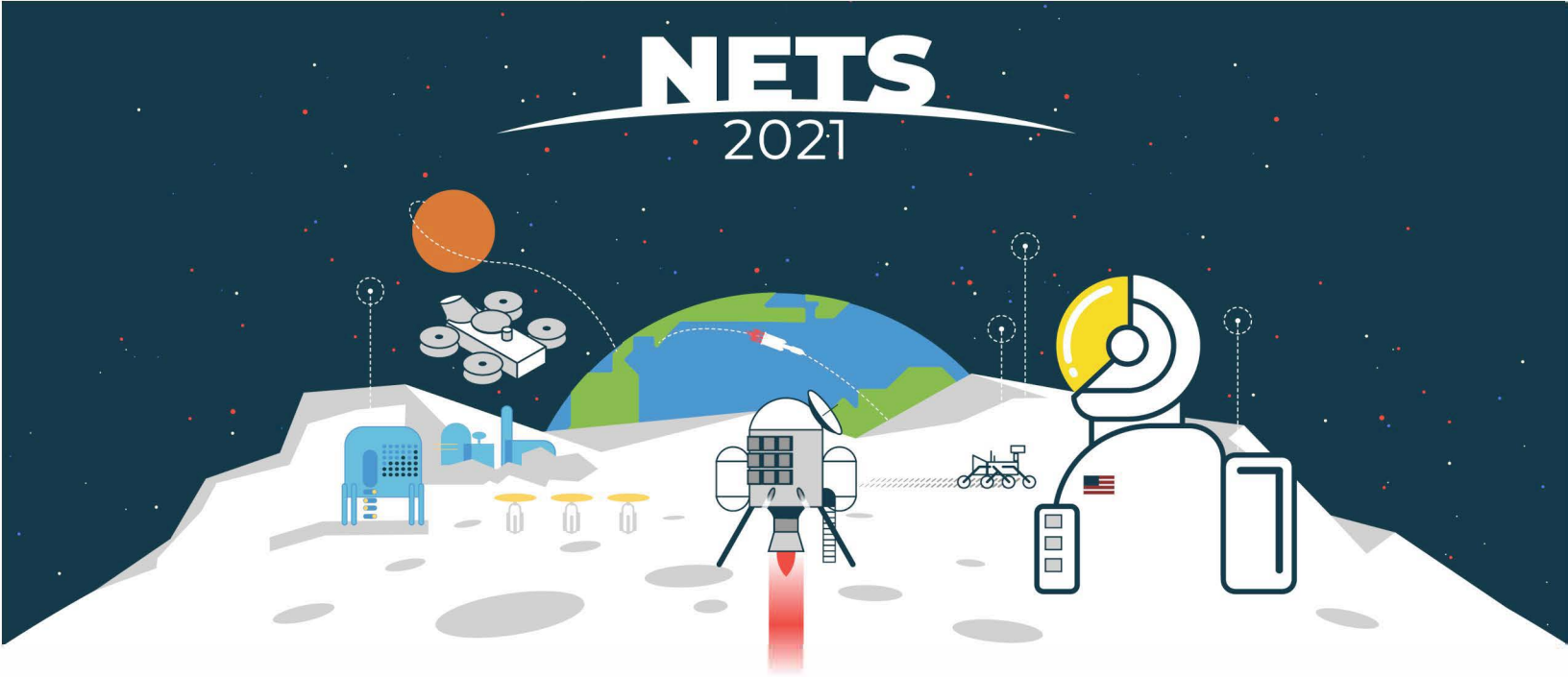

NUCLEAR and
EMERGING
TECHNOLOGIES for
SPACE

CONFERENCE PROCEEDINGS

Hosted by Oak Ridge National Laboratory

April 26th-30th, 2021

Track 2: Nuclear Fission Power and Propulsion

Technical Track Chair(s): Paolo Venneri

U.S. DEPARTMENT OF ENERGY

https://nets2021.ornl.gov

OAK RIDGE National Laboratory

Author	Title
Ang, Caen	Pulsed Electric Current Sintering for Fuel Element Fabrication
Bess, John D.	Upgrading Test Vehicle Capacity to Enable Future Space and Microreactor Testing In TREAT
Colgan, Nathan	Mass Optimization of a Convective Heat Exchanger for Mars Surface Reactor Waste Heat Rejection
Cornell, Bryce	Design And Modeling of a Centrifugal Nuclear Thermal Rocket
Deason, Wesley	Pylon: Scalable Power for The Emerging Space Economy
Dorville, Joffrey	Design of a Low Enrichment Uranium Nuclear Reactor to Power a Future Martian Colony – Neutronic Aspects
Eades, Michael	Nuclear Thermal Propulsion Demonstration Concept
Glatt, Conner	Design of a Low-Enrichment Uranium Nuclear Reactor to Power a Future Martian Colony – Heat Rejection
Gustafson, Jeremy	Space Nuclear Propulsion Fuel and Moderator Development Plan Conceptual Testing Reference Design
Kim, Chan S.	Development of Key Technologies for Korean Space Heat Pipe Reactor
Manickam, Vigneshwar	Preliminary System Framework for The Startup Analysis of a Low Enriched Nuclear Thermal Propulsion Engine
Mason, Lee	Nuclear Power Concepts for High-Power Electric Propulsion Missions to Mars
Mendoza, Jesus A.	Dual Moderator Space Reactor Cores
Mendoza, Mario	Nuclear Thermal Propulsion Immediate Xenon Restart Threshold for Short Burn Durations
Nikitaev, Dennis	In-Situ Alternative Propellants for Nuclear Thermal Propulsion
Palomares, Kelsa	Nuclear Space System Analysis and Modelling (NSSAM): A Software Tool to Efficiently Analyze the Design Space of Space Reactor Systems
Palomares, Kelsa B.	Moderator Considerations for Space Nuclear Power and Propulsion Systems
Park, Gyutae	Increasing Cermet Fuel Thermal Margin with Thoria for Nuclear Thermal Propulsion
Pratt, Micah	Simulation of an Inductively Heated Multi-Channel Nuclear Thermal Rocket Model
Rader, Jordan D.	Development Of Multi-Purpose Dynamic Nuclear Thermal Rocket System Models
Schleicher, Robert W.	Safety Design Considerations for Nuclear Reactor Powered Spacecraft
Selby, Aaron	Progress on Decay Heat Modeling and Mitigation in NTP Systems
Shirvan, Koroush	MIT Reactor Irradiation Capabilities for Space Nuclear Technology Deployment

Smith, Corey	Core Loading Pattern Optimization of a Tie-Tube Nuclear Thermal Propulsion Reactor Using a Simulated Annealing Algorithm for Nodal Diffusion Solvers
Tellez, Jacob	Design of a Low Enrichment Uranium Nuclear Reactor to Power a Future Martian Colony – Thermal Hydraulics
Widdicombe, Teyen	Design of Nerva-Derived HALEU Reactor ("EMU") for Nuclear Thermal Propulsion
Wood, Emily	Alternatives for Electrical Power Production from a Nuclear Thermal Propulsion Engine
Zymbaluk, Jaden G.	A Survey of High-Temperature Moderators for Space Nuclear Reactor Applications

Nuclear and Emerging Technologies for Space
Sponsored by Oak Ridge National Laboratory, April 26th-30th, 2021.
Available online at https://nets2021.ornl.gov

PULSED ELECTRIC CURRENT SINTERING FOR FUEL ELEMENT FABRICATION

Caen Ang[1], Matthew Scott[1], Ethan Deters[1], Aaron Selby[2]
[1]*University of Tennessee, Department of Nuclear Engineering, 1412 Circle Dr, Knoxville, TN, 37996*
[2]*USNC-Tech, 2356/120 West Commodore Way, Seattle, WA, 98199*
Primary Author Contact Information: cang@utk.edu

ZrC is a candidate material for nuclear thermal propulsion core structures. There has been significant progress in controlling the sintering to produce dense, bulk structures with embedded channels via control of the Zr-C system kinetics and chemical thermodynamics. Preliminary hot hydrogen tests at 2500K illustrate promising performance of ZrC-based materials. Challenges in geometry and design remain when considering Pulsed Electric Current Sintering for near-net shape fabrication.

I. INTRODUCTION

Nuclear thermal propulsion (NTP) systems use a nuclear reactor to heat hydrogen to temperatures >2000K. This provides a high thrust, high I_{sp} solution to space travel, enabling faster transit times to Mars and beyond. These higher temperatures are incompatible with historical nuclear fuels, which requires new and advanced fuels to enable the deployment of NTP systems.

This study focused on the development of an NTP reactor fuel that consisted of TRIstructural ISOtropic (TRISO) particles embedded within a dense ZrC matrix. These TRISO particles contain a fissionable core such as UO_2 surrounded by a buffer layer of porous carbon, an inner layer of pyrolytic carbon (IPyC), an impermeable SiC shell, and a final outer layer of pyrolytic carbon (OPyC). These layers serve as a fission product barrier and pressure vessel. These TRISO particles are then encased in a fully dense matrix of ZrC, which serves as a secondary fission product barrier.

Since 2011, work has been performed in consolidating TRISO particles in a dense SiC matrix for terrestrial reactors. USNC-Tech has implemented this technology for space applications; first developing SiC-based NTP reactor fuel then enhancing that technology with the implementation of the ZrC matrix. This ZrC matrix is an ultra-high temperature material that can withstand temperatures >2700K, extending the maximum operating temperature of the NTP reactor fuel by over 20% and enabling 900s I_{sp}.

The challenge of producing this ZrC-based NTP fuel is in producing fully dense ZrC at conditions that accommodate the TRISO particles. This requires producing ZrC at temperatures and pressures much lower than standard production methods.[1] This study focused on producing ZrC using a sintering method compatible with TRISO particles, characterizing those samples, and testing ZrC coupons in Compact Fuel Element Environmental Test (CFEET) facility located at NASA George C. Marshall Space Flight Center.

The lessons from the final NF-1 test (1973) provide key insights as to the required microstructural design in developing carbide materials. To briefly review Lyon et al[2], this was the last test of US-designed carbide fuel elements, which included composite-graphite elements coated with ZrC and NbC (which constituted the majority of the test cells). The difficulty in fabrication relative to the composite-graphite elements was highlighted. In both materials, coolant channel integrity appeared to be a priority. This is a significant challenge to the fabrication and microstructure that prefers thicker walls, which help to increase thermal gradients and corresponding stresses. When compared to the (U,Zr)C in graphite, solid-solution carbide observed less cracking due to FP gas, decrease in thermal conductivity and strength. An additional advantage was the projected lifetime of hours at 2800-3100K derived from individual component tests. However, a key problem observed in the carbide elements was longitudinal cracking, particularly at temperatures of 1500-1800K, which is below the onset of acceptable mechanical response of ZrC.[3]

Understanding the pre-requisites to high density ZrC-based materials is crucial, particularly with respect to the mechanisms of sintering that dominate the fabrication of these materials. Subsequent infrastructure for verification of fabrication, supporting characterization and component testing is essential. Such a strategy will provide a framework for iterative fabrication, characterization and testing that address the remaining challenges with ZrC-based NTP systems.

I.A. Kinetics of initial stage sintering

Sintering of ZrC as a structural material for high temperature refractory environments was explored via densification experiments. ZrC powders (H.C. Starck, Grade B, AB134580, Lot 26011/18 and (US Res. Nano. Inc, US2168, (99+%, 80nm, Cubic)) were sintered to ~1875°C at up to 30 minutes under Pulsed Electric Current sintering mode (LABOX-675 (NJS Co. Ltd, Japan)) under an applied pressure of 10-30 MPa. In these experiments, the length change of the ZrC green body articles were determined by recording the displacement changes during sintering. The identical sintering sequence was conducted on graphite tooling. The time steps were synchronized and a subtraction of the displacement values

at each time step was used to reveal the change in length of the ZrC green body article as a function of time or temperature. This experiment requires specific tooling that minimizes lateral expansion and maximizes axial expansion, as well as insulating against significant temperature variations. Once calibrated, the experiment provides usable data for the Constant Rate Heating (CRH) method published by Young et al, resulting in activation energies for shrinkage, and specifically for sintering provided a rate constant *n* is specified for a particular mechanism (viscous, volume or grain boundary diffusion).[4]

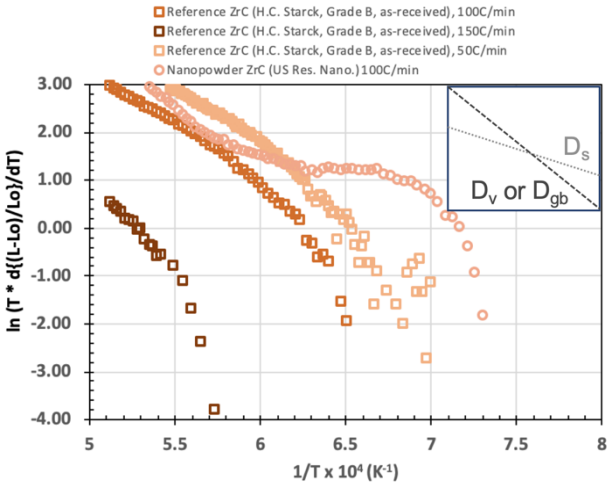

Figure 1. Differential CRH plot for sintering of ZrC at different heating rates and two different particle sizes (d50 = 0.3 um and 0.08 um). The inset shows a schematic of the effect of surface diffusion on CRH plots.

Figure 1 shows the differential plots for ZrC materials heated at different heating rates (50, 100 and 150C per minute) as well as nano-size powders. All compacts were prepared at 150 MPa uniaxial pressing, ensuring significant contact between particles and limiting grain boundary sliding[1] and other redistribution mechanisms. Since the y-axis represents a shrinkage rate as the heating rate is increased, the onset of shrinkage in the powder compact is delayed; this may be explained by the non-uniform temperature distribution in the powder compact. The use of nano-sized powder lead to an earlier onset of shrinkage than the micron-sized powder, explained by the higher potential as a result of the greater curvature in the nano-sized powder. The reader is directed to these references for the fundamentals of the experiment. However, the inset of Figure 1 explains that the CRH experiment should show one gradient assuming only one mechanism and all particles are mono-sized. As noted by Young et al[4], changes in slope are associated with the radius of the particles in the specimen, a change in diffusion mechanisms or the distribution of competing mechanisms. Since surface diffusion builds the neck radius without bringing the particle centers closer, a reduced rate of shrinkage is observed. The result is less shrinkage at higher temperature.

This type of calculation permits the derivation of activation energies and/or change in major mechanisms at the initial stage of sintering. As noted, non-linearity in sintering plots arise from size distributions and can reportedly be used to distinguish particle size distributions. Figure 1 shows that in the nano-size powder, the rate of shrinkage per temperature increment is rapidly reduced. This might be explained by rapid surface diffusion enhancing neck growth without shrinkage, or the establishment of inter-agglomerate networks no longer allowing conventional sintering mass transport. (Both theories are typical problems associated with nanosized powders for sintering.) The value of nQ/3R for the initial stage shrinkage gradients of -12.2 to -14.7 correspond to 610-735 kJ/mol if n = ½ for lattice (volume) diffusion. These values correspond to slightly higher than the bond enthalpy in ZrC noted as 5.812 eV (561 kJ/mol)[3], which would be in general agreement with the values obtained here. Determining sintering kinetics may be crucial to fabrication of extruded core structures; typically, ZrC densifies via intergranular glide at low pressures (~25 MPa) and a dislocation mechanism at high pressures (~100 MPa)[1], but such options may be problematic for extruded core structures. The applied experimental efforts reported here are useful tools in determining both the effect of relative particle sizes and the role of dopants in the Zr and C sublattices that may be needed to alter the processing conditions required for sintering on initial stage sintering.

I.B. Chemical stability of ZrC during sintering

As noted, the high bond enthalpy results in high temperatures required for consolidation of ZrC materials. However, focusing on the kinetics alone misrepresents the difficulty in fabrication of fully dense ZrC parts. A significant problem associated with densification of any ceramic is the contribution from surface or vapor diffusion, which deposits matter at the sink of the neck and thereby reduces the diffusion potential that is driven by defect populations in curvature. One of the problems in ZrC is the presence of oxygen, which preferentially forms ZrO_2. The presence of ZrO2 is otherwise difficult to remove because its vapor pressure is relatively low with respect to even these sintering conditions. As a result, its presence stabilizes pore curvatures by reducing surface energy (~1.2-1.6 J/m^2)[5], and results in grain expansion due to the relative difficulty and insufficient energy to extend grain boundaries. However, the chemical stability can be determined by the Gibbs free energy (1):

$$\Delta G = \Delta H - T\Delta S \qquad (1)$$

where the negative value of free energy corresponds to a favorable reaction. It is known that carbothermal reduction of ZrO_2 in the presence of excess carbon can be written in the form of (2):

$$ZrO_{2(s)} + 3C_{(s)} \rightarrow ZrC_{(s)} + 2CO_{(g)} \quad (2)$$

And this reaction[6] becomes favorable above ~1928K (1655°C). Therefore, excess carbon is a potential solution to eliminate residual ZrO2, provided at $CO_{(g)}$ can be removed from the pore network.

It is often proposed that sintering additives may play a role in densification. Certainly, the inclusion of dopants at the 0.1-1 mol% level should contribute high defect populations relative to equilibrium thermal vacancy concentrations.

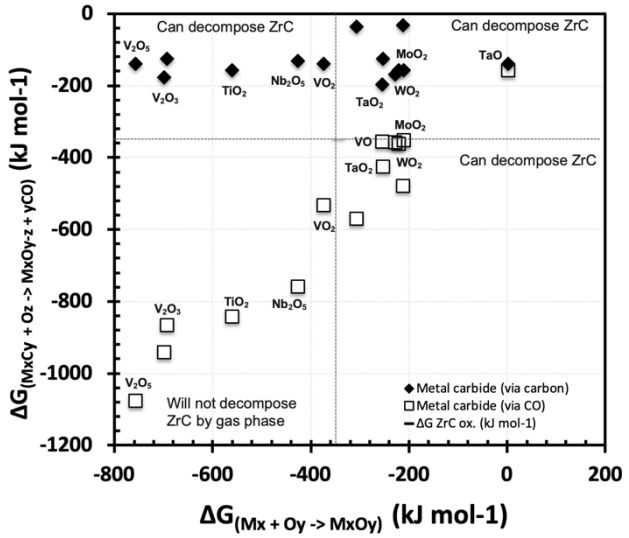

Figure 2. Thermodynamic stability plot comparing the Gibbs formation free energy for oxides of Ti, W, Ta, Nb, Mo, and V at 2148K (1875°C). The results show that ZrC will be oxidized by all additives in solid oxide form, but some vapor phase oxides will not decompose ZrC.

Methods of addition are typically based on powder which poses another challenge. The mixing always leads to the addition of oxygen via the native oxides always present in the added dopant (e.g. a nitride or carbide). This leads to a significant problem where the addition of dopants may not appear effective in practice. In applying equation (1) to formation of several transition metal oxide impurities, a sintering additive should not decompose ZrC via either the direct carbon reaction or via carbon monoxide.

Figure 2 shows the results of the thermodynamic calculations[6]. The horizontal and vertical lines represent the equation (3):

$$ZrC_{(s)} + O_{2(g)} \rightarrow ZrO_{2(s,l)} + 2C_{(s)} \quad (3)$$

while each position represents the carburization reactions via carbon or carbon monoxide (CO). Effectively, Figure 2 illustrates the challenges in sintering additives for ZrC; practically any oxygen species of these transition metals will oxidize ZrC into ZrO2. This is not an unexpected result due to the known oxygen affinity of Zr. Therefore, an added carbide or nitride will be stable and provide a composite structure, but it will also lead to an increase of the amount of ZrO_2. At higher temperatures, formation of a carbide additive via CO will not oxidize ZrC, which does suggest possible compromises in a potential thermodynamic system. The above experimental analysis will prove useful in determination of suitable sintering additives for monolithic ZrC, as well as determining the thermal stability of ZrC composites.

I.C. Monolithic ZrC in hot hydrogen environments

Material corrosion tests from 2000-2500K were conducted at the Compact Fuel Element Environmental Test (CFEET) facility, at the NASA George C. Marshall Space Flight Center. Detailed experimental conditions are described elsewhere[7], but it includes a flow rate of 0.5 SLPM to maintain 1 atm H_2 pressure, and a heating rate of 400°C/min for isotherms of typically 30 min, where mass and dimensions were obtained during the intervals.

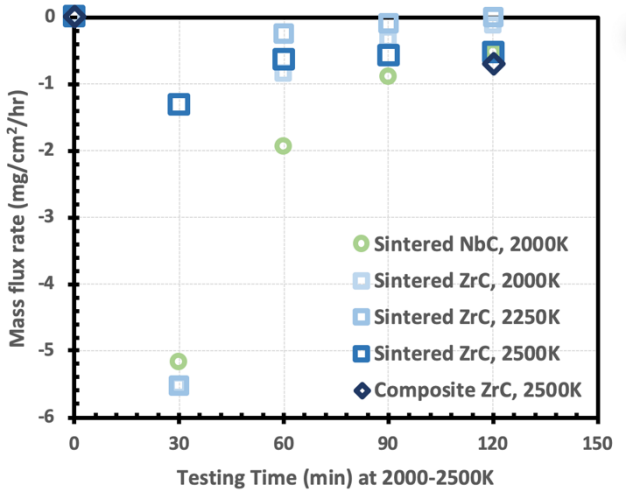

Fig. 3. Mass loss rate of monolithic and composite ZrC materials at 2500K. For comparison, sintered NbC (2000K)[8] and ZrC (2000 and 2250K) are included.[7]

Figure 3 shows that ZrC materials all experience a high mass loss in the first 30 min exposure test. However, given that sintered NbC[8] also shows this mass loss, the change is attributed to the presence of identified impurities such as Fe observed at the grain boundary. The presence of these impurities is dissimilar between tests, as noted by a lower initial mass loss in ZrC at 2500K compared to higher initial mass loss in ZrC at 2250 and 2000K. These results came from a similar powder feedstock, although not the same batch/lot. A composite

ZrC fabricated at UTK was also tested with similar mass losses, which represents a promising basis for addressing reported high strain / high cracking at specific stations of NF-1. Further testing is planned at representative hydrogen pressures expected in NTP composites.

I.D. Design and architecture of fuel elements

The legacy fuel elements were fabricated by powder processes; for example (U,Zr)C was formed via ZrC, UO_2, ZrO_2, and C.[2] The excess carbon was specifically important for part release and as well as U and Zr carbothermal reduction (essence of Figure 2). A difficult design challenge is the stability and tolerance of channels; a major concern in materials fabricated by PECS/SPS. Figure 4 shows a photograph of fabricated parts with embedded channel structures. Minor issues such as channel roughness and debris are correctable in post-fabrication.

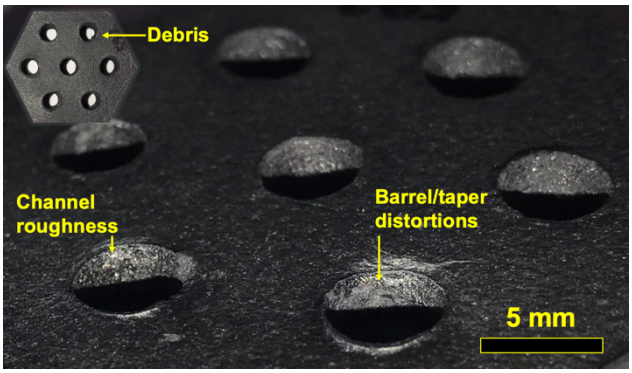

Figure 4. Fabrication challenges from embedding multiple channels in parts via PECS/SPS. The identified flaws appear to increase with frequency as additional channels (3, 7, 19, etc) are added.

However, it is possible that debris originated during fabrication represents weakness in the channel due to reaction with the volatile mandrel materials. Barreling or tapering of the channels are observed. This is attributed to fundamental challenges in both sintering stress and controlling of current. These included as-yet not well understood feedback of current-temperature profiles during sintering, due to non-conductive mandrels, which will be published in a future manuscript.

II. CONCLUSIONS

The study of zirconium carbide (ZrC) sintering provides a basis for understanding not only monolithic, but also composite forms needed for more flexible materials properties highlighted by historical NTP testing. Both CRH experiments and chemical thermodynamics analysis confirm the problematic contributions from loss of shrinkage rate and zirconium oxide formation. Successfully fabricated composite and monolithic ZrC materials show not only promising hot hydrogen test results but also simple architectures able to satisfy NTP designs by PECS/SPS.

ACKNOWLEDGMENTS

The authors thank Paolo Venneri (USNC-Tech) for inception and useful discussions. Brandon Connor provided editorial review. Caen Ang discloses employment and financial interests in USNC. The work presented in this paper was partially funded by Jacobs Technology Inc. Contract No. 80MSFC18C0011 supporting Versatile NTP. Work was conducted on equipment owned/donated by Ultra Safe Nuclear Corporation (Seattle, WA, USA).

REFERENCES

[1]M. GENDRE, A. MAITRE, and G. TROLLIARD, "A Study of the Densification Mechanisms During Spark Plasma Sintering of Zirconium (Oxy-) Carbide Powders," *Acta Mater.*, 58[7] 2598-2609 (2010).

[2]L. L. LYON, "Performance of (U, Zr) C-Graphite (Composite) and of (U, Zr) C (Carbide) Fuel Elements in the Nuclear Furnace 1 Test Reactor." Los Alamos Scientific Lab., N. Mex.(USA), 1973.

[3]Y. KATOH, G. VASUDEVAMURTHY, T. NOZAWA, and L. L. SNEAD, "Properties of Zirconium Carbide for Nuclear Fuel Applications," *J. Nucl. Mater.*, 441[1–3] 718-742 (2013).

[4]W. S. YOUNG and I. B. CUTLER, "Initial Sintering with Constant Rates of Heating," *J. Am. Ceram. Soc.*, 53[12] 659-663 (1970).

[5]A. V. RADHA, O. BOMATI-MIGUEL, S. V. USHAKOV, A. NAVROTSKY, and P. TARTAJ, "Surface Enthalpy, Enthalpy of Water Adsorption, and Phase Stability in Nanocrystalline Monoclinic Zirconia," *J. Am. Ceram. Soc.*, 92[1] 133-140 (2009).

[6]E. T. TURKDOGAN, "Physical Chemistry of High Temperature Technology (Gibbs Free Energy Tables)," (1980).

[7]K. BENENSKY, Romnes, C., Eades, M., Venneri, P., Terrani, K., and Zinkle, S., "Evaluation of Novel Refractory Carbide Matrix Fuels for Nuclear Thermal Propulsion, 2018 Nuclear and Emerging Technologies for Space. February 26 – March 1. Las Vegas, Nv. Presentation and Proceedings. ," 2018.

[8]C. ANG, L. SNEAD, and K. BENENSKY, "Niobium Carbide as a Technology Demonstrator of Ultra-High Temperature Ceramics for Fully Ceramic Microencapsulated (Fcm) Fuels," *International Journal of Ceramic Engineering & Science*, 1 92–102 (2019).

Nuclear and Emerging Technologies for Space
Sponsored by Oak Ridge National Laboratory, April 26th-30th, 2021.
Available online at https://nets2021.ornl.gov

UPGRADING TEST VEHICLE CAPACITY TO ENABLE FUTURE SPACE AND MICROREACTOR TESTING IN TREAT

John D. Bess, Nicolas E. Woolstenhulme, Daniel B. Chapman, Aaron S. Epiney, Justin T. Johnson, Matthew R. Ramirez, Wesley T. Smith, Kevan D. Weaver

Idaho National Laboratory, Idaho Falls, ID 83415-3855

Primary Author Contact Information: (208) 206-1286 and john.bess@inl.gov

I. INTRODUCTION

The Transient Reactor Test (TREAT) facility is an air-cooled, graphite-moderated and -reflected reactor fueled with dilute concentrations of uranium oxide. The TREAT reactor provides nuclear-heated transient testing paired with well-designed experiment vehicles to enable a range of conditions to support tests and missions of various needs to characterize nuclear fuels, materials, and instrumentation. TREAT experiment vehicles are generally self-contained and engineered with the capabilities to safety contain hazards, support the specimens and accompanying instrumentation, and deliver desired specimen boundary conditions throughout the test[1].

More recent historically utilized experiment test vehicles include the M-series culminating in M8CAL[2] and also the AN-CAL experiments[3]. The M-series experiments typically comprised a sodium loop within coupled stainless-steel pipes representing the test fuel region and return leg for pumped coolant. A dysprosium filter was utilized in the test region to reduce the thermal component of the neutron flux. These test vehicles displaced a 4 in. by 8 in. (10.16 cm by 20.32 cm) region in the center of the reactor core, enclosed within a secondary containment vessel also made from stainless steel. The AN-CAL experiment test vehicles consisted of a concentric pair of containment vessels with an outer diameter of 7.625 in. (~19.4 cm). The outer vessel was stainless steel, and the inner vessel either aluminum or stainless steel. Both of these testing envelopes extended the full height of the core, with the testing region specifically focused within the active fueled height of the core of approximately 48 in. (~1.22 m).

The contemporary test vehicle employed in transient testing is called the Broad Use Specimen Transient Experiment Rig (BUSTER), which continues to provide ample versatility supporting testing missions within the same in-core footprint of the M-series experiments[4]. The burden of the primary safety containment falls upon the stainless-steel pipe providing an approximately 6-cm-inner-diameter testing environment. A secondary stainless-steel containment vehicle fits within the core to host the primary containment within the confines of the reactor core. While the secondary containment of BUSTER provides experimental facilities within the full height of other TREAT assemblies, the available vertical testing volume is slightly limited due to placement of a graphite block at the bottom of the secondary containment in an effort to reduce axial neutron leakage.

Although the BUSTER test vehicle continues to support current transient testing needs in TREAT, there is a growing need to develop a larger vehicle to increase the volumetric testing capacity within TREAT. Larger BUSTER-type vehicles can provide additional space for hosting test environment modules, instrumentation, integrated modular systems, and/or advanced test loops concepts. Recent activities at Idaho National Laboratory (INL) have focused upon designing the new Big-BUSTER test vehicle and refining said design for implementation in future TREAT transient test experiments.

II. BIG-BUSTER DESIGN AND ANALYSIS

There are numerous challenges associated with moving to a larger design: reduced fuel in the core center of TREAT, introduction of a greater mass of neutronically absorbing material that impacts total core excess reactivity and transient testing performance, and the introduction of larger neutron streaming paths that also impact core performance. A key requirement is that Big-BUSTER still allows for continued support of existing BUSTER-sized experiments while enabling a wider range of new experimental applications. There is also a desire to follow the trajectory of previous test vehicle designs via a dual-containment system that can be tightly emplaced within the TREAT core.

The current Big-BUSTER design was evaluated to provide only the secondary containment vessel for future experiments. This choice was made to provide more flexibility in experiment design, such that the primary containment shall be designed to accommodate the commensurate needs of the selected experiment, because not all experiments in TREAT will incur testing environments requisite for containment of high-temperature and high-pressure conditions. Such adaptability in design was desirable to enable the provision of testing conditions suitable of advanced

transient testing of microreactors, such as proposed for the Nuclear-heated Irradiations for Microreactor Benchmarks and Linked Experiments (NIMBLE)[5]. Microreactors are a burgeoning area of interest for advanced reactor deployment with great promise for nontraditional applications that includes miniaturization benefits simplifying siting, operations, transportation, and manufacturing. Smaller-scale design accommodates innovation in the advanced manufacturing of components, applications of autonomous controls, and demonstration of heat removal technologies atypical to conventional full-sized power reactors. Microreactors benefit from the decades of research invested in the development of space reactor technologies. Furthermore, space reactors represent microreactor concepts uniquely designed to support space power needs.

Tests hosted in TREAT would not be established to contain a complete microreactor, nor to provide extended operations supporting accumulated burnup or neutron damage. Complete subassembly-type microreactor components can undergo transient testing to evaluate system-scale experiments with full representation of nuclear physics. Furthermore, existing infrastructure at INL can support extended burnup tests at the Advanced Test Reactor (ATR) that can be pre- and post-processed at the Hot Fuel Examination Facility (HFEF). Irradiated specimens can be assembled into NIMBLE tests within Big-BUSTER to provide insight into the irradiated performance of microreactor core materials and systems.

The small size of space and microreactors makes it possible to fit not only a portion of the fuel, but also part of the heat removal and power conversion system into Big-BUSTER. This enables TREAT experiments for microreactors to test (in addition to the traditional fuel characterization) also their heat removal systems under prototypic as well as accidental conditions in prototypic irradiation environments.

Big-BUSTER is designed to accommodate a configurable heat exchanger hood that can connect to the microreactor's heat removal mechanism, e.g. heat pipes or circulating gas. This heat exchanger can evacuate heat during a test, to be able to reproduce prototypical temperature and power distributions in the test section. In addition, this heat exchanger can also be used to simulate loss of heat sink or loss of cooling situations. During such tests, power, and temperature re-distribution in the microreactor test section can be investigated using actual direct nuclear heating feedback.

A comprehensive reactor physics analysis of Big-BUSTER was recently completed to support a final design review in preparation for construction of several test vehicle units and supporting hardware components[6]. The evaluated Big-BUSTER design consists of a Zircaloy-2.5Nb pipe that is 87.941 in. (~2.2 m) in length with an outer diameter of 9.7 in. (~24.6 cm) and inner diameter of 8.75 in. (~22.2 cm). The bottom of the tube has an 8 in.(~20.3 cm) long end cap, and the tube top has an 8 in. (~20.3 cm) long end fitting with flanged adapter to accept the test vehicle hood. The components are welded together to form a single hermetic testing environment. The final Big-BUSTER design will more likely have an outer diameter of 9.5 in. (~24.1 cm) to provide some additional margin in transportation and handling; this slight modification is not expected to have a significant impact upon the computed results.

Integration of Big-BUSTER into the TREAT core will require displacement of the central 3 × 3 assembly positions within the core matrix to allow a footprint of 12 in. (30.48 cm) on each side. Additional core interface hardware is required to yield desirable neutronic conditions and ensure a tight fit between the TREAT core assemblies and the Big-BUSTER testing environment. Unfueled filler assemblies are to be specifically manufactured to adapt the round test vehicle to completely fill the vacated square hole. A similar concept was employed during the AN-CAL experiment series[3]. The filler assemblies consist of Zircaloy-4 cladding, axial graphite reflectors, and aluminum end fittings. Steel bolts sandwich graphite or BeO moderator material in each filler assembly to match with the vertical position of the fueled active core region of TREAT. The filler assemblies are also designed to ensure a vertical gap within this region of the core immediately to the north and south of the test vehicle to accommodate fast neutron hodoscope imaging capabilities. Visualization of Big-BUSTER within TREAT is shown in Figure 1.

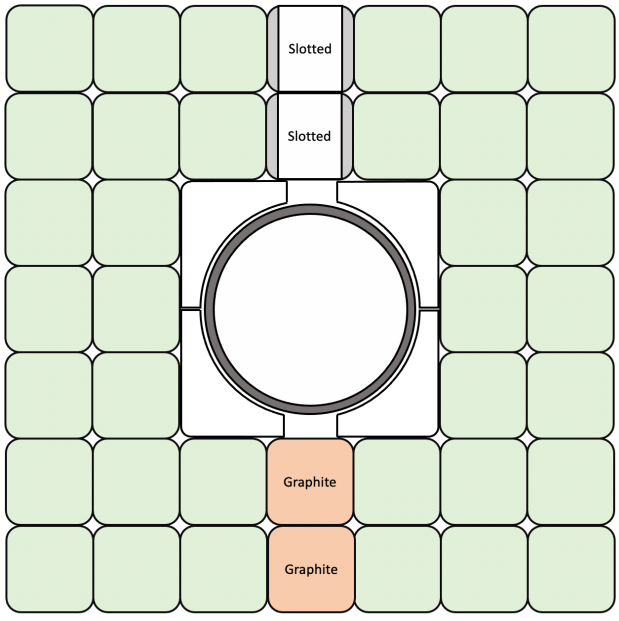

Fig. 1. Depiction of Big-BUSTER Test Vehicle Installation in TREAT.

It was concluded that the Big-BUSTER design is expected to exceed or meet the programmatic and safety requirements necessary to allow for its implementation in TREAT. Those results are reported elsewhere[6], but key findings relevant to this work are discussed herein.

III. SUMMARY OF KEY RESULTS

The worth of the Big-BUSTER test vehicle with BeO filler assemblies is -0.41 ± 0.01 and +1.25 ± 0.01 %Δk/k, respectively. For the same components with the graphite-moderated filler material, the worths are -0.34 ± 0.01 and +0.99 ± 0.01 %Δk/k, respectively. There is clear value in provisioning the uniquely designed filler assemblies to provide a physical and neutronic coupling between the TREAT core and Big-BUSTER. The significance of the small neutron worth of the empty Big-BUSTER test vehicle should be noted. A similar double-canned calculation of concentric Zircalloy canisters only increased the magnitude of the worth by ~0.2 %Δk/k. These results can be compared against a similar design with stainless steel 304 double canisters that resulted in a further increase in negative worth of ~3.4 %Δk/k. The current stainless steel 316 BUSTER test vehicle has a worth of only approximately -2.0 %Δk/k, pre-BUSTER designs for possible Inconel-718 testing environments were similarly around -3.6 %Δk/k. For reference, the M8CAL experiments were worth about -3.4 %Δk/k, and AN-CAL experiments -4.0 %Δk/k for the double-steel canisters and -2.2 %Δk/k for the aluminum-in-steel containment pair. Therefore, the worth of the current Big-BUSTER design is significantly less than prior experiments, allowing for the incorporation of various neutron absorbing materials in future experiment design.

The evaluated core loading with Big-BUSTER was assessed to provide $\geq$ 4.2 %Δk/k to enable transient testing. Because fuel and dummy assemblies can be swapped around to adjust total core excess reactivity, the true limitation for available excess reactivity to support an experiment will be that the temperature of the fuel does not exceed 600 °C, so as to prevent oxidation of the fuel assembly Zircaloy-3 cladding. The evaluated TREAT loading for the Big-BUSTER experiments had an estimated excess reactivity of +7.08 ± 0.01 %Δk/k. Further adjustment of the core loading to accommodate either a full- or half-slotted core in support of the hodoscope facilities would adjust the available excess reactivity by -0.92 ± 0.01 to +1.05 ± 0.01 %Δk/k, respectively. A hodoscope slot completely filled with fuel assemblies is estimated to increase total core excess reactivity +2.80 ± 0.01 %Δk/k. There is more than sufficient reactivity to support transient test of increased negative worth, as well as sufficient reactivity that can be removed to accommodate microreactor subassembly tests possibly introducing significant positive reactivity into the TREAT core.

A requirement for the neutron flux environment within Big-BUSTER is that the peak total neutron flux in the empty test vehicle be $\geq 7.8 \cdot 10^{12}$ n/cm^2•s•MW. The evaluated neutron flux for the BeO and graphite filler assemblies is $8.41 \cdot 10^{12}$ and $8.43 \cdot 10^{12}$ n/cm^2•s•MW, respectively. These results are comparable to previous computational characterization of BUSTER that yielded $7.79 \cdot 10^{12}$ and $8.64 \cdot 10^{12}$ n/cm^2•s•MW for the full- and half-slotted cores, respectively[4]. The 3-group neutron spectra at the peak position are as follows for the BeO moderated Big-BUSTER: 45.4 % thermal (< 0.625 eV), 41.6 % epithermal, and 13.0 % fast (> 100 keV). The neutron spectra are very similar for the graphite-moderated test vehicle: 41.5 % thermal (< 0.625 eV), 43.3 % epithermal, and 15.2 % fast (> 100 keV). The current BUSTER test vehicle has the following spectra: 30 % thermal (< 0.625 eV), 50 % epithermal, and 20 % fast (> 100 keV). The steel in BUSTER suppresses the thermal component of the neutron flux. The evaluated photon flux for the BeO and graphite filler assemblies is $1.21 \cdot 10^{12}$ and $1.26 \cdot 10^{12}$ p/cm^2•s•MW, respectively. These results are slightly less than previous computational characterization of BUSTER that yielded $2.88 \cdot 10^{12}$ and $3.20 \cdot 10^{12}$ p/cm^2•s•MW for the full- and half-slotted cores, respectively[4].

The current design uses Cerafiber® Wet Pack as thermal insulation. Preliminary thermal hydraulic considerations suggest that relatively high operating temperatures of up to 1250 K can be reached in experiments in Big-BUSTER, while the containments and TREAT fuel stays within their operational limits. However, to achieve such high temperatures, electrical heaters will have to be used to preheat the experiment prior to the test. Then nuclear heating can be used during the portions of interest of the transient experiment. Analysis shows that for this high temperature case, heat loss through Big-BUSTER is on the order of ~5 kW[7]. This is encouraging as to the potential to accommodate a wide array of microreactor designs.

The computed values for Big-BUSTER are expected to change with the introduction of test components and, if necessary, a primary test vehicle. Characterization, design, and safety calculations will be required on a per-experiment basis to assess the versatility in experiment capabilities and their impact upon testing environment and reactor physics performance. However, it is clear from the current design and safety requirements[6] that Big-BUSTER is suitable for providing a larger-volume transient testing environment to support future transient experiments. The accommodation of a larger test vehicle within TREAT enables subassembly-sized experiments supporting system-scale experimentation for microreactor and space reactor designs.

IV. CONCLUSIONS

Design calculations were performed to evaluate programmatic and safety requirements supporting the feasibility of incorporating a larger-volume test vehicle within the center of the TREAT core. Larger transient testing capacity enables additional versatility in maintaining support of current testing missions while providing flexibility to design new system-scale experiments with full representation of nuclear physics. These types of experiments allow for transient tests in support of microreactor and space reactor design concepts. The current design review of the proposed Big-BUSTER test vehicle is just completing, with manufacture of containment vessels and supporting core interface hardware will commence. It is currently planned to insert Big-BUSTER into the TREAT core by the summer of 2022.

ACKNOWLEDGMENTS

This research made use of the resources of the High-Performance Computing Center (HPC) at Idaho National Laboratory (INL), which is supported by the Office of Nuclear Energy of the U.S. Department of Energy (US DOE-NE) and the Nuclear Science User Facilities (NSUF) under Contract No. DE-AC07-05ID14517.

REFERENCES

1. N. E. WOOLSTENHULME, D. M. WACHS, and A. B. BEASLEY, "Transient Experiment Design for Accident Tolerant Fuels," *Trans. Am. Nucl. Soc.*, **111**, 604 (2014).
2. W. R. ROBINSON and T. H. BAUER, "The M8 Power Calibration Experiment (M8CAL)," ANL-IFR-232, Argonne National Laboratory (1994).
3. W. R. ROBINSON, R. J. PAGE, and A. E. WRIGHT, "TREAT NPR Calibration Experiment AN-CAL," ANL/NPR-92/11, Argonne National Laboratory (1992).
4. J. D. BESS, et al., "Nuclear Characterization of a General-Purpose Instrumentation and Materials Testing Location in TREAT," *Ann. Nucl. Energy*, **124**, 270 (2019).
5. J. D. BESS, et al., "Enabling Future Microreactor Testing with the NIMBLE Platform in TREAT," *Trans. Am. Nucl. Soc.*, **123**, 482 (2020).
6. J. D. BESS, et al., "Reactor Physics Analyses of the Big-BUSTER Testing Environment in TREAT," *Trans. Am. Nucl. Soc.*, **124** (2021).
7. A. S. EPINEY, et al., "NIMBLE Microreactor Testing Platform for TREAT: Preliminary Thermal-Hydraulic Considerations," *Trans. Am. Nucl. Soc.*, **123**, 1825 (2020).

Nuclear and Emerging Technologies for Space
Sponsored by Oak Ridge National Laboratory, April 26th-30th, 2021.
Available online at https://nets2021.ornl.gov

MASS OPTIMIZATION OF A CONVECTIVE HEAT EXCHANGER FOR MARS SURFACE REACTOR WASTE HEAT REJECTION

Nathan Colgan[1], Gregory Nellis[1], and Mark Anderson[1]

[1]*UW-Madison, 1500 Engineering Drive, Madison, WI, 53706*

Primary Author Contact Information: 610-608-0556, ncolgan@wisc.edu

A numerical model of a finned-tube heat exchanger is developed and optimized to determine the mass-optimal heat exchanger geometry for waste heat rejection to the Martian atmosphere for a range of heat exchanger materials, configurations, and power loads. The optimizer uses a non-linear adaptive differential evolution optimization algorithm to find the optimal tube length, tube diameter, and fin pitch while a gradient descent method is used to find the optimal number of tube rows and columns. For a 100 kW stainless steel heat exchanger suitable for use with a supercritical CO_2 (sCO_2) closed Brayton cycle direct-cooled reactor, the optimal heat exchanger mass is found to be 27.0 kg with a frontal area of 3.94 m^2. This is 95% less mass and area than a comparable radiator and requires 638 W of fan power (or 0.6% of the output power) to operate. Optimal geometries are also found for heat rejection loads of 1 kW to 500 kW across a range of coolant and atmosphere temperatures, indicating wide applicability of this technology for Martian heat rejection applications such as cryofuel refrigeration, in-situ resource utilization (ISRU) plant cooling, or large-scale power generation.

I. INTRODUCTION

The development of a new compact and reliable power generation system will be required for future crewed Mars surface missions. Nuclear fission is an attractive power source for these missions, however waste heat rejection from the associated power block is a considerable challenge in space applications. Even the most efficient Brayton cycles only have thermal efficiencies approaching 40-50%; therefore, for a power system that is large enough to sustain a prolonged crewed mission, 10's to 100's of kWs of heat will need to be transferred to the environment to maintain steady operation[1]. Radiative heat rejection systems have a long flight heritage, however radiative heat transfer is relatively inefficient except at very high absolute temperature which leads to high heat rejection system mass and a relatively high mass-optimal cycle heat rejection temperature, reducing the cycle thermal efficiency. This effect is demonstrated by Sondelski[2], who modelled a mass-optimal Mars fission power cycle using a radiator for heat rejection and determined that the radiator accounted for the majority of the system mass. A Mars surface reactor may be able to avoid these issues by rejecting heat convectively to the atmosphere using a forced-convection heat exchanger. Convection offers much higher effective heat transfer coefficients than radiation and a weaker dependence on temperature allowing the power block to operate at lower heat rejection temperatures; this is particularly important for sCO_2 cycles that need to operate near the vapor dome. Convection heat transfer surfaces do not need to be exposed to the sky, allowing for a much more compact structure and eliminating the need for the complex deployment mechanisms required by a large radiator due to launch vehicle limitations. If a convective heat exchanger that transfers waste heat to the atmosphere without significant parasitic power loss and that is less massive than a similarly-performing radiator can be built, such a system would provide substantial mass, cost, and complexity savings to a future Mars surface mission. Such a system would also be useful for a wide range of other Martian heat rejection applications such as cryofuel refrigeration, in-site resource utilization (ISRU) plant cooling, or rover and habitat thermal regulation.

II. MODELING

The thin Martian atmosphere is a challenging heat transfer medium. The average surface pressure and temperature of 600 Pa and 220 K (Ref 3), respectively, result in a low-density environment which drastically reduces the forced convection heat transfer coefficient, requiring a high volumetric flow rate through the heat exchanger causing a relatively large pressure loss. The pressure rise that can be achieved using conventional fan technology also decreases at low air density, which further increases the difficulty of atmospheric heat rejection in this environment. Therefore, to determine if these conditions are suitable for convective waste heat

rejection, a numerical model of a plane-finned crossflow heat exchanger is developed using the effectiveness-NTU method. This heat exchanger architecture was chosen because it offers both low pressure loss and high conductance. When supplied with the desired rate of heat rejection, Q, sCO_2 mass flow rate, $\dot{m}_h$, and inlet temperature, $T_{h,in}$, ambient air temperature, $T_{c,in}$, heat exchanger material and tube pitch to diameter ratio, PD, and configuration, i.e. staggered or in-line, the model determines the minimum heat exchanger mass, the required fan power, and the geometry of the minimum-mass heat exchanger. All results presented in this work use a sCO_2 pressure of 9 MPa and an atmospheric pressure of 600 Pa. Figure 1 illustrates the staggered-tube heat exchanger geometry.

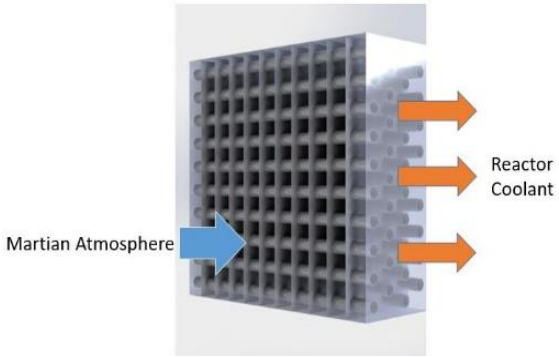

Fig. 1. Diagram of a finned-tube heat exchanger.

II.A Heat Exchanger Model

The heat exchanger model has five geometrical parameters that must be optimized. Three of these parameters, the tube length, L, tube diameter, D, and fin pitch, p_{fin}, are continuous while the number of tube rows, N_{rows}, and the number of tube columns, N_{cols}, are both integers. The maximum tube length and overall heat exchanger height are set at 4 m based on typical launch vehicle fairing size, the number of tube columns is limited to 10 to match the range of the pressure drop correlation used in the model, the minimum tube diameter is 0.5 mm as this is approximately the smallest size tubing found in commercially-available heat exchangers. The minimum tube length is 0.1 m and the minimum number of tube rows is 10; these limits were necessary to prevent erroneous edge cases. The fins are modelled as 0.1 mm thick copper sheets.

A flow diagram of the process to calculate the heat exchanger mass is shown in Figure 2. To determine the heat exchanger mass for a given geometry and thermal input parameters, first the thermal conductivity, density, and yield stress, σ_Y, of the tube material and the conductivity, density, and specific heat capacity of the sCO_2 and atmosphere are determined at the average temperature on the high-pressure and low-pressure side respectively from property tables. As the low-pressure outlet temperature is not initially known, atmospheric properties are initially found at the atmospheric inlet temperature. The tube wall thickness is then calculated according to Eq. (1):

$$t_{wall} = \frac{DP_h MOS}{2(\sigma_Y + P_h)}. \quad (1)$$

Where MOS, the margin of safety, is 1.25.

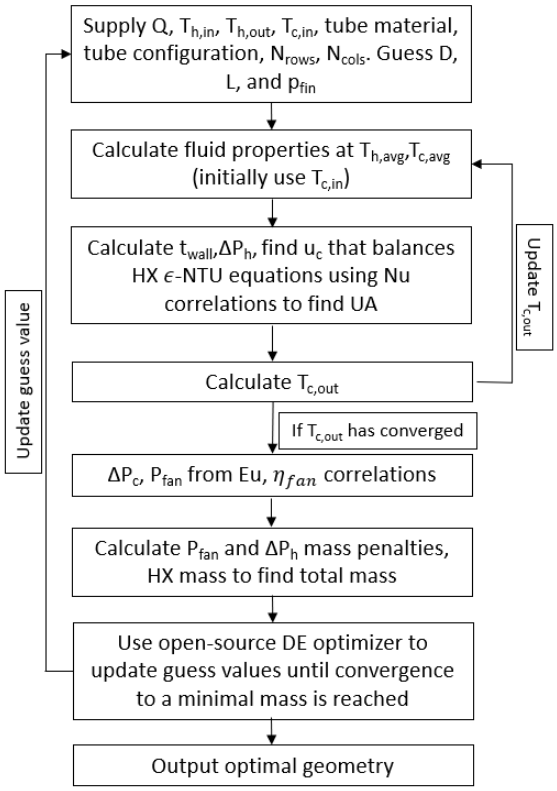

Fig. 2. Flow diagram of the continuous variable optimization.

The sCO_2 pressure drop is calculated using the Zigrang and Sylvester[4] correlation for turbulent flow and the correlation given in Nellis and Klein[5] for laminar flow in a smooth circular duct. The required

atmosphere velocity through the heat exchanger to produce the desired heat rejection rate is then determined using the effectiveness-NTU method as described in Nellis and Klein[5]. The heat exchanger conductance, UA, depends on the tube heat transfer coefficient, found by using the correlation provided by the Engineering Sciences Data Unit[6] for tube banks in low Reynolds number flows, and the fin heat transfer coefficient is given by the Shah and London[7] correlation for a rectangular duct.

The heat exchanger will be balanced when the following equality is satisfied:

$$Q = \epsilon \dot{C}_{min}(T_{h,in} - T_{c,in}) \quad (2)$$

Where Q is the total heat transfer rate. ϵ, the heat exchanger effectiveness is given in Table 8-1 of Nellis and Klein[5] and is a function of UA, and $\dot{C}_{min}$ is the minimum heat capacity rate of the heat exchanger. Both of these terms depend on the velocity so by finding the root of Eq. (2), the required atmosphere velocity can be determined. From this, the low-pressure outlet temperature can be determined. This procedure is repeated while updating the atmosphere thermal properties at the new average temperature until convergence is reached. From the velocity, the pressure drop is calculated using the Euler number correlations given in the *Heat Exchanger Design Handbook*[8] and the fan power is derived from the fan efficiency correlations described in Eppel et al.[9] for low-speed axial fans. The mass of the fan is then calculated based on the heat exchanger frontal area and a specific motor power of 5.75 kg/kW based on commercially-available electric motors. A mass penalty is also applied to account for the additional reactor mass required to supply the fan power and is derived from the Sondelski[2] Mars fission power cycle optimization model. A mass penalty based on the sCO_2 pressure loss is also derived from this model. Headers, modelled as tubes with a diameter equal to the total depth of the heat exchanger, are also included in the mass estimation. The total mass of the heat exchanger plus the associated mass penalties is then calculated to simplify the optimization to a single objective value.

II.B Geometry Optimization

The optimization is split into two processes. The inner process, shown in Figure 2, determines the values of the continuous geometrical parameters L, D, and p_{fin}, that result in the minimum heat exchanger mass for a given set of input thermal parameters and given values for the discrete geometrical parameters N_{rows} and N_{cols}. An open-source non-linear optimization package, BlackBoxOptim[10], is used. This optimizer uses an adaptive differential evolution approach which does not require that the function be differentiable. The mass model uses a number of correlations that are not smooth at Reynolds number regime boundaries and the effectiveness-NTU method implementation is nonlinear so this type of solver is required. The solver has been found to converge within 2500 iterations across the range of geometries and conditions investigated. Once the solver has determined the optimal mass for a given N_{rows} and N_{cols}, this value is passed to the outer process.

A flow diagram of the outer process, which determines the optimum values for N_{rows} and N_{cols}, is shown in Figure 3. The discrete solver to determine the optimal number of tube rows and tube columns uses the first order two-dimensional gradient descent method. When provided with a set of thermal parameters, tube material and configuration, the discrete solver guesses an initial pair of values for N_{rows} and N_{cols} and calls the continuous solver to determine the minimum mass heat exchanger using these values and neighboring values. Next the step size to the next test point is calculated for both parameters from the local partial gradients of the optimal mass using first-order finite differencing

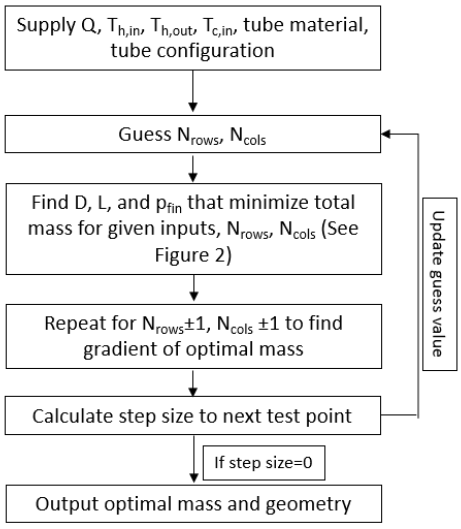

Fig. 3. Flow diagram of the discrete parameter solver.

. Once the step size for each parameter is determined, the test point is updated by incrementing by the step sizes while checking to ensure that this does not place the test point outside the search area. This process is repeated until the step size for both parameters is 0, at which point the optimal geometry and mass are reported. The optimal mass is convex across the whole search area so the gradient descent method is able to consistently find the global minimum regardless of the initial guess values.

III. RESULTS

III.A Optimal Geometries

Table 1 shows the optimal geometry and mass for steel staggered-tube heat exchangers of various sizes, with a pitch to diameter ratio of 2 and at an ambient temperature of 220 K and pressure of 600 Pa and coolant pressure of 9 MPa. The 1 kW and 10 kW low-temperature examples are relevant to applications such as cryofuel refrigeration, ISRU plant or rover cooling while the 100 kW and 500 kW high-temperature examples are relevant to reactor cooling. For all sets of inlet conditions studied, the optimal fin pitch equaled the tube length; this corresponds to removing all fins and using bare tubes. The increase in the heat transfer from the fins did not outweigh the associated mass and pressure drop increase at any fin density. This behavior is noticeably different than typical heat exchanger design in standard atmospheric conditions, stemming from the fins' lower heat transfer coefficient in the low-conductivity flow and the optimization for mass instead of volume. To confirm this observation, the optimal 400 kW heat exchanger geometry in 100 kPa CO_2 is determined while limiting the length and height to 0.4 m. The optimal geometry for this case is shown in the last column of Table 1; notice that the heat exchanger has a fin pitch of 0.245 mm corresponding to a typical finned-tube design.

Table 1: Optimal stainless steel heat exchanger geometry examples.

Parameter	Value				
Atmospheric Pressure [kPa]	0.6	0.6	0.6	0.6	100
Heat Load [kW]	1	10	100	500	400
Inlet Temp, [K]	400	400	625	625	625
Outlet Temp, [K]	350	350	525	525	525
Length, [mm]	102	479	1072	3977	400
Tubes/row	358	470	736	627	25
Tube Diam [mm]	1.215	1.733	2.478	3.190	7.124
Height, [mm]	870	1629	3648	4000	356
Depth, [mm]	4.9	10.4	14.9	31.9	128.2
Tube rows	2	3	3	5	9
Fin Pitch, [mm]	102	479	1072	3977	0.245
Fan Power, [W]	9.4	130.4	637.9	4695	4747
Optimal Mass, [kg]	0.493	5.258	27.0	226.5	100.8

III.B Effect of Heat Rejection Rate on Optimal Heat Exchanger Geometry

Figure 4 shows the dependence of the optimal mass on the rate of heat rejection from 1 kW to 180 kW using 316 Stainless Steel, 6061-T6 Aluminum, Copper, Inconel 740H, and R56400 Titanium tubes. The materials result in similar optimal heat exchanger masses for the range of heat rejection rates studied, although Aluminum resulted in the lowest overall mass. Across this range of heat rejection rates, optimal heat exchanger mass increases nearly linearly with heat rejection rate, indicating that this method of heat rejection is very scalable and suitable for a wide range of applications.

Figure 5 demonstrates how the geometry and low-pressure-side pressure drop of the optimal heat exchanger vary with heat rejection rate from 1 kW to 1 MW for a stainless steel heat exchanger at an inlet temperature of 625 K. The heat exchanger height reaches its maximum limit between 100 and 200 kW, so once the frontal area of the heat exchanger can no longer be increased, the air velocity and number of tube columns must increase to raise the heat transfer rate, leading to a higher pressure rise and fan power.

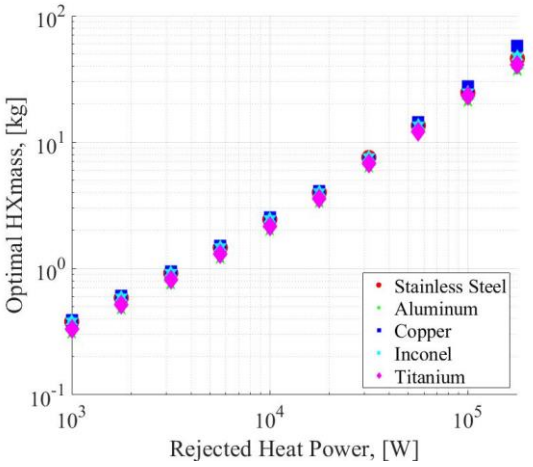

Fig. 4. Optimal heat exchanger mass vs heat rejection rate for a staggered tube HX, PD=2. The coolant is sCO_2 at an inlet temperature of 625 K and outlet temperature of 525 K.

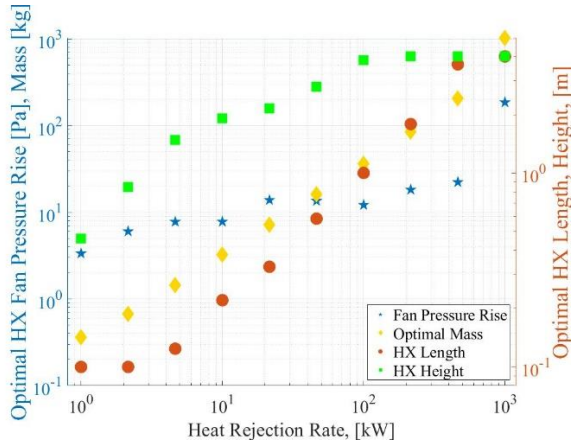

Fig. 2. Optimized geometry parameters vs heat rejection rate for a stainless steel heat exchanger.

Above 600 kW, the fan motor mass accounts for the majority of the system mass. Pressure rises above 25 Pa may be difficult to obtain in the Martian environment so a heat rejection of higher than 500 kW may require multiple heat exchangers.

3 different tube pitch to diameter ratio values were investigated for both staggered and in-line tube arrangements. These configurations were selected due to the existence of existing heat transfer and pressure loss correlations. Figure 6 shows the trend of optimal mass with rejected heat power for these 6 configurations. In all cases, the staggered, PD=2 arrangement provided the lowest mass. Even though the in-line arrangement provides lower pressure loss as a given Reynolds number, the decreased conductance requires a higher flow rate, negating the benefit of the more streamlined geometry.

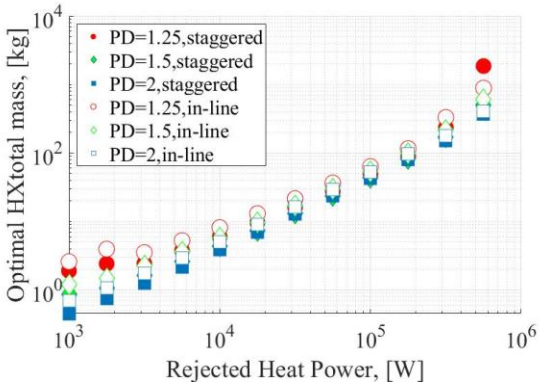

Fig. 7. Optimal heat exchanger mass vs rejected heat power for various tube configurations. Coolant inlet temperature is 625 K.

III.C Effect of Coolant Inlet Temperature on Optimal Mass

Figure 7 demonstrates the dependence of the optimal mass on the high-pressure inlet temperature. For low inlet temperatures, Aluminum heat exchangers have the smallest mass. However, at higher temperatures its yield strength decreases and the tube walls become thicker, increasing the mass.

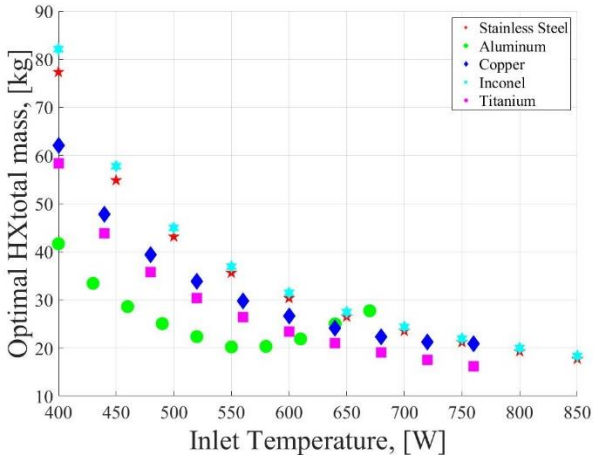

Fig. 7. Optimal 100 kW heat exchanger mass vs high-pressure inlet temperature. The high-pressure temperature change in the heat exchanger is 100 K for all cases.

Above 625 K, Titanium becomes the lowest-mass option. However it likely based on the Sondelski[2]

model results that heat rejection temperatures for a mass-optimal fission power system will be between 400-500K to increase efficiency so Aluminum may be the preferred heat exchanger material for this application.

III.D Effect of Ambient Temperature on Optimal Mass

The low-pressure inlet temperature was varied from 220 K to 310 K, which corresponds to approximately the highest daytime temperatures observed near the Martian equator[3], in order to ascertain the effect of local air temperature of heat exchanger performance. As shown in Figure 8, optimal mass increased approximately 19% over this range, but even at the highest temperatures the heat exchanger still drastically outperforms a radiator.

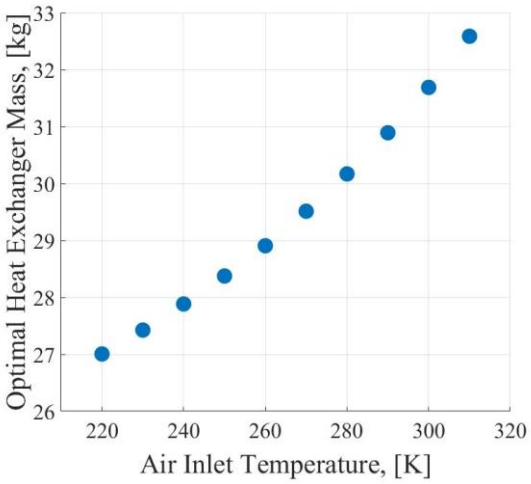

Fig. 8. Optimized heat exchanger mass vs atmospheric temperature for a stainless steel 100 kW heat exchanger with a coolant inlet temperature of 625 K and a temperature drop of 100 K.

IV. CONCLUSION

Overall, the predicted heat exchanger performance across all conditions and applications compares extremely favorably in Martian conditions to current radiator-based heat rejection systems and suggests that this technology could be beneficial to any future Mars missions. Heat exchangers up to 500 kW are compact enough to deploy to the Martian surface using current launch vehicles without requiring in-situ deployment mechanisms. In all cases under Mars conditions the optimal heat exchanger geometry contained no fins. At low coolant temperatures aluminum tubing led to the lowest optimal mass but at higher temperatures titanium and stainless steel produced lower masses.

V. FUTURE WORK

Experimental validation of these results is planned for the near future. A vacuum chamber will be filled to typical Martian conditions and a heat exchanger of similar design to the optimal geometry described above will be operated inside it to measure the heat exchanger conductance, pressure drop, and fan efficiency. Additionally, this model will be integrated with the Sondelski[2] model to determine how to use of a convective waste heat rejection system effects the overall cycle design of a Mars fission power system.

REFERENCES

1. NASA-SP-2009-566, Human Exploration of Mars Design Reference Architecture (DRA) 5.0, National Aeronautics and Space Administration, Washington, D.C. (2009).
2. B. SONDELSKI, Mass Optimization of a Supercritical CO_2 Brayton Cycle with a Direct Cooled Nuclear Reactor for Space Surface Power. Master's Thesis, University of Wisconsin, Madison, (2019)
3. R. M. HABERLE, "Solar System/Sun, Atmospheres, Evolution of Atmospheres Planetary Atmospheres: Mars", *Encyclopedia of Atmospheric Sciences*, 2015
4. D. J. ZIGRANG and N. D. SYLVESTER, "Explicit Approximations to the Solution of Colebrook's Friction Factor Equation," *AIChE Journal*, **28,** 514 (1982)
5. G. NELLIS and S. A. KLEIN, *Heat Transfer*, Cambridge University Press, New York, NY (2009)
6. Engineering Sciences Data Unit, *Convective Heat Transfer During Crossflow of Fluids Over Plain Tube Banks*, ESDU Data Item No. 7303J, London, November (1973)
7. R.K SHAH and A.L. LONDON, *Laminar Flow Forced Convection in Ducts*, pp. 196-222Academic Press, (1978)
8. Heat Exchanger Design Handbook Vol. 1, Hemisphere, New York, (1983)
9. P.H. EPPEL, F. DURST, and A. DELGADO, "A Theoretical Derivation of the Cordier Diagram for

Turbomachines", *Proc. IMechE* Vol. 225, p. 1-15, (2010)
10. R. FELDT. BlackBoxOptim.jl, (2019), Github Repository, https://github.com/robertfeldt/BlackBoxOptim.jl

Nuclear and Emerging Technologies for Space
Sponsored by Oak Ridge National Laboratory, April 26th-30th, 2021.
Available online at https://nets2021.ornl.gov

DESIGN AND MODELING OF A CENTRIFUGAL NUCLEAR THERMAL ROCKET

Bryce Cornell,[1,2] Ethan Fisher,[1,3] C. Miller McSwain,[1,4] Michael G. Houts,[1] Darrin Leer,[1,5] and Mark Patterson[6]

[1]*NASA Marshall Space Flight Center, MSFC, AL 35812*
[2]*Auburn University, Auburn, AL 36849*
[3]*Mississippi State University, Mississippi State, MS 39762*
[4]*University of Tennessee, 1412 Circle Drive, Knoxville, TN 37996*
[5]*University of North Carolina – Charlotte, 9201 University City Blvd, Charlotte, NC 28223*
[6]*Southern Research, Birmingham, AL, 35255*

Primary Author Contact Information: (901) 573-9481 and btc0027@auburn.edu

A computational fluid dynamic model of the Centrifugal Nuclear Thermal Rocket propulsion system is necessary prior to physical experimentation and development. In this paper, a simulation of a rotating centrifugal fuel element is discussed and evaluated. The model was developed and simulated using ANSYS Fluent and will help lay the foundation for future modeling of the system. This task was one of the first needed to kickstart progress towards the optimization of the Centrifugal Nuclear Thermal Rocket.

I. INTRODUCTION

The Centrifugal Nuclear Thermal Rocket (CNTR) is a high performance nuclear thermal propulsion (NTP) system designed to support advanced space exploration missions including a 420-day round-trip human Mars mission. NTP systems use the heat produced by nuclear fission to excite propellant which expands through a nozzle to create thrust. The first conceptual study of liquid-core high performance NTP was conducted by McCarthy and published in 1954.[1] He proposed that a single cylinder with molten fissionable material be used.[1] Ten years after McCarthy's publication, Nelson modified McCarthy's conceptual design to include 19 cylinders of molten fissionable material.[2] This new design had a predicted specific impulse (I_{sp}) of 1200 s.[2] The CNTR is designed to provide a high I_{sp} of up to 1800 s with hydrogen propellant and up to 1000 s with passively storable propellant such as CH_4 or NH_3. The CNTR is quite advantageous as it allows the use of molten fuels that can operate at much higher temperatures than solid fuels thereby generating a higher specific impulse. Additionally, the CNTR's propellant flexibility expands its mission capabilities and could be essential in supporting crewed missions to Mars.

II. BENEFITS OF THE CNTR

The CNTR offers many benefits and advantages when compared to other NTP and non-nuclear propulsion systems. To begin, as mentioned above, the CNTR will have an I_{sp} upwards of 1800 s compared to first generation NTP systems which boasted I_{sp} values of just 900 s; this difference in thrust capability enables a 14-month round-trip to Mars compared to the 24-month trip promised with traditional, first-generation NTP systems.[4] The CNTR also supports a variety of propellants which sets it apart from many other propulsion systems which lack propellant flexibility. Additionally, the CNTR is designed to operate such that the structural materials operate at temperatures under 1000 K to avoid any complications that could be associated with extreme temperatures. The CNTR also promises excellent heat transfer between the fuel and propellant as the propellant passes directly through the liquid fuel layer in each element. Finally, as each fuel element is independently rotated, experiments to test the system's viability should be relatively straightforward. This will reduce the Advancement Degree of Difficulty (AD^2) and accelerate the CNTR's development.

III. CNTR DESIGN

The design of the CNTR features a liquid-core similar to that of the NTP system proposed by McCarthy over 60 years ago.[1] The CNTR contains a matrix of rotating centrifugal fuel elements (CFEs) as well as moderator blocks and a radial reflector to stabilize the neutronics of the CNTR. Figure 1 depicts a 19 CFE matrix but configurations with differing numbers of elements are also being considered.

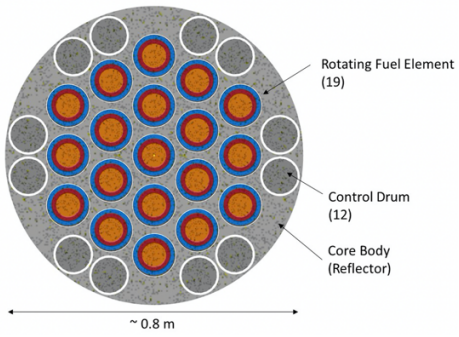

Fig. 1. Matrix configuration of 19 CFEs.

Each CFE features a molten uranium fuel source and a porous inner wall. The porous wall allows the propellant to flow radially inward through the uranium since the centrifugal forces created by the rotation of the centrifuge hold the uranium against the walls.

The heat transferred to the propellant as it flows radially through the molten uranium layer causes the propellant to expand axially through the nozzle. However, the use of the propellant is three-fold; along with being excited to create thrust, the propellant is used to cool various components of the system and power the rotation of the centrifuge prior to its contact with the molten uranium. The propellant flow path through a CFE is depicted in Figure 2.

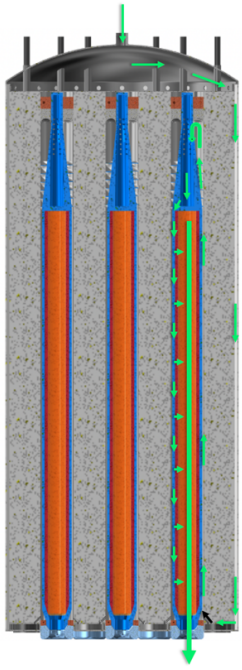

Fig. 2. CNTR propellant flow path from inlet to nozzle.

The propellant enters the system at the top inlet before flowing around, and thus cooling, various external components of the system such as the moderator blocks, radial reflectors, and core drums to an ideal temperature below 800 K. The propellant then enters the gas inlet manifold, permeates the moderator block below the centrifuges, and travels upward along the CFEs cooling the nozzles. Once it reaches the top of the centrifuges, it passes through the turbines which rotate the centrifuges before being redirected back down between the centrifuge outer wall and the porous silicon carbide inner wall. The propellant then passes through the porous wall into the molten uranium where it is heated to a target temperature of over 5000 K before entering the center cavity created by the centrifuge rotation. Finally, the propellant is expelled out of the nozzle to create thrust.

III.A. CFE Design and Temperature Profile

Each CFE within the CNTR is made up of 6 “layers”: the outer wall, the cooling passage, the porous SiC layer, the ZrC coating layer, the molten uranium, and the central cavity. These regions and their expected temperatures are depicted in Figure 3.

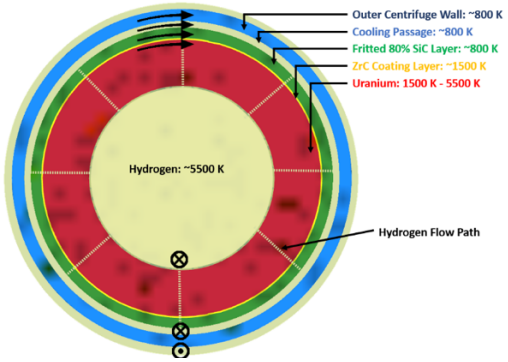

Fig. 3. Cross section of CFE with labeled layers.

It is within the molten uranium layer that the propellant is heated before entering the central cavity and being ejected out the nozzle to create thrust. By heating the propellant, it becomes excited and its velocity increases as explained by equation (1). This is essential as thrust is related to exit velocity by equation (2).

$$V_e = M_e\sqrt{\gamma R T_e} \tag{1}$$

$$F = \dot{m}V_e + (p_e - p_o)A_e \tag{2}$$

where V_e, M_e, γ, R, T_e, F, $\dot{m}$, p_e, p_o, and A_e are exit velocity, exit Mach, specific heat ratio, gas constant, exit temperature, thrust, mass flow rate, exit pressure, free stream pressure, and exit area, respectively.

The layers adjacent to the cooling passage will be kept around 800 K while the molten uranium and propellant in the central cavity are predicted to reach temperatures upward of 5500 K. This is thanks to the liquid core of the CFE which allows the total heat transferred to the propellant to be much greater than that of a solid core system. Although 5500 K is above the boiling point of uranium, the pressure in the system will exceed the vapor pressure of the molten uranium which will reduce vaporization and promote the condensation of the uranium.

III.B. Uranium Entrainment in the CNTR

While the conditions within the CFEs should prevent molten uranium leakage and promote entrainment, uranium leakage is still a primary concern. To prevent leakage, each fuel element is contained within a rotating centrifuge hence the nomenclature, CFE. The CFE rotates at a constant angular velocity forming a molten uranium vortex. The nature of the vortex pushes the molten uranium against the walls of the centrifuge which provides the propellant with a central cavity that leads to the nozzle for expulsion. However, given the nature of the fluid dynamics of the gaseous propellant flowing radially inward through the liquid fuel layer, it is possible for some liquid uranium droplets or gaseous vapors to become entrained in the propellant flow. Along with the centrifugal rotation, the end of the CFE will be tapered to reduce uranium leakage as shown in Figure 4. The tapered region will be kept at a lower temperature to promote condensation of the uranium vapor. The condensed uranium will then be pushed back into the fuel layer by the centrifugal forces.

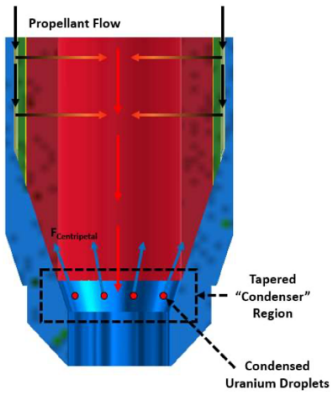

Fig. 4. Condenser region of a CFE in the CNTR.

Reducing entrainment to an acceptable level will be a challenge due to the complexity associated with the fluid dynamics of the propellant and liquid uranium as well as the limited knowledge of material properties at the system's extremely high temperatures. However, the goal is to address these complexities by conducting several experiments to gain a better understanding of the complex propellant-uranium interface.

IV. MODELING CFE ROTATION

To begin the extensive process of designing the CNTR and its intricacies, one of the first tasks will be to accurately model the molten uranium surface profiles in a rotating CFE. As the angular velocity is increased, the centrifugal forces will increase as well. Since the CNTR will be utilized in both gravitational and non-gravitational environments, it is important to note that, in environments with gravity, the hydrostatic pressure combined with the centrifugal forces will yield a parabolic surface profile. In environments without gravity, on the other hand, there will be no hydrostatic pressures to account for so the surface profile will be uniform along the length of the centrifuge. However, as the CNTR is designed to generate thrust in a rocket, it can be assumed that the thrust generated will create a less substantial, artificial gravity; this artificial gravity will generate some hydrostatic pressure which will need to be accounted for.

This first task will yield data on surface profiles and initiate the creation of a complete CFD model of the system. Using water as the operating liquid will simplify the model and allow for easier modification prior to application in a system that more accurately reflects the uranium-propellant system. If surface profiles can be accurately predicted using this model, it could be used to study and optimize entrainment in the system as well as the startup and shutdown processes in the future.

To begin, the parabolic surface profile was predicted using the forced vortex equation, equation (3).

$$z - z_0 = \frac{\omega^2 r^2}{2g} \tag{3}$$

where z, z_0, ω, r, and g are the height of the fluid, the lowest point of the vortex, the angular velocity, the radius, and the gravitational acceleration, respectively. Figure 5 depicts an example case of the system with an angular velocity of 50 rad/s, a radius of 10 cm, and a gravitational acceleration of 9.81 m/s^2. Using equation (3), the fluid vortex had a predicted height of 31.8 cm. Fisher used ANSYS Fluent to construct a CFD model using a coupled k-ω Shear Stress Transport turbulence equation paired with a volume of fluids setup that accurately simulates a fluid vortex.[5] After tweaking the model to obtain a solution more efficiently, it predicted the height of the fluid vortex to be 27.25 cm when rotated at 50 rad/s, as shown in Figure 6. This model predicted the vortex height with a percent error of 14% which is adequate for the preliminary purposes of the model.

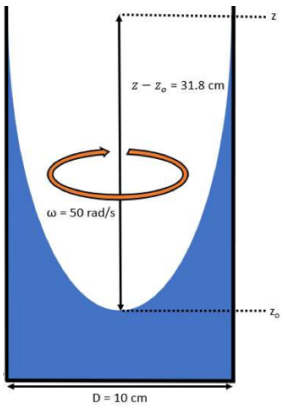

Fig. 5. Diagram of Fisher's fluid vortex model.[5]

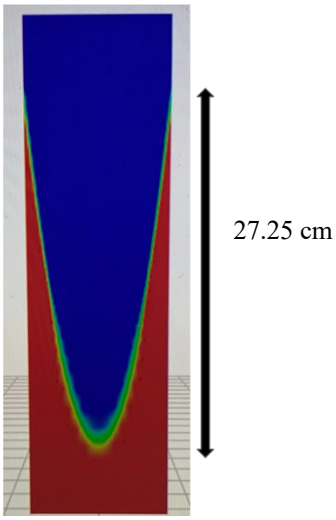

Fig. 6. Result of fluid vortex simulation when run at 50 rad/s.

After adjusting simulation settings, adapting the geometries, and optimizing the mesh, a model was developed for a CFE rotating at 500 rad/s, or about 32% of the expected angular velocity of 1580 rad/s. This model was also run in a gravitational environment with a gravitational acceleration of 9.81 m/s^2. Figure 7 shows the uniform fluid distribution along the height of the CFE forming a constant width central cavity for propellant expulsion.

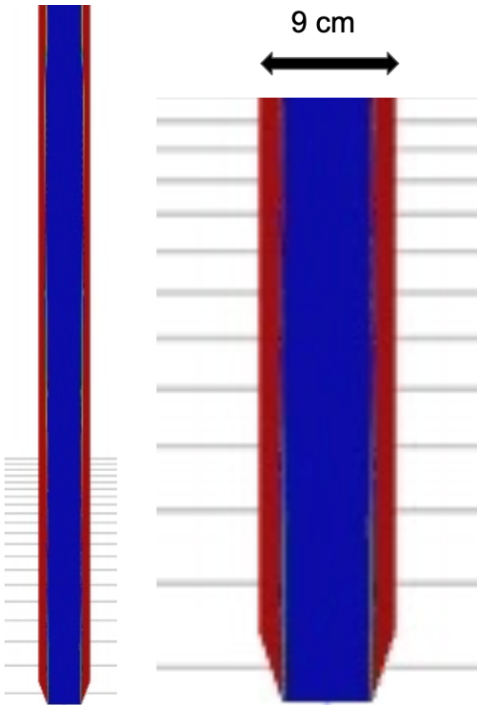

Fig. 7. Result of rotating CFE simulation when run at 500 rad/s.

This is due to the increasing centrifugal forces associated with the higher angular velocity. Although this model only represents 32% of the expected angular velocity, the parabolic surface profile is not expected to change much with the full 1580 rad/s as it has already reached uniformity.

V. CONCLUSION

Although this model has started to help prove the efficacy of the CNTR, there are still many design challenges that must be addressed; some of the most critical include examining the propellant-uranium interface behaviors, studying the effects that the unfamiliar extreme temperatures will have on the neutronics of the system, and mocking up a physical proof of concept. Future experiments will be conducted to help overcome these challenges and make the CNTR a realizable tool for advanced space exploration missions. As discussed throughout this paper, accurately modeling the rotating CFEs will be critical in the development of the CNTR as a whole. As more experiments are performed, a better understanding of the system will be achieved and even more accurate models can be generated. These efforts will accelerate the CNTR's development and enable its use in future advanced space exploration missions.

ACKNOWLEDGEMENTS

This work was supported by Universities Space Research Association, NASA Marshall Space Flight Center, and Argonne National Laboratory.

REFERENCES

1. J. McCarthy, "Nuclear Reactors for Rockets," *American Rocket Society*, Vol. 24, p. 36–37 (1954).
2. S. T. Nelson and J. Grey, "Conceptual Study of a Liquid-Core Nuclear Rocket," Tech. Rep. 665, Princeton University (1964).
3. M. Patterson, M. Johns, J.Allen, M.Houts, F.Heidet and. N.Smith, "Concept Design and Considerations for Advanced Nuclear Thermal Propulsion", American Nuclear Society; Winter Meeting (2020).
4. M. Houts, C. Joyner, J. Abrams, J. Witter, P. Venerri, "Versatile Nuclear Thermal Propulsion", *70th International Astronautical Congress* (2019).
5. E. Fisher, "CNTR: Explanation of Propellant Flow and Description of Initial Experiments," *American Nuclear Society* (2020).

Nuclear and Emerging Technologies for Space
Sponsored by Oak Ridge National Laboratory, April 26th-30th, 2021.
Available online at https://nets2021.ornl.gov

PYLON: SCALABLE POWER FOR THE EMERGING SPACE ECONOMY

Wesley Deason[1], Ethan Chaleff[1]

[1]*USNC-Tech, 2356 W. Commodore Way Seattle, WA 98199*

Primary Author Contact Information: 206-889-8177; w.deason@usnc-tech.com

USNC-Tech's Pylon space reactor architecture enables a safe and scalable approach to implement nuclear power in space. Pylon leverages USNC's proprietary nuclear fuel technology, FCM™, to achieve high performance at any power level, from 10's of kilowatts to multi-megawatts. When coupled with a gas-cooled Brayton cycle and solid neutron moderators, no configuration changes are required from initial demonstration to full commercial application.

I. INTRODUCTION

Can the same reactor architecture that is used to demonstrate the viability of lunar fission surface power also be used to support the higher power levels of established human lunar outposts? We believe it must be. If not, the risk is high that insufficient technology heritage will be available to provide greater power in the future when it is demanded.

In 2019, we published our first paper on the Pylon space reactor[1]. The design presented in that publication targeted a power level of 150 kWe and demonstrated the high-power capabilities of USNC's FCM™ fuel technology. This power level was selected based on our analysis and market survey of the minimum amount of power needed to establish a sustainable human presence on the lunar surface. While near-term priorities focus on demonstration reactors at 1-10 kWe levels, these power levels will be inadequate to service any reasonable sustained human presence.

Unfortunately, the uses of high-power space reactors differ markedly from those needed at an initial lunar outpost. High-power space reactors will need to energize rovers, process regolith for raw materials, power less austere human habitats, and provide a significant reserve power margin. Low-power space reactors will provide only life-support and science experimentation.

Both the low power and high power concepts are heavily mass constrained. For example, higher power reactors deployed after some infrastructure is established can plausibly take advantage of lunar regolith for shielding. An early demonstration reactor would likely not.

The current pathway to support and develop lunar fission surface power aims at selecting architectures optimized between 10 and 40 kWe to demonstrate the viability and practicality of building and launching a lunar power reactor. This optimization will tend to select technology architectures (such as fuel, moderator, and power conversion designs) that are not necessarily amenable to higher power levels.

I.A. Power Needs for an Early Lunar Outpost and Research Station

Initial or temporary lunar research outposts will not be particularly power intensive. Studies indicate that power needs for early-stage lunar outposts may be around 10 kWe up to 40 kWe depending on activities[2,3]. However, as these habitats become more established, power demand will increase significantly. The most power-intensive activities are those related to the demonstration of in-situ resource utilization (ISRU). Lunar ISRU is the use of locally available sources of water, oxygen, and other minerals, rather than obtaining these materials through shipment from Earth. ISRU's power intensity is due to the processing required to separate these minerals from lunar regolith – a hint towards what could drive a commodity-driven market for power on the moon and space.

While initial lunar outposts will sustain themselves through shipment of supplies from the earth, any sizable human research presence on the moon will require supplementation through ISRU. By analogy, the ISS has an average power capacity between 80 and 240 kWe (ref. 4) and receives regular supply shipments from earth, supporting fewer than 10 astronauts[5]. Notably, these astronauts are always within one hour of a gravity-assisted return to earth.

I.B. Leveraging Early Lunar Opportunities into Commercial Space Nuclear Power

Very recently, the US government, including NASA and DOE, have announced that they are interested in private entities proposing commercial solutions for powering a lunar outpost for the Artemis program[6]. As expected, the draft request for proposals (RFP) lays out the need for 10 kWe with a total system mass of less than 3500 kg. Other system requirements for the desired system are less well-defined. This presents an excellent opportunity for companies with a commercial interest in space nuclear power to propose a scalable architecture. By fulfilling its role as a market catalyst, the government is giving companies pursuing scalable space nuclear architectures a chance to prove their technologies. Companies that do this

will have a leg up over companies that pursue non-scalable architectures.

II. SELECTING A SCALABLE SPACE NUCLEAR ARCHITECTURE

Several different high uranium density fuel types can be coupled to many different high-temperature power cycles using several different heat transport methods. Choosing the different combinations can yield very different results.

This section describes the high-level architecture choices selected to produce a reasonable mass and degree of technology confidence for demonstration levels, while enabling significant performance benefits at greater than 150 kWe levels.

II.A. Architecture Summary

The Pylon architecture uses a SiC-matrix FCM™ fuel, ZrH moderator, a helium-xenon recuperated Brayton power conversion system. We believe that these technologies represent the best balance of near-term demonstration with improved scaling to higher power levels and are discussed in more detail below.

II.B. Fuel

USNC's FCM™ (fully ceramic micro-encapsulated) fuel technology was a clear choice for Pylon. FCM™ is a particle-based fuel form where self-contained nuclear fuel particles such as TRISOs or BISOs are encapsulated in a fully ceramic matrix. There are multiple options for ceramic matrix material based on temperature limits, but for applications less than 2000 K, and especially with HALEU, SiC is the preferred matrix. An assembly schematic for the Pylon fuel element is shown below in Figure 1.

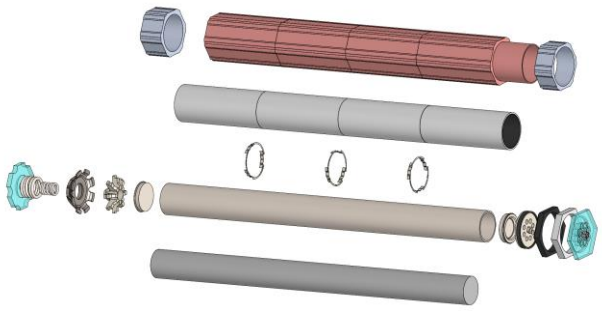

Fig 1. Pylon fuel and moderator assembly.

In addition to already being implemented in the MMR™, USNC's terrestrial nuclear power plant design, the high-temperature capability, and fuel loading flexibility make it ideal to be used in a scalable space reactor architecture. The low neutron absorption matrix also allows for a mass optimized system with HALEU (or even LEU for heavier, but higher power systems) compared to other high-temperature capable fuels, like W/Mo CerMets and TaC-containing CerCers.

For low power implementations of Pylon, we can take advantage of high fuel loading fractions and low fission product inventories to produce a compact nuclear reactor core. For high power implementations, fuel loading can be decreased and take advantage of the higher thermal conductivity matrix and better management of fission product volatiles.

The traceability to terrestrial system improves licensing and testing capability while leveraging commercial manufacturing facilities and irradiation campaigns. Ground testing is a critical concern for a complex spaceflight power system; ground safety and licensing benefits of mechanistic dose models associated with TRISO particles encapsulated in a dense SiC matrix may significantly decrease the cost of demonstration and testing facilities.

II.C. Moderator

There are significant debates and a wide range of options on moderator materials for FSP systems. USNC-Tech believes that a Zirconium Hydride approach is both warranted and technologically feasible for fission surface power systems under the given constraints and performance objectives. ZrH improves the system performance relative to other moderators and unmoderated cores. We are encouraged by recent strides at ORNL on the formation and canning of ZrH in C26M2 alloy with thermally grown oxides[7]. Additionally, USNC-Tech is actively investing in efforts to improve the TRL and performance of these systems.

II.D. Power Conversion and Heat Transport System

The heat transfer method used in a space nuclear power system can significantly affect its capabilities and performance. Three systems are viable for surface power: liquid metal coolant, heat pipes, or gas coolant. At lower powers, heat pipes are an attractive option due to their fully passive operation and high specific power. When coupled to low power conversion systems like sterling generators, they significantly reduce the mass, complexity and operation of the power conversion system. They do come with a neutronic penalty, especially in thermal spectrum and low enrichment fuels.

Liquid metal coolants, particularly when implemented within a liquid metal Rankine power conversion system, are good options for transporting and converting heat into electricity in space reactors. The constant temperature condensing portion of the Rankine cycle allows for a higher temperature radiative surface, which reduces the necessary size of the waste heat radiators. Additionally, power scaling is excellent and neutronic impact is minimal with liquid metal coolants. Unfortunately, temperature scaling is difficult to achieve without redevelopment,

requiring evolution from potassium to sodium, then lithium for the highest temperature applications.

When coupled to a Brayton power conversion system, gas coolants allow for flexible power arrangements and reactor system geometries. Gas coolants also have a minimal neutronic impact on the reactor (though not negligible) and are easily scaled within the same architecture to higher power levels. One way use of gas coolant can affect core neutronics is the need for increased coolant flow area fractions. Compression losses are significant compared to liquids and too high pressure drops can reduce cycle efficiency significantly. Gas also reduces corrosion issues and is not sensitive to changes in power levels or temperatures.

There are certainly challenges associated with Brayton power conversion, especially at lower power levels. While there are technology analogs to various terrestrial and aerospace applications, it cannot be denied that the TRL of Brayton electric systems in nuclear space applications is low. However, Brayton systems present the best balance of technology maturity and scalability. One of the major issues with Brayton cycles is operating with the small turbine and compressor wheel diameters for optimized systems at the sub 10 kWe level. Brayton technology has advanced significantly over demonstration systems like the NASA BRU[8]. Brayton can operate at different temperatures more easily than liquid metal Rankine or Sterling cycles, accommodating variable power operation and different use cases.

III. CONCLUSIONS

Fission Surface Power systems will be required to enable long-duration stable human presence on the lunar surface. However, to do that will require overcoming the temptation to pursue only the simplest and most proven technologies. Although the deployment costs are high, USNC-Tech believes that cultivating a slightly more aggressive technological vision will enable the actual use, rather than the mere demonstration, of fission surface technology on the lunar surface.

REFERENCES

1. M. EADES et al., “THE PYLON: COMMERCIAL LEU NUCLEAR FISSION POWER FOR LUNAR, MARTIAN, AND DEEP SPACE APPLICATIONS,” Proceeding of NETS 2019, Richland, WA, Feb 2019, American Nuclear Society (2019)
2. R. L. CATALDO et al., “Power Requirements for the First Lunar Outpost (FLO),” NASA Technical Memorandum 105925, Proceedings of the Tenth Symposium on Space Nuclear Power and Propulsion, Albuquerque, NM, January 1993, University of New Mexico (1993)
3. Z. KHAN et al., “Power System Concepts for the Lunar Outpost: A Review of the Power Generation, Energy Storage, Power Management and Distribution (PMAD) System Requirements and Potential Technologies for Development of the Lunar Outpost,” NASA/TM—2006-214248; DOE/NV/11718–1118, National Aeronautics and Space Administration (2006)
4. NASA, “About the Space Station Solar Arrays,” Webpage, last updated Aug 3, 2017, retrieved Feb 19, 2021, Available: https://www.nasa.gov/mission_pages/station/structure/elements/solar_arrays-about.html
5. E. HOWELL, “International Space Station: Facts, History & Tracking,” Web Article, Published Feb 8, 2018, retrieved Feb 19, 2021, Available: https://www.space.com/16748-international-space-station.html
6. DOE, “Fission Surface Power Project: Draft RFP,” Available https://beta.sam.gov/opp/24744267c3794298bd7ffce0db947b62/view
7. Y. YAMAMOTO et al., “Report on Exploration of New FeCrAl Heat Variants with Improved Properties,” ORNL/TM-2019/1290, August 2019, Oak Ridge National Laboratory, Available https://info.ornl.gov/sites/publications/Files/Pub130413.pdf
8. L. MASON et al., “Status of Brayton Cycle Power Conversion Development at NASA GRC,” NASA/TM—2002-211304, January 2002, Glenn Research Center, Available https://ntrs.nasa.gov/api/citations/20020038204/downloads/20020038204.pdf

Nuclear and Emerging Technologies for Space
Sponsored by Oak Ridge National Laboratory, April 26th-30th, 2021.
Available online at https://nets2021.ornl.gov

DESIGN OF A LOW ENRICHMENT URANIUM NUCLEAR REACTOR TO POWER A FUTURE MARTIAN COLONY – NEUTRONIC ASPECTS

Joffrey Dorville, Jacob Tellez, Conner Glatt, and Jeffrey King

Colorado School of Mines, 1500 Illinois St, Golden, CO 80401

joffreydorville@mines.edu, jtellez@mines.edu, cglatt@mines.edu, kingjc@mines.edu

Moderator, fuel, and core geometry configuration options are reviewed for the preliminary design of a low enrichment uranium megawatt-class nuclear reactor intended to provide 2 MW_e to a colony established on the surface of Mars. The initial calculations suggest that using a cylindrical fuel block and yttrium hydride as moderator could be beneficial to achieve desired neutronic performance and reduce the mass of the system. The cylindrical design using yttrium hydride, dimensioned from this analysis, has a total diameter of 90 cm and a total height of 126.4 cm for the core and the reflector. The total mass of the core with the reflector is 2,900 kg. The control drum worth, the shutdown margin, and the excess reactivity, calculated for cold clean conditions with MCNP6.2, are \$15.0 ± \$0.5, \$9.94 ± \$0.33, and \$5.10 ± \$0.15, respectively.

I. INTRODUCTION

The renewed and internationally shared interest in establishing human colonies on Mars and the Moon leads to the important question of how to power these installations. Nuclear reactors have been used since the Space Nuclear Auxiliary Power (SNAP) program to provide reliable sources of electricity for space applications; and, surface solutions like the Kilopower project appear promising.[1,2] Most of these designs include High Enrichment Uranium (HEU, uranium containing > 20% uranium-235) as fuel to take advantage of the high power density and reduced mass possible with HEU fuel.

However, the recent Presidential Space Policy Directive 6, signed on December 16, 2020, mandates that any sponsoring agency which develops space nuclear power and propulsion systems demonstrate that they reviewed all Low Enrichment Uranium (LEU, uranium containing < 20% uranium-235) fuel options.[3] In this context, the Colorado School of Mines is studying a Fission Surface Power system to provide electricity to an advanced Martian colony based on LEU fuel options, as part of the 2020-2021 reactor design class.

The Megawatt Implementation of a NuclEar ReActor using Low enrichment uranium (MINERAL) will deliver 2 MW_e of steady state electric power with a minimum lifetime of 10 years. The reactor will use available technologies and materials to reduce the risks associated with the development phase. To decrease the amount of supplies sent from the Earth, MINERAL will, as much as possible, take advantage of available resources on Mars. With well-known technologies and in-situ resource utilization, the MINERAL concept aims at being safe, reliable, easily developed, and resilient once deployed in its final location. The main challenge of this concept is the mass optimization, as LEU fueled reactors are typically larger than their HEU fueled counterparts for the same power output.

Adding moderating material to an LEU reactor is an effective technique to reduce the overall mass of the system. However, the integration of a moderator can be challenging due to the impact on the reactor lifetime and the thermal limits associated with the moderating materials.[4] Zirconium hydride (ZrH) was studied as a moderator directly incorporated in a uranium zirconium hydride (U-ZrH) fuel in the SNAP program and is still used in TRIGA reactors today.[5] Despite its good moderating quality, hydrogen density, and high thermal conductivity, U-ZrH fuel is constrained by its hydrogen dissociation temperature (~900K).[5] Yttrium hydride (YH) is a potential high-temperature alternative currently under development with a limiting dissociation temperature of 1173K.[6,7] A higher temperature results in an improved efficiency for the power conversion unit; but, a tradeoff exists in terms of core efficiency due to the reduced moderating ratio of YH compared to ZrH.

II. MINERAL REACTOR CONCEPT

The MINERAL reactor produces energy from a direct Brayton cycle loop using pure carbon dioxide as the working fluid. The composition of the Martian atmosphere includes significant concentrations of CO_2 which can be processed directly on Mars to provide the reactor's coolant. A potential advantage of using a coolant which is abundant in the atmosphere is the opportunity to compensate for small coolant losses during operation with a dedicated purification and makeup system.

Figure 1 represents a conceptual view of a deployed MINERAL unit on the Martian surface. The reactor is partially buried in the Martian regolith to provide shielding for the ionizing radiation emitted by the core during operation. This configuration reduces the size and mass of the shield for the same dose requirements,

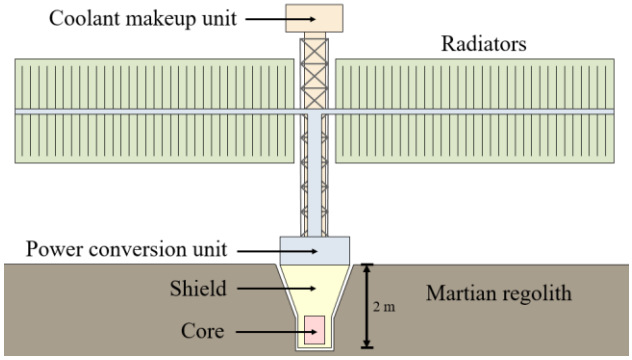

Fig. 1. Axial cross section of the MINERAL system (not to scale).

compared to a reactor placed directly on the surface.[8] The buried reactor could potentially be placed closer to the colony compared to the on-surface configuration and thus reduce the mass of power cables needed.[9]

The excess heat from the power conversion system is removed by a secondary closed loop connected to the primary Brayton cycle loop through a heat exchanger.[10] The energy transfer between the secondary loop and the environment is accomplished by several radiator panels deployed above the power conversion unit.[11] The size of the panels are dependent on the efficiency of the power conversion unit. Increasing the temperature operating range of the core will reduce the surface area needed to reject the excess heat and thus decrease the mass of the system.

Figure 2 illustrates the layout of the core and shield of the reactor. The core consists of a fuel block traversed by coolant channels and surrounded by a cylindrical reflector. Control drums integrated with the reflector control the reactivity of the core. The coolant coming from the power conversion unit passes along the outside

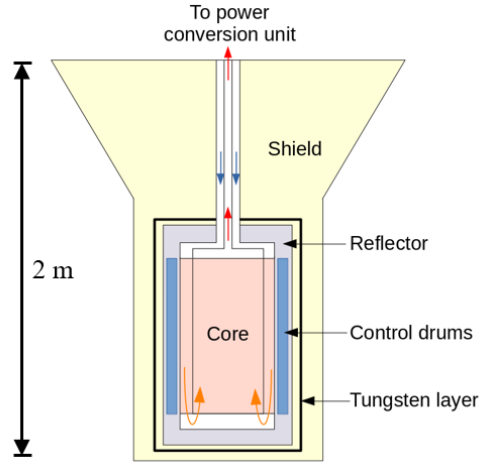

Fig. 2. Axial cross section of the reactor core and shield (not to scale).

of core to the bottom of the reactor.[10] Then, the coolant is heated through the core on the way back to the power conversion unit.

The preliminary design of the radiation shield is based on a lithium hydride (LiH) structure with a layer of tungsten to provide attenuation of neutrons and gamma-rays, respectively. This shield design is informed by the experience obtained from the SNAP program[12]; but, this project will explore other solutions, including utilization of in-situ resources like liquefied or solidified CO_2.

III. MODEL DESCRIPTION

The preliminary design phase for the reactor consisted of reviewing possible core configurations and evaluating their performance based on the control drum worth, the excess reactivity, and the shutdown margin. The initial assessment is focused on four main core configurations obtained from two fuel options (U-ZrH and U-YH) and two geometric options for the fuel block (cylindrical and hexagonal options represented by shapes (1) and (2) in Figure 3, respectively). An iterative search process with the following variables determined the four main core configurations: the pitch, the coolant channel radius, the number of rings, the core height, the reflector radius, and the height of the axial reflectors. The search objective was to find an excess reactivity and a shutdown margin close to \$5 and \$10, respectively.

The initial analysis considers cold clean conditions (room temperature, beginning of life, and no fission products in the core). MCNP6.2 performed the neutronic simulations using nuclear data from the ENDF/B-VII.1 evaluation.[13,14] The criticality calculations included 20,000 particles per cycle with 50 inactive cycles and 950 active cycles. The initial source distribution is contained in a cylinder surrounding the core with a Watt energy spectrum. The 2σ uncertainties are less than 0.04% in all cases.

An in-house Python framework can generate MCNP core geometries from the main geometric variables. This neutronic framework is also coupled with a coolant channel model to quantify the overall performance of the reactor with respect to the material temperatures.[10]

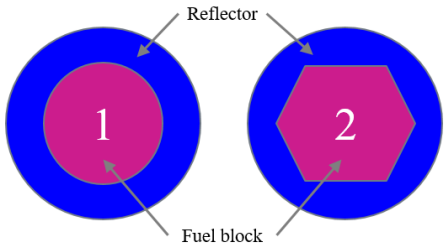

Fig. 3. Axial cross sections of the cylindrical (1) and hexagonal (2) configurations (not to scale).

Figure 4 presents a radial cross-section of the reactor core in the cylindrical configuration. The fuel block is composed of several fuel/coolant cells arranged in a hexagonal lattice defined by the distance between two cell centers (pitch). The fuel/coolant cells are arranged in rings around the first central cell. Each cell consists of a coolant channel filled with CO_2 and clad with 0.2 cm of molybdenum – 14 wt% rhenium (Mo-14Re) alloy surrounded by a homogeneous mixture of fuel and moderator. The fuel block is also clad with Mo-14Re with a thickness of 0.2 cm.

The first fuel option is a typical TRIGA type U-ZrH alloy with 45 wt% of low-enrichment uranium (19.75 wt% of uranium-235). The second fuel option is a homogeneous mixture of low-enrichment uranium and yttrium hydride based on the same mass ratio (45 wt% of uranium). This choice is based on the similarity to the U-ZrH option and the ability to model the fuel block as a homogeneous mixture. U-YH fuel has not been well documented at this time and the current development pathway for YH implies a heterogeneous moderator.[6]

The reflector is composed of one radial part and two axial parts (superior and inferior). Each part is composed of beryllium oxide. The scattering library for beryllium oxide is used at the room temperature (be/o.10t). The current MCNP model omits penetrations through the reflector for the coolant channels and the mechanisms used to rotate the control drums.

The control drums are located outside the core and inside the radial reflector. A specifically developed algorithm automatically adjusts the number of control drums to fill the available space in the reflector. The control drums are beryllium oxide with a boron carbide segment which acts as a neutron absorber. The thickness of the coating is 1 cm and the covered angle is 120°. The boron segment is 100% enriched in boron-10. Each control drum is contained in a 0.1 cm thick Mo-14Re cladding.

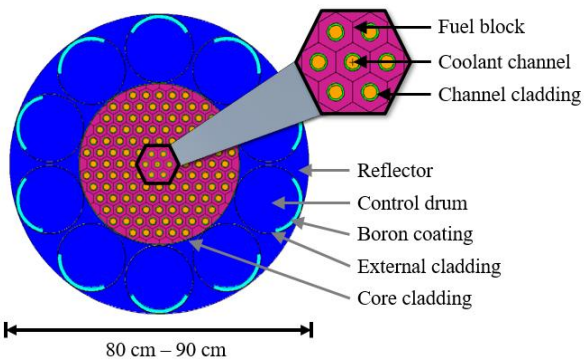

Fig. 4. Radial cross-section of the cylindrical core.

IV. RESULTS

The control drum worth is calculated from the difference in reactivity between the most reactive and least reactive states (referred to as the open and closed states, respectively). In the open state, the boron coating is in the farthest position from the core. Inversely, the boron coating is directly facing the core in the closed state. The excess reactivity corresponds to the reactivity in the open configuration and the shutdown margin is the reactivity obtained in the closed state. To express reactivity in dollars, the effective delayed neutron fraction is calculated for the open state based on the prompt method.[15]

Tables I and II present the neutronic results achieved after the iterative search with U-ZrH and U-YH configurations, respectively. While acceptable results are obtained for cylindrical configurations with both fuel options, the excess reactivity of the hexagonal reactors do not reach the objective of $5. For the hexagonal cores, the limiting factor might be the size of the reflector as the iterative search stopped at its maximal value. The algorithm which calculates control drum positions is constrained to produce a 12 control drums configuration for hexagonal cores. The maximal reflector size is reached when it is no longer possible to fit 12 control drums without intersection.

Tables III and IV present the geometric parameters obtained for U-ZrH and U-YH configurations, respectively. Figure 5 illustrates the four configurations at the same scale. Configurations with U-ZrH appear to have a more compact fuel block compared to U-YH, which could be explained by the better moderating ratio of ZrH. Preliminary estimation of core mass shows that the hexagonal cores are lighter (2,200 kg for both fuel options) than cylindrical cores. However, the difference in neutronic performance makes them difficult to compare on the same basis. The cylindrical U-YH core weighs 2,900 kg, while the U-ZrH version only weighs 2,500 kg.

TABLE I. Neutronic results for U-ZrH.

Core configuration	Cylindrical	Hexagonal
Control drum worth ($)	14.7 ± 0.6	12.1 ± 0.4
Shutdown margin ($)	9.2 ± 0.4	8.71 ± 0.32
Excess reactivity ($)	5.51 ± 0.21	3.43 ± 0.11

TABLE II. Neutronic results for U-YH.

Core configuration	Cylindrical	Hexagonal
Control drum worth ($)	15.0 ± 0.5	13.6 ± 0.5
Shutdown margin ($)	9.94 ± 0.33	9.78 ± 0.35
Excess reactivity ($)	5.10 ± 0.15	3.80 ± 0.12

TABLE III. Geometric results for U-ZrH.

Core configuration	Cylindrical	Hexagonal
Pitch (cm)	3.52	3.52
Coolant channel radius (cm)	0.83	0.81
Number of rings	7	7
Core height (cm)	90	90
Reflector radius (cm)	40	36.8
Axial reflector height (cm)	36	36

TABLE IV. Geometric results for U-YH.

Core configuration	Cylindrical	Hexagonal
Pitch (cm)	3.6	3.6
Coolant channel radius (cm)	0.7	0.66
Number of rings	7	7
Core height (cm)	90	90
Reflector radius (cm)	45	37.5
Axial reflector height (cm)	36	36

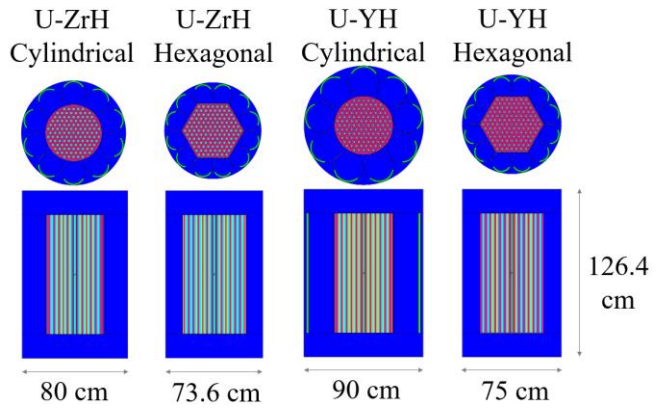

Fig. 5. Radial and axial representations of the selected configurations.

V. SUMMARY AND CONCLUSIONS

The preliminary design calculations for a megawatt-class reactor to provide electricity to a future Martian colony determined four core configurations from a combination of U-ZrH or U-YH fuel options and cylindrical or hexagonal core shapes. The results obtained in this initial analysis suggest that the cylindrical option offers more possibilities to adjust the core parameters to obtain acceptable neutronic performance. The hexagonal configuration imposes more constraints to the design and makes it more difficult to optimize with the chosen geometric parameters. For cylindrical cores, the difference in size and mass between U-ZrH and U-YH options can be compensated by the gain in maximum temperature using YH, which will result in a lighter power conversion unit.

The cylindrical U-YH version is therefore selected to be considered for the next optimization step of the design process. From the preliminary design calculations, the total diameter of the core with reflector is 90 cm and the total height is 126.4 cm. The total mass of the core with the reflector is 2,900kg. The control drum worth, the shutdown margin, and the excess reactivity, calculated for cold clean conditions with MCNP6.2, are \$15.0 ± \$0.5, \$9.94 ± \$0.33, and \$5.10 ± \$0.15, respectively.

Future work will include a review of heterogenous fuel/moderator configurations using yttrium hydride in the cylindrical core configuration. Systematic optimization based on reactor total mass (including the shield and the radiator) for equivalent neutronic performance will also be performed. Lifetime and coefficients of reactivity will be estimated, and reactivity calculations at operating temperatures will be performed.

REFERENCES

1. W. R. Corliss, *SNAP Nuclear Space Reactors*. Oak Ridge, Tennessee: U.S. Atomic Energy Commission / Division of Technical Information, 1969.
2. D. I. Poston et al., "KILOPOWER REACTORS FOR POTENTIAL SPACE EXPLORATION MISSIONS," *Nuclear and Emerging Technologies for Space (NETS-2019), American Nuclear Society*, Feb. 2019.
3. Department of Energy, Presidential Policy Directive 6 (Space Policy), "National Strategy for Space Nuclear Power and Propulsion," Office of the Secretary, *Department of Energy*, 85 FR 83923, 2020.
4. L. de H. Mencarini and J. C. King, "Fuel geometry options for a moderated low-enriched uranium kilowatt-class space nuclear reactor," *Nuclear Engineering and Design*, vol. 340, pp. 122–132, Dec. 2018, doi: 10.1016/j.nucengdes.2018.09.017.
5. D. Olander et al., "Uranium–zirconium hydride fuel properties," *Nuclear Engineering and Design*, vol. 239, no. 8, pp. 1406–1424, Aug. 2009, doi: 10.1016/j.nucengdes.2009.04.001.
6. X. Hu et al., "Fabrication of yttrium hydride for high-temperature moderator application," *Journal of Nuclear Materials*, vol. 539, p. 152335, Oct. 2020, doi: 10.1016/j.jnucmat.2020.152335.
7. J. L. Anderson et al., "Reactivity control of fast-spectrum reactors by reversible hydriding of yttrium zones." NASA, Lewis Research Center, NASA-TN-D-4615, 1968.

8. A. E. Craft and J. C. King, “Radiation Shielding Options for a Nuclear Reactor Power System Landed on the Lunar Surface,” *Nuclear Technology*, vol. 172, Dec. 2010.

9. L. Mason et al., “System Concepts for Affordable Fission Surface Power,” NASA, Glen Research Center, NASA/TM-2008-215166, p. 18, 2008.

10. J. Tellez et al., “Design of a Low Enrichment Uranium Nuclear Reactor to Power a Future Martian Colony - Thermal Hydraulics”, *Nuclear and Emerging Technologies for Space (NETS-2021)*, April 26-30, paper 35997, Oak Ridge National Laboratory (2021).

11. C. Glatt et al., “Design of a Low Enrichment Uranium Nuclear Reactor to Power a Future Martian Colony – Heat Rejection”, *Nuclear and Emerging Technologies for Space (NETS-2021)*, April 26-30, paper 35998, Oak Ridge National Laboratory (2021).

12. S. S. Voss, “SNAP reactor overview - Final Report,” Air Force Weapons Laboratory – Air Force Systems Command, Kirtland Air Force Base, NM 87117, AFWL-TN-84-14, Aug. 1984.

13. C. J. Werner et al., “MCNP USER’S MANUAL Code Version 6.2.” Los Alamos National Laboratory, Oct. 27, 2017.

14. M. B. Chadwick et al., “ENDF/B-VII.1 Nuclear Data for Science and Technology: Cross Sections, Covariances, Fission Product Yields and Decay Data,” *Nuclear Data Sheets*, vol. 112, no. 12, pp. 2887–2996, Dec. 2011, doi: 10.1016/j.nds.2011.11.002.

15. R. K. Meulekamp and S. C. van der Marck, “Calculating the Effective Delayed Neutron Fraction with Monte Carlo,” *Nuclear Science and Engineering*, vol. 152, no. 2, pp. 142–148, Feb. 2006, doi: 10.13182/NSE03-107.

Nuclear and Emerging Technologies for Space
Sponsored by Oak Ridge National Laboratory, April 26th-30th, 2021.
Available online at https://nets2021.ornl.gov

NUCLEAR THERMAL PROPULSION DEMONSTRATION CONCEPT

Michael Eades[1], Wes Deason[1], and Ethan Chaleff[1]

[1]*USNC-Tech 2356 W Commodore Way #120, Seattle, WA 98199*

Primary Author Contact Information: Michael Eades (206) 906-974, m.eades@usnc-tech.com

USNC-Tech was honored to participate in the NASA-funded Industry Lead Nuclear Thermal Propulsion (NTP) Fight Demonstrator study managed by AMA. This program surveyed the industry for input into how a near-term NTP demonstration system could be designed and built. Under this project, USNC-Tech produced the R2DTO concept that leveraged USNC-Tech Technology to enable a near-term demonstration of NTP systems. This paper provides a high-level overview of R2DTO that highlights key technology choices and advantages.

I. INTRODUCTION

R2DTO (Ready to Demonstrate Technology in Orbit) is a near-term NTP concept designed to demonstrate the key required technology to enable human transit to mars. R2DTO is a beryllium-moderated NTP system utilizing ZrC-FCM™ derived fuel, also known as "CerCer" (ceramic matrix, ceramic fuel). This high-temperature coated particle fuel enables high-temperature nuclide retention with robust mechanical properties suitable for high-confidence ground-testing and extreme performance during flight missions. Fig. 1 presents a rendering of the R2DTO concept, and key design properties are presented in Table 1.

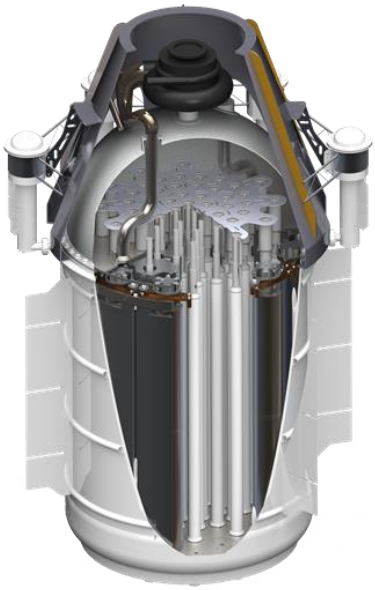

Fig. 1. A rendering of USNC-Tech's R2DTO concept

TABLE I. Key R2DTO Design properties

Property	Value
Thrust Class	10,000 lbf
Specific Impulse (s)	~900 s
Reactor Mass	~2500 kg
Fuel material	UN/ZrC FCM™ derived
Moderator material	Be Metal
Total HALEU mass (kg)	~120 kg

R2DTO intends to allow sufficient safety and radionuclide retention to be capable of ground testing without sacrificing performance while being flight ready for space-flight demonstration, should this be a desired national priority. As envisioned, R2DTO operates at a subscale thrust compared to what would be required for a human Mars class NTP system. However, it shares identical or nearly identical systems as would be required for the flight system, including fuel operating conditions, control systems, and core structures. Furthermore, a subscale demonstration will develop and exercise supply chains, regulatory pathways, and program management processes necessary for a full-scale NTP system.

II. KEY DESIGN FEATURES

The following sections describe the key technical and performance features of the R2DTO concept.

II.A. Passive Decay Heat Management

Post-shutdown decay heat cooling is typically accommodated by using a reserve propellant to cool the reactor following shutdown. This design strategy compromises I_{sp} to reduce weight in the reactor. USNC-Tech modeling has consistently demonstrated that a high-temperature capable reactor requiring less cooling can more than offset required mass gains in the reactor.

R2DTO addresses decay heat through a number of unique design features, the most apparent of which are the small radiators affixed to the outside of R2DTO's pressure vessel. Figure 2 shows a rendering of the R2DTO core where the radiators are prominent. Prior research has indicated that increasing the surface area and emissivity of the vessel can reduce period of active cooling during decay heat, coast period of operation by 20%-50% compared to an uncoated, cylindrical vessel.[1]

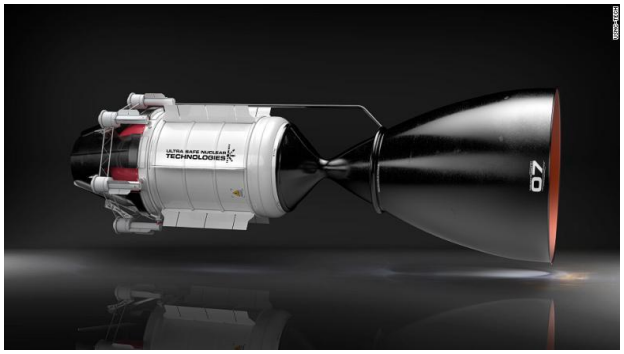

Fig. 2. A rendering of USNC-Tech's R2DTO concept showing the radiators.

Secondly, the vessel has been designed utilizing high-performance, commercially available steel alloys to reduce the mass of cooling systems in the vessel and enable higher vessel temperatures during cooldown cycles. The design leverages recent research and development from hydrogen storage systems to avoid hydrogen embrittlement issues in service without necessitating novel alloys or auxiliary cooling systems.

In addition to the vessel material and fins, higher decay heat temperatures also require a range of additional design features within the reactor to accommodate decay heat generation and transport without violating thermal limits in any structures. This does result in a noticeably more massive NTP subsystem. The mass savings are only realized system-wide as a reduction in stored additional hydrogen and cryogenic tank systems not typically accounted for as part of NTP design assessments.

II.B. Round 37/61 Channel Fuel elements

R2DTO employs round, 37-channel (or 61, in larger systems) fuel elements to minimize in-element peaking and maximize manufacturability. Figure 3 presents a drawing of a 37-channel version of the R2DTO fuel. Notable when compared to legacy solutions, manufacturing challenges with forming CerCer fuel have also been addressed by increasing minimum hole spacing in a cookie design.

Smaller 37- and 61-channel fuel elements also reduced in-element peaking compared to larger diameter 91-channel fuel elements. Larger fuel elements reduce the center neutron flux (due to non-fissile fuel absorption), thus increasing peaking in outer channels. Design space studies indicate that larger fuel elements with more coolant channels and larger diameter do enable lower mass cores, assuming a given I_{sp} and other key parameters such fuel material, moderator, and thrust stay constant. However, in-element peaking concerns are not trivial. In-element peaking is associated with increased pressure drop and local hot spots that limit the NTP system's overall performance, likely canceling out this benefit.

Round fuel elements also reduce peaking relative to hexagonal elements. Round fuel elements remove corners where neutron flux can "pinch" and cause localized peaks, as was seen with NERVA-derived hexagonal fuel elements. Round fuel elements are also more amenable to manufacturing through available processes.

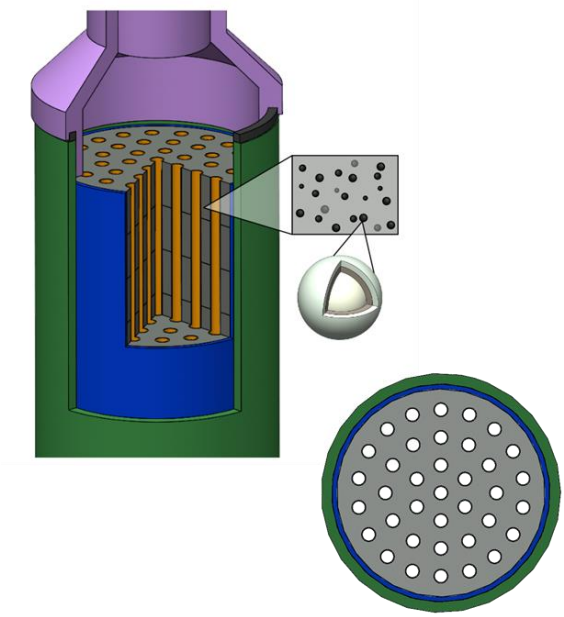

Fig. 3. 37-channel fuel element in the "cookie" geometry

Finally, smaller fuel elements are easier to manufacture as reducing the number of channels reduces the pressures needed for the various extrusion and compaction processes needed to make a CerCer fuel element. Additionally, reducing the number of channels decreases the chances of a defect in a fuel element during manufacturing.

II.C. Beryllium Metal Block Moderator

The block moderator configuration employed by R2DTO surrounds the circumference of each fuel element with a moderator. In R2DTO, the block moderator is made of beryllium metal, though other options were evaluated. Beryllium was selected based on a system optimization for mass, performance, and technology readiness; optimization is included in other design basis documents. The moderator is effectively a set of monolithic discs with holes for fuel assemblies and control drums and machined features for alignment and flow routing.

Block moderator configurations depart from NERVA clustered arrangements of hexagonal tie tube and fuel elements, however, the block moderator configuration still has a strong heritage for reactors. High power research reactors such as MARIA and BR2 (Figure 4) use

beryllium as a moderator in a block configuration. The Aircraft Test Reactor (Figure 5) and nuclear ramjet Tory series reactors (Figure 6) used BeO in a block configuration.

Fig. 4. The BR2 reactor with a Be moderator tubes[2]

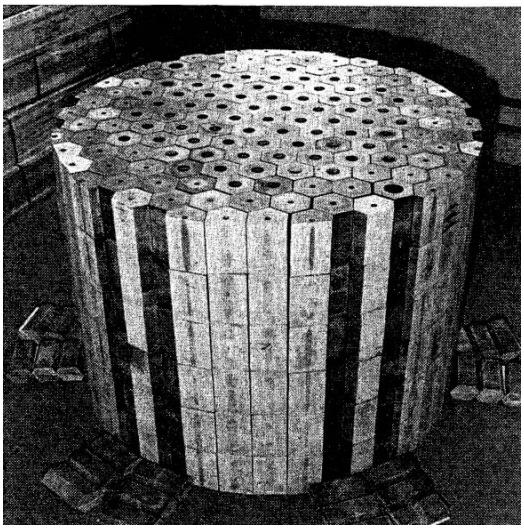

Fig. 5. Aircraft Reactor Experiment with a BeO prismatic block moderators[3]

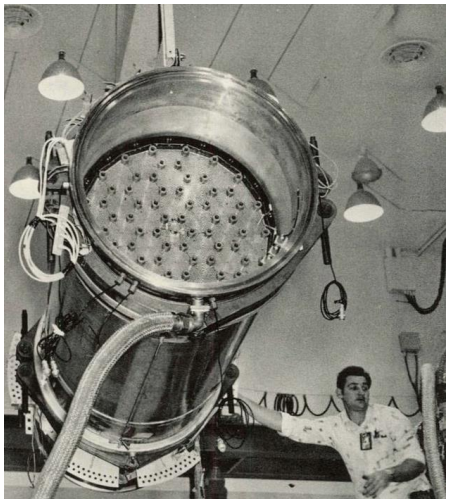

Fig. 6. Tory IIA reactor with monolithic BeO Block moderator[4]

Finally, the Strategic Defense Initiative (SDI) Timberwind/SNTP NTP system concept and the Soviet RD-0410 NTP system (Figure 7) tests used hydride moderators in a disc block moderator configuration. However, the use of hydride moderator adds complexity not warranted in R2DTO. The complexities related to using hydride moderator are expanded upon in the following section.

Fig. 7. ZrH block used for the RD-0410 moderator[5]

III. PERFORMANCE IMPROVEMENT PATHWAYS

The R2DTO concept is the product of multiple design factors aimed at reducing uncertainty and improving applicability and amenability to ground or flight testing. As performance objectives are resolved during the mission design process, the R2DTO provides the design framework to adapt to a range of mission specifications.

One avenue to notably reduce the size and mass of the R2DTO concept is by the inclusion of ZrH pin in the Be metal block moderator. In this concept, cooling passages surrounding the ZrH pins cool the material with hydrogen parallel to cooling passages in the Be metal block moderator. Initial studies indicate that ZrH pins can reduce active core mass by more than 20%. Figure 8 shows a cross-section a modified R2DTO with this feature. Of course, it should be noted that the inclusion of ZrH pins necessitates the development, characterization of ZrH technologies and complicates the moderator's design. It may introduce additional thermal challenges as ZrH is unlikely to handle the same temperatures as beryllium metal and can cause uneven power distribution in the fuel elements. A ZrH moderated NTP would also face the challenge of hydrogen density varying with temperature distribution, and in turn affecting power distribution. While none of these are trivial, USNC-Tech is actively developing and improving the technology

associated with the manufacturing and modeling of ZrH in NTP cores should this path prove desirable.

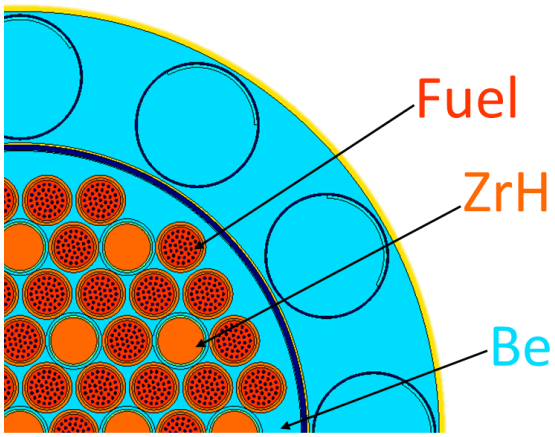

Fig. 8. Cross section of a modification of the R2DTO concept with ZrH Pins added to the Be block moderator.

Achieving higher operating temperatures may also be possible with the addition of part per thousand (ppt) hydrocarbons to the hydrogen propellant stream. Seeding compound mixtures of hydrocarbons into hydrogen propellant will significantly reduce the hydrogen corrosion in ZrC based NTP fuels like those used in R2DTO.[5,6] Hydrogen corrosion occurs when carbon bonds to hydrogen in the propellant and forms a hydrocarbon. Seeding the propellent with hydrocarbons before it contacts the fuel will bring the carbon-leaching reaction to equilibrium and stop hydrogen corrosion in the fuel.

Experiments conducted by the U.S. and the Soviet Union in the 1970s and 1980s found that hydrocarbon seeding was an effective method of slowing hydrogen corrosion.

IV. CONCLUSION

R2DTO is a near-term NTP concept that can demonstrate key aspects for human Mars class NTP systems in-space test or a ground test. Features highlighted that minimize risk and maximize performance include its ZrC FCM™ derived fuel, beryllium Block moderator, and small diameter fuel elements.

ACKNOWLEDGMENTS

This work was done in part in support of the NASA funded Industry Lead Nuclear Thermal Propulsion (NTP) Fight Demonstrator study managed by AMA. This work was done in contract 80LARC170003.

REFERENCES

1. L.B. CARASIK, M. EADES, V. PATEL, "Decay Heat Studies to Reduce Active Cooling Time of a Nuclear Thermal Propulsion System." *Proceedings of NETS 2019*, American Nuclear Society (2019) [online] Available at: <http://anstd.ans.org/NETS-2019-Papers/Track-4--Space-Reactors/abstract-75-0.pdf> [Accessed 19 February 2021].
2. K. EYMAN, M.C. HASYCHAK, "Materion Supplies Beryllium for Retrofit of World-leading Nuclear Test Reactor." 2016 [online] Businesswire.com. Available at: <https://www.businesswire.com/news/home/20160922005843/en/Materion-Supplies-Beryllium-for-Retrofit-of-World-leading-Nuclear-Test-Reactor> [Accessed 19 February 2021].
3. E. S. BETTIS et al, "The Aircraft Reactor Experiment-Design and Construction", Nuclear Science and Engineering, 2:6, 804-825, (1957) DOI: 10.13182/NSE57-A35495
4. H. REYNOLDS, "The Pluto Program," Lawrence Radiation Laboratory (1961) DOI: /10.2172/4073736
5. A. LANIN *Nuclear Rocket Engine Reactor* (2013th ed.). Springer, Berlin, Germany (2014)
6. E. STORMS, "The Behavior of ZrC(1-x) and U(y)Zr(1-y)C(1-x) in Flowing Hydrogen at Very High Temperatures", Report No. LA-12043-MS. Los Alamos, New Mexico: Los Alamos National Laboratory (1992)

Nuclear and Emerging Technologies for Space
Sponsored by Oak Ridge National Laboratory, April 26th-30th, 2021.
Available online at https://nets2021.ornl.gov

DESIGN OF A LOW-ENRICHMENT URANIUM NUCLEAR REACTOR TO POWER A FUTURE MARTIAN COLONY – HEAT REJECTION

Conner Glatt, Jacob Tellez, Joffrey Dorville, and Jeffrey King

Colorado School of Mines, 1500 Illinois St, Golden, CO 80401

cglatt@mines.edu, jtellez@mines.edu, joffreydorville@mines.edu, kingjc@mines.edu

This paper explores the design characteristics of the heat rejection system for a Martian surface reactor sized to produce 2 MW_e of electric power for at least ten years. The heat rejection analysis explores the effects of Martian weather on waste heat rejection and how control systems might be used to maintain the desired levels of power dissipation. The resulting adaptive radiator system maintains constant power dissipation by balancing radiative and convective heat transfer through variations in the rejection temperature and the radiator panel geometry. The worst-case hot environment (mid-day during the Martian summer with no wind) dictates the minimum system size, with 3744 m^2 of radiator panel area necessary to reject 4.9 MW_{th} of power through radiation and natural atmospheric convection. Preventing heat escape during the worst-case cold conditions with a fixed effective radiator area requires the implementation of variable rejection temperatures, radiative view factors, and convective angles-of-attack.

I. INTRODUCTION

The 2020-2021 Colorado School of Mines Reactor Design class was tasked with developing a reactor power system for use on the Martian surface. The reactor will be fueled with Low Enrichment Uranium (LEU; uranium containing <19.75% uranium-235) and will provide 2 MW_e of electric power for at least ten years of full power operation. The Megawatt Implementation of NuclEar ReActor using Low-enrichment uranium (MINERAL) concept has a real thermal to electric conversion efficiency of 29%; and, while excess thermal power will likely be in high demand for any Martian outpost, sufficient heat rejection systems must be in place to dissipate up to 4.9 MW_{th} of waste heat. Two other papers in these proceedings detail the neutronic[1] and thermal-hydraulic[2] performance of the MINERAL reactor, respectively. This paper describes the design of the reactor's heat rejection system.

The MINERAL heat rejection system takes advantage of convective heat transfer to the Martian atmosphere, supplementing the typical radiative heat transfer that lunar and deep-space radiator systems rely on. Bi-modal heat dissipation increases the efficiency of heat rejection per unit area, reducing the overall mass of the system. The Martian weather introduces high levels of variability, primarily by way of intermittent wind speeds which can cause the system to be too effective at dissipating heat and requiring implementation of an active control system. Maximizing the control margin while maintaining a balance between radiative and convective heat transfer to minimize total mass was the primary design challenge for this portion of the MINERAL system.

II. RADIATOR DESIGN

The MINERAL reactor produces energy via a direct Brayton cycle using supercritical carbon dioxide (CO_2) as the working fluid. The core thermal-hydraulics are limited by the uranium zirconium hydride (U-ZrH) homogeneous fuel and the potential disassociation of ZrH at higher temperatures, leading to a core outlet temperature of 762 K. The coolant exits the turbine at 535 K and is returned to the compression cycle at 325 K, necessitating 4.9 MW_{th} of heat removal.[1,2]

MINERAL's heat rejection system removes power from the reactor's primary loop via a CO_2-CO_2 counterflow heat exchanger between the turbine and compressor. Rejection loop coolant flows out of the heat exchanger at temperature T_{hot}, through the heat rejection radiators, across parallel banks of water heat pipes embedded in the radiator panel sections, and returning to the heat exchanger at temperature T_{cold}. Each panel section is three meters wide and four meters tall and is mounted on a motorized central axis such that the angle of the panel with respect to the Martian surface may be altered in response to changing atmospheric conditions.

Figure 1 shows the buried reactor configuration with the radiator panels in the fully vertical (90°) position. The

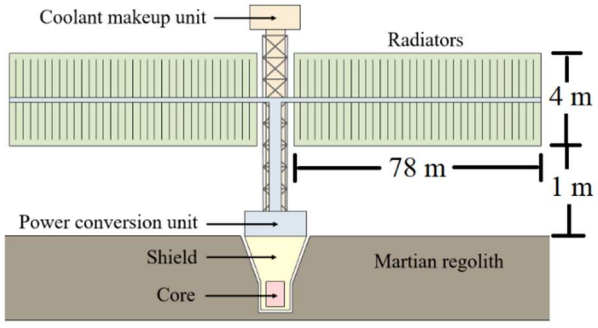

Fig. 1. Buried reactor configuration with the radiator panels in the fully vertical position (not to scale).

panel material is assumed to have a sufficiently high thermal conductivity that the temperature gradient to the surface of the panel is negligible and the panel heat rejection temperature is the average of T_{hot} and T_{cold}. The radiator panels utilize both radiation and atmospheric convection to dissipate heat from the reactor coolant loop. The angle of the panels controls the balance between radiative and convective heat transfer, allowing active control of the rate of heat rejection.

II.A. RADIATIVE HEAT REJECTION

The radiative heat transfer design approach is predicated on maximizing the view factors to the lowest temperature sinks and utilizing materials with a high emissivity and low absorptivity. On the Martian surface the regolith and the sky serve as the primary radiative sinks. The panels are assumed to be a constant temperature across the reactor emplacement, so no radiative heat transfer occurs between them. The Sun serves as a source of radiative heat transfer into the radiator. Eq. 1 governs radiative heat transfer:

$$Q_{rad} = \sigma \varepsilon A_{eff}(T_s^4 - T_{sink}^4), \quad (1)$$

where ε is assumed to be 0.9 for the panels and A_{eff} is equivalent to A multiplied by the view factor vf. Table I presents the approximations used to calculate the view factors to the regolith, the Sun, and the adjacent panel(s).

The view factor of the panel to the sky is assumed to be the difference between the sum of the other components and unity. In the current six-panel configuration, the view factor to the adjacent panel represents a power transfer 'dead zone' if the isothermal panel assumption is used. If the panels are rotated, their projection in the horizontal plane shrinks and greatly reduces the height-to-width ratio seen by adjacent panels, decreasing the 'Panel to Adjacent Panel' view factor and increasing the 'Panel to Space' and 'Panel to Regolith' view factors.

TABLE I. Applicable view factor approximations.

Radiative Component	View Factor Approximation[3]
Panel to Regolith	$vf = \dfrac{\left[\begin{array}{l}(x_1^2 - 2x_1y_2\cos(\alpha) + y_2^2)^{\frac{1}{2}} \\ + (x_2^2 - 2x_2y_1\cos(\alpha) + y_1^2)^{\frac{1}{2}} \\ - (x_2^2 - 2x_2y_2\cos(\alpha) + y_2^2)^{\frac{1}{2}} \\ - (x_1^2 - 2x_1y_1\cos(\alpha) + y_1^2)^{\frac{1}{2}}\end{array}\right]}{2(x_2 - x_1)}$
Panel to Sun	$\boldsymbol{vf = \dfrac{\pi R_{sun}^2}{2\pi Dist_{sun}^2}}$
Panel to Adjacent Panel	*Two Rectangles with a Common Edge and Included Angle of* α (see Ref. 3)

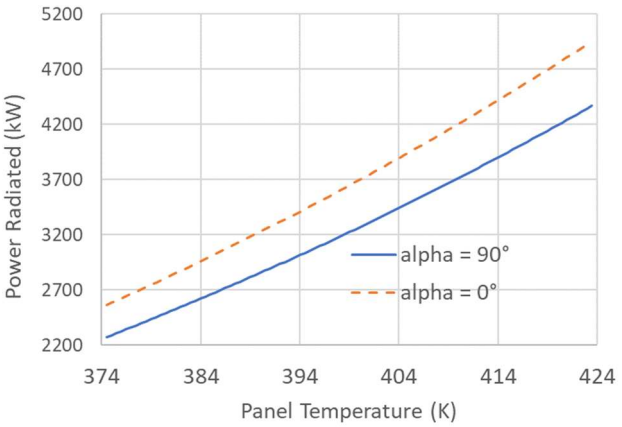

Fig. 2. Heat radiated by the heat rejection system in a 293 K environment.

The difference between the space sink temperature and the regolith sink temperature is insignificant compared to their respective differences from the panel temperatures, so the variability in radiated heat due to panel angle can be attributed to changes in the view factor to adjacent panels. Figure 2 represents the total power radiated to the sinks in the hottest expected environment[4], regolith at 293 K and 293 K atmospheric temperature, as a function of the panel temperature with the panels in the parallel (0°) and perpendicular (90°) configurations and a total emitting area of 3744 m^2.

II.B. CONVECTIVE HEAT REJECTION

Mars' atmosphere, which is 95 wt% carbon dioxide, 2.6% nitrogen, 1.9% argon, 0.16% oxygen, and 0.06% carbon monoxide, regulates the surface temperature to a moderate degree.[4] The commonly cited average Martian surface air temperature is 210 K, although hot temperatures of 293 K at the lower latitudes and cold temperatures of 146 K at the poles have been recorded, meaning that the atmospheric sink temperature can vary as much as 147 K depending on the time of year.[5] For the model baseline, the atmospheric composition was assumed to be 100% carbon dioxide at 210 K at 0.7 kPa with the properties shown in Table II.

TABLE II. Properties of CO_2 at 210 K and 0.7 kPa.

Property	Value[6]
Specific Heat, C_p	0.735 $\frac{kj}{kg*K}$
Kinematic Viscosity (μ)	4.42x10^{-6} $\frac{m^2}{s}$
Dynamic Viscosity (ν)	10.88x10^{-6} $Pa*s$
Thermal Conductivity (k)	0.0095 $\frac{W}{m*K}$
Prandtl Number (Pr)	3.420x10^{-4}

The American Society of Heating, Refrigeration, and Air-conditioning Engineers (ASHRAE) Vertical Plate Natural Convection correlation provides the Nusselt number for still air at the radiator panel (Ref. 7):

$$Nu = \left[0.825 + \frac{0.387Ra^{1/6}}{(1+(\frac{0.492}{Pr})^{9/16})^{8/27}}\right]^2 . \quad (2)$$

Eq. 3 yields the corresponding heat transfer coefficient:

$$h_{nat} = \frac{Nu*k}{L}. \quad (3)$$

To accommodate the changes to h_{nat} resulting from the inclination of the panel, an angle dependent first-degree approximation was derived from empirical data on orientation-dependent surface conductivity (Ref. 8):

$$h_{nat} = h_{nat} + [(h_{nat} * -0.00595) * (\alpha - 90)]. \quad (4)$$

ASHRAE's Nusselt number correlation for forced convection over a flat plate[7], valid for all Reynolds' Numbers, provides the forced convection heat transfer coefficients:

$$Nu = 0.037Re^{0.8}Pr^{1/3}. \quad (5)$$

The forced heat transfer coefficient gained from Eq. 3, h_f, and the natural convection heat transfer coefficient h_{nat} from Eq. 4 are combined using the empirical formula provided by Eq. 6 (Ref. 9):

$$h_{tot} = (h_f^{3.2} + h_{nat}^{3.2})^{1/3.2}, \quad (6)$$

where h_{tot} is the overall heat transfer coefficient. This avenue of determining the overall heat transfer coefficient is justified by a Richardson number of 0.14 at the highest-wind condition, meaning that natural convection is never considered negligible. The overall heat transfer coefficient allows the calculation of the total heat rejected by convection:

$$Q_{conv} = h_{tot}A(T_s - T_\infty). \quad (7)$$

Temperature variation in the low atmosphere and ground-level air on Mars can happen much more rapidly than changes to the regolith temperature. The low thermal inertia of the atmosphere can result in daily air-temperature swings of 100 K, meaning that the contribution from natural or forced convection can be vary wildly depending on the time of day.

During a calm day where the forced convection component is zero, the contribution from natural convection to the overall heat transfer can be as little as 72 kW in the vertical configuration, the configuration most conducive to two-sided natural convection.[8] Conversely, in a dust storm with 100 m/s winds during a low temperature condition, the power dissipated by combined natural and forced convection can be 4395 kW. Figure 3 displays how the power dissipated by convection from 3744 m^2 of radiator panels at 400 K and an angle of 90° changes as a function of wind speed.

II.C. CONTROL STRATEGY

The radiator must provide sufficient rejection in the worst 'hot' case, meaning no wind at mid-day during a Martian summer while also being able to limit heat escape during the worst 'cold' case, meaning a night-time dust storm during a Martian winter. The assumption of an imperfect counterflow heat exchanger necessitates a temperature drop of 10K between the primary outlet and the secondary inlet, so the radiator must reject 4.9 MW_{th} of heat to provide a maintain the conditions illustrated in Figure 4.

Altering the angle of the panels and changing the coolant 'hot' temperature through manipulation of the mass flow rate of the coolant provide two methods of controlling the rate of heat rejection from the panels. The total heat rejection coefficient, h_{tot}, is minimally impacted by the angle of the surface, presenting an opportunity for limited heat transfer control if a gimbal is incorporated at the panel joints. Equation 8 shows the relationship between mass flow rate and the coolant hot temperature:

$$T_{hot} = \frac{Q_{in}}{\dot{m}c_p} + T_{cold}, \quad (8)$$

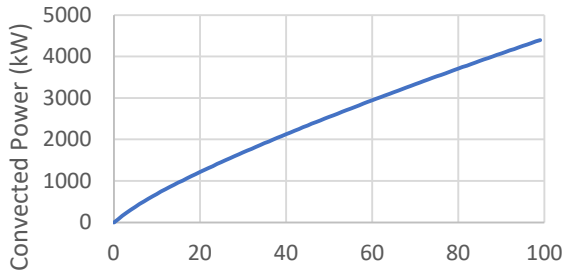

Fig. 3. Heat dissipated by convection at an atmospheric temperature of 146 K as a function of wind speed.

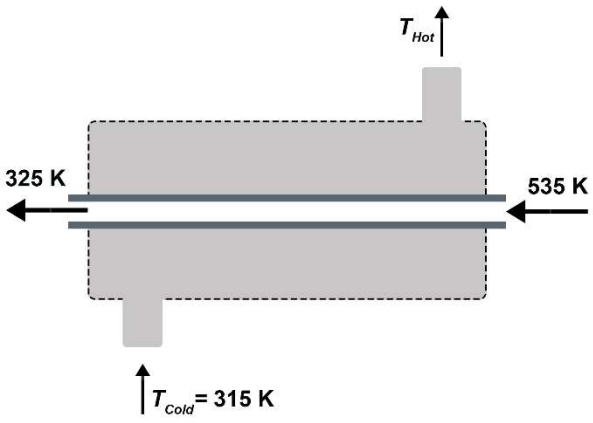

Fig. 4. Heat exchanger between the primary core loop and the heat rejection loop.

where T_{hot} and T_{cold} are measured at the outlet and inlet, respectively, in Figure 4.

The radiator control model attempts to match output power to input power while maintaining a constant return temperature. Given a set of environmental conditions, the model guesses a panel temperature, calculates the power rejected by radiation and convection, and compares it to the input power. The control model then checks this power difference against an arbitrary resolution factor that differentiates between major and minor discrepancies.

If the power discrepancy is large, the model increments or decrements the panel temperature guess, and recalculates the output power. If the power discrepancy is small, the model adjusts the panels' angle with respect to the ground, inducing finer changes to both the radiative view factors and angle-of-attack for convective heat transfer.

Figure 5 illustrates a simplified state diagram for the control system implemented in Python, representing the path to reach equilibrium between input power and output power. Once the input and output power are equal, the model calculates the mass flow rate necessary to achieve T_{hot} at the given input power.

III. RESULTS

The heat rejection system attempts to maintain a constant level of power dissipation in response to changing environmental conditions. As an example, Figure 6 depicts how the control system would manage T_{hot} as the wind speed varies at constant temperature. The scenario presented in Figure 6 is the worst-case 'cold' environment, nighttime with an atmospheric temperature and regolith temperature of 146 K[5].

In Figure 6, the power rejected due to convection increases logarithmically as natural convection is quickly outpaced by forced convection. The control system responds by lowering the panel temperature, exponentially reducing the effectiveness of radiative heat transfer. By

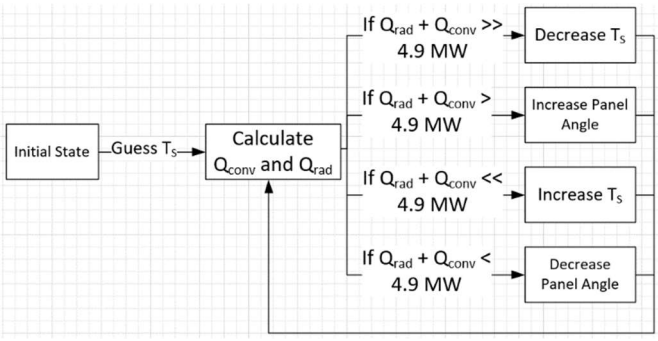

Fig. 5. Simplified control system state diagram.

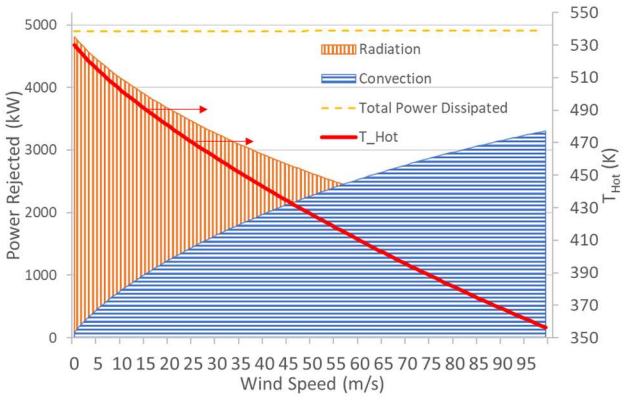

Fig. 6. Management of the power dissipated by the control system at an environmental temperature of 146 K.

manipulating the radiator coolant temperature (T_{hot}), and by extension, the panel temperature, the total power dissipated remains constant and the reactor core and power conversion system temperatures are unaffected.

The overall efficiency of the rejection system is limited by the daytime 'hot' case with no wind at an environmental temperature of 293 K. In this case, the panels are at 0° (fully horizontal) and T_{hot} is ~535 K, the maximum temperature attainable from the heat exchanger in the reactor power conversion loop. The panel surface area required to dissipate 4.9 MW_{th} in this configuration is 3744 m^2, yielding a specific heat rejection of 1309 W/m^2. From Figure 6, the worst-case nighttime 'cold' condition corresponds to an ambient temperature of 147 K with 100 m/s wind speeds and zero solar insolation. In this scenario, convection dominates the heat transfer and T_{hot} is forced down to 356 K.

IV. SUMMARY AND CONCLUSIONS

Heat rejection on the Martian surface is contingent on the management of both radiative and convective heat transfer. This paper outlines the design considerations and modeling of a radiator system that is equally effective in a summer daytime 293 K environment as in a winter nighttime 146 K environment.

The MINERAL reactor's heat rejection system has the opportunity to use the Martian atmosphere for bi-modal heat dissipation. Weather phenomena like wind and variable environmental temperatures necessitate the implementation of a controlled system that can remove constant power from the primary reactor loop. The design incorporates sufficient panel area to dissipate 4.9 MW_{th} by radiation and natural convection in the worst case 'hot' environment, and has the control margin to limit heat escape in the worst case 'cold' environment by increasing adjacent panel view factors and reducing the effective

panel temperature. Future work will include the exploration of alternative control methods such as variable efficiency heat exchangers and adaptive wind shielding.

NOMENCLATURE

A – surface area of the convecting surface
A_{eff} – effective radiating surface area
α - angle of rejection surface with respect to ground
c_p – specific heat capacity
ε - radiative emissivity
k – thermal conductivity
L – characteristic length of convecting surface
$\dot{m}$ – mass flow rate
Nu – Nusselt number
Pr – Prandtl number
Q_{conv} – power dissipated by convection
Q_{rad} – power dissipated by radiation
Q_{in} – waste heat from reactor system
Ra – Rayleigh number
Re – Reynolds number
σ - Stefan-Boltzmann constant
T_{cold} – rejection system heat exchanger coolant inlet temperature
T_{hot} – rejection system heat exchanger coolant outlet temperature
T_∞ - temperature of the Martian air
T_s – surface temperature of the panel
T_{sink} – sink temperature for radiative heat transfer

REFERENCES

1. J. DORVILLE et al., "Design of a Low Enrichment Uranium Nuclear Reactor to Power a Future Martian Colony -Neutronic Aspects", *Nuclear and Emerging Technologies for Space (NETS-2021)*, April 26-30, paper 35996, Oak Ridge National Laboratory (2021).
2. J. TELLEZ et al, "Design of a Low Enrichment Uranium Nuclear Reactor to Power a Future Martian Colony -Thermal-Hydraulics", *Nuclear and Emerging Technologies for Space (NETS-2021)*, April 26-30, paper 35997, Oak Ridge National Laboratory (2021).
3. J. HOWELL, "A Catalog of Radiation Heat Transfer Configuration Factors", University of Texas at Austin, Austin, TX (2010).
4. NASA, "Mars Facts", National Aeronautical and Space Administration, NASA Quest (2015).
5. L. SHEKHTMAN, "With Mars Methane Mystery Unsolved, Curiosity Serves Scientists a New One: Oxygen", National Aeronautical and Space Administration, Goddard Space Flight Center, Greenbelt, MD (2019).
6. NIST, "Carbon Dioxide: Gas phase thermochemistry data", United States Department of Commerce, 2018.
7. ASHRAE, "ASHRAE Fundamentals Handbook", American Society of Heating Refrigerating and Air Conditioning Engineers Inc, Atlanta, GA (2009).
8. A. JAFFER, "Convection from a Rectangular Plate", Massachusetts Institute of Technology, Cambridge MA (2019).
9. D. L. SIEBERS et al, "Experimental Mixed Convection Heat Transfer From a Large Vertical Surface in a Horizontal Flow", SAND83-8225, Sandia National Laboratories, Albuquerque NM (1983).

Nuclear and Emerging Technologies for Space
Sponsored by Oak Ridge National Laboratory, April 26th-30th, 2021.
Available online at https://nets2021.ornl.gov

SPACE NUCLEAR PROPULSION FUEL AND MODERATOR DEVELOPMENT PLAN CONCEPTUAL TESTING REFERENCE DESIGN

J. Gustafson[1], M. Krecicki[1,2], R. Swanson[1], B. Zilka[1], and J. K. Witter[1]

[1]*BWX Technologies, Inc, Lynchburg, VA, 24501*
[2]*Georgia Institute of Technology, Atlanta, GA, 30318*

Primary Author Contact Information: jlgustafson@bwxt.com

As future National Aeronautics and Space Administration (NASA) missions aim for destinations farther out into the solar system, Space Nuclear Propulsion (SNP), and in particular Nuclear Thermal Propulsion (NTP), is the only feasible near-term technology able to provide specific impulses of 900 seconds or greater and thrust in the range of tens of thousands of pounds. To maximize the success of the SNP program as a whole, a Fuel and Moderator Development Plan (FMDP) was created to mature mission critical technology, such as the reactor fuel form and moderator material. This paper details the conceptual testing reference design that provides the basis for the FMDP for future design and testing activities to meet NASA's goals.

I. INTRODUCTION

The SNP FMDP activities are coordinated by NASA and the Department of Energy (DOE) and include the following requirements to develop a subscale nuclear engine that demonstrates the viability of the NTP propulsion system and is scalable to the Mars mission needs:

1. Develop a High Assay-Low-Enrichment Uranium (HA-LEU) solid fuel form that can provide reactor exit temperatures greater than or equal to 2700 K.

2. Develop a moderated reactor conceptual design which includes, but is not limited to, a moderator block concept.

3. Develop a sub-scale, non-nuclear engine for early testing that leverages the benefits from conventional system development processes with the infusion of advances in nuclear fuel and reactor technology development.

This paper incorporates the initial summary issued via technical note [1] and further summarizes the design assessments completed. The reactor subsystem (RSS) conceptual testing reference design activities support decisions regarding technology development and the integrated fuel assembly in the moderator block unit cell test at the Idaho National Laboratory (INL) Transient Reactor Test (TREAT) facility. While the scaled configuration tests with a fuel assembly/moderator assembly in hydrogen is further out in calendar year 2022/2023, efforts made in advance assist with building toward the capstone tests.

I.A. FMDP Ground Rules

The proposed FMDP RSS testing reference design concept is based on the following ground rules:

1. The reactor uses a HA-LEU Uranium Nitride (UN) fuel kernel embedded in zirconium carbide (ZrC), referred to as cercer fuel, or molybdenum/tungsten (Mo/W), referred to as cermet, matrix material in a moderator block arrangement.

2. The gas (hydrogen) nozzle chamber temperature must be sufficient to reach an engine specific impulse (I_{sp}) of 900 sec. This is analogous to an approximate fuel channel exit gas temperature of ~2700 K.

3. The engine thrust is in the range of 12,500 to 15,000 lb_f.

4. The dry RSS mass limit is ~3,800 kg. This does not include turbomachinery, nozzle or external shielding mass allocations. This mass limit does include the necessary internal shielding.

5. The fuel elements are circular in shape with internal cooling channels.

Fabrication of the cermet fuel form is expected to be performed via spark plasma sintering (SPS) furthering development of the processing parameters developed under Game Changing Development (GCD). A thin refractory metal coating is applied to the UN kernel to protect the kernel from exposure to the atmosphere during handling as well as to promote bonding with the matrix material during fabrication of the composite fuel form. BWX Technologies, Inc. (BWXT) has previously manufactured W-coated UN particles. These particles will be tested in the very near future as part of the SNP FMDP test plans. The leading fuel particle proposed for the SNP cercer fuel is a UN kernel with a ZrC protective coating. The primary purpose of the coating is to prevent or slow carbon interaction with the UN kernel during operation [2][3]. Investigating fuel performance will be a major focus of future FMDP design activities.

II. DESIGN DESCRIPTION

The RSS conceptual testing reference design conforms to the typical NTP reactor arrangement, utilizing a neutron reflecting material surrounding the active core region using control drums lined with a neutron absorbing material and flow plenums for directing coolant flow through regions within the RSS. The FMDP conceptual testing reference design is available within the registered content on the NASA Technical Reports Server (NTRS) [4].

The active core region utilizes a moderator block design. Several historical reactor designs relied on slab moderator configurations. For example, the Experimental Beryllium Oxide Reactor (EBOR) utilized cylindrical assemblies inserted into blocks of beryllium oxide (BeO) [5]. The Heat Transfer Reactor Experiment (HTRE) design utilized solid moderator blocks of zirconium-hydride (ZrH) in a similar arrangement [6]. The moderator block configuration allows for more efficient neutron moderation and reduced intra-element power gradients, allowing for a significant increase in exit gas temperature.

The moderator material selection is a multi-faceted, inter-disciplinary trade-off between cost, manufacturability, mechanical integrity, reactor weight and active core volume. When all of these factors are considered, a ZrH moderator block is recommended. The ZrH moderator material allows for significantly reduced core diameter, which minimizes the reactor radial reflector and support structure masses. With the hydride moderator block design concepts, the better moderating properties relative to other solid moderators produce improvements in the U235 fission cross section and capture to fission ratio, and decrease in leakage [10]. These improvements offset any potential mass penalties due to a higher material density and parasitic loss to hydrogen absorption due to the optimized neutron economy. The choice of a ZrH moderator, therefore, also reduces the required amount of HA-LEU UN fuel, a valuable resource, resulting in improved sustainability.

Two potential fuel forms are proposed for the testing reference design. The first fuel form is cermet, utilizing a Molybdenum (Mo) 30 weight percent (wt%) W alloy (Mo:30W) which has been previously utilized in NASA GCD program efforts and several academic research papers [7][8][9]. The second fuel form is a cercer fuel with a ZrC matrix. While each fuel type has advantages and disadvantages, both must follow a similar development progression to ultimately be integrated as part of the SNP engine. The moderator block architecture improves cost and risk management by decoupling RSS development from fuel and moderator development. While core loading patterns and coolant channel element geometries may vary between fuel forms, the outer diameter of the fuel element is constrained such that either fuel form can be used in the same RSS design. This is made possible by fitting the fuel element(s) into a cartridge-like fuel assembly, which is then placed within the moderator block region to assemble the reactor core. This allows for the design of the RSS to be adaptable to multiple fuel forms and mature independently of the fuel form.

Cooling channels are directly integrated into the moderator block to ensure the temperature limits of ZrH are not violated during engine operation. The coolant in the moderator block enters at the bottom of the core and makes a single pass through the moderator block before recombining with the flow from the radial reflector. The active core region contains 61 fuel assemblies and each fuel assembly contains 91 internal coolant channels. The coolant enters the fuel channels from the top of the reactor and makes a single pass through the fuel assemblies before entering the rocket nozzle chamber.

III. DESIGN ASSESSMENTS

This section contains discussion on a selected sub-set of analyses performed on the conceptual testing reference design including neutronic, thermal hydraulic, and stress assessments.

III.A. Neutronics

BWXT's internally developed machine learning based optimization tools were leveraged to provide a conceptual reactor design that met all of the required performance criteria, while in accordance with the FMDP ground rules. The continuous energy Monte-Carlo particle transport code MCNP6.2 was used to conduct all neutronic analysis.

Energy deposition distribution by reactor component was considered for both core designs. The values include both neutron and photon direct energy deposition. The results demonstrate that the majority of the energy produced is directly deposited in the fuel element. One notable difference between the two designs is that the cercer design has 1.31% more energy directly deposited outside the fuel elements.

Additional optimization was performed to flatten the radial power profile for both designs to achieve maximum thermal performance and minimize the pressure drop from orificing.

The profiles were tailored by adjusting the fuel to matrix volume ratio in each fuel assembly, with an upper limit of 65 volume percent (vol%) of fuel particles. The fuel kernel uranium enrichment was kept constant at 19.75 wt% ^{235}U to minimize parasitic absorption in ^{238}U. The cermet fueled core was able to obtain a smoother radial power profile, with a maximum radial peaking

factor of 1.02 and a minimum of 0.96. The cercer core also achieves a satisfactory radial power peaking, with a maximum of 1.03 and a minimum of 0.97.

Values were determined at beginning of life (BOL) hot full power operational conditions, with the drums rotated 120 degrees from fully inserted. It should be noted that the cores are slightly super critical at a 120-degree drum rotation. This reserves some excess reactivity for future design trade-offs. The direct energy deposition distribution parameters do not change much over the expected reactor lifetime. The integral drum worth represents the total change in reactivity from rotating the drums from their completely inserted position to a completely removed position.

The H:^{235}U ratio for cercer was 306:1 and cermet 41:1, which accounts for the hydrogen present in the moderator block and excludes any hydrogen present in the coolant channels.

One of the major advantages of the moderator block design over discrete moderator elements is an improved neutron economy. Neutron economy ties to the material in which the neutrons are being absorbed and their proportional worth of the total available reactivity for a RSS. The ^{235}U worth fraction of neutron economy must be above 1.00 for reactivity criticality and a viable core design. The moderator block configuration provides reactivity margin, which can be used to improve thermal hydraulic performance and reduce reactor mass.

III.B. Thermal and Mechanical Assessment

The thermal and mechanical analyses of the hot fuel assembly and surrounding moderator unit cell was a primary focus during the conceptual testing reference design phase due to the peak fuel-to-moderator coolant temperature differences, which could lead to thermally and mechanically conservative results for the entire reactor core. Required changes to the entire RSS could be inferred from the performance of this assembly.

The assessment of the hot fuel assembly was performed using ANSYS Mechanical APDL finite element analysis (FEA) software [11] to evaluate a series of 2D planar models. Each planar model represented an 11 mm length of the hot assembly with the geometry and mesh. The thermal load and boundary conditions for each model were determined using a combination of analytic methods that translated the FMDP ground rules (Section I.A.) and direct energy depositions into plant power balance data, which were then used in combination with axial and radial power profiles to calculate channel-and-elevation-specific fluid temperatures and convection coefficients.

The fuel and moderator assembly thermal analysis considered axial and radial power peaking factors. The effects of intra-element peaking were not included, but are recommended to be included in future work. Hydrogen gaps between fuel assembly components were included in the analysis. Although considered stagnant gaps, the effects of conduction, thermal radiation and changes to gap size were included in the thermal analysis. The effect of natural convection within these gaps was shown to be negligible and was therefore not included. The hot channel temperature profiles for the cermet and cercer designs were determined.

Both the cercer and cermet peak fuel temperatures are under the design temperature target of 2850 K. The peak moderator temperature for the cermet concept is below the ZrH temperature limit. The peak moderator temperature for the cercer concept is also below the ZrH temperature limit. Heat transfer between the fuel assembly and moderator is considered in the calculation of thermal boundary conditions. Extrapolating from the hot assembly analysis, the estimated heat conducting to the moderator for the entire core is 5.64 MWt in the cermet design and 6.18 MWt in the cercer design. The combination of the greater fuel-assembly-to-moderator heat transfer and direct energy deposition in the moderator cause the higher peak temperatures in the cercer moderator.

A comparative linear elastic steady state structural analysis of both the cermet and cercer concepts was completed. Planar stresses and displacements were calculated using the temperature profiles determined in the thermal analysis. The peak stresses in the insulator, outer wall and moderator are comparable for both fuel assembly concepts. The cermet concepts have higher stresses in the fuel cladding. The stresses in the insulator wall are high relative to the material strength. The stresses in the structural outer wall are reasonable in comparison to the material capabilities. Peak moderator stresses indicate the potential for mechanical failure in the moderator block; however better material properties are required for a more accurate evaluation. The peak stresses in the insulator, outer wall and moderator are comparable for all fuel assembly concepts. The largest differences are observed in the fuel meat and cladding where the cermet concepts have higher stresses in the fuel cladding. The CTE mismatch between the cladding and the fuel meat is a significant factor in these stresses.

IV. SUMMARY AND CONCLUSIONS

Two reactor design concepts were developed to support the FMDP: one utilizing a cermet fuel form and the other utilizing a cercer fuel form. Both designs adhere to the FMDP ground rules detailed in this paper and meet the performance requirements. A view of the reactor design is provided in Figure 1.

The supporting neutronic, thermal hydraulic and mechanical analysis demonstrates the viability of both designs and provides valuable insights to inform development and testing to progress technology maturation important for SNP NTP applications. The cercer fuel form needs approximately seven times less HA-LEU, reduced maximum fuel meat stress and is about 400 kg lighter than the cermet fuel form. However, the cermet design leverages a previously manufactured fuel form with a beneficial epi-thermal neutron spectrum. Future work will focus on further study and refinement of the conceptual testing reference design summarized herein, in support of the FMDP development of the cercer and cermet fuel forms for integration in a complete SNP engine.

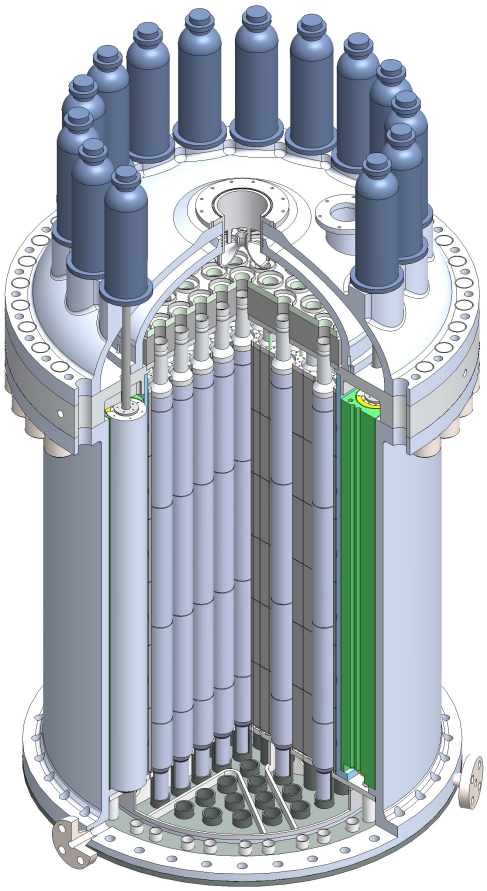

Fig. 1. Reactor subsystem cross section

ACKNOWLEDGMENTS

This work was authored by BWXT under Contract No. 80MSFC17C0006 with the National Aeronautics and Space Administration and Department of Energy Contract and Department of Energy subcontract through Idaho National Laboratory in Battelle Energy Alliance, LLC Contract No. BEA 00212687. The United States Government retains and the publisher, by accepting the article for publication, acknowledges that the United States Government retains a non-exclusive, paid-up, irrevocable, worldwide license to reproduce, prepare derivative works, distribute copies to the public, and perform publicly and display publicly, or allow others to do so, for United States Government purposes. All other rights are reserved by the copyright owner. The authors would like to thank Matt Ales (BWXT), Jim Inman (BWXT), Zach Moore (BWXT), Stephen Leff (BWXT), Ted Thome (BWXT), Eric Barringer (BWXT), Daniel Galicki (BWXT), Kalen Braman (NASA MSFC), Luke Scharber (NASA MSFC), Mark Stewart (NASA GRC), for the support to complete this paper.

REFERENCES

1. J. Gustafson, Space Nuclear Propulsion Fuel and Moderator Development Plan Conceptual Testing Reference Design, Nuclear Technology, DOI: 10.1080/00295450.2021.1890991.
2. Argonne National Laboratory, Bhattacharyya, S.K., “An Assessment of Fuels for Nuclear Thermal Propulsion,” ANL/TD/TM01-22, December 2001.
3. A.A. Salamatin, F. Peng, K. Rider, K.G. Kornev, “Non-stoichiometry Effects and Phase Equilibriain the Uranium-Carbon-Nitrogen Ternary System”, Met Trans A, 2020.
4. J. Gustafson, R. Swanson, “Space Technology Mission Directorate Technology Demonstration Mission Program Space Nuclear Propulsion Project Fuel and Moderator Development Plan Conceptual Testing Reference Design Task 3.1 PCB/ECB 8/20/20,” Aug. 27, 2020, NTRS Document ID 20205008398. NTRS Registered Content Link https://ntrs.nasa.gov/search?q=20205008398
5. “Experimental Beryllium Oxide Reactor Program,” Quarterly Progress Report or the Period, January 1 through March 31, 1962; April 25, 1962; San Diego, CA.
6. “Introduction to Nuclear Propulsion – Introduction and Background Lecture 1”, Feb. 26-28, 1963. NASA-CR-52961. https://ntrs.nasa.gov/archive/nasa/casi.ntrs.nasa.gov/19640019868.pdf
7. M. Krecicki, D. Kotlyar. ‘Low enriched nuclear thermal propulsion neutronic, thermal hydraulic, and system design space analysis’ Nuclear Engineering and Design Volume 363, July 2020.

8. M. Krecicki, D. Kotlyar. 'Neutronic Feasibility Of A Low Enriched Fast Spectrum Nuclear Thermal Propulsion Engine', Nuclear and Emerging Technologies for Space (NETS) 2020 Conference Proceedings, Knoxville, TN 2020, April 6th – 9th (Meeting cancelled due to COVID-19). Web: https://nets2020.ornl.gov
9. M. Krecicki, et. Al. 'Quantification of Intra-Element Peaking In Low-Enriched Nuclear Thermal Propulsion Cores', Nuclear and Emerging Technologies for Space (NETS) 2020 Conference Proceedings, Knoxville, TN 2020, April 6th – 9th (Meeting cancelled due to COVID-19). Web: https://nets2020.ornl.gov
10. J. R. Stehn 'Naval Reactors Physics Handbook Volume III: The Physics of Intermediate Spectrum Reactors' Knolls Atomic Power Lab, 1958. https://www.osti.gov/biblio/348907-naval-reactors-physics-handbook-volume-physics-intermediate-spectrum-reactors
11. ANSYS Mechanical APDL, Release 18.2, ANSYS Inc., Canonsburg, PA, USA, 2016.
12. "MCNP6 User's Manual Version 1.0" LA-CP-13-00634 Los Alamos National Lab (2013).

Nuclear and Emerging Technologies for Space
Sponsored by Oak Ridge National Laboratory, April 26th-30th, 2021.
Available online at https://nets2021.ornl.gov

DEVELOPMENT OF KEY TECHNOLOGIES FOR KOREAN SPACE HEAT PIPE REACTOR

Chan Soo Kim[1*], Sung Nam Lee[1], Byung Ha Park[1],Sung Deok Hong[1] and Sung Hoon Choi[1]

[1]*Korea Atomic Energy Research Institute, Daejeon, Republic of Korea, 34057*

**Primary Author Contact Information: +82-42-868-8747 and kcs1230@kaeri.re.kr*

The sustainable energy supply is important to carry out the various mission in space environment. The development of the fission power system for space, independent on the distance and direction of sun, is necessary for the surface power and the deep space exploration. Heat pipes can simplify the reactor design and remove the pump, piping and others. The objectives of the Korean space heat pipe reactor development program are the code development for space heat pipe reactor and the experimental evaluation of the thermal performance of the alkali metal heat pipe, which is manufactured by Korean company. This paper summarizes the research progress for Korean space heat pipe reactor technologies.

I. INTRODUCTION

In the future, the human space mission during long period in moon or mars will require the sustainable large nuclear power independent on the circumstance including the distance and direction of sun. Space fission power system should have a simple and reliable design. Its mass should also be as small as possible. Since the reactor maintenance in space is almost impossible, the number of components should be minimized to reduce unexpected events.

The advantages of heat pipe as the reactor cooling system include zero gravity operation, mechanical simplicity, relatively light weight and others. Therefore, the fission heat of heat pipe reactor can be transported from the core to the power conversion system without pumping power and gravity assistance. The fully passive heat removal without the moving part results in the simple design and maintenance. NASA and LANL has been developing a small fission power system called Kilo Power which uses sodium heat pipes and the stirling engines[1]. China[2] is also performing the basic study for the space heat pipe reactor.

Korean government makes comprehensive nuclear energy promotion plan every five years since 1997. This 5th plan (2017~2021) required that Korean nuclear technology should be spread and linked to future strategic fields and non-electric applications. Space application was one of the future strategic fields. Therefore, Korea Atomic Energy Research Institute could start the development of key technologies for space reactor in April 2019. Its objectives are to develop the design technology for space heat pipe reactor and to experimentally improve the thermal performance of the bendable alkali metal heat pipe. This paper summarizes the progress of Korean space heat pipe reactor R&D.

II. DEVELOPMENT OF REACTOR CONCEPT AND DESIGN TECHNOLOGY

II.A. Core Concept

In accordance with the U.S.-Republic of Korea Nuclear Cooperation Agreement, a study on the development of the concept of a space heat pipe reactor was conducted using a low-enriched uranium with an enrichment of less than 20wt%. The core concept of the space heat pipe reactor is designed to the following requirements,

- Life time > 10years
- Thermal power: 5kWth
- U-235 enrichment < 20.0wt%
- Mass < 1200kg, height < 5m, diameter < 2m
- Shielding design to protect the reactor system

II.A.1. Space heat pipe reactor core design

According to the design requirements, two core concepts were designed as shown in Figure 1, a fast and an epithermal reactor.

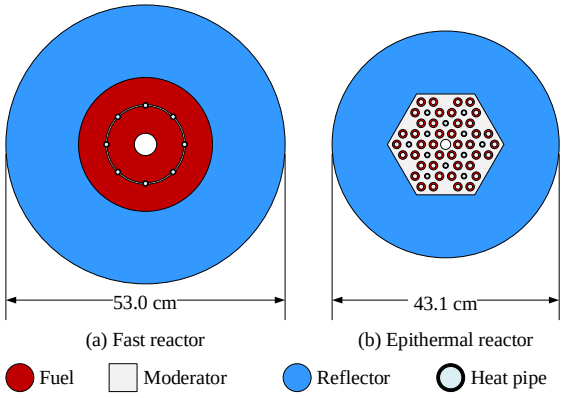

Fig. 1. Conceptual core design of the (a) fast and (b) epithermal space heat pipe reactor

The fast reactor design is a practical near-term solution by reducing material and engineering complexity, and is designed in a simple form consisting of U-Mo fuel

and BeO reflector. In the fast reactor, the annular fuel is divided into internal and external parts, and there is a void and a heat pipe between them. It is designed to improve heat transfer performance by contacting the heat pipe during thermal expansion of the fuel.

The epithermal reactor is designed to increase the neutronics efficiency using a moderator and significantly reduce the mass compared to the fast reactor. U-metal nuclear fuel, ZrH moderator, and BeO reflector are used. The dpa values of reflector surface for 10 years are about 0.04 of which is less than 0.1 dpa. The neutron fluence values are also about $7.7x10^{19}$ nvt, far less than the maximum permissible dose of BeO reflector.

In order to increase the contact area between the fuel and the moderator, the annular fuel was used and a moderator rod was inserted inside. This design achieved the criticality by using less fuel than the core using the cylindrical fuel, which further reduced the reactor mass.

II.A.2. Reactor shielding design

The radiation shielding design requirements for space reactors applied in this study were a fast neutron fluence (>100keV) of 10^{14}n/cm^2 and an absorbed dose of 10MRad or less at the stirling engine for one year[1]. The shielding design was performed assuming that the stirling engine was located 100cm away from the center of the core, and the shielding material was selected as LiH with 90wt% of Li-6, and the whole was surrounded by thin SS316. Figure 2 shows the mass comparison of fuel, moderator, reflector, and radiation shield of the core applying the shielding design requirements. The mass of the fast reactor is about 600 kg and the epithermal reactor is about 260 kg.

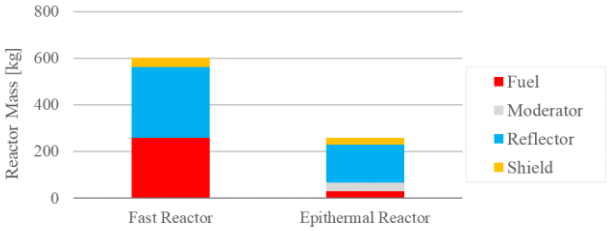

Fig. 2. Mass comparison of the fast/epithermal space heat pipe reactor

II.B. Design Technology

KAERI has been developing the reactor analysis codes to predict the core temperature and reactor performance capacities. First, the heat pipe simulation code named LUHPIS has programmed to simulate transient heat transport under the hot temperature condition with working fluid of sodium. The LUHPIS code can be used both stand-alone and dll with other CFD S/W like ANSYS CFX. Second, a core heat transport code HEPITOS has developed to analyze the core temperature distribution in the core during normal operation. Third, a space reactor system code SPAR-LM has been developing to analyze the system performance capacity from core to heat sink.

The LUHPIS code may simulate the steady and transient condition heat pipe with one dimensional model. The code adopted various wick type to simulate various heat pipe type. Fig. 3 represents the simulation results of LUHPIS for LANL transient heat pipe test results[3].

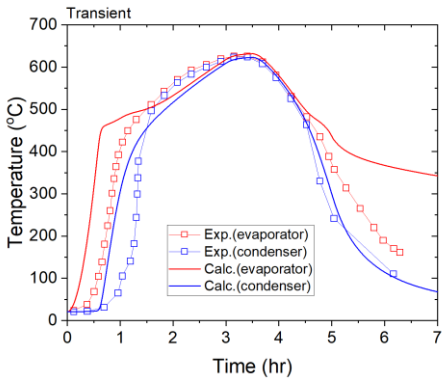

Fig.3. LUHPIS results for LANL transient test.

The HEPITOS code predict the steady heat transport in the core. The HEPITOS uses unit cell to generate mesh and can analyze two type of cores, monolith and groove. Fig. 4 shows the temperature distributions in the fuel and moderator region the 5 kWth epithermal reactor with 700℃ heat pipe temperature condition.

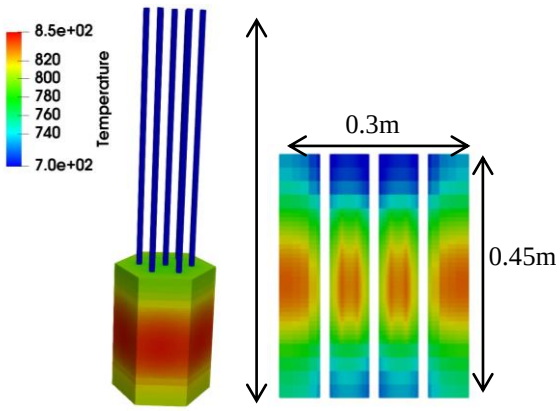

Fig. 4. HEPITOS mesh and calculated results.

The SPAR-LM code investigates a reactor core, heat pipe, stirling converter, radiator panel. Fig. 5 represents the temperature profile from the panel to the reactor core under the lunar ambient temperature of -20℃

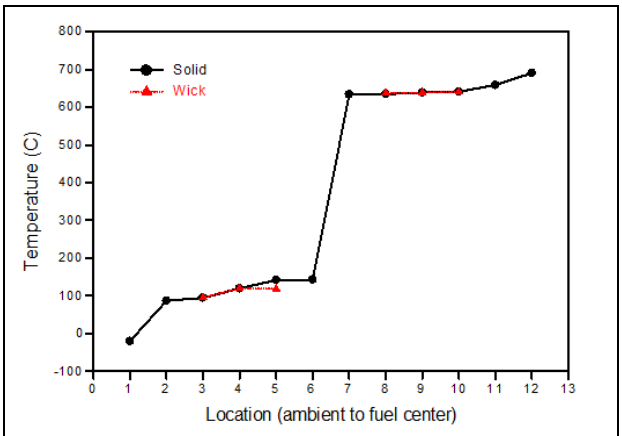

1	Lunar ambient
2	Inner side of radiator panel contacting to heat pipe
3,4,5	Condenser, adiabatic, and evaporator of the water heat pipe
6,7	Cooler and heater of stirling engine
8,9,10	Condenser, adiabatic, evaporator of the alkali metal heat pipe
11,12	Inner side of moderator and center of fuel

Fig. 5. Temperature profile in the system

III. DEVELOPMENT OF HEAT PIPE TECHNOLOGIY FOR SPACE REACTOR

III.A. Design of Bendable Wick Structure

Straight heat pipes are simple and cost effective but room is limited for the space purpose. Bendable heat pipes are good to maximize space utilization. Design and manufacturing of bendable heat pipes is a challenge for a heat pipe cooled reactor in space bases. The selection of wick material is a key for the manufacturing. Sintered metal powder and screen mesh are widely used for high temperature application. Sintered metal powder heat pipes showed crack when it was bended. Screen wick heat pipes showed reduction in vapor flow passage and capillary force[4].

Braided wire wick structure is possible option to manufacture bendable heat pipes. Braided wire wick is soft and strong. It has a good elasticity. Permeability of braided wire wick was an unknown parameter for design of heat pipe. Capillary rise rate experiments with simulant heat pipes were conducted to measure the permeability.

Bendable heat pipes were designed with utilizing in-house heat pipe design program. Braided wire wick was good in terms of pressure drop but it was poor in capillary force. We select sintered wick for the evaporator section and braided wire wick for adiabatic and condenser section.

Figure 6 shows a simulant heat pipe which is bendable. Wick structure is well attached to the surface. The vapor flow passages are maintained in the bended part.

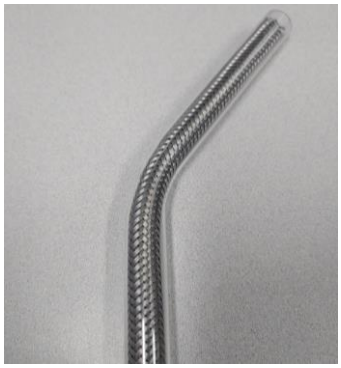

Fig. 6. Simulant bendable heat pipe

III.B. Thermal Performance Test

The experimental apparatus is composed of a evaporator, a condenser, a water cooling system and adiabatic zone formed by Kaowool insulator as shown in the Fig. 7.

The evaporator is a furnace type heater simulating reactor core thermal condition (Max. temperature to 1425℃). A Kanthal heater molded with Ceramic Kaowool material can generate up to 6 kW thermal power. The heater is surrounded by thick Kaowool-insulator to minimize heat loss to the environment. Two variable AC autotransformers, the voltage controller slidacses are connected to the evaporator to control the power manually.

The apparatus has the gas-cooled condenser because of the frozen startup failure and sonic limit[5]. It has a thermocouple port, an assembling flange and a high-temperature (870℃) sealing adapter.

Figure 7 also shows the layout of test section installed in both evaporator and condenser with the surface temperature measurement points. 25cm of HP is inserted into the evaporator and 20cm inserted condenser, and the other 55cm is opened at adiabatic region. K-type thermocouples are attached on the HP wall surface.

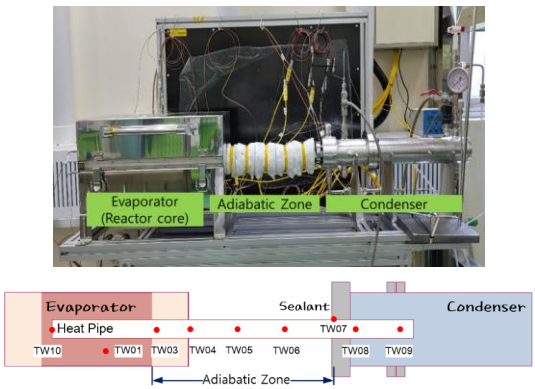

Fig. 7. HP experimental apparatus

Sodium Heat Pipe (HP) is 3/4" diameter and 1.0 m length of tube. It has the screen wick with annular artery. The cross section view of the HP is represented in the Figure 8. Geometric data of the wick structure are listed in the Table I. The HP is filled with 50 grams of sodium that is the amount of emerging all the screen wicks installed in the HP internal.

Table I. Characteristic of the test section (wick structure)

Parameter		Unit	Value
Wick	Type	-	Screen wick
	Mesh		#400
	Screen thickness	mm	0.063
	Artery type		Annulus
	Material		SUS316

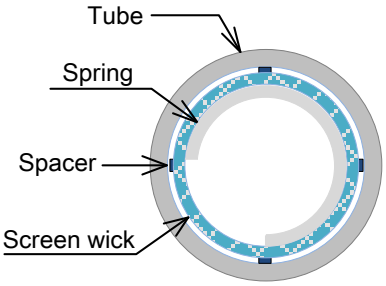

Fig.8. Cross-sectional View of Test section

The gas condenser is easily controlled the frozen state startup failure and can operate up to 3.0 kW power of the evaporator as shown in the Figure 9. The gas flow and thermal loss in the condenser removed 2.6 kW from the sodium heat pipe. The temperature gradient of the heat pipe surface in the condensing region resulted from the temperature difference between the inlet and outlet of the cooling gas flow.

IV. CONCLUSIONS

Heat pipe reactor is very suitable to fission power system for space application, because it has simple design, self-regulating reactivity feedback, and the passive safety. Korea Atomic Energy Research Institute has been developing the key technologies for space heat pipe reactor since April 2019. The core concept and the analysis codes is being developed for the space heat pipe reactor design. The wick structure was selected for the bendable heat pipe. The test facility was prepared for the thermal performance test facility of the alkali metal heat pipe at the high temperature condition.

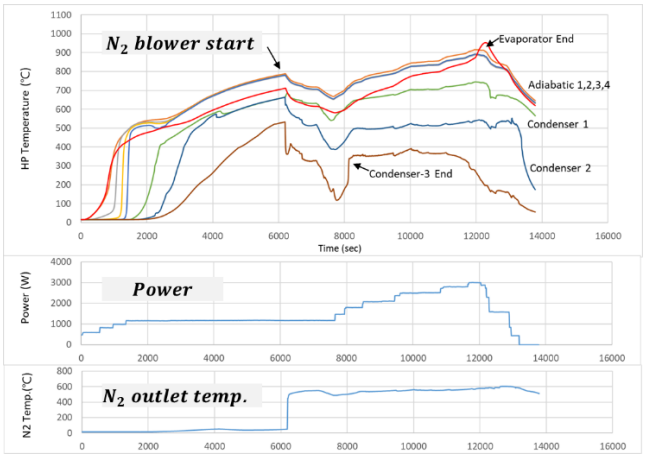

Fig. 9. Temperature history of sodium heat pipe with a nitrogen cooled condenser

ACKNOWLEDGMENTS

This study was supported by Nuclear Research and Development Program (2019M2D1A1058139) of the National Research Foundation of Korea (NRF) grant funded by the Korean Government (MSIP).

REFERENCES

1. D. I. Poston, M. Gibson, P. McClure, "Kilopower reactor for potential space exploration missions," *Nuclear and Emerging Technologies for Space*, Richland, WA, Feb. 25-28, ANS (2019).
2. W. Zhang, D. Zhang, C. Wang, W. Tian, S. Qui, G. H. Su, "Conceptual design and analysis of a megawatt power level heat pipe cooled space reactor Power System," *Annals of Nuclear Energy*, **144**, 107576 (2020).
3. R. S. Reid J. T. Sena, A. L. Martinez, "Sodium Heat Pipe Module Test for SAFE-30 Reactor Prototype," Space Technology and Application International Forum-2001(STAIF-2001), AIP Conference Proceedings 552, pp. 876-874, Feb. 11-14, 2001,Albuquerque, NM, AIP (2001).
4. D. Odhekar, D. Harris, "Experimental Investigation of Bendable Heat Pipes Using Sintered Copper Felt Wick," *Thermal and Thermomechanical Proceedings of 10th Intersociety Conference on Phenomena in Electronics Systems*, May 30-June 2, 2006, IEEE (2006).
5. J. M. Tournier, M. S. El-Genk, "Startup of a horizontal lithium-molybdenum heat pipe from a frozen state," *International Journal of Heat and Mass Transfer*, **46**, 4, pp. 671-685 (2003).

Nuclear and Emerging Technologies for Space
Sponsored by Oak Ridge National Laboratory, April 26th-30th, 2021.
Available online at https://nets2021.ornl.gov

PRELIMINARY SYSTEM FRAMEWORK FOR THE STARTUP ANALYSIS OF A LOW ENRICHED NUCLEAR THERMAL PROPULSION ENGINE

Vigneshwar Manickam, Matt Krecicki, and Dan Kotlyar

Georgia Institute of Technology, George W. Woodruff School, Nuclear and Radiological Engineering, Atlanta, Georgia 30332-0405, USA
Primary Author Contact Information: vigneshwar.manickam@gatech.edu

This paper presents a preliminary computational framework for start-up sequence analysis and design of nuclear thermal propulsion (NTP) low enriched uranium (LEU). The computational framework provides a modular package for the integrated transient modeling of key engine components. Additionally, this paper introduces the control of core reactivity and chamber pressure in a modern LEU NTP system based on previous work that was investigated for the control of NERVA engines.

I. INTRODUCTION

Currently, extensive research is being conducted on high fidelity steady-state calculations to determine performance factors to analyze LEU NTP designs. The general approach is to decouple the engine components (*e.g.*, pumps) from the reactor-core. Some uncertainties arise from adopting the decoupled approach, but overall it is a reasonable assumption. As the turbomachinery components operate under nearly constant conditions, the boundary conditions (*e.g.*, inlet pressures and temperatures) to the core can be well established. Transient operations, however, such as engine startups, require modelling the entire integrated system. The Computational Reactor Engineering (CoRE) group in Georgia Institute of Technology is developing an integrated system framework that will enable to model fast startups and restarts. Our approach is to develop a modular system that will allow using varying level of fidelity (e.g., the core is model as a single channel vs. each channel is modeled separately). Here, we present only preliminary results that demonstrate the overall structure of the framework, and present initial results that follow the hydrogen propellant from the cryogenic tanks up to the nozzle. The overreaching goal is to develop an open-source package that compliments NPSS by increasing the flexibility of every key component through time dependent analysis and expanding the spatial analysis of the reactor core.

I.A. Current System Frameworks

NASA Glenn Research Center presents a Large NERVA Derived Engine created in the Numerical Propulsion System Simulation (NPSS) framework that uses design parameters from the Small Nuclear Rocket Engine (SNRE) (Ref. 1). This concept is capable of generating approximately 112.1 kN of thrust and delivering 555 MW of thermal power. NPSS is capable of solving for the outlet temperature and pressure of each key component in the engine design based on fuel element and turbomachinery constraints. The program uses a lumped model methodology to solve the temperature and pressure parameters for significant engine components. The program also currently uses power deposition profiles from Monte Carlo N-Particle (MCNP5) to model the reactor core.

I.B. Reference NERVA Startups

The NERVA program presented unique operational requirements and challenges based on different phases of their startup procedure. Figure 1 shows the typical operational phases for a typical NERVA engine. The startup procedure is initiated with a conditioning phase in which turbopumps are chilled, the reactor is brought to critical, and the drums are used to raise reactor temperature to the next phase. Bootstrapping of the engine involves gradually increasing the chamber pressure with a control sequence of the turbine inlet, outlet, and bypass valve. The drums are used to correct for the change in chamber temperature during this sequence. Once the bootstrapping procedure is complete at a set chamber pressure, the engine is ready to be ramped up toward a nominal full thrust level (Ref. 2).

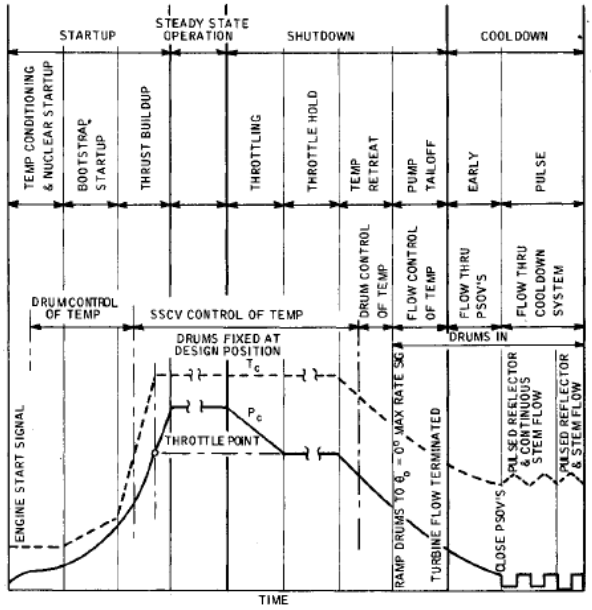

Fig. 1. NERVA engine operational phases

A similar type of startup sequence is expected for a LEU NTP design along with similar constraints in which the engine must startup without being precluded by ^{135}Xe at any time. This adds more challenges to the design of a startup sequence due to unfavorable reactivity penalties associated with LEU cores. Additionally, the current LEU NTP designs incorporate the use of moderator elements (ME) in conjunction with ceramic metallic (cermet) fuel elements (FE) to negate these reactivity penalties. An adequate startup analysis with the inclusion of MEs is currently not being undertaken. The neutronic and thermal-hydraulic transient analysis of MEs could exploit new startup strategies or allow for a pathway for future NTP designs.

II. INTEGRATED SYSTEM

The reference startup profile shows the importance of controlling the chamber pressure and chamber temperature of the engine. The control sequence allows the user to input desired chamber temperature and pressure ramps in order to control the startup trajectory. In summary, the integrated system requires one input to control a single set of parameters: the turbine bypass valve (TBCV) controls the chamber pressure, and the control drums control the chamber temperature. The dynamic time dependent nature of this analysis requires a robust numerical scheme to solve numerous differential equations for each time iteration. The code leverages the use of the SciPy Odeint package that solves initial value problems for stiff or non-stiff first order differential equations using adaptive time meshing (Ref. 4). As shown in Figure 2, the code currently houses several modules that are able to be rapidly customized with future higher fidelity modules. An array of time dependent parameters of the NTP are housed in the State Class. Each separate component module stores steady state algebraic equations and transient differential equations specific to the component. SciPy Odeint calls the transient equations from the component modules in order to solve the equations at every time step in the solve.py script. The Solution class holds an array for the solutions of these equations and updates the solutions for each state parameter in the State Class. The Solution Class also incorporates plotting functions that is helpful for post-processing of the results.

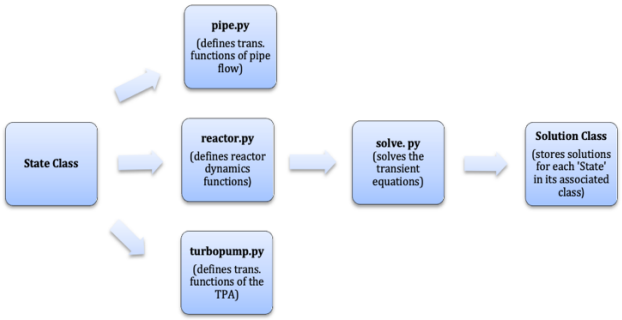

Fig. 2. Modular design of transient package

II.A. Reactor Framework

SERPENT, a multi-purpose three-dimensional (3D) Monte Carlo particle transport code, was used to calculate reactivity coefficient correlations (Ref. 3). A simplified methodology was implemented where each region was perturbed separately from hot full power conditions in order to develop the following reactivity coefficients: fuel temperature, moderator temperature, fuel gas density, moderator supply gas density, moderator return gas density and control drum rotation. SERPENT was also used to calculate the delayed neutron fractions, decay constants, and the associated effective generation time for the reactor design. These kinetic parameters along with the feedback and control reactivities are used in the point kinetics equations. These equations handle the neutronic part of the lumped reactor core model, where the solutions of these equations provide the power and delayed neutron precursor concentration at every time step. The reactor is currently modeled as a lumped model, using the point kinetics equations and a time dependent heat transfer relationship between coolant and fuel. Future work involves axially discretizing the fuel and moderator element and incorporating local changes in temperature and density in each layer.

The maximum fuel temperature limits compounded by the cooldown and heat up rates of cermet fuels add additional constraints to the startup. The most important aspect of this model is the precise control of nuclear kinetics and reactivity. The MIT/SNL Alternate Period-Generated Minimum Time Control Law computed by Eq. 1, was derived from the point kinetics equations to precisely generate any desired power profile with little or no power overshoot (Ref. 5). The control law provides a rate of change of reactivity required to produce an instantaneous reactor period.

$$\dot{\rho}_c = (\beta - \rho)\omega_s - \lambda_{eff}\rho - \sum_{i=1}^{I} \beta_i(\lambda_i - \lambda_{eff}) - \dot{\rho}_f + \Lambda\,[\dot{w}_s + \omega_s(\omega_s + \lambda_{eff})] \quad (1)$$

where, standard nomenclature is used to represent decay constants, λ, delayed neutron fraction, β, reactivity ρ, and the dot operator represents the time derivative. The desired inverse period, ω_s, is calculated for a given power trajectory using Eq. 2. The user defines the final power level (P_f), initial power level (P_o) and the time ramp (t_{ramp}) required to reach this final power.

$$\omega_s = \frac{\ln\left(\frac{P_f}{P_o}\right)}{t_{ramp}} \quad (2)$$

A desired rate of change of the inverse period, shown in Eq. 3, is calculated by comparing the calculated desired inverse period to the measured inverse reactor period of the reactor at every time step. The measured inverse reactor period (ω_t) is simply the rate of change of power divided

by the power at the time step. At the start of the problem, the measured inverse reactor period is zero, due to the reactor being in steady state and by definition having an infinite reactor period. The initiation of the transient causes the measured inverse period to be a non-zero number. The desired inverse period is set to zero once the power reaches the desired power level and is maintained at zero until the start of the next power transient.

$$\dot{\omega_s} = \frac{\omega_s - \omega_t}{t_{ramp}} \quad (3)$$

The law takes into account the reactivity due to control drums, feedback, and the population of the delayed neutron precursors at every time step in order to develop an adequate rate of change of control reactivity to keep the reactor at the required inverse period to reach the desired final power or temperature level. The rate of change of reactivity is used as the actuator signal for the drum speed for the purpose of rotating the drums at the associated speed. If this calculated drum speed is larger than the user defined maximum drum speed, then the latter is used instead. The control laws can be modified to take in temperature signals and temperature trajectories which will be useful to model the reference chamber temperature ramp profile as shown above (Ref. 6).

Several sensitivity studies regarding the number of time steps required to reach the specified power trajectory was conducted using in-house built differential equation solvers. The control law exhibited significant power overshoot if fewer time steps were used and produced fast drum speed if many time steps were used. The reactor framework leverages the adaptive time meshing scheme of the SciPy Odeint package, which dynamically adjusts the number of time steps used to solve all differential equations that describe the model. The adaptive time meshing allowed for tighter control of the change of reactivity and thus minimum power overshoot without using power tolerance bands.

II.B. Component Framework

The model currently consists of piping, tees, valves, turbopump, turbine, regenerative nozzle and control drums; where all the components are treated as lumped volumes Constant parameters of each component are defined by the user in an input file, making all components customizable. The hydrogen fluid properties are taken from a data set provided by NASA's Lewis Research Center (Ref. 7). Each component is connected to one another and the hydrogen properties at the outlet of each component serve as the boundary conditions to inlet of the next component. The current system framework seeks to build a transient model of the SNRE, using the NPSS Large NERVA derived engine. At each time iteration, the enthalpy and pressure of the hydrogen fluid is updated. The pressure drop across each component uses a predictor-corrector approach where the inlet and outlet hydrogen properties of the components are both used to calculate an accurate pressure drop based on friction and acceleration losses.

The framework uses the momentum integral methodology to conserve the fluid momentum across a component. This quasi-steady state assumption assumes that the SciPy Odeint solver's time step is small enough to assume that the flow rate is constant at any time step (Ref. 8). The mass flow rate of the system is updated at every time step and is based on the choked nozzle flow rate equation which takes the chamber temperature and pressure as inputs.

User-defined pump curve characteristics and pump curve data is required to capture pump performance. The shaft speed of the turbopump assembly (TPA) is found from the solution of a time dependent differential equation that balances the torque imbalance of the pump and turbine sharing the same shaft. The transient program solves for the pressure rise across the pump based on a dynamic TPA shaft speed. A similar control logic is required to regulate the chamber pressure ramps of the system. The choked nozzle flow assumption allows for the chamber pressure to be nearly proportional to the system mass flow rate for a constant chamber temperature. Relating the dynamic manipulation of the TBCV based on user-defined chamber pressure ramps under the choked flow assumption is currently under investigation.

III. DEMONSTRATION OF POWER RAMP

The MIT/SNL Alternate Period-Generated Minimum Time Control Law using SERPENT generated physics parameters for a LEU NTP core is demonstrated. Figure 3 shows the change of reactor of power from an initial power level of 100 MW to a final power level of 500 MW using a time ramp of 6 seconds. Figure 4 shows the population of 6 delayed neutron precursor groups.

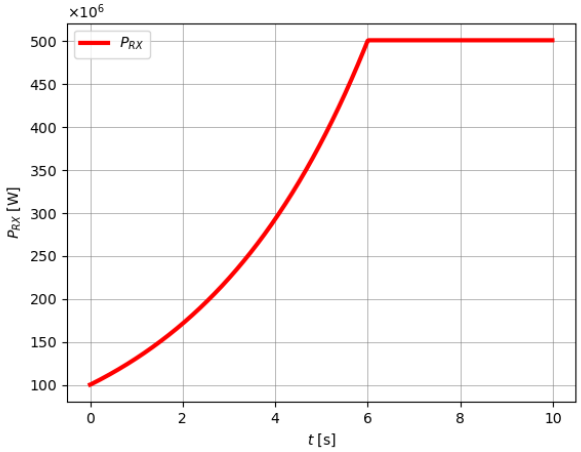

Fig. 3. Power ramp to 500 MW in 6 second

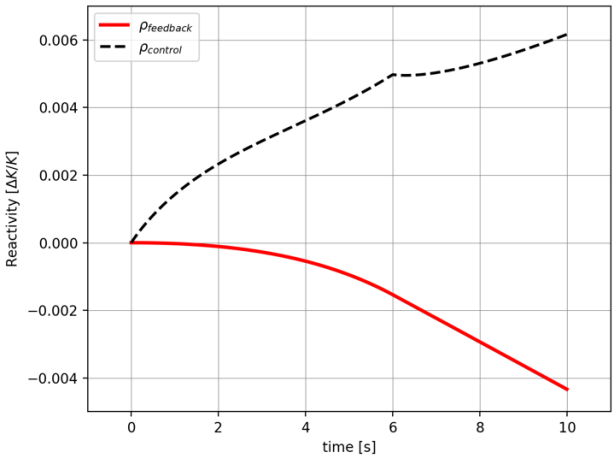

Fig. 4. Change in control and feedback reactivity

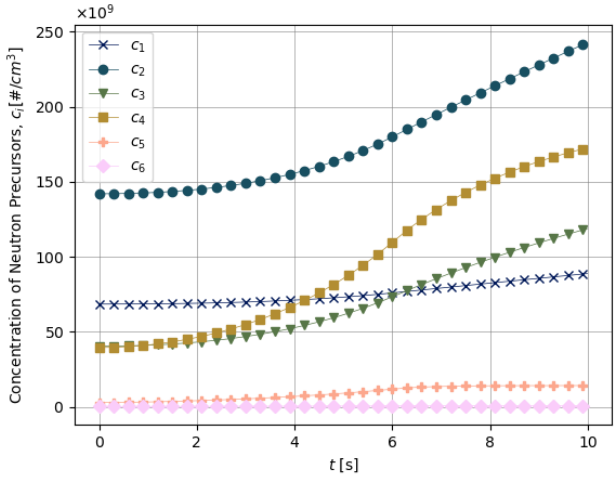

Fig. 5. Change in delayed neutron precursors

These figures demonstrate that the control law achieves a final reactor power of 500 MW with no power overshoot in 6 seconds. The control law reactivity is able to keep an infinite reactor period and stabilize at 500 MW by correcting for the increase in delayed neutron precursor levels by inserting negative reactivity into the core. Currently the code incorporates hydrogen gas density and fuel temperature perturbations into total feedback reactivity.

IV. CONCLUSIONS

This current framework has shown the ability to simulate a transient startup of an LEU NTP system through the precise control of control reactivity with minimal power overshoot. The framework enables a modular design that allows for vast customization of components in the rocket. This current preliminary stage had the primary motivation of developing a foundation to control the neutronics of an LEU core at a point kinetics level. Future work will involve the control of chamber pressure by varying the pressure rise across the turbopump through the turning of the TBCV position. User-defined chamber temperature ramps and chamber pressure ramps will allow for integrated startup analysis for later LEU design concepts.

ACKNOWLEDGMENTS

This work is funded by the US Navy's Naval Education and Training Professional Development Center via the Graduate Education Voucher Program. The primary author also acknowledges James Kennington of Penn State, in his help to develop a baseline framework for the SciPy Odeint solver that enables fast transient simulations.

REFERENCES

1. M. L. BELAIR, C. J. SARMIENTO, and T.M. LAVELLE, "Nuclear Thermal Rocket Simulation in NPSS," *AIAA Joint Propulsion Conference*, San Jose, CA, July 14–17, Joint Propulsion Conference (2013) DOI:10.2514/6.2013-4001.
2. J. H. ALTSEIMER, G. F. MADER, and J. J. STEWART, "Operating Characteristics and Requirements for the NERVA Flight Engine," *Journal of Spacecraft and Rockets*, **8**, 7 (1971). DOI:10.2514/3.59723
3. LEPPÄNEN, L., PUSA, M., VIITANEN, T., VALTAVIRTA, V., KALTIAISENAHO, T., 2015., The Serpent Monte Carlo code: Status, development and applications in 2003. Ann. Nucl. Energy 82, 142-150.
4. VIRTANEN, P. et al., "SciPy 1.0: Fundamental Algorithms for Scientific Computing in Python," *Nature Methods*, **17**, 3 (2020). DOI:10.1038/s41592-019-0686-2
5. J. A. BERNARD and D. D. LANNING, "Considerations in the Design and Implementation of Control Laws for the Digital Operation of Research Reactors," *Nuclear Science and Engineering*, **110**, 425 (1992). DOI: 10.13182/NSE92-A23916
6. J. K. WITTER, "Modeling for the Simulation and Control of Nuclear Reactor Rocket Systems," *PhD Thesis, Department of Nuclear Engineering, Massachusetts Institute of Technology*, (1993).
7. J.T. WALTON, "Computer program for thermal and transport properties of parahydrogen from 20 to 10,000K," NASA Lewis Research Center, Cleveland, Ohio, (1993). NASA-TP-3378
8. W.E. CASEY, "Thermal-Hydraulic Transient Analysis of a Packed Particle Bed Reactor Fuel Element," *MS and Naval Engineer Thesis, Department of Nuclear Engineering, Massachusetts Institute of Technology*, (1990)

NOMENCLATURE

$\dot{\rho_c}$	Rate of change of control reactivity
$\dot{\rho_f}$	Rate of change of feedback reactivity
ρ	Total reactivity
β	Total fraction of delayed neutrons
β_i	Fraction of delayed neutrons of group 'i'
C_i	Delayed neutron group 'i'
λ_i	Precursor decay constant of group 'i'
λ_{eff}	$= \frac{\sum \lambda_i {}^2 C_i}{\sum \lambda_i C_i}$, Effective decay constant
ω_s	Desired inverse reactor period
ω_t	Measured inverse reactor period
Λ	Effective generation time

Nuclear and Emerging Technologies for Space
Sponsored by Oak Ridge National Laboratory, April 26th-30th, 2021.
Available online at https://nets2021.ornl.gov

NUCLEAR POWER CONCEPTS FOR HIGH-POWER ELECTRIC PROPULSION MISSIONS TO MARS

Lee Mason[1], Steve Oleson[2], Paul Schmitz[2], Lou Qualls[3], Michael Smith[3], Brian Ade[3], and Jorge Navarro[3]

[1]*NASA Headquarters, Space Technology Mission Directorate*
[2]*NASA Glenn Research Center, COMPASS Team*
[3]*Oak Ridge National Laboratory*

Primary Author Contact: 216-536-5430, lee.s.mason@nasa.gov

Under the Mars Transportation Assessment Study, NASA and DOE are performing analyses and generating concepts for crewed Nuclear Electric Propulsion (NEP) missions to Mars. This paper presents the results of trade studies and concept development for the nuclear electric power system, consisting of the fission reactor, radiation shielding, power conversion, heat rejection and power management & distribution (PMAD). The nuclear power team completed trade studies to evaluate different reactor and power conversion technologies and developed preliminary concepts for the crew shielding, waste heat radiators, and PMAD. The initial results suggest that a modified terrestrial microreactor combined with supercritical CO_2 Brayton conversion could be used to perform the crew and cargo missions with satisfactory performance and modest risk.

I. MARS NEP MISSION CONCEPT

Mission studies conducted by the Glenn Research Center (GRC) COMPASS Team identified the need for a 1.9 MWe power system to perform a 2-year round-trip crewed mission to Mars using a hybrid NEP/chemical propulsion architecture, as shown in Figure 1. The COMPASS studies evaluated multiple crewed mission opportunities spanning 2035 to 2042 that utilize a Low Earth Orbit (LEO) aggregation orbit, un-crewed LEO-to-Near Rectilinear Halo Orbit (NRHO) spiral where the NEP vehicle rendezvouses with the deep-space crew habitat, and 760-day opposition-type round-trip mission that includes a 30-day Mars stay. Additional mission analysis indicated that a duplicate NEP stage, using the same 1.9 MWe nuclear power system and EP thrusters but without the chemical propulsion, could perform pre-crew cargo missions delivering payloads of about 200t to Mars after a LEO spiral and 535-day one-way Mars trip.

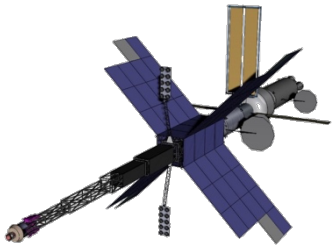

Fig. 1. Hybrid NEP/Chem Vehicle Concept

II. POWER SYSTEM CONCEPT

The reactor cooling method and power conversion choice is a major influence on system design and reliability. Figure 2 presents examples of the design space for reactor heat transfer and power conversion in nuclear fission systems. The three major primary heat transfer methods for space reactors are heat pipes, pumped liquid metal, and pumped gas. Heat pipes work on a passive two-phase evaporation/condensation cycle that requires no external power, while liquid metal or gas cooling requires drive pumps or compressors to circulate the fluid. The benefit of active cooling over passive heat pipes is flexibility in design and higher thermal throughput. Typical liquid metals used in pumped cooling loops are lithium, sodium, potassium, or a mixture of sodium and potassium (NaK). Gas-cooled systems have the option of directly coupling to a Brayton converter, simplifying the reactor heat transport. However, this leads to a single shared gas circuit for the reactor and power conversion, which impacts the system fault tolerance.

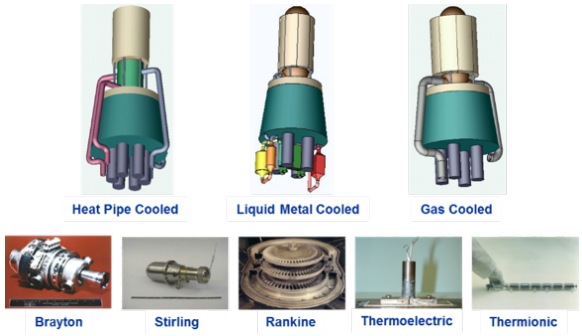

Fig. 2. Potential Reactor-Power Conversion Options

Among the power conversion options are Stirling, Brayton, and Rankine thermodynamic cycles, as well as thermoelectric and thermionic devices. Each option presents different characteristics on conversion efficiency and power throughput, and therefore on the system mass. On the low end of the efficiency scale, thermoelectric conversion has a long history of use in radioisotope power systems. However, the lower efficiency is a challenge for high power fission systems due to the larger reactor, radiation shield, and waste heat radiator. The Stirling cycle has high efficiency but does not scale well to higher power. HeXe Brayton systems fair better at higher power

but the lower heat rejection temperature results in a larger radiator. A supercritical CO_2 (or perhaps other supercritical working fluid) Brayton system may perform better than the HeXe system but that technology has been mainly focused on terrestrial applications. A potassium Rankine cycle has the potential for high efficiency and heat rejection temperature, but the two-phase system design is a challenge and the maturity is low.

Rejecting the power conversion waste heat represents a major design challenge. The vacuum of space requires radiative heat rejection, which is dependent on large, bulky radiators. In fact, the limiting design factor for the reactor power system in this study was the stowed radiator volume that could be accommodated in a single launch vehicle. Preliminary radiator stowage concepts have indicated a maximum radiator area of approximately 2500 m^2 for the 8.4 m Space Launch System (SLS) fairing. The 2500 m^2 radiator limit proved to be the primary design constraint in determining the maximum NEP power output.

Figure 3 shows a parametric analysis of radiator area and system mass across a range of relevant power levels for three different reactor-Brayton combinations. System mass includes the reactor, shield, power conversion, heat rejection and PMAD. Given the 2500 m^2 SLS radiator limit, the 1200 K HeXe case (A) permits 1.6 MWe maximum power output, the 1200 K SCO_2 case (B) permits 1.9 MWe, and the 1500 K HeXe case (C) permits 2.9 MWe. The 1200 K SCO_2 case was selected as the study reference, supplying 1.9 MWe with a total system mass under 25 MT. While the 1500 K case may appear attractive from a performance standpoint, it introduces considerable development risk relative to the other two cases. The 1500 K reactor would require a new fuel form and refractory alloy cladding/structural material beyond what was demonstrated during the SP-100 Program. It would also require new higher-temperature materials for the Brayton converters and radiators beyond the current experience base for those technologies.

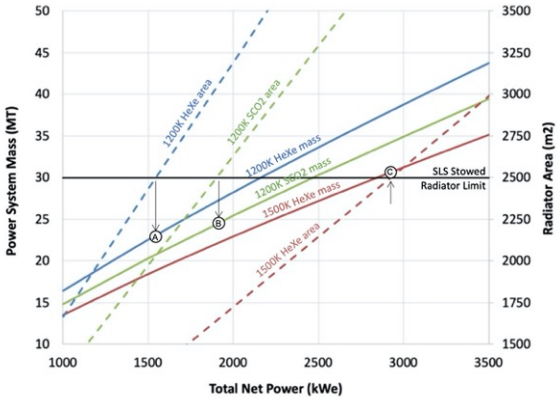

Fig. 3. Parametric System Analysis

II.A. Reactor and Shield Subsystems

The reactor concept in the parametric analysis above assumed a fast-neutron spectrum core with pin-type refractory-clad fuel using Highly Enriched Uranium (HEU). The DOE's Oak Ridge National Laboratory (ORNL) was added to the team to evaluate different reactor design options and fuel enrichment levels. They evaluated two reactor concepts: a) a fast-spectrum SP-100 derived system using UN pin fuel with pumped Li primary heat transport, and b) a derivative of the Transformational Challenge Reactor (TCR) using UN particle fuel in a solid SiC element with interspersed YH moderator. The TCR derivative could use either direct Brayton gas cooling or the primary Li loop, although the Li option was the preferred configuration for this study based on overall system reliability. Both the SP-100 and TCR reactor approaches were evaluated with HEU (93% enrichment) and High-Assay Low Enriched Uranium (HA-LEU, 19.75% enrichment).

The ORNL reactor study assumed a thermal power of 10 MWt, coolant outlet temperature of 1200 K, and operational life of two years at full power. The results showed the SP-100 HEU option to be the lightest mass reactor at approximately 2400 kg including fuel, vessel, reflector, instrumentation & control, and Li primary loop. The LEU version of the fast-spectrum SP-100 reactor was found to be prohibitively heavy. The HEU TCR option with YH moderator had a similar reactor mass as the fast-spectrum HEU SP-100, but the larger reactor diameter resulted a 70% increase in shield mass. The mass of the LEU TCR reactor with YH moderator was about twice the HEU version at 4800 kg and required the heaviest shield because of the large reactor diameter. However, the total 3500 kg mass increase (including the shield) for the LEU TCR option relative to the HEU SP-100 option did not significantly impact the mission design. The LEU TCR reactor shown in Figure 4 was selected as the reference approach for the mission study, with the HEU SP-100 as the study alternative. The 10 MWt thermal power rating provides approximately 40% thermal power margin at 1.9 MWe.

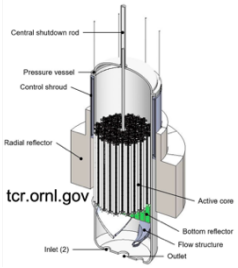

Fig. 4. TCR-Derivative Reactor Concept for NEP

A key challenge for the reactor is to shield the mixed neutron and gamma radiation field. The amount of radiation is directly correlated to the thermal power and

operating duration of the reactor, which adds an additional motivation for high power conversion efficiency. The need for shielding is driven by both electronic and materials tolerance as well as human dose limits for crewed missions. Low-atomic-number materials like hydrogen, beryllium, lithium, and boron provide efficient shielding for the neutron flux, while high-atomic-number materials like tungsten or depleted uranium effectively shield the gamma flux.

For this study, ORNL compared several design variants for their effectiveness in attenuating radiation at three key locations: a) the Brayton units, b) the PMAD electronics, and c) the crew habitat. The starting point was a conical LiH/W shield with a 26 deg half angle that limited radiation to 25 krad and 10^{11} n/cm^2 at 50 m from the reactor (at the PMAD electronics) after two years of reactor operation. Further analysis revealed that this shield design was not sufficient for the crew habitat. Figure 5 presents the four shield configurations evaluated by ORNL. The LiH/W starting point assumed a constant shield thickness for the entire 26 deg half angle. The two compound shields assumed a thicker central section, or "plug" for increased protection of the vehicle centerline elements and crew habitat (within a 3 deg half angle). One of the compound shields assumed a combination of Be/B_4C/LiH/W, while the other assumed only LiH/W. The fourth shield option used LiH/W and retained the central plug but included cutouts in the perimeter to form a cruciform with four 26 deg extensions corresponding with the location of the radiator wings.

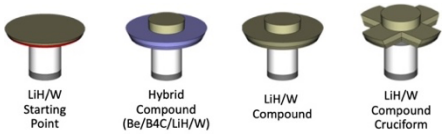

Fig. 5. Shield Options Evaluated

The desire to limit radiation at the crew habitat to 50 rem/yr became the driving requirement for shield mass. The ORNL analysis incorporated the benefits provided by the in-line Brayton engines, reactor boom, PMAD equipment, Xe propellant and tanks in attenuating crew radiation. The mass comparison among the four configurations revealed that the full-thickness LiH/W shield was the heaviest at 13800 kg, followed by the hybrid compound at 4800 kg, the LiH/W compound at 3500 kg and the LiH/W compound cruciform at 2800 kg. The compound cruciform was selected as the design reference, and the corresponding radiation flux maps are presented in Figure 6. This shield results in a total absorbed gamma dose at the Brayton converters and PMAD electronics after two years of operation of 100 Mrad and 25 krad, respectively. The effective human dose at the forward external face of the crew habitat is 3 mrem/hr, corresponding to 100 rem in two years. The total mass of the reference HA-LEU reactor and crew-rated radiation shield is about 7600 kg. The equivalent HEU-version is about 4100 kg.

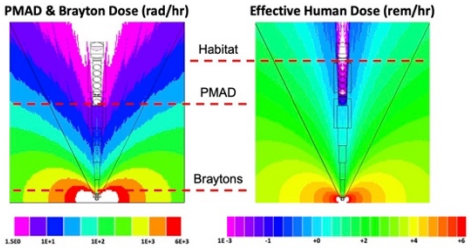

Fig. 6. Radiation Map for Compound Cruciform Shield

II.B. Power Conversion Subsystem

The power conversion trades comparing HeXe and Supercritical CO_2 Brayton favored the SCO_2 option. The SCO_2 option yielded a ~20% increase in power output for the same total radiator area. The reference 1.9 MWe power system concept assumes four SCO_2 Brayton converters each producing 25% of the total power, shown in Figure 7 coupled to the Li-cooled reactor through four liquid-to-gas heat exchangers. The use of a primary loop with separate HXs permits the system to produce partial power should one or more Brayton units fail. Each Brayton unit includes a turboalternator-compressor, recuperator, and gas cooler. The development of a ~500 kWe-class Brayton unit represents a significant scale-up from the experience base for HeXe Brayton technology, represented by the 10 kWe Brayton Rotating Unit (BRU), the 2 kWe mini-BRU, the 36 kWe converter for the Space Station Freedom Solar Dynamic Power Module, and the 100 kWe converter for the Prometheus/Jupiter Icy Moons Orbiter mission. Legacy HeXe Brayton technology, with superalloy hot-side materials that permit turbine inlet temperatures up to 1150 K, has undergone considerable NASA testing to demonstrate performance in relevant environments and for extended operating times (e.g., ~50,000 hours of BRU testing).

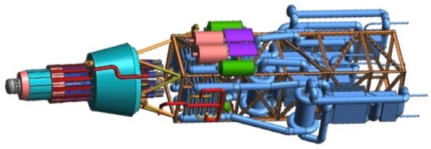

Fig. 7. NEP Reactor-Brayton Configuration

Conversely, SCO_2 Brayton development has focused on MWe-class power levels but has been mostly limited to terrestrial applications with systems that are not designed for space use. If SCO_2 Brayton is pursued for Mars NEP, the emphasis will be on adapting high power terrestrial technology and demonstrating performance in relevant environments. If HeXe Brayton is pursued, the emphasis will be on scaling the legacy technology to higher power levels. The four 500-kWe SCO_2 Brayton converters in the reference concept have a total mass of about 2100 kg.

II.C. Heat Rejection Subsystem

The heat rejection subsystem (HRS) assumes each Brayton converter has a dedicated pumped-NaK cooling loop and a one-fourth segment radiator assembly. The NEP radiators would operate at temperatures between 375 and 550 K and reject about 4 MWt. This temperature regime was studied extensively during the Prometheus and Fission Surface Power projects. Technology development was completed on high temperature Ti/H_2O heat pipes (both life testing and microgravity research), polymer-matrix composite (PMC) radiator panels (both sub-scale and full-scale thermal-vacuum tests), and pumped NaK fluid loops (at temperatures up to 875 K). Leveraging those developments, the NEP radiators use PMC panels with embedded Ti/H_2O heat pipes. The 2500 m^2 total NEP radiator surface is comprised of four radiator segments each having 17 individual radiator panels (~4 m x 5 m) that are coupled to the NaK coolant manifold, as shown in Figure 8 (for comparison, the total radiator area for the International Space Station is about 1200 m^2). The total mass of the NEP HRS concept is about 9500 kg with 68 radiator panels at ~100 kg each.

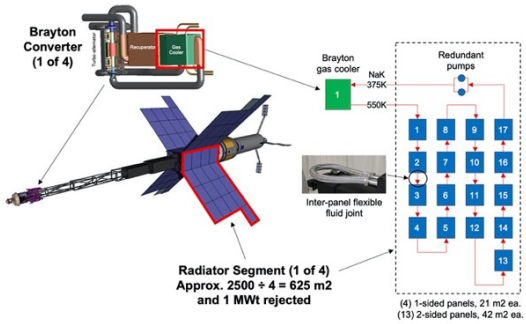

Fig. 8. NEP Radiator Configuration

II.D. PMAD Subsystem

The NEP PMAD electrical schematic is shown in Figure 9. The four Brayton units produce high frequency (~2.5 kHz) 3-phase power at 960 Vac that is transmitted through cables to the PMAD electronics located 50 m away. The power system produces sufficient electric output to power the EP thrusters, spacecraft bus, and system parasitic loads. Each Brayton has a dedicated PMAD channel with a high voltage AC bus that feeds the 650 Vdc Hall thruster direct drive units (DDU) and 120 Vdc spacecraft bus using the appropriate voltage conversion stages. Brayton rotor speed control is accomplished via a pulse-width modulated DC parasitic load radiator (PLR) that maintains a constant load on the alternator. The PLR is sized to reject the entire 500 kWe Brayton output (at 550 deg C) allowing the Brayton units to operate at full power even if there are no external loads. The four PLRs (~30 m^2 each) are located on the perimeter of the truss sections that comprise the reactor boom. The spacecraft receives power from the Brayton units, but also supplies power for startup and control via batteries and solar arrays. Startup power is delivered to a start inverter that allows the Brayton units to be electrically motored. The spacecraft also feeds power to the PMAD controller/processor that manages system operations and distributes DC power to the auxiliary loads (pumps, drive motors, etc.). Each of the four PMAD channels includes a cold plate and dedicated thermal radiator (~20 m^2 each) that rejects 15 kWt (~3%) at 100 deg C. The total PMAD mass for the four channels including cabling, electronics, and thermal management is about 5800 kg.

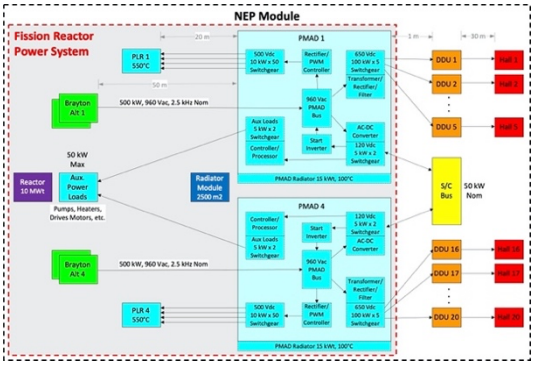

Fig. 9. NEP PMAD Schematic

III. CONCLUSIONS

Trade studies and analyses were performed to produce a nuclear electric power system conceptual design suitable for 1.9 MWe crewed Mars NEP missions. The reference concept uses a modified Li-cooled terrestrial microreactor with HA-LEU fuel, LiH/W crew-rated radiation shield, SCO_2 Brayton power conversion, pumped-NaK heat rejection with composite heat pipe radiators, and 960 Vac PMAD. Key design drivers were the maximum radiator size that could be accommodated in the SLS fairing, the high-voltage EP electrical interface and the crew radiation dose. The reference concept has a total system mass of about 25000 kg (~13 kg/kWe). The use of HEU for the reactor could reduce the system mass by 3500 kg (14%).

REFERENCES

1. J.F. MONDT, "Development Status of the SP-100 Power System," AIAA-89-2591, 25th Joint Propulsion Conference, Monterey CA (1989).
2. J.L. SANZI and D.A JAWORSKE, "Heat Pipes and Heat Rejection Component Testing at NASA Glenn Research Center," NASA/TM-2012-217205 (2012).
3. L.S. MASON, "Dynamic Energy Conversion: Vital Technology for Space Nuclear Power," *Journal of Aerospace Engineering*, Vol 26, Issue 2 (2013).
4. S.R. OLESON, et al., "Mars Opposition Piloted Nuclear Electric Propulsion (NEP)-Chem Vehicle," AIAA 2020-4055, ASCEND 2020, Virtual (2020).

Nuclear and Emerging Technologies for Space
Sponsored by Oak Ridge National Laboratory, April 26th-30th, 2021.
Available online at https://nets2021.ornl.gov

DUAL MODERATOR SPACE REACTOR CORES

Jesus A. Mendoza, Vanessa Linero, Cameron Schade, Jeffrey C. King

Colorado School of Mines, 1500 Illinois St, Golden, CO 80401
jmendoza1@mines.edu, vlinero@mines.edu, cschade@lanl.gov, kingjc@mines.edu

Space reactors fueled with Low Enrichment Uranium will most likely require moderators to reduce the size and mass of the reactor. This paper considers combinations of beryllium, yttrium hydride, and zirconium hydride as moderators for a 250 kW_e fission power reactor. A dual moderated system can include a more thermally favorable material with less effective moderating capabilities near the fuel and a less thermally favorable, but more effective moderator away from the fuel. This arrangement reduces the impact of the less desirable qualities of both materials. The zirconium hydride cases resulted in the highest infinite multiplication factors (above 1.30 in each case). Zirconium hydride is only viable up to 900 K. Yttrium hydride has an upper operating limit of 1173 K. As a sole moderator, yttrium hydride produced an infinite multiplication factor of 1.24715; but, adding beryllium around the coolant channels increased the infinite multiplication factor to 1.24853. This result, along with beryllium's superior thermal conductivity, indicates that a mixed moderator configuration may be more ideal for a high temperature reactor.

I. INTRODUCTION

The desire to establish a permanent lunar presence by 2024 requires a stable orbital transit system from the Earth to the Moon in order to replenish supplies and to transport materials for a lunar base. A cargo transport vehicle using Nuclear Electric Propulsion is one possible solution to this need. Such a vehicle could efficiently transfer cargo and supplies between the Earth and Lunar orbits. The 2019 – 2020 Nuclear Reactor Design course at the Colorado School of Mines considered the design of a reactor to provide 10 years of 250 kW_e steady state electric power for such a spacecraft. The reactor is fueled using low enrichment uranium fuel elements that do not exceed 19.75% uranium-235 by weight. The difficulty of obtaining highly enriched uranium, as well as the proliferation risks associated with the material make the development of a low enrichment uranium system desirable. Section 3 B of Space Policy Directive 6, issued on December 23, 2020, directly states that highly enriched uranium may only be used in space nuclear applications when no other alternative is viable.[1]

This paper considers the combined use of two different moderating materials to reduce the average neutron energy in the core to increase the effective fission cross-section of fuel in the reactor. Previous high temperature reactor designs like the HTRE-3 have considered heterogeneous moderators in the form of core moderators and reflectors.[2] This paper looks at the benefits of heterogeneous moderators within the core. The inclusion of a more thermally favorable material that may be less effective as a moderator with a more effective moderator that may not be as thermally stable can give the benefits of both materials in the reactor core without having to rely on one material that has deficits in either thermal stability or moderation ability. In this scheme, a primary moderator surrounds the fuel pins in the reactor and a secondary moderator surrounds the coolant channels. While this paper only considers macroscopically heterogeneous moderators, other researchers are considering two-phase composite moderators.[3] This paper considers beryllium, yttrium hydride, and zirconium hydride as possible moderating materials. Beryllium has been widely considered as an excellent reflector due to its scattering cross section, as well as having a reaction where it can absorb a neutron and subsequently emit two neutrons[4]. Recent developments in the fabrication of yttrium hydride show that it is possible to fabricate crack-free yttrium hydride with a homogenous hydrogen distribution for use in a reactor.[5] The maximum operating temperatures of beryllium, yttrium hydride, and zirconium hydride are 1560 K[6], 1173 K[7], and 900 K[7], respectively, which make these materials useful as moderators in high temperature reactors. This paper considers the possible combinations of beryllium, yttrium hydride, and zirconium hydride to determine the most effective moderator configuration, based on the thermal hydraulic design limits of the reactor.

II. REACTOR DESIGN

The reactor core, shown in Figure 1 with the corresponding material details in Table I, consists of a hexagonal lattice of fuel pins and coolant channels. The uranium mononitride fuel elements contain uranium enriched to 19.75% uranium-235 by weight and are surrounded by the primary moderator. The coolant channels are surrounded by the secondary moderator. Each fuel pin is adjacent to three coolant channels, and each coolant channel is surrounded by six fuel pins. The reactor power system uses a Brayton cycle power conversion system with helium-xenon gas composition (made up of 78 wt% He and 22 wt% Xe) as the coolant and working fluid. Twelve control drums positioned at the edge of the core control the reactor power by rotating a neutron poison

section in or out. The drums span the height of the core and are made up of beryllium and a 120° section of boron carbide enriched to 95% boron-10 by weight. For this project, the reactor had to be relatively small so that the control systems could reside outside of the reactor and adequately control the reactor's operating conditions without internal moving parts. Determining the k_∞ of the reactor core gave insight for the patterns in k_{eff} of the reactor with regards to the core's inner geometry and materials.

III. OPTIMIZATION MODEL

The Monte Carlo N-Particle (MCNP) version 6.2[10] based optimization simulations determined the optimal system geometry and moderator with respect to the system's neutronics. The MCNP simulations estimated the infinite multiplication factor (k_∞) of the reactor based on a unit cell, shown in Figure 2. The unit cell consists of a coolant channel surrounded by fuel elements with reflective boundary conditions (dashed outline) on all sides except the top and bottom (in and out of the page). In all of the simulations, the coolant channel outer radius and element height stayed constant (1.1 cm and 36 cm, respectively). The moderator around the fuel (the primary moderator) could differ from the moderator around the coolant channels (the secondary moderator).

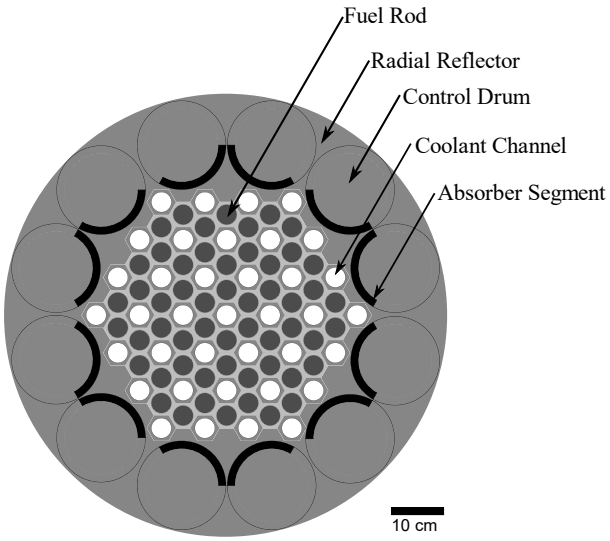

Fig. 1. Axial view of the reactor core.

TABLE I. Material densities of reactor components.

Section	Material	Density (g/cm^3)
Fuel	UN	14.32[8]
Reflector	Be	1.85[6]
Absorber	B_4C	2.38[9]
Coolant Cladding	SS-316	8.00[9]

The optimization simulations considered combinations of metallic beryllium, yttrium hydride (YH_2), and zirconium hydride (ZrH_2) in each moderator position. Zirconium hydride and yttrium hydride used a 1:2 metal-to-hydrogen ratio to have comparable atomic ratios for the metal hydrides, as the thermal scattering libraries for yttrium hydride only apply to that atomic ratio. The optimizations ran in a grid format where a python script wrote an input file with an initial pitch; ran simulations with a fixed set of radii (in increments of 0.05 cm); increased the pitch by 0.05 cm; ran simulations with the same set of radii; and then repeated the process for the next desired pitch value. The specific pitch and radii values for each combination varied in order to have the peak value close to the center of the resulting plot. The peak values provided reactivity information to determine the potential under- and over-moderated configurations of the reactor for thermal feedback considerations.

Each simulation used the ENDF/B-VIII.0 continuous neutron energy libraries evaluated at 293.6 K.[4] The simulations also used the ENDF/B-VIII.0 re-released S(α,β) thermal scattering data evaluated at 294 K for beryllium metal, zirconium hydride, yttrium hydride, and iron-56.[11] The KCODE simulations ran 25 inactive cycles and 200 active cycles running 5×10^4 source neutrons per cycle.

IV. RESULTS AND DISCUSSION

The neutronic analysis of the reactor core looked at different moderator combinations to determine the most effective configuration for this reactor. This analysis also required a look at some of the thermophysical properties of

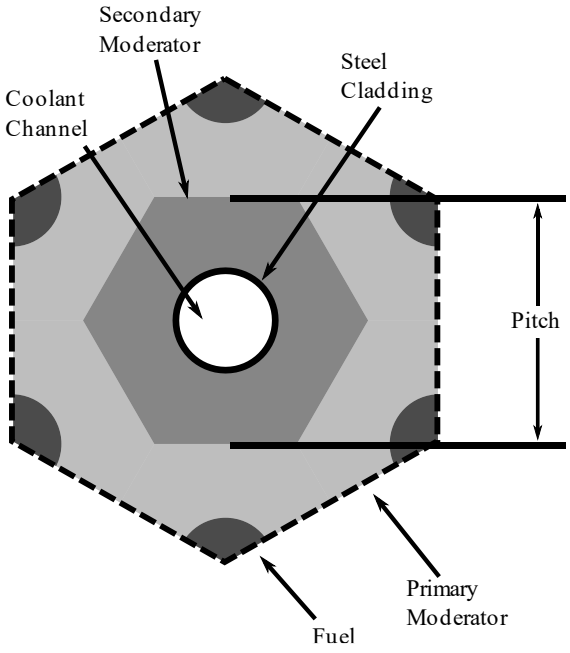

Figure 2. Unit cell used in the optimization simulations.

the moderator to determine which materials are more suitable for high temperature operating conditions. The thermophysical considerations lead to a more comprehensive look at the more notable moderator configurations for a more complete neutronic analysis.

IV.A. General Results

Table II shows the peak infinite multiplication factor (k_∞) values with the corresponding fuel radii and pitch for each moderator combination. This paper uses the notation of "Primary Moderator – Secondary Moderator" to identify the different combinations of primary and secondary moderator. All of the simulations had a 3σ variance of less than 0.00084.

The pure beryllium moderated system did not have radius and pitch values that corresponded to a global maximum. The k_∞ values for the pure beryllium system continuously increased with increasing radii and pitch. The values shown in the table are the maximum values considered since there does not appear to be a global maximum and the all-beryllium configuration with a maximum predicted k_∞ of 1.16182 is not superior to the beryllium-yttrium hydride and beryllium-zirconium hydride configurations with calculated k_∞ values of 1.22902 and 1.28960, respectively.

The yttrium hydride-primary systems show more promise than the beryllium-primary configurations. The mixed yttrium hydride-primary systems produced k_∞ values of 1.24853 and 1.29401 which are both higher than the pure yttrium hydride system that produced a peak k_∞ value of 1.24715. The mixed yttrium hydride-primary systems did have the downside of requiring larger radii and pitch values for their peak k_∞. The more notable dimensional increase was in the pitch values which increased from 3.90 cm for the pure yttrium hydride configuration to 4.45 cm and 4.95 cm for the mixed systems containing zirconium hydride and beryllium, respectively. The macroscopic thermal neutron absorption cross sections for beryllium, yttrium hydride, and zirconium hydride are 0.00245 cm^{-1}, 0.0947 cm^{-1}, 0.0613 cm^{-1}, respectively[4,6,7], which provides an explanation for why the pure yttrium hydride configuration was less effective than the mixed yttrium hydride-primary configurations.

TABLE II. k_∞ values for optimized unit cells with different moderators.

Scenario (Primary – Secondary)	Peak k_∞	Fuel Radius (cm)	Pitch (cm)
Be – Be	1.16182	10.45	21.1
Be – YH_2	1.22902	2.60	5.40
Be – ZrH_2	1.28960	2.60	5.45
YH_2 – Be	1.24853	1.75	4.95
YH_2 – YH_2	1.24715	1.55	3.90
YH_2 – ZrH_2	1.29401	1.95	4.45
ZrH_2 – Be	1.33949	1.20	3.90
ZrH_2 – YH_2	1.30466	1.00	3.05
ZrH_2 – ZrH_2	1.34434	1.15	3.35

The zirconium hydride-primary scenarios provided a higher k_∞ than the other configurations, showing that zirconium hydride is a more effective moderator than beryllium or yttrium hydride. The results in the table are consistent with zirconium hydride's higher theoretical hydrogen density (7.3 atoms/b-cm compared to 5.8 atoms/b-cm for yttrium hydride), zirconium hydride's lower absorption cross section, and the better moderating capabilities of hydrogen compared to beryllium.[12]

IV.B. Thermophysical Considerations

The choice for which moderators to use is not only governed by the neutronics properties. The thermophysical properties of the moderators must also be considered to fully decide which materials are better suited for high temperature reactors. Zirconium hydride starts to dissociate at around 900 K[7] which is less ideal; but, with a lower power reactor, the thermal hydraulic conditions become less of an issue. Lower power reactors can provide an opportunity for the use of an yttrium hydride-zirconium hydride configuration or any of the zirconium hydride primary systems.

As temperatures in a reactor increase, less effective but more thermally stable moderators are more desirable. The inclusion of one moderator that is more thermally favorable and another that is less thermally favorable but more effective as a moderator can result in a more optimal reactor. The yttrium hydride-beryllium mixed moderator system has the moderating capabilities of yttrium hydride and the benefit of the thermophysical properties of beryllium. Due to beryllium's melting point and thermal conductivity (1560 K[6] and 103 W/m-K[13]) surpassing yttrium hydride's hydrogen disassociation temperature and thermal conductivity (1173 K[7] and 45 W/m-K[14]), the yttrium hydride-beryllium scenario is the more favorable configuration.

IV.C. Optimal Configurations

Figures 3, 4, and 5 display the results of the optimization simulations for the beryllium-yttrium hydride, pure yttrium hydride, and the yttrium hydride-beryllium configurations, respectively. The dashed line represents the maximum k_∞ value for each pitch with an "o" marking the location of the peak value in the plot. The gray shaded area represents the section of the plot where the radius of the fuel would be greater than the pitch, which is not geometrically feasible. In Figures 3, 4, and 5, the under-moderated region is above and to the left of the dashed line since that region is where there is less than the ideal moderator content. In each case, increasing the fuel

radius decreased the primary moderator content and decreasing the pitch decreased total moderator content. It is important for a reactor to be under-moderated to have a negative thermal feedback coefficient. As the temperature increases, the moderator density decreases reducing the overall moderator and decreasing the reactivity of the reactor. An over-moderated system results in a positive thermal feedback coefficient where the decreased moderator content (from an increase in temperature) increases the effectiveness of the moderator. This increased effectiveness increases the reactivity of the reactor, increasing the power, and increasing the temperature leading to a potentially out-of-control reactor.

Figure 3 shows the simulation set with beryllium as the primary moderator and yttrium hydride as the secondary moderator. In this configuration, there appears to be no under-moderated region. This was the case in all three scenarios with beryllium surrounding the fuel. The simulations with a homogeneous beryllium moderator produced a k_∞ that increased as the reactor elements got larger. As a result, there appears to be no system with beryllium surrounding the fuel that would have a negative thermal feedback coefficient.

Figures 4 and 5 show the other two configurations of main interest. Each configuration has yttrium hydride surrounding the fuel with either yttrium hydride or beryllium surrounding the coolant channels. Both scenarios, as well as the scenarios with zirconium hydride surrounding the fuel, have under- and over-moderated regions. Figure 5 shows a larger under-moderated region than Figure 4. The inclusion of a larger under-moderated region is favorable in order to have a larger range of values for the thermal hydraulic considerations where it may be more ideal to have more fuel for a smaller power density leading to a lower moderator temperature.

V. SUMMARY AND CONCLUSIONS

A moderated low enrichment uranium fueled reactor could feasibly power a cargo spacecraft using nuclear electric propulsion in order to efficiently transfer cargo and supplies between the Earth and Lunar orbits for a lunar base. This paper considered the use of a reactor core containing two different moderators. The neutronic analysis analyzed combinations of moderators to determine the most effective moderator combination for such a spacecraft when also considering the thermophysical properties of the moderators.

A combination of different moderators around the fuel and coolant channels can lead to more desirable operating conditions than possible with a single moderator. Zirconium hydride around the fuel yields the highest k_∞ values (all of which are greater than 1.3), with pure zirconium hydride being the optimal configuration at a k_∞ of 1.34434; however, the hydrogen dissociation temperature of zirconium hydride will limit the reactor

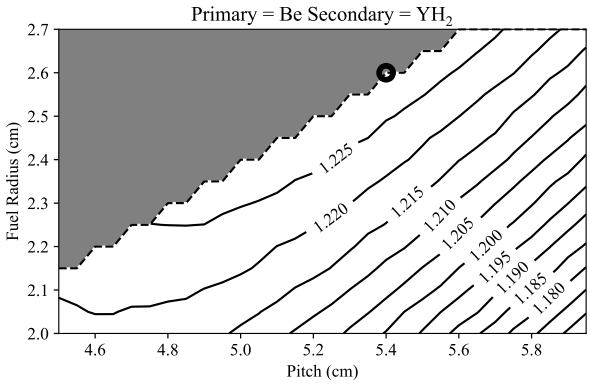

Fig. 3. Optimization results for the beryllium-yttrium hydride configuration.

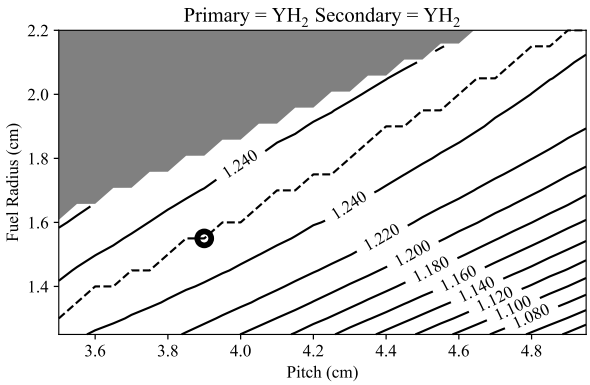

Fig. 4. Optimization results for the pure yttrium hydride configuration.

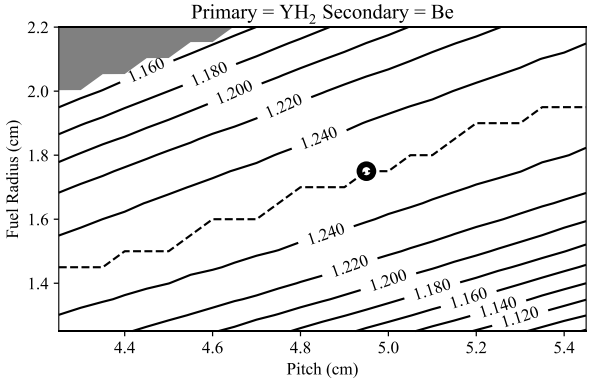

Fig. 5. Optimization results for the yttrium hydride-beryllium configuration.

operation temperature to less than 900 K. Beryllium and yttrium hydride are better suited for reactor operations above 900 K and can provide favorable neutronic conditions. Configurations with beryllium around the fuel did not produce useful results since they provided no under-moderated geometries and would be expected to have a positive temperature feedback coefficient. The configurations with yttrium hydride around the fuel resulted in useful under-moderated geometries. Adding beryllium around the coolant channels with yttrium hydride around the fuel produced the highest k_∞ (1.24853), compared to a pure yttrium hydride moderated system which only reached a k_∞ of 1.24715.

The thermophysical properties of the moderators suggested the use of beryllium and yttrium hydride in the system in order to tolerate operating temperatures greater than the 900 K limit imposed by zirconium hydride. Yttrium hydride's neutronic performance makes it more favorable than beryllium when considering the moderating material around the fuel, since no beryllium – primary system produced an under-moderated geometry. Beryllium's thermal conductivity of 103 W/m-K is more favorable than yttrium hydride's thermal conductivity of 45 W/m-K. Beryllium's thermal performance and the performance of the yttrium hydride-beryllium mixed moderator configuration indicate that the inclusion of beryllium in the reactor is desirable for high temperature operating conditions.

REFERENCES

1. "Posting of the Presidential Policy Directive 6 (Space Policy), 'National Strategy for Space Nuclear Power and Propulsion,'" *Federal Register*, **85**, no. 247, 83923-83927 (2020).
2. "Summary of Report of the HTRE No. 3 Nuclear Excursion", APEX-509, Cincinnati, OH, 1965.
3. E. M. DUCHNOWSKI, R. F. KILE, J. R. TRELEWICZ, and N. R. BROWN, "Reactor Performance and Safety Characteristics of Two-Phase Composite Moderator Concepts for Modular High Temperature Gas Cooled Reactors," *Nuclear Engineering and Design*, **368**, 110824 (2020). DOI:10.1016/j.nucengdes.2020.110824.
4. D. A. BROWN, M. B. CHADWICK, R. CAPOTE, et al., "ENDF/B-VIII.0: The 8th Major Release of the Nuclear Reaction Data Library with CIELO-project Cross Sections, New Standards and Thermal Scattering Data", *Nuclear Data Sheets*, **148**, 1-142 (2018). DOI:10.1016/j.nds.2018.02.001.
5. X. HU, D. SCHAPPEL, C. M. SILVA, and K. A. TERRANI, "Fabrication of Yttrium Hydride for High-Temperature Moderator Application," *Journal of Nuclear Materials*, **539**, 152335 (2020). DOI:10.1016/j.jnucmat.2020.152335.
6. V. Y. BODRYAKOV, "Joint Study of Temperature Dependences of Thermal Expansion and Heat Capacity of Solid Beryllium," *High Temperature*, **56**, 185-192 (2018). DOI:10.1134/S0018151X18020049.
7. J. L. ANDERSON, W. MAYO, and E. LANTZ, "Reactivity Control of Fast-Spectrum Reactors by Reversible Hydriding of Yttrium Zones," NASA TN-D-4615, Lewis Research Center, Cleveland, Ohio, 1968.
8. S. L. HAYES, J. K. THOMAS, and K. L. PEDDICORD, "Material Property Correlations for Uranium Mononitride," *Journal of Nuclear Materials*, **171**, 262-318 (1990), DOI:0.1016/0022-3115(90)90374-V.
9. R. J. MCCONN JR, R. J. GESH, R. T. PAGH, R. A. RUCKER, and R. G. WILLIAMS III, "Compendium of Material Composition Data for Radiation Transport Modeling," PIET-43741-TM-963 PNNL-15870 Rev. 1, Richland, WA, 2011.
10. C. J. WERNER, J. S. BULL, C. J. SOLOMON, et al., "MCNP Version 6.2 Release Notes," LA-UR-18-20808, Los Alamos, NM, 2018, DOI:10.2172/1419730.
11. D. K. PARSONS and C. A. TOCCOLI, "Re-Release of the ENDF/B VIII.0 S(α,β) Data Processed by NJOY2016," LA-UR-20-24456, Los Alamos, NM, 2020.
12. R. VAN HOUTEN, "Selected Engineering and Fabrication Aspects of Nuclear Metal Hydrides (Li, Ti, Zr, and Y)," *Nuclear Engineering and Design*, **31**, 434-448 (1974). DOI:10.1016/0029-5493(75)90178-8.
13. J. J. G. HSIA and G. C. Y. WANG, *Thermophysical Properties of High Temp. Solid Materials Vol. 1*, pp. 55, The Macmillan Company, New York, NY (1967).
14. M. ITO, J. MATSUNAGA, D. SETOYAMA, H. MUTA, K. KUROSAKI, M. UNO, and S. YAMANAKA, "Thermal Properties of Yttrium Hydride," *Journal of Nuclear Materials*, **344**, 295-297 (2005). DOI:10.1016/j.jnucmat.2005.04.058.

Nuclear and Emerging Technologies for Space
Sponsored by Oak Ridge National Laboratory, April 26th-30th, 2021.
Available online at https://nets2021.ornl.gov

NUCLEAR THERMAL PROPUSLION IMMEDIATE XENON RESTART THRESHOLD FOR SHORT BURN DURATIONS

Mario Mendoza[1]

[1]*USNC-Tech, 2356 W Commodore Way Unit 120, Seattle, WA, 98199*

281-726-9656 | m.mendoza@usnc-tech.com

For nuclear thermal propulsion systems, the concentration of xenon in the core produced during operations reduces the reactivity in the system and can prevent the reactor from restarting for subsequent burns if not enough time has elapsed to allow for the xenon to decay. Since the amount of xenon produced is dependent on power and time of operation in this application, different burn durations require different lengths of minimum wait-time. By analyzing the maximum xenon negative reactivity insertion after different burn durations, an immediate restart threshold was developed for immediate reactor restarts for extraneous situations not included in mission plans. An NTP burn less than the immediate restart threshold (42.19 min in this case) can afford an immediate second cycle without dropping its k_{eff} below 1 after the second burn. For any burn duration longer than the immediate restart threshold, the same required wait-time between burns will produce sustainable cycles.

I. INTRODUCTION

Nuclear thermal propulsion (NTP) rockets are a proven technology that provide an attractive alternative to conventional chemical rockets for space travel due to their high specific impulse, high thrust, its lower initial mass in Low Earth Orbit (LEO), and higher tolerance to payload mass growth (Ref. 1). In fact, NTP rockets have been identified as the preferred flight method for Mars Transit Vehicles (MTV) (Ref. 2). NTP systems achieve propulsion by passing a propellant (hydrogen) through a nuclear reactor core where it absorbs heat from fissioning ^{235}U atoms and is then expanded through a nozzle to produce thrust. Although different designs exist for NTP cores, USNC-Tech is exploring a thermal spectrum core with High Assay Low Enriched Uranium (HALEU). Even though low-enriched fuel presents higher technology readiness levels and lower nuclear proliferation concerns, it can cause the reactor core to be more susceptible to negative reactivity effects from fission products produced during operations. The presence of some fission products in the core, specifically ^{135}Xe, can prevent the core from reaching criticality depending on concentration levels.

Typical NTP Mars missions, like the NASA Design Reference Architecture 5.0, involve burning the NTP core for durations of 60 minutes or less with multiple days or months between each burn (Ref. 1,2,3,4). Operating a reactor within this regime typically avoids running into any negative reactivity effects from ^{135}Xe buildup. However, this paper presents the concept of the immediate xenon restart threshold for second burns to help mission designers plan for emergency events or difficult rendezvous and docking maneuvers. If the core is burned for a duration below the threshold, it can afford an immediate restart for a burn of a similar duration while maintaining a k_{eff} end-of-cycle greater than or equal to critical for the second cycle. Any initial burn durations longer than the threshold, however, must have a minimum wait-time before ensuring that a second burn will not experience negative feedback from xenon.

I.A. Theory: Xenon Reactivity Feedback

During fission reactions in a reactor core, ^{235}U atoms reach an excited state when absorbing neutrons and subsequently decay by fission into two lighter isotopes, or fission products, as well as neutrons, gammas, and other types of radiation. It is then that these neutrons born from fission induce other fission reactions in the fuel to maintain a chain reaction and keep the reactor operational. Each new fission in the system not only produces more neutrons, but they also produce more fission products. These fission products stay within the core and interact with neutrons until they are transmutated or decayed. The fission product of greatest importance for reactor operations on the order of NTP burn durations is ^{135}Xe. Eq. (1) below shows the typical production and destruction rates of ^{135}Xe in a reactor where $N_{Xe}(\vec{r},t)$ is the atom density of ^{135}Xe in the core, $\Sigma_f(\vec{r},E,t)$ is the fission cross-section of ^{235}U, $\varphi(\vec{r},E,t)$ is the neutron flux in the core, $N_I(\vec{r},t)$ is the atom density of ^{135}I, λ_I and λ_{Xe} are the decay constants of ^{135}I and ^{135}Xe, $y_{Xe}(E)$ is the yield for ^{135}Xe from fission, and $\sigma_{Xe}^{a}(\vec{r},E,t)$ is the absorption cross-section for ^{135}Xe (Ref. 5).

$$\frac{dN_{Xe}(\vec{r},t)}{dt} = \Sigma_f(\vec{r},E,t)\varphi(\vec{r},E,t)y_{Xe}(E) + \lambda_I N_I(\vec{r},t) - \lambda_{Xe}N_{Xe}(\vec{r},t) - N_{Xe}(\vec{r},t)\sigma_{Xe}^{a}(\vec{r},E,t)\varphi(\vec{r},E,t) \quad (1)$$

As can be seen above, ^{135}Xe is created from fission and the decay of ^{135}I (another fission product) and is destroyed through neutron absorption and decay. As a reactor core operates and fissions keep occurring, the concentration of xenon keeps building up until an equilibrium concentration is reached. It's not until the reactor is shutdown that the

production ^{135}I and ^{135}Xe halt that the concentration of ^{135}Xe begins to fall. It is important to keep track of xenon concentrations for reactor operations because of its enormous absorption cross-section of $2.7 * 10^6$ barns for thermal neutrons, causing a negative reactivity feedback (Ref. 5). Eq. 1 above only serves as a description of how xenon is created or destroyed within a reactor. The effects of xenon in this paper were calculated by measuring the effective multiplication factor throughout different burn simulations using the Monte-Carlo based code, Serpent (Ref. 6).

II. Analysis Setup

The analysis for the xenon restart threshold was completed on an NTP core designed by USNC-Tech for a NASA flight demonstration study (Ref. 7). One of the goals for the flight demonstration study was to develop an NTP core which could have multiple restarts of 5, 20, and 60-minute burns. The NTP core was designed with 19.75% enriched uranium in the form of USNC's patented Fully Ceramic Microencapsulated (FCM™) fuel. The core also utilized a solid beryllium moderator and control drums within the radial reflector region. The NTP core operates at a 180 MW_{th} power level.

III. Initial Lifetime Calculations

An initial burnup analysis for the core at full power nominal operating conditions was completed to analyze the core's criticality for a 2-hour long burn. The core was simulated at 8 different time steps, 15 min apart starting at 0 hours and finishing at 2 hours. The overall change in reactivity throughout the core is represented in units of percent mille (pcm) of reactivity and can be seen in Figure 1. The core produced a beginning-of-life k_{eff} of 1.03158 and underwent a total 655 pcm change in reactivity throughout the 2-hour life cycle.

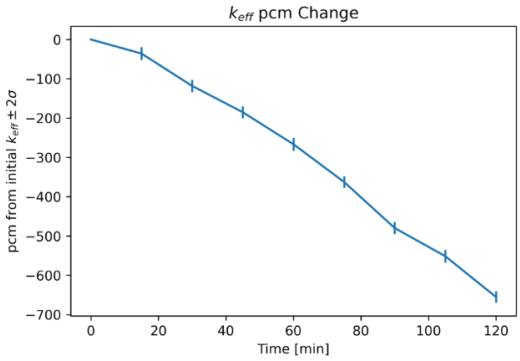

Fig. 1. Total reactivity change for a 2-hour burn.

As is evident, the core's criticality decreases as it burns. To analyze the impact of xenon on the loss of reactivity compared to other fission products, an NTP core was modeled during another 2-hour burn while setting the xenon concentration to zero at each step. By eliminating xenon from the core, the reactivity effects from other fission products and fuel depletion can be observed. As is seen in Figure 2, it was found that during the 2-hour burn without xenon present, the k_{eff} of the core stayed the same, within error, throughout the core lifetime. Therefore, the change in reactivity within the NTP core during operation can be approximated to be due entirely to the buildup of xenon concentrations. Reactivity changes due to other fission products, like samarium, are negligible during the 2-hour maximum burn of the reactor.

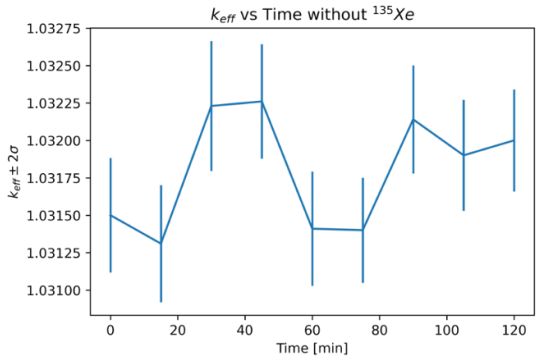

Fig. 2. The k_{eff} during a 2-hour burn with zero xenon.

IV. Immediate Restart Threshold

Once an NTP core completes a burn cycle, depending on the concentration levels of xenon at shutdown, the removal of control systems might not overcome the xenon reactivity effects. Therefore, a certain period of time must elapse for the xenon concentration to decrease through decay. For this analysis, the restart capabilities for three different burn scenarios of 5, 20, and 60 minutes at full power for a flight demonstration were studied. The core was simulated for each burn length at full power for the duration of operations, followed by two days of the NTP core at zero power, representing a reactor shutdown. This type of analysis demonstrates xenon's effect on the core's reactivity as its concentration builds up after shutdown and then decays. Figure 3 shows the k_{eff} after 5, 20, and 60-minute burns. For all three types of burn lengths, the xenon concentration in the core had a significant effect on the k_{eff} soon after the reactor is shut down. Also, as was expected, the negative xenon worth in the core increased with burn duration since equilibrium concentrations are not reached at these short burn durations.

As can be seen from Figure 3, the k_{eff} manages to stay above 1 after each of the three burn durations. This means that the impacts of the negative xenon reactivity effects are not large enough to prevent a restart of the core at any moment after shutdown of the first cycle. However, an immediate restart is not always appropriate. For example, the maximum xenon worth that the reactor experiences after a 60-min burn is around -2000 pcm. The reactor could theoretically restart for another 60-min cycle at any moment after its first shutdown, but a second cycle will add an additional -2000 pcm of total reactivity. If enough xenon

is still present in the core, a second cycle will cause the reactor to drop well below critical after that cycle and prevent a third reactor startup until after all the xenon has decayed. For this reason, a reactor must wait to restart once its xenon concentration is low enough that a second cycle will not cause the reactor to drop below critical after a new cycle from the new xenon buildup. Waiting this necessary period of time assures that the reactor will always have enough reactivity at full power to facilitate operations in a neutronic and thermohydraulic sense for multiple cycles in certain emergency or rendezvous and docking situations.

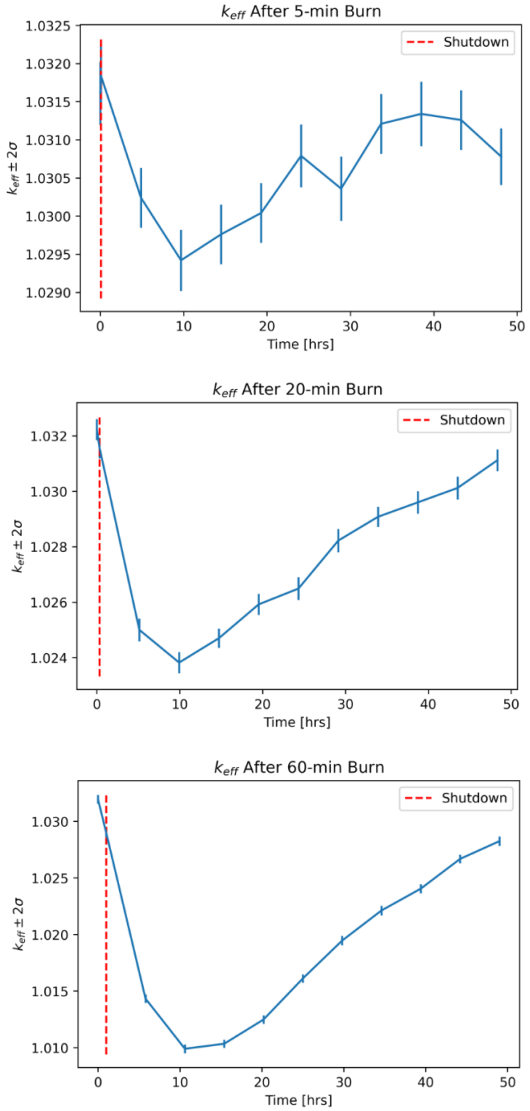

Fig. 3. The k_{eff} for two days after a 5 (top), 20 (middle), and 60-min (bottom) burn.

To calculate the NTP wait-times, the maximum xenon worth for each separate burn duration was subtracted from their k_{eff}'s, simulating the total reactivity effect from an immediate second cycle. The time it takes for this new, reduced k_{eff} to reach criticality due to xenon decay is the total wait-time needed for a second reactor startup. Waiting until the new k_{eff} reaches criticality ensures the k_{eff} of the system does not drop below 1 after the end of second cycle. In Figure 4, it is seen that a second startup after a 5 or 20-minute burn does not require a wait-time, while a 60-minute burn requires a wait-time of 32.24 hours after shutdown.

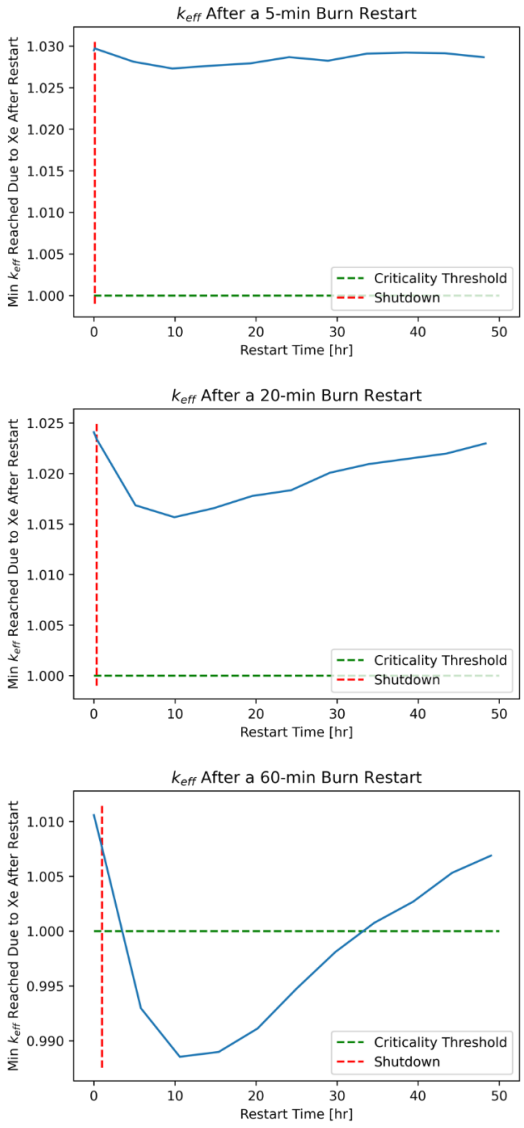

Fig. 4. The minimum k_{eff} of the system when maximum xenon worth is reached after a second core start-up after waiting a certain restart time for a 5 (top), 20 (middle), and 60-min (bottom) burn.

Since the minimum k_{eff} reached after a second cycle for the 5 and 20-min burns never drops below 1, the reactor will still have favorable reactivity conditions after a second cycle, so it can afford to restart immediately after shutdown of the first cycle. After comparing the difference in restart times between the burn durations, an immediate restart threshold can be defined, as seen in Figure 5. Any burn

durations producing a xenon worth above the threshold line in the figure can afford a successful restart at any time after first shutdown. In other words, any reactor burn time of 42.19 min or less does not require a waiting periods before its second reactor startup. For burn durations to the right of the intersection, a certain amount of wait-time must pass before a core restart at full power.

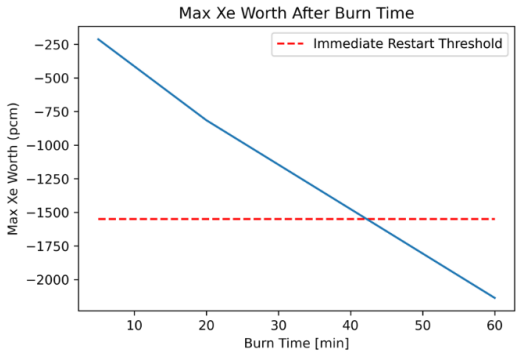

Fig. 5. The maximum xenon worth reached after a single burn duration.

It is important to note that an immediate restart for those burn times which can afford it are only for a second cycle, and to ensure criticality does not drop below 1 after said cycle. If the reactor underwent a third, immediate 20-minute burn cycle, for example, the xenon concentration after three consecutive 20-minute cycles will resemble the concentration after a continuous 60-minute burn. In which case, a wait time like that of a 60-minute burn is required before a fourth startup. Further analysis is needed for determining the negative xenon effects after multiple subsequent cycles for burn durations under the immediate restart-time threshold. However, for any burn duration longer than the immediate restart threshold, the same required minimum wait-time between burns can produce sustainable cycles. In this context, sustainable cycles are those which produce similar start and end k_{eff}'s while waiting the same amount of time between each cycle. As was mentioned, however, typical Mars missions do not require multiple subsequent NTP core burns immediately after each other or after the minimum wait times. The immediate restart threshold displayed in Figure 5 presents mission planners with burn duration options for possible emergency situations without jeopardizing the core's reactivity levels after those maneuvers.

III. CONCLUSIONS

Typical Mars mission plans include burns at specific durations and intervals that are not necessarily affected by the negative reactivity effects of fission products from a previous reactor burn. In the case of emergency situations or difficult rendezvous and docking maneuvers, it may be required for an NTP core to experience multiple subsequent burns within a short period of time. This paper presented the idea of an immediate restart threshold to inform mission designers in such scenarios. If the core is burned for a duration below the threshold, it can afford an immediate restart for a burn of a similar duration while maintaining a k_{eff} end-of-cycle greater than or equal to critical for the second cycle. Any initial burn durations longer than the threshold, however, must have a minimum wait-time before ensuring that a second burn will not experience negative feedback from xenon. For the NTP core analyzed in this work, as designed by USNC-Tech for a NASA flight demonstration program at a power of 180 MW_{th}, the immediate restart threshold is at a burn duration of 42.19 min.

ACKNOWLEDGMENTS

I'd like to thank my colleagues at USNC-Tech for all their help.

REFERENCES

1. S. K. BOROWSKI, D. R. McCURDY and T. W. PACKARD, "Nuclear Thermal Propulsion (NTP): A proven growth technology for human NEO/Mars exploration missions," *2012 IEEE Aerospace Conference*, Big Sky, MT, USA, 2012, pp. 1-20, doi: 10.1109/AERO.2012.6187301.
2. "Human Exploration of Mars Design Reference Architecture 5.0", B. G. DRAKE, ed., National Aeronautics and Space Administration, NASA-SP2009-566, Washington, DC, July 2009.
3. S. K. BOROWSKI, D. R. McCURDY and T. W. PACKARD, "7-Launch NTR Space Transportation System for NASA's Mars Design Reference Architecture (DRA) 5.0", AIAA-2009-5308, August 2009.
4. M. J. EADES and J. A. CAFFREY, "Time Dependence of Fission Energy Deposition in Nuclear Thermal Rockets," Proc. Nuclear & Emerging Technologies for Space, Albuquerque, New Mexico, February 23–26, 2015, p. 260, (2015)
5. P. TSVETKOV, "9. Core Composition Changes during Reactor Operation", NUEN 601 Reactor Theory Lecture Notes, Texas A&M University (2020).
6. J. LEPPÄNEN, et. al, "The Serpent Monte Carlo Code: Status, Development and Applications in 2013," Joint International Conference on Supercomputing in Nuclear Applications and Monte Carlo, p. 06021, EDP Sciences (2014).
7. Ultra Safe Nuclear Technologies, "Ultra Safe Nuclear Technologies Delivers Advanced Nuclear Thermal Propulsion Design to NASA", 19 Oct 2020; https://usnc.com/ (current as of 1 Feb).

Nuclear and Emerging Technologies for Space
Sponsored by Oak Ridge National Laboratory, April 26th-30th, 2021.
Available online at https://nets2021.ornl.gov

IN-SITU ALTERNATIVE PROPELLANTS FOR NUCLEAR THERMAL PROPULSION

Dennis Nikitaev[1] and L. Dale Thomas[1]

[1]*University of Alabama in Huntsville*

Primary Author Contact Information: 702-287-6852 dn0038@uah.edu

Nuclear Thermal Propulsion (NTP) produces heat by nuclear fission allowing any fluid to function as a propellant if it does not degrade the reactor materials. Liquid hydrogen is commonly considered due to its low molecular weight yielding a high specific impulse (Isp) of up to 900 seconds. However, its density is 7% that of water and increases the dry mass of the vehicle to store it. There are two alternative propellants, water, and ammonia, that are abundant resources in the Solar System, and both are much denser than liquid hydrogen and do not require post processing, such as electrolysis, to be used directly.

At the temperatures found inside the NTP reactor, water will oxidize most materials. Recent work on silicon carbide coatings of water reactors has shown that during reactor accidents, this coating will protect the fuel up to 100-200 hours at temperatures up to 2273 K. Therefore, if a silicon carbide coating is used, then it will allow the engine to operate between 100 to 200 hours, much longer than there is uranium in a low-enriched uranium reactor to support engine operation. Ammonia, on the other hand, is not expected to cause any significant reactor degradation due to its slow kinetics.

NTP expander cycle engine models of 25,000 lbf thrust class were constructed in Simulink which yielded a Isp of 336 seconds for water and 388 seconds for ammonia. Although this Isp is lower than the most efficient chemical engines, since pure water and ammonia are used directly and are stored as such, a propellant tank volume decrease of up to 75% for water and 69% for ammonia are possible. This will decrease the number of launches, given that the tanks are not fully fueled at time of launch and Lunar resources are used to fill the tanks completely.

I. WATER

Water will be an abundant resource in space once the mining of it on the Moon becomes established. Water contains oxygen and hydrogen which can both be used as rocket propellant. Water can also be easily stored in space with no boil off and kept in liquid form.[1] However, chemical rocket engines cannot directly use water as the propellant without it undergoing splitting such as thermolysis (splitting by high temperature) or electrolysis (splitting by electricity). The splitting of any molecule requires delivering energy in the form of either electricity or heat equivalent to the Gibbs free energy of the molecule. However, Nuclear thermal Propulsion (NTP) can use any fluid as the propellant provided that chemical reactions between the propellant and the reactor do not occur or are negligible to the integrity of the engine.

A Cornell University study has shown that rapid electrolysis (splitting water at the same rate as required by the propulsion system which is in kg/s) could be achieved via pulsing where a capacitor stores enough energy to generate a large pulse of electricity to split water equivalent to that of the required (pulsed) flow rate. The Cornell study mentions that rapid electrolysis is much slower than the combustion process and the specific impulse (Isp) in chemical engines suffers from this if pulsing is not used. However, it was assumed that all the electrical power delivered to the system would come from solar arrays and the attempt to lower the mass of these arrays played a factor in the engine performance. The Cornell study also conducted a performance analysis where water would be split during coasting periods and the oxygen and hydrogen would be stored in separate tanks to allow for more control over the combustion process.[2]

It is well known that the process of electrolysis becomes highly efficient at high temperatures in terms of the electrical energy supplied and the electrical energy (that splits the water molecule) equivalent to water's Gibbs free energy[3]. Furthermore, the Gibbs free energy decreases as temperatures rise[4]. The current study will focus on Aerojet Rocketdyne's (AR) nuclear thermal propulsion (NTP) engine[5] as a baseline and will modify it to use water as the propellant. The goal will be to develop a Steam Nuclear Thermal Propulsion (SNTP) engine model in Simulink like that of the UAH NTP Simulink model[6] and analyze both steady state and transient vehicle performance. The baseline mission architectures will be AR's conjunction[7] and opposition[8] class crewed Mars missions. Furthermore, performance comparisons will be made for vehicles using the following propulsion propellants: baseline pure hydrogen[5], seeded hydrogen[9], steam, water (with slow electrolysis), oxygen augmented NTP, and chemical propulsion[2].

To generate comparable thrust to the baseline Aerojet Rocketdyne (AR) Low Enriched Uranium (LEU) NTP engine of 25,000 lbf, the mass flow rate of water would need to be between 26 and 35 kg/s depending on the Isp. This translates to around 175-200 MWe required to completely split the water which could be achievable with turbomachinery if the pump pressurized the water in the

GPa range and the turbine pressure ratio resulted in a turbine output pressure of around 10 MPa or 100 atm. The mass of such a pump or a series of pumps would be at least that of the engine based on historical relations[5,10]. Partial splitting that is also useable is an option with a required pump output pressure of at least 150 MPa or roughly 1500 atm which could produce electrical power levels in the vicinity of 40 MWe for which electrical generators currently exist[11]. However, despite being able to produce this amount of electrical power, the size of the electrolyzer would be that of a large plant for a single engine with current technology. This is because state of the art electrolysis plants can only produce 0.04 kg/s of hydrogen from water[12] whereas a usable electrolyzer for a NTP engine would have to produce at least ten times that amount. All of this results in that although thermodynamically possible, current electrolyzer technologies would have to be scaled down thousands of times to be useable for NTP engine applications.

If electrolysis is not used, then the reactor would need to make up the lost Isp with temperature gain. To produce a Isp of 420 seconds without electrolysis, the required reactor outlet temperature would have to be 3500 K, just under the melting point of tungsten and above melting points of current nuclear fuels[13]. Furthermore, all metals except beryllium react with water[14] by oxidization at temperatures above 800-1200 K[15-17]. Therefore, even liquid fuel elements would be at risk due to the oxidization of the structure supporting the fissioning liquid core. Furthermore, if a bare fuel were used, specifically the commonly considered uranium dioxide UO2, even though it is still oxidized, oxidation will still be an issue since oxygen tends to diffuse into uranium dioxide and form U3O8 which will degrade the fuel element at very high temperatures[18]. Therefore, a coating or cladding material is essential for a steam NTP engine. An excellent candidate is silicon carbide SiC which has shown to be resistant to oxidization and can protect the fuel underneath for 100-200 hours at a surface temperature of 2473 K[19-22], therefore, a Isp above 400 seconds will not be possible with existing materials.

Due to the purpose of using water as a propellant and its high density, a Isp of at least 300 seconds should be acceptable[23]. To produce this Isp, the exit temperature of the reactor would have to be 2000 K which should be within the capabilities of the SiC cladding. In comparison with AR's LEU NTP baseline engine, the reactor exit temperature was 2650 K and a maximum surface temperature was 2750 K[5]. Based on this, it is reasonable to expect that the maximum possible exit temperature of the steam should be around 2350 K which will produce a Isp of 336 seconds.

The advantage of using water for a Mars mission was shown by using the Tsiolkovsky's ideal rocket equation. The AR's conjunction class mission[7] vehicle parameters used in the analysis included the ΔV schedule, vehicle mass, propellant mass, and propellant volume along with the respective storage densities of liquid hydrogen and water. It was found that for water to achieve the same ΔV performance while assuming a 300 second Isp, the required volume would be 26% that of liquid hydrogen. This is, in fact, less than the volume of a single inline stage tank of AR's conjunction class vehicle architecture[7]. Other studies have shown the same level of advantages, especially when considering using distilled water obtained from In-SITU resources. Although many studies have looked at 1st order performance of a steam NTP engine and even performed mass analysis, no study currently exists which shows a detailed power balance and considers duct and line pressure losses with variable fluid properties.[1,2,24-26] There is also no work currently available for an expander cycle which involves using all the stored water without it being dumped after the turbine. An analysis such as this will help further understand how a steam NTP engine will operate and identify areas where current research and technology are lacking.

A preliminary expander cycle analysis on a steam NTP Engine was conducted with the goal of producing 25,000 lbf of thrust (baseline[5]) at a specific impulse of over 300 seconds. The schematic of the proposed engine is shown in Figure 1. The required mass flow rate of water resulted in 34 kg/s. This is almost three times the mass flow rate of pure hydrogen which is about 12.8 kg/s[5]. The selected reactor exit (chamber) temperature was 2350 K which produced 329.1 sec Isp and required a total reactor power of 312.9 MWt. To prevent boiling and work with supercritical water, the pump output pressure was set to be 300 atm (to handle pressure losses) and the temperature of the water reservoir was assumed to be 300 K. These values correspond to State 1 in Figure 1.

To facilitate water's transition into the supercritical phase, the regenerative cooling lines of the nozzle and control drums along with the moderator element cooling lines will not split the flow as they do in the baseline[5]. Instead, the flow will cascade from the regenerative cooling to the moderator cooling. By assuming that the same fraction of heat will be taken from each of these lines as in the baseline[5,6], the resulting outlet temperature from the cascaded lines was found to be 510 K with a pressure of 274 atm (pressure losses were assumed). These values correspond to State 2 in Figure 1.

However, water is still a liquid at this pressure and temperature, therefore, a U-loop through 35% of the fuel elements is necessary to bring the water to a supercritical state to use in the turbine. The resulting temperature coming out of the U-loop of fuel elements is 750 K at a pressure of 232 atm. This temperature has not shown significant water interactions and is not expected to cause oxidization. These values correspond to State 3 in Figure 1.

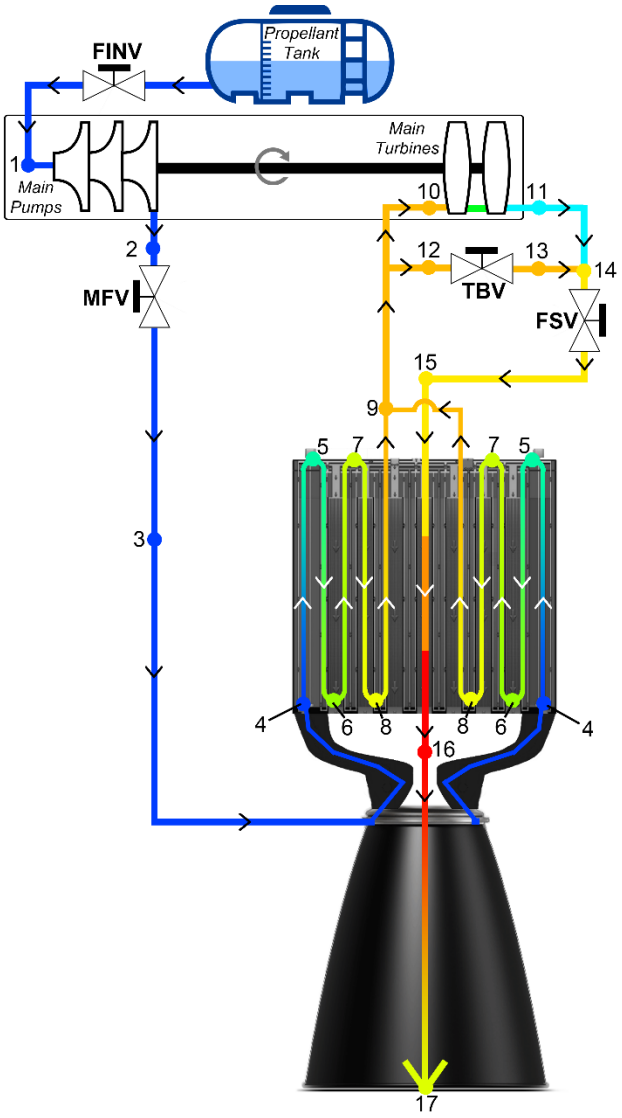

Fig. 1. NTP Engine Schematic

The supercritical water enters a turbine circuit with a bypass valve. The turbine pressure ratio and efficiency were arbitrarily assumed to be 2 and 0.5 respectively for conservative estimations. These values yield that 45% of the total flow will be bypassed. As a rule of thumb, about 10% should remain as bypassed to retain control of the turbine throttling resulting in 35% of the flow being available to produce other work[27]. The turbine circuit output temperature and pressure corresponding to State 4 in Figure 1 are 657 K and 116 atm respectively.

After passing through the turbine, the flow passes through a final shut off valve and the pressure is reduced by 10% to provide a pressure margin[27]. Afterwards, it enters the other 65% of the fuel elements and gets heated up to 2350 K with an outlet pressure of 83.4 atm. These values correspond to State 5 in Figure 1.

Finally, the flow enters the nozzle and expands. The diameter of the throat is 0.091 m with an area ratio of 400. Increasing the area ratio to 1000 will increase Isp by 7 seconds, however, this difference may be marginal given the additional mass needed.

Referring to State 3, these values are rough, although the water would flow through double the length of the fuel elements, it will flow through 17.5% of the total fuel elements at a time. Due to the skewed sinusoidal power curve of a nuclear thermal reactor in a rocket engine, the flow is expected to cool down somewhat as it goes through the upper portion of the second set of fuel elements. The flow schedule would likely result in water going in and out of the outer fuel elements to provide energy to the turbines while the inner elements will provide the final addition of heat as shown in Figure 2.

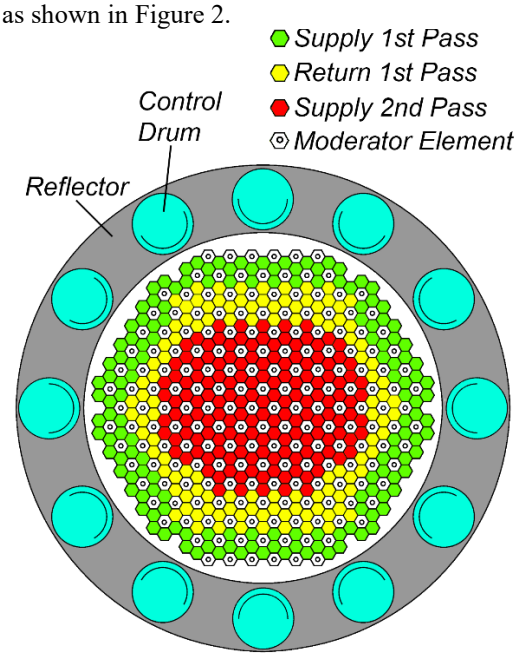

Fig. 2. Reactor Fuel Element Flow Schedule

II. AMMONIA

The Soviet Union looked at an Ammonia/Alcohol propellant for their NTP engine system ЯРД [YaRD] for the 3rd stage of the N-1 Lunar rocket but this engine never left the drawing board. This propellant was primarily chosen due to their inability to store liquid hydrogen at the time (1965). However, detailed engine schematics or power balance diagrams are not available for this engine. It is unclear if dissociation of ammonia via thermolysis was considered either.[28]

To analyze an ammonia engine, the same approach for water will be taken: pressurizing ammonia beyond its critical pressure (112 atm), heating it to beyond its critical temperature (405 K) to get a supercritical fluid, expand it through a set of turbines to drive the pump and get ammonia vapor coming out of the turbines, run this fluid

through the reactor for final heating, and then expand it through the nozzle[29,30]. A key performance measure is the amount of dissociation by thermolysis, species present, and how the species concentration with respect to temperature curves change as the pressure is increased. Furthermore, metals such as tungsten can serve as catalysts for hydrogen production by absorbing the nitrogen in ammonia. This will result in nitride layers which penetrate more with increasing pressure.[31] It is critical for the coating to not serve as a catalyst and not react with either nitrogen or hydrogen at high pressures and temperatures. A study was done that examined solar thermal propulsion and concluded that due to ammonia's extremely slow kinetics, the propellant will be substantially undissociated at temperatures below 2500 K. Furthermore, any degree of dissociation has shown to increase the specific impulse, albeit by tens of seconds.[32] Therefore, it is both reasonable and conservative to assume that no significant dissociation occurs inside the engine even at the baseline chamber temperature of 2650 K. Due to the slow kinetics of ammonia, it is also assumed that the baseline tungsten coating will be sufficient to withstand corrosion even with trace amounts of free nitrogen. It was found that nitrogen is reactive but only above the considered temperatures[33].

III. MISSION ANALYSIS

A code was constructed to analyze the required travel time to and from Mars using the conjunction class mission architecture as the baseline[7] with the mission starting in 2033. Table 1 summarizes the 1st order results of using hydrogen, water, seeded hydrogen (max seed), H2/LOX augmentation[34], and ammonia (no thermal dissociation). The propellant volume and vehicle dry mass were kept constant in all cases, and it was assumed that the launch vehicle can lift the larger masses to the same orbit. When looking at all these cases together, water provides the highest ΔV and the shortest travel times followed by H2/LOX and ammonia. This confirms the fact that water is a viable solution given its superb performance in terms of ΔV and accessibility across the Solar System.

TABLE I. 1st Order Mission Analysis of Propellant Performance

Propellant	Total DV (m/s)	E to M Time (days)	M to E Time (days)
H2	4222	179	178
H2+Ar	4790	163	161
H2O	6753	135	133
H2+LOX	6466	138	136
NH3	6393	139	137

The same analysis was performed but the ΔV was kept constant and the propellant volume was varied along with the dry mass of the inline tanks. Table 2 shows the summary of the previously considered propellants. Here, both pure hydrogen and seeded hydrogen perform relatively similarly without any savings to the number of inline tanks. However, water, H2/LOX, and ammonia reduce the number of inline tanks to one. Furthermore, water outperforms both H2/LOX and ammonia in terms of decreasing the propellant volume. The vehicle that uses water resulted in being the heaviest of all with an 89.1563% mass gain as opposed to H2/LOX with 11.2625% and ammonia with 55.6312% mass gains. Although ammonia is present on the Moon and other bodies in the Solar System, it is still not as abundant as water and does not have the dual functionality as a consumable for both the engine and the life support system[35,36]. This will require additional efforts and facilities to mine ammonia specifically. Coupling this with ammonia's worse performance, the use of ammonia in an NTP engine is not justified.

TABLE II. 1st Order Mission Analysis of Propellant Volume

Propellant	Initial Mass (mton)	Mass Increase (%)	Propellant Volume (m^3)	Volume Decrease (%)
H2	217.27	0.000	1292	0.0000
H2+Ar	275.68	26.8836	1131	12.4613
H2O	410.98	89.1563	318.61	75.3398
H2+LOX	241.74	11.2625	375.73	70.9187
NH3	338.14	55.6312	401.35	68.9358

II. CONCLUSIONS

A preliminary engine model was constructed to analyze NTP engine performance using water or ammonia since both resources are available on the Moon. A brief overview of the reactor materials was also performed and determined that no changes are required for ammonia, but the channel coating had to be changed to SiC and the reactor exit temperature lowered to 2250 K. The mission analysis showed that there could be significant vehicle volume savings from using these propellants directly without any conversion via electrolysis or thermolysis. Future work will analyze specific mission architectures in more detail and a detailed engine model will be constructed.

ACKNOWLEDGMENTS

NASA

REFERENCES

1. Kleinhenz, J. E., and Paz, A. Case Studies for Lunar ISRU Systems Utilizing Polar Water. Presented at the ASCEND, Virtual Event, 2020.
2. Doyle, K. P., and Peck, Mason A. "Water Electrolysis for Propulsion of a Crewed Mars Mission." Journal of Spacecraft and Rockets, Vol. 57, No. 6, 2020, pp. 1103–1117. https://doi.org/10.2514/1.A34632.

3. Hauch, A., Ebbesen, S. D., Jensen, S. H., and Mogensen, M. “Highly Efficient High Temperature Electrolysis.” Journal of Materials Chemistry, Vol. 18, 2008, pp. 2331–2340. https://doi.org/10.1039/b718822f.

4. MacDonald, G. J. F. “GIBBS FREE ENERGY OF WATER AT ELEVATED TEMPERATURES AND PRESSURES WITH APPLICATIONS TO THE BRUCITE-PERICLASE EQUILIBRIUM.” The Journal of Geology, Vol. 63, No. 3, 1955, pp. 244–252. https://doi.org/10.1086/626253.

5. Joyner, C. R., Eades, M., Horton, J., Jennings, T., Kokan, T., Levack, D. J. H., Muzek, B. J., and Reynolds, C. LEU NTP Engine System Trades and Mission Options. Presented at the Proceedings of the Nuclear and Emerging Technologies for Space, Richland, WA, 2019.

6. Nikitaev, D., and Thomas, L. D. “Seeding Hydrogen in Nuclear Thermal Propulsion Engines.” Journal of Spacecraft and Rockets, 2020, pp. 1–11. https://doi.org/10.2514/1.A34711.

7. Levack, D. J. H., Horton, J. F., Jennings, T. R., Joyner, C. R. I., Kokan, T., Mandel, J. L., Muzek, B. J., Reynolds, C., and Widman, F. W. J. Evolution of Low Enriched Uranium Nuclear Thermal Propulsion Vehicle and Engine Design. Indianapolis, IN, 2019.

8. Reynolds, C. B., Joyner, C. R. I., Kokan, T., Levack, D. J. H., and Muzek, B. J. NTP Robustness for Mars Conjunction and Opposition Class Missions. Presented at the ASCEND, Virtual Event, 2020.

9. Nikitaev, D., and Thomas, L. D. “Seeded Hydrogen in Mars Transfer Vehicles Using Nuclear Thermal Propulsion Engines.” Journal of Spacecraft and Rockets, 2020, pp. 1–10. https://doi.org/10.2514/1.A34722.

10. Tizon, J., and Roman, A. A Mass Model for Liquid Propellant Rocket Engines. Presented at the 53rd AIAA/SAE/ASEE Joint Propulsion Conference, Atlanta, GA, 2017.

11. General Electric Company. Industrial Generators. https://www.gepowerconversion.com/sites/default/files/product/GEA32349%20Power%20When%20It%20Matters%20-%20Industrial%20Generators%20Brochure%20-%20July%202016.pdf. Accessed Dec. 2, 2020.

12. ITM Power. “UK to Build World’s Largest Hydrogen Electrolysis Plant in Germany.” Construction Review Online, Jul 12, 2019.

13. Yacout, Abdellatif. Nuclear Fuel. https://www.ne.anl.gov/pdfs/nuclear/nuclear_fuel_yacout.pdf. Accessed Dec. 2, 2020.

14. Samal, Sneha. High-Temperature Oxidation of Metals. In High Temperature Corrosion, 2016.

15. Bostrom, W. A. The High Temperature Oxidation of Zircaloy in Water. Publication WAPD-104. Westinghhouse Atomic Power Dvision, Pittsburgh, PN, 1954.

16. Sabourin, Justin L., and Yetter, Richard A. “High-Temperature Oxidation Kinetics of Tungsten-Water Reaction with Hydrogen Inhibition.” Journal of Propulsion and Power, Vol. 27, No. 5, 2011, pp. 1088–1096. https://doi.org/10.2514/1.B34093.

17. Nelson, A. T., Sooby, E. S., Kim, Y. J., Cheng, B., and Maloy, S. A. “High Temperature Oxidation of Molybdenum in Water Vapor Environments.” Journal of Nuclear Materials, Vol. 448, Nos. 1–3, 2014, pp. 441–447. https://doi.org/10.1016/j.jnucmat.2013.10.043.

18. Dobrov, B. V., Likhanskii, V. V., Ozrin, V. D., and Solodov, A. A. “Modeling of the Oxidization of Uranium Dioxide in a Steam Atmosphere.” Atomic Energy, Vol. 82, No. 2, 1997, pp. 109–115. https://doi.org/10.1007/BF02413460.

19. Rashkeev, Sergey N., Glazoff, Michael V., and Tokuhiro Akira. “Ultra-High Temperature Steam Corrosion of Complex Silicates for Nuclear Applications: A Computational Study.” Journal of Nuclear Materials, Vol. 444, No. 1, 2014, pp. 56–64. https://doi.org/10.1016/j.jnucmat.2013.09.021.

20. Avincola, V. Angelici, Grosse, M., Stegmaier, U., Steinbrueck, M., and Seifert, H. J. “Oxidation at High Temperatures in Steam Atmosphere and Quench Ofsilicon Carbide Composites for Nuclear Application.” Nuclear Engineering and Design, Vol. 295, No. 1, 2015, pp. 468–478. https://doi.org/10.1016/j.nucengdes.2015.10.002.

21. Pint, B. A., Terrani, K. A., Brady, M. P., Cheng, T., and Keiser, J. R. “High Temperature Oxidation of Fuel Cladding Candidate Materials in Steam–Hydrogen Environments.” Journal of Nuclear Materials, Vol. 440, No. 1, 2013, pp. 420–427. https://doi.org/10.1016/j.jnucmat.2013.05.047.

22. Duan, Zhengang, Yang, Huilong, Satoh, Yuhki, Murakami, Kenta, Kano, Sho, Zhao, Zishou, Shen, Jingjie, and Abe, Hiroaki. “Current Status of Materials Development of Nuclear Fuel Cladding Tubes for Light Water Reactors.” Nuclear Engineering and Design, Vol. 316, No. 1, 2017, pp. 131–150. https://doi.org/10.1016/j.nucengdes.2017.02.031.

23. Zuppero, Anthony. (No Subject). Dec 02, 2020.

24. Zuppero, Anthony, Schnitzler, Bruce, and Larson, Thomas. Nuclear-Heated Steam Rocket Using Lunar

Ice. Presented at the 33rd Joint Propulsion Conference and Exhibit, Seattle, WA, 1997.

25. Zuppero, Anthony, and Richins, William. Pump and Pressure Vessel Considerations for Nuclear Heated Steam Rocket. Presented at the American Nuclear Society 1998 Annual Meeting, Boston, MA.
26. Zuppero, Anthony, Larson, Thomas, Schnitzler, Bruce, Werner, James E., Rice, John W., Hill, Thomas, J., Richins, William, and Parlier, Lynn. Origin Of How Steam Rockets Can Reduce Space Transport Cost By Orders Of Magnitude. In AIP, No. 458, 1999, pp. 1211–1216.
27. Orbit Transfer Vehicle Engine Study, Phase A - Extension (Volume II-A: Study Results). Publication NASA-CR-161515. Rocketdyne, Huntsville, AL, 1980.
28. Buran. Ракетно-космический комплекс Н1-Л3 [Space-Rocket Complex N1-L3], , 2019.
29. Lemmon, E. W., Bell, I. H., Huber, M. L., and McLinden, M. O. 10.0. NIST Standard Reference Database 23: Reference Fluid Thermodynamic and Transport Properties-REFPROP. National Institute of Standards and Technology.
30. WebBook, N. I. S. T. C. NIST Standard Reference Database Number 69. National Institute of Standards and Technology, 2018.
31. Shindo, Hitoshi, Egawa, Chikashi, Onishi, Takaharu, and Tamaru, Kenzi. “Reaction Mechanism of Ammonia Decomposition on Tungsten.” Journal of the Chemical Society Faraday Transactions 1, Vol. 76, No. 1, 1980, pp. 280–290. https://doi.org/10.1039/f19807600280.
32. Colonna Gianpiero, Capitta, Giulia, Capitelli, Mario, Wysong, Ingrid J., and Kennedy, Fred G. “Model for Ammonia Solar Thermal Thruster.” Journal of Thermophysics and Heat Transfer, Vol. 20, No. 4, 2006, pp. 772–779. https://doi.org/10.2514/1.18380.
33. Emrich, William J. Jr., and Schoenfeld, Michael P. Lessons Learned from Recent Testing in the Nuclear Thermal Rocket Element Environmental Simulator. Presented at the Nuclear Emerging Technologies for Space, Las Vegas, NV, 2018.
34. Bulman, M. J., Neill, T. M., and Borowski, S. K. LOX-AUGMENTED NUCLEAR THERMAL ROCKET (LANTR) ENGINE SYSTEM INTEGRATION. Presented at the 40th AIAA/ASME/SAE/ASEE Joint Propulsion Conference and Exhibit, Fort Lauderdale, Florida, 2004.
35. Pizzarello, Sandra, Williams, Lynda B., Lehman, Jennifer, Holland, Gregory P., and Yarger, Jeffery L. “Abundant Ammonia in Primitive Asteroids and the Case for a Possible Exobiology.” Proceedings of the National Academy of Sciences of the United States of America, Vol. 108, No. 11, 2011, pp. 4303–4306. https://doi-org.elib.uah.edu/10.1073/pnas.1014961108.
36. Phillips, Tony. “Lunar Impact Uncovered More Than Just Moon Water.” NASA, Oct 21, 2010.

Nuclear and Emerging Technologies for Space
Sponsored by Oak Ridge National Laboratory, April 26th-30th, 2021.
Available online at https://nets2021.ornl.gov

NUCLEAR SPACE SYSTEM ANALYSIS AND MODELLING (NSSAM): A SOFTWARE TOOL TO EFFICIENTLY ANALYZE THE DESIGN SPACE OF SPACE REACTOR SYSTEMS

Kelsa Palomares[1], Christopher Harnack[2], Corey Smith[1], Reed Herner[1], William Machemer[2], Samantha Rawlins[1], Emanuel Grella[2], Adam Boylston[2,3]

[1] *Advanced Projects Huntsville, Analytical Mechanics Associates, Huntsville, AL, 35806*
[2] *Advanced Projects Denver, Analytical Mechanics Associates, Denver, CO, 80211*
[3]*Department of Aerospace Engineering, University of Colorado, Boulder, CO, 80303*
Primary Author Contact Information: kelsa.b.palomares@ama-inc.com

Space reactors have the potential to play a key role in future NASA exploration activities due to their capability to enable sustainable power and advanced propulsion systems. To enable assessment of the space reactor design space, the nuclear space system analysis and modelling (NSSAM) software was developed by Analytical Mechanics Associates. NSSAM leverages a scalable and extensible software architecture which automates reactor analysis to perform coupled engine-reactor and reactor physics-thermal hydraulics calculations. This allows space reactor systems to be evaluated by a wider number of users with a consistent analysis approach to compare designs. NSSAM has been developed with multiple use cases to tailor the analysis to the level of detail desired by the user and computing resources. This summary overviews the NSSAM architecture and development approach, current capabilities (including design variants and use cases) and analysis approach for reactor and system component models.

THIS MANUSCRIPT IS UNDER EXPORT REVIEW BY THE SPONSORING ORGANIZATION AND WILL BE RELEASED ONCE APPROVED

ACKNOWLEDGMENTS

This work was funded under Contract No. 80LARC17C0003. Rachael Collins served as software architect and significantly contributed to the overall software development of NSSAM including all services, controllers, and testing methodologies. AB supported the development of software tests. KP oversaw the technical approach of reactor model and controller development. CH served as engine lead and with support from EG were responsible for the development of the engine models. CS and WM were responsible for the development of the fuel and reactor component thermal hydraulic models. RH and SR were responsible for the development of the reactor physics models in MCNP and Serpent respectively.

REFERENCES

1. TODREAS, N. et. al. *Nuclear Systems Volume I: Thermal Hydraulic Fundamentals, Second Edition.* Book, 2nd Ed. CRC Press, Taylor & Francis (2011).
2. CLOUGH, J. "Integrated Propulsion and Power Modeling for Bimodal Nuclear Thermal Rockets." *Thesis.* University of Maryland. (2007).
3. PATEL, V. "Temperature Profile in Fuel and Tie-Tubes for Nuclear Thermal Propulsion Systems" *Nuclear and Emerging Technologies for Space* (2015).
4. MCCARTHY, J. R. & WOLF, H., "The Heat Transfer Characteristics of Gaseous Hydrogen and Helium," Rocketdyne, RR-60-12 (1960).
5. SPARROW, E. M., "Temperature Distribution and Heat-Transfer Results for an Internally Cooled, Heat-Generating Solid," *ASME*, J. Heat Transfer, 82(4): 389–392 (1960).
6. BINDER, M., TOMSIK, T., & VERES, J. P. "RL10A-3-3A Rocket Engine Modeling Project." NASA-TM-107318. (1997).
7. BRUGGE, N. "Evolution of Pratt & Whitney's Cryogenic Rocket Engine RL-10." (2019). http://www.b14643.de/Spacerockets/index.htm

Nuclear and Emerging Technologies for Space
Sponsored by Oak Ridge National Laboratory, April 26th-30th, 2021.
Available online at https://nets2021.ornl.gov

MODERATOR CONSIDERATIONS FOR SPACE NUCLEAR POWER AND PROPULSION SYSTEMS

Kelsa Benensky Palomares[1]

[1] *Advanced Projects Huntsville, Analytical Mechanics Associates, Huntsville, AL, 35806*
Primary Author Contact Information: kelsa.b.palomares@ama-inc.com

Nuclear reactors have the potential to provide high energy density to enable sustainable surface power and advanced propulsion methods needed for human exploration activities at the moon and mars. Current mission planning is surveying different reactor types for space power and propulsion application. Of these reactor types, the use of a moderator within the reactor can enable reduced enrichment, reduce overall fuel loadings, and minimize the critical size of the reactor compared to unmoderated reference systems. This proceeding summarizes some moderator materials identified for space reactor applications: zirconium hydride, yttrium hydride, beryllium, and beryllium oxide, and the unique design considerations inherent to surface power and nuclear thermal propulsion reactor designs. It was found that there are four key considerations during the moderator selection and design process: nuclear properties, thermophysical & mechanical properties, manufacture & readiness, and environmental compatibility. Surface power reactors can benefit from moderators which minimize overall system mass and are capable of surviving high temperature irradiation environments for years with little degradation. Nuclear thermal propulsion reactors can benefit from moderators which are capable of retaining structural integrity under multiple burns while being exposed to a wide temperature range (40 < T < 500+ K). Moderator materials which exhibit good stability under irradiation and high temperature operation, minimize fuel pitch, and are high readiness are desirable for near term implementation.

THIS MANUSCRIPT IS UNDER EXPORT REVIEW BY THE SPONSORING ORGANIZATION AND WILL BE RELEASED ONCE APPROVED

ACKNOWLEDGMENTS

This proceeding summarizes contributions from the 2020 nuclear power and propulsion moderator-insulator technology interchange meetings hosted by NASA's space nuclear technology portfolio. Fission Surface Power and Space Nuclear Propulsion Project team members from Los Alamos National Laboratory, Idaho National Laboratory, Oak Ridge National Laboratory, NASA Marshall Space Flight Center, NASA Glenn Research Center, NASA Langley Research Center, and supporting industry contractors contributed to identifying applicable materials and figures of merit. Dr. DV Rao (LANL) and Dr. Steven Zinkle (UTK, ORNL) provided critical review of the original manuscript. A thank you to Dr. Jonathan Witter is given for his inputs on moderator considerations and use conditions for NTP. This work was performed in support of NASA's Space Nuclear Propulsion project under contract no. 80LARC17C0003.

REFERENCES

1. WITTER, J. "Space Nuclear Propulsion (SNP) Moderator Environments" Report No. NTP1-PPT-20-0240, BWX Technologies, Lynchburg, VA (2020).
2. Los Alamos National Laboratory. Report No. LA-CP-20-20258
3. "NTP Engine HA-LEU Reactor Quick Look Sprint" Report No. NTP1-RPT-0070, BWX Technologies, Lynchburg, VA (2020).
4. GALICKI, D. "Space Nuclear Propulsion (SNP) Moderator Trade Study" Report No. NTP1-PPT-20-0216, BWX Technologies, Lynchburg, VA (2020).
5. VOSS, S. "TOPAZ II system description" Report No. LA-UR--94-4, Los Alamos National Laboratory, Los Alamos, NM (1994).
6. BAUGNET, J. et. al. "The BR2 Materials Testing Reactor, Past, Ongoing, and Under-study Upgradings *International Group on Research Reactors Conference*; Knoxville, TN 28 Feb - 2 Mar 1990, p. 83-115; International Atomic Energy Agency (1990).
7. SNEAD, L. L. and ZINKLE, S. J. "Use of Beryllium and Beryllium Oxide in Space Reactors" *Space Technology and Applications International Forum* Albuquerque, NM. 13 Feb – 17 Feb 2005 **746**, p.768-775 (2005).
8. VOIT, A.P. "Thermal-desorption decomposition of erbium and yttrium hydrides: experiment and mathematical simulation." (in russian) *IHISM'06 JUNIOR*, Russian Federation p.127. (2006).

Nuclear and Emerging Technologies for Space
Sponsored by Oak Ridge National Laboratory, April 26th-30th, 2021.
Available online at https://nets2021.ornl.gov

INCREASING CERMET FUEL THERMAL MARGIN WITH THORIA FOR NUCLEAR THERMAL PROPULSION

Gyutae Park[1], Franklin Schulte[2], Lance Snead[3], Koroush Shirvan[4]
Massachusetts Institute of Technology, MA, 02139
[1]park_g@mit.edu, [2]fschulte@mit.edu, [3]snead@mit.edu, [4]kshirvan@mit.edu

The addition of thoria to urania was investigated as means to increase the fuel melting temperature of a Low-Enriched Uranium (LEU) Nuclear Thermal Propulsion (NTP) reactor core. Space Capable Cryogenic Thermal Engine (SCCTE) model[1, 6] was reproduced and tested to investigate the use of thorium dioxide (ThO_2)-uranium dioxide (UO_2)-tungsten (W) cermet to achieve higher fuel melting point, operating temperature, and specific impulse (Isp) for human Mars missions. A critical NTP model with additional fuel thermal margin was achieved with adjustments in the axial fuel composition and the tie tube geometry to minimize the fuel enrichment penalty.

I. BACKGROUND

I.A. SCCTE Model

Developed by the NASA Marshall Space Flight Center (MSFC) and the Center or Space Nuclear Research (CSNR), the SCCTE concept is a LEU NTP design that uses W-UO_2 cermet as fuel and zirconium hydride ($ZrH_{1.8}$) as moderator. [6] The reactor design and features produced by CSNR are presented in Figure 1. The specific design was chosen in this study for the following reasons:

- LEU fuel Design
- High thermal conductivity of tungsten
- Axial and radial enrichment zoning for a lower radial peaking factor
- Nominal Isp of 894.2 s (Ref 6)

High thermal conductivity of tungsten and enrichment zoning contribute to a flatter temperature profile, allowing higher operation temperatures and a nominal specific impulse of 894.2 s.

I.B. Use of Thorium

Given the goals of human Mars missions, NTP models with greater than 900 Isp are of specific interest. High specific thrust is achieved by greater reactor operating temperatures: a feature that is limited by material thermal properties. Thus, materials with better thermal properties help achieve shorter travel times for an NTP model.

The addition of thoria to the fuel offers benefits in this regard. Table V presents some properties of interest for UO_2 and ThO_2. Figure 2 describes the melting point of UO_2-ThO_2 mixture at different UO_2 mole fractions. Thoria has a higher melting point, higher thermal conductivity, and lower density than urania. Thus, a thoria-urania mixture raises the fuel solidus point and thermal conductivity while reducing the overall density of the fuel. These changes help designs reach flatter radial temperature profiles, higher operating temperatures, and lighter rocket mass.

Furthermore, the addition of thoria improves the chemical stability of the fuel, [2] limits vaporization of fuel at very high temperatures, [2] and improves irradiation performances of the fuel. [4] All these factors contribute to a more robust NTP design.

On the other hand, the lower fissile inventory will reduce the core reactivity and further challenge the ability to maintain critically with LEU fuel. Consequently, the decreased reactivity will have to be compensated by adding additional fissile or moderator material.

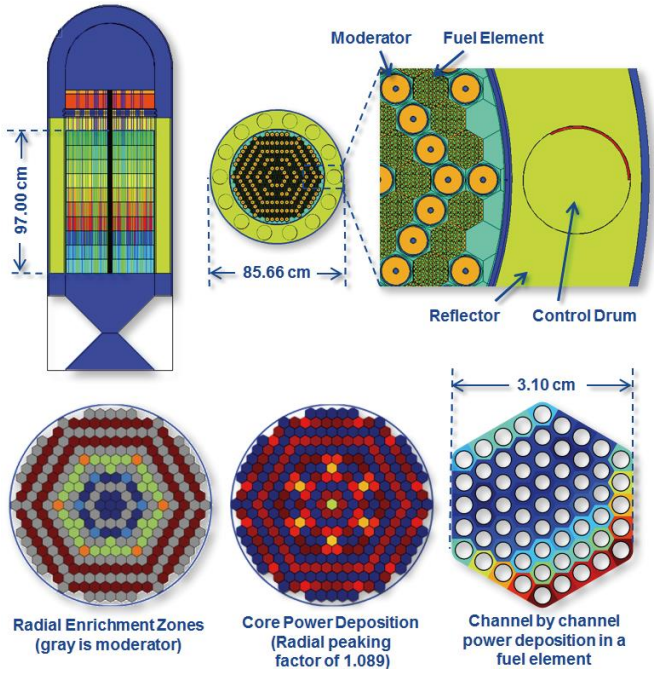

Fig. 1. SCCTE Reactor design and description[6]

TABLE I. Comparison of density, melting point, and thermal conductivity between UO_2 and ThO_2 is shown.

Property	UO_2	ThO_2
Density (300K)	10.96 g/cm^3	10.00 g/cm^3
Melting Point[2]	3120 ± 30 K	3640 ± 30 K
Thermal Conductivity[4] (500~2000K)	8~2.5 W/m·K	14~3 W/m·K

II. Methodology

Serpent[5], a monte-carlo particle transport code was used to reproduce the SCCTE based on Ref. 1. Heat deposition in fuel cells was tallied to determine the axial heat generation rate. A simplified equivalent annulus model of a fuel element with a 1-D coolant flow channel was used to calculate the axial coolant and fuel temperature profiles.

The same analysis was performed with a varied reactor design. Axial U-235 enrichment, fuel thoria fraction and tie-tube geometry were adjusted, as shown in Table IV, to maintain criticality while achieving a higher fuel melting point. Table II describes the reactor and fuel model specifications.

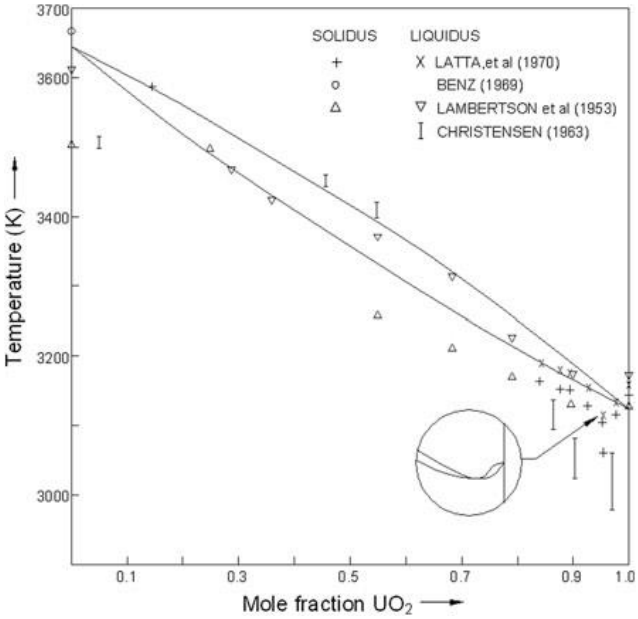

Fig. 2. ThO_2-UO_2 mixture solidus and liquidus line[4]

TABLE II. SCCTE Fuel and Model details[1]

Metrics	Value
Reactor Power (MW)	765.6
Fuel Geometry	Hexagonal fuel with cylindrical coolant channel
Number of Fuel elements	151
Number of Tie tube elements	150
Coolant channels per fuel cell	61
Fuel Composition	W-UO2-ThO2
Oxide volume fraction (vol%)	60.0
ThO2 in Oxide (mol%)	6 ~ 40
W-184 enrichment (at %)	98
Fuel enrichment (wt.%)	12.989 ~ 19.549
Percent Theoretical Density (%)	98%

III. Results

Reactor Criticality

The lower portion (near the coolant exit) of each fuel cell was replaced with higher thorium fraction ThO2-UO2-W cermets. The bottom 38.8 cm in the core fuel zone was adjusted. Only the lower portion of the fuel was considered for increased ThO_2 fraction to limit the negative reactivity worth of thorium while achieving higher thermal margins (fuel and coolant temperatures are well under the material melting point near the coolant entrance). Table III compares the change in core reactivity as a function of thoria fraction in fuel oxide. The six mol percent case is provided for the replicated reference core with the lowest melting point of 3141.1 K.

As demonstrated in Table III, the addition of thoria to cermet fuel results in a noticeable increase in fuel melting point with each 10 mol% addition resulting in a 50 K increase in the range of interest. This study focuses on 50 mol% thoria-urania tungsten cermet, which yields a nearly critical reactor with about a 200 K increase in fuel melting point.

TABLE III. Fuel melting point for various ThO_2 fraction in fuel oxide and the resulting multiplication factor for the adjusted SCCTE core

ThO_2 fraction in oxide (mol%)	Multiplication factor (k_{eff})	Fuel melting point (K)
6.00	1.00537 ± 0.00038	3142.1
20.0	0.99987 ± 0.00033	3210.0
30.0	0.99690 ± 0.00036	3260.0
40.0	0.99419 ± 0.00027	3310.0
50.0	0.99184 ± 0.00032	3360.0

To compensate for the loss of reactivity, the following options were considered: increasing axial U-235 enrichment, and increasing the moderator thickness within tie-tubes. Table IV shows the reference presented by Patel et al.[6] and the tested axial and radial enrichment pattern. Table V shows the change in reactivity given the new enrichment pattern.

TABLE IV. Enrichment Pattern for SCCTE[6]
Reference enrichment pattern with row-wise axial enrichment and column-wise radial enrichment.

Radial / Axial	Inner				Outer
Inlet	0.1975	0.187625	0.1975	0.187625	0.1975
	0.1975	0.187625	0.1975	0.187625	0.1975
	0.1975	0.187625	0.1975	0.187625	0.1975
	0.1975	0.187625	0.1975	0.187625	0.1975
	0.1975	0.187625	0.1975	0.187625	0.1975
	0.158	0.1501	0.158	0.1501	0.158
	0.13825	0.131338	0.13825	0.131338	0.13825
	0.13825	0.131338	0.13825	0.131338	0.13825
Outlet	0.13825	0.131338	0.13825	0.131338	0.13825

Adjusted enrichment pattern with constant axial enrichment and column-wise radial enrichment.

	Inner				Outer
Axially const.	0.1975	0.187625	0.1975	0.187625	0.1975

TABLE V. Core multiplication factor for reference and adjusted fuel enrichment pattern with modified axial ThO_2 fraction in fuel

ThO_2 fraction in oxide (mol%)	Reference k_{eff}	Adjusted k_{eff}
40.0	0.99419 ± 0.00027	0.99813 ± 0.00031
50.0	0.99184 ± 0.00032	0.99472 ± 0.00031
50.0 w/ Tie tube adjustment	-	1.00223 ± 0.00031

The increase in axial fuel enrichment resulted in limited multiplication factor improvement due to the following contributions demonstrated in Figure 3:

- The axial neutron reflector is located above the coolant inlet zone leading to reduced fission rate near the coolant exit.
- The increase in fuel thorium concentration near the coolant exit increases neutron absorption rate near the core bottom.

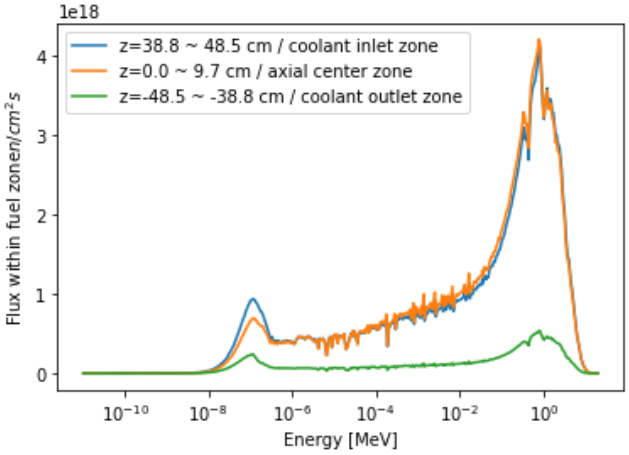

Fig. 3. Average flux in the adjusted fuel with 50 mol% ThO_2 in fuel oxide for 3 axial segments: coolant inlet, axial-center, and coolant outlet.

Adjustment of the tie-tube dimensions yielded a more significant impact on the core reactivity. Figure 4 depicts the tie-tube design and Table VI describes the replicated, and adjusted tie-tube dimensions. The thickness of the insulating zirconium carbide (ZrC) layer and the coolant cross-sectional area were kept constant to limit the resulting temperature changes in the tie tube elements. The overall thickness of the graphite body has been reduced to increase the amount of $ZrH_{1.8}$ moderator.

The adjustments in tie tube dimensions lead to a multiplication factor of 1.00223 ± 0.00031, with a total moderator mass increase of 8.94 kg. The increase in moderator mass is compensated by the reduction in fuel mass that was introduced by the higher thoria fraction in the fuel. Thus, adjusting the axial fuel composition and tie tube geometry results in a critical reactor with temperature margins of approximately 200 K, a fuel mass decrease of 6.1 kg, and a moderator mass increase of 8.94 kg.

Fuel Temperature Margin

With the updated SCCTE model, temperature, and fuel margin to melting point were calculated and compared to the replicated original model. First, a comparison was performed assuming the same coolant inlet temperature of 291K[1]. An equivalent annuli model of a single coolant channel was considered for both the reference and the adjusted models. Both simulations were normalized to the same operation power of 765.6 MW. Convective and radiative heat transfer between the fuel and the coolant were considered. Figure 5 shows the comparison between the two models.

The high number of coolant channels within a fuel cell along with turbulent coolant flow resulted in a marginal difference in the fuel and coolant temperature. The adjusted model has a higher average fuel temperature due to the increased moderator mass in the reactor core.

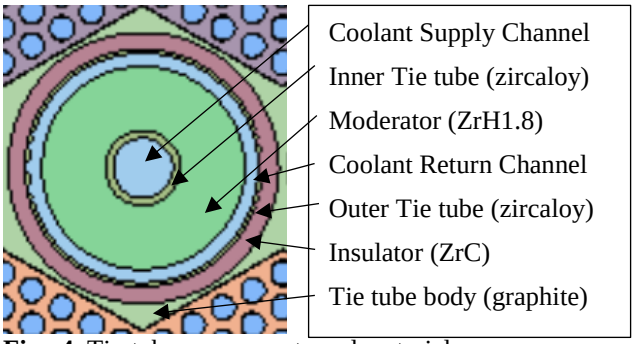

Fig. 4. Tie-tube components and material

TABLE VI. Tie-tube dimensions
Original → Adjusted

Fuel Pin Component	Inner Radius (cm)	Outer Radius (cm)
Coolant Supply Channel	-	0.3305
Inner Tie tube	0.3305	0.4135
Moderator	0.4135	1.1205→1.1431
Coolant Return Channel	1.1205→1.1431	1.2680→1.2880
Outer Tie tube	1.2680→1.2880	1.3095→1.3295
Insulator	1.3095→1.3295	1.4950→1.5150
Tie tube body	3.10 (flat-to-flat)	

The higher fuel temperature margin of the ThO_2-UO_2-W cermet allows the reactor to operate at a higher temperature by adjusting the inlet hydrogen temperature.

The adjusted core was able to achieve an overall operating temperature increase of 150 K while keeping the fuel temperature margin constant at the outlet as shown in Figure 6. Axially-varied introduction of ThO_2 in the fuel should potentially achieve a greater temperature increase and is left as future work.

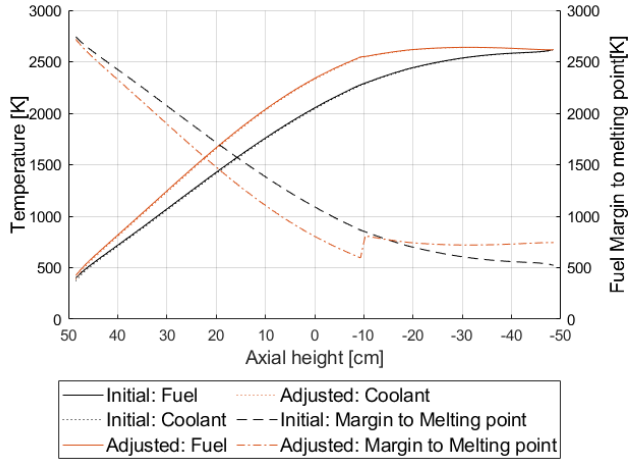

Fig. 5. Comparison of Fuel, coolant, and fuel temperature margin between replicated and adjusted SCCTE model

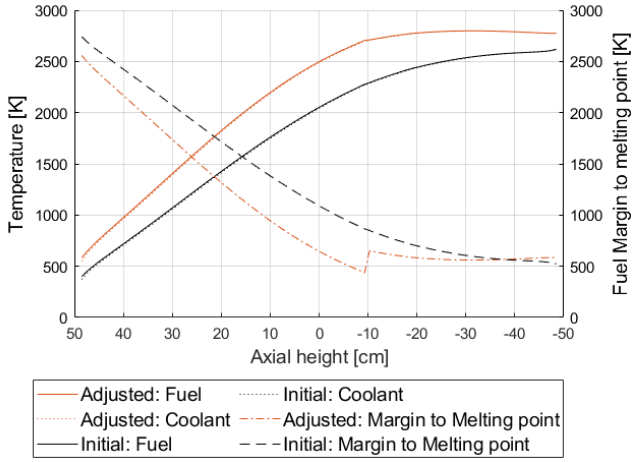

Fig. 6. Comparison of Fuel, coolant, and fuel temperature margin between replicated and adjusted SCCTE model with different inlet temperature for the adjusted model.

IV. CONCLUSION and FUTURE WORK

Adjustments to the SCCTE NTP concept were made to investigate the possibility of greater than 3,000 K fuel and coolant temperatures. Partial axial adjustment of fuel composition with 50 mol%-in-oxide-ThO_2-UO_2-W cermet over the original 6 mol%-in-oxide cermet was investigated. With relevant adjustments to the tie tube design, the adjusted fuel yields a critical NTP core with a possible 150 K increase in operation temperature while keeping the fuel thermal margin near the coolant exit.

To verify and further test the adjusted SCCTE model, a non-comprehensive list of future works is presented below.

- An in-depth feasibility study of the adjusted SCCTE model
- Investigate a finer axial adjustment of fuel composition to reduce the loss in reactivity from thorium addition
- Model neighboring tie tubes to verify that the adjustments to tie tube geometry does not result in a significant loss in tie tube structural strength or in exceeding the tie tube melting point
- Investigate fuel and moderator temperature profile in finer meshes to consider radial and axial temperature distribution of fuel and moderator elements

VIII. REFERENCES

1. Michael Eades, et al., SCCTE: An LEU NTP Concept with Tungsten Cermet Fuel. Transactions of the American Nuclear Society, Vol. 113, Washington, D.C., (2015).
2. Belle J. and Berman RM, Thorium dioxide: properties and nuclear applications. Naval Reactors Office, United State Department of Energy, Government Printing Office, Washington (1984).
3. Webb, Analysis and fabrication of tungsten cermet materials for ultra-high temperature reactor applications via pulsed electric current sintering, University of Idaho. (2012)
4. Dasarathi Das and S. R. Bharadwaj, Thoria-based Nuclear Fuels. Springer (2013).
5. Leppänen, J., et al. "The Serpent Monte Carlo code: Status, development and applications in 2013." Ann. Nucl. Energy, 82 (2015) 142-150.
6. Patel, et al., Center for Space Nuclear Research (CSNR) NTP Design Team Report. Idaho National Laboratory. Idaho Falls, Idaho. (2015).

Nuclear and Emerging Technologies for Space
Sponsored by Oak Ridge National Laboratory, April 26th-30th, 2021.
Available online at https://nets2021.ornl.gov

SIMULATION OF AN INDUCTIVELY HEATED MULTI-CHANNEL NUCLEAR THERMAL ROCKET MODEL

Micah Pratt[1], Colin Coane[1], Kayden Elmer-Schurr[1], Aram Shahinyan[1], and Breece Phipps[1]

[1]*The Advanced Spacecraft Propulsion and Energy Laboratory, University of Southern California, Los Angeles, CA, 90007*

(727) 481-9618; Micahpra@usc.edu

Nuclear thermal rocket propulsion offers an alternative to traditional liquid rockets, yielding similar amounts of thrust combined with two to three times the efficiency. The Hyperion-I project was designed to model solid core nuclear thermal propulsion using induction heating methods to simulate and experimentally validate this model. Here, a coupled electromagnetic and computational fluid dynamic model was created for a 7-channeled test article using ANSYS Maxwell and ANSYS Fluent and was subjected to experimental conditions. Nitrogen gas was flowed through each channel at a 0.25 g/s mass flow rate with an inlet temperature of 288.16 K. The total ohmic loss in the test article from induction heating was 24.72 W, of which 1.87 W was lost to the environment due to convection. The average outlet gas temperature was 307±1 K, yielding a temperature increase of 19±1 K across the article. Future hardware testing will experimentally validate these temperature measurements and will include testing of a full-scale core.

GLOSSARY OF TERMS

T	temperature
P	pressure
T_0	inlet temperature
T_{out}	outlet temperature
ΔT	change in temperature
ΔP	change in pressure

I. HYPERION-I CAMPAIGN INTRODUCTION

The University of Southern California's Advanced Spacecraft Propulsion and Energy (ASPEN) Laboratory's Hyperion-I project is a three-phase campaign designed to model Nuclear Thermal Rocket Engines (NTRE's) through experimentally validated simulations. Phase I aimed to refine the proposed experimental setup and simulation methodology, and was completed in Spring 2020.[1] Phase II, which is currently underway, aims to demonstrate the effectiveness of modeling a multi-channeled NTRE engine geometry. Each phase increases the model's fidelity through increasing the complexity of the engine's reactor subsystem, and the final phase, Phase III, aims to model a full scale NTRE core.

Liquid bi-propellant rocket engines are an essential element in most modern space vehicle architectures. These propulsion systems, however, are limited to maximum specific impulses of approximately 450 seconds, necessitating large fuel tanks and, in turn, limiting vehicle and mission design due to additional fuel weight. Electric propulsion provides much higher specific impulse, on the order of 1000's of seconds, but is limited by thrust several orders of magnitude lower than that of liquid propulsion, leading to much longer mission durations due to the need for prolonged acceleration. NTRE's benefit from thrust on par with liquid bi-propellant rockets while providing specific impulses of more than 800 seconds, two to three times that of conventional bi-propellant systems.[2]

The Hyperion-I engine system utilizes nitrogen gas as its working fluid and consists of three main subsystems: the feed system, the reactor core test article, and the thrust chamber. The feed system regulates the flow of nitrogen from commercial gas cylinders to the reactor subsystem, allowing for adjustable reactor model inlet pressures to meet test and safety standards. The feed system also contains instrument ports to allow the acquisition of pressure and temperature data at key points, such as the reactor inlet and outlet. The reactor core model consists of a multi-channeled steel fuel element inserted into the feed system.

Fig. 1. Proposed Hyperion-I Phase III engine core test article.

In lieu of using fissile materials, the reactor model is heated by an induction heater to provide a safer testing environment, a method which has been implemented in NASA's Nuclear Thermal Rocket Element Environmental Simulator (NTREES) to simulate the volumetric heating effects of a fission-based propulsion system.[3] Three test articles will be tested over the span of the Hyperion-I campaign. For Phase I, a single length of stainless-steel tubing was used, which greatly simplified testing and modeling due to its simple geometry. Maraging steel test articles additively manufactured by USC's Center for Advanced Manufacturing[4] will be used as the reactor test articles in Phases II and III, possessing 7 channels for Phase

II and 61 channels for Phase III. A model of the proposed Phase III test article is given in Figure 1. The reactor subsystem works by volumetrically heating the propellant as it flows axially through the reactor channels. As the propellant flows from inlet to outlet, it will heat up and accelerate, be directed into a thrust chamber consisting of an exhaust plenum and exit nozzle, and then expanded outward to generate thrust.

I.A. Phase I Results

Phase I of the Hyperion-I campaign confirmed the validity of the proposed experimental setup and heating method, and the feasibility of experimentally validating a Multiphysics NTRE fuel element model in ANSYS.[1] Along with verifying the experimental setup functioned properly, Phase I also served to refine the feed system setup and data-acquisition capabilities for future physical tests. For modeling simplicity, a single section of 3/16" (4.76 mm) outer diameter stainless-steel tubing was used for the reactor subsystem in place of a more sophisticated reactor test article. Exit data was successfully captured, which indicated that when the test article was inductively heated, the outlet temperature of the working fluid (nitrogen) was equal at steady state to the outlet temperature predicted by the ANSYS model. This was the primary area of interest, as this quantity could be readily validated through direct measurement. This indicated the model was valid, and the test was ruled a success. However, due to design issues during the first day of testing and the unintentional heating of a thermocouple fitting at the test article inlet, experimental temperature difference ΔT and pressure difference ΔP between the inlet and outlet faces were not properly resolved. Thermocouple noise also drastically skewed data gathered during the test's heating phase due to RF interference between the thermocouple operation-amplifiers and the induction heater. These issues were addressed in follow up tests through the redesign of the induction heater coil, the inclusion of a dedicated NI USB - 9213 thermocouple reader, and additional RF shielding to enable more reliable temperature readings.

I.B. Phase II Purpose and Goals

Hyperion-I Phase II seeks to increase the reactor model's sophistication by simulation and experimental validation of an additively manufactured test article. The test article was a 250 mm long hexagonal cylinder with 7 teardrop shaped channels, each with a hydraulic diameter of 2.3 mm. The model's geometry was chosen as it is similar to the design of many hexagonal nuclear fuel elements[2], with the exception of channel geometry. The channel shape was chosen as the test article was additively manufactured, and the teardrop shape allowed the article to be printed horizontally. The Phase II test article was produced at USC's Center for Advanced Manufacturing from DMLS MS1 maraging steel and was post-machined at the USC on-campus machine shop. End caps that attach the test article to the feed system have also been manufactured by the USC Undergraduate Fabrication Lab.

The primary objective of Phase II is to ensure the effectiveness of modeling multi-channeled test articles by simulation and validating this model experimentally. Validating the simulation will allow for scaling the test article to the proposed full core model with 61 teardrop channels. This will be done by verifying that Phase II ANSYS simulations produce physical results, and by validating the model's accuracy by comparing outlet temperature and ΔT between the test article inlet and outlet faces predicted by ANSYS with those observed experimentally in upcoming tests. Physical experiments will also resolve the pressure drop across the multi-channeled article, which is of interest as a pressure-based solver is used in the ANSYS model. This paper presents the results from Phase II ANSYS simulations of the 7-channel test article.

II. ANSYS MODELING METHODOLOGY

The inductive heating of the test article was simulated using the Maxwell 3D electromagnetic module in ANSYS. The electromagnetic simulation consisted of the 7-channel test article situated within a model of the induction heater coil to be used for physical tests. The test article geometry was created in Siemens NX and imported into the ANSYS Workbench and Maxwell, while the copper induction coil geometry was created natively in Maxwell. The model setup is shown in Figure 2. A 300 Amp alternating current was applied to the coil with a frequency of 70 kHz as determined by a prior test of the heater used in physical testing. A base mesh was applied to the coil and the test article, with additional skin-depth based meshing on the test article to increase the simulation fidelity of eddy currents and heating behaviors. A bounding region of air was defined around the induction coil and test article. The system was then solved for magnetic field vectors in the coil and the ohmic losses in the test article.

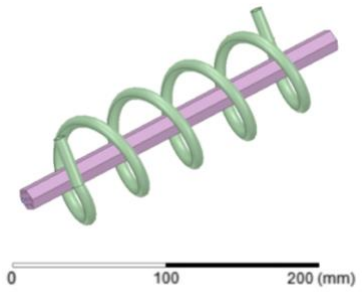

Fig. 2. ANSYS Maxwell model setup showing the test article and induction coil.

The results of the electromagnetic simulation were then used to simulate the heating of the test article and subsequently of the working fluid in the ANSYS Fluent computational fluid dynamics (CFD) module. First, the ohmic loss contour from the Maxwell simulation was imported as a volumetric heat source onto the test article geometry in Fluent. Gaseous nitrogen was then assigned to fill the volume of each of the test article's channels. Internally developed NTRE sizing scripts were used to determine a target mass flow rate of 0.25 g/s per channel and predicted flow velocities for the model, and test article inlet and outlet pressures were estimated by numerical solutions to the Darcy-Weisbach equation. These values were then prescribed in the model as boundary conditions for the working fluid. A convective heat loss boundary condition was applied to the outside of the test article to simulate natural convection with ambient air around the article, and the convection coefficient used was determined by approximating the test article as a horizontal cylinder. A pressure-based solver was utilized and default Fluent CFD settings were used aside from these mentioned. The system was then solved for the temperature profiles of the working fluid and of the test article itself, and the heat loss due to convection with the environment was also recorded.

III. RESULTS & DISCUSSION

Induction heating produces eddy currents in the test article which in turn generate ohmic losses, heating the article. The total ohmic loss over the entire test article was 24.72 W. The region of greatest ohmic loss was located directly beneath the coil itself, and the regions of least ohmic loss are situated at the inlet and outlet of the article. Since heating is proportional to ohmic loss, heating was expected to be greatest near the center of the test article and least at the inlet and outlet. The steady-state temperature profile of the test article is shown in Figure 3. Observed temperature was greatest near the article's center and decreased outwards towards the article's inlet and outlet, indicating successful coupling between the imported Maxwell ohmic loss contour and the Fluent simulation.

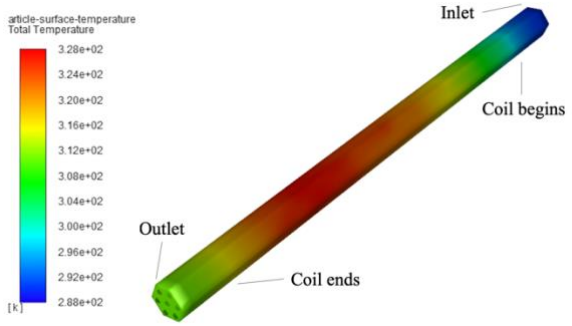

Fig. 3. Temperature profile of the test article surface.

As mentioned in the model setup, a convection condition was assigned to the test article's outer body to simulate natural convection with air. Heat loss to the environment due to convection was 1.87 W. Additionally, the total power output of the Fluent model was 24.69 W. This was within 0.1% of the 24.72 W ohmic loss imported from Maxwell, confirming that energy was conserved in the model.

Figure 4 displays the full temperature profile of gas in the test article channels. As gas flows through the channels, the test article volumetrically heats the gas, and so temperature was expected to gradually increase as gas flowed from inlet to outlet. The simulation results yielded a smoothly increasing temperature gradient as gas flows through the article, confirming this prediction.

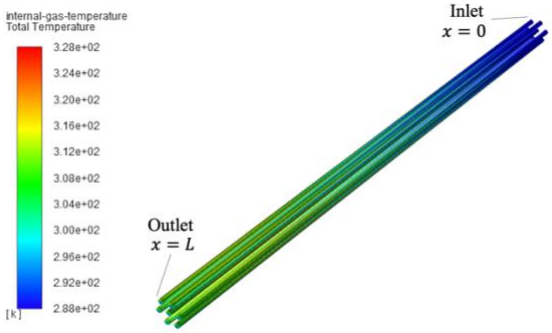

Fig. 4. Temperature profile of gas flowing through the test article channels.

Figure 5 displays the average and maximum gas temperatures over the length of the article. The inlet is defined as the location $x = 0$, while the outlet is defined as location $x = L$. Both average and maximum temperatures gradually increase along the article and peak around $x/L = 0.75$, gradually decreasing afterwards. This heating profile correlates with the test article temperature, as in both cases temperature decreases slightly near the outlet after the coil ends.

The main results of interest from the CFD model were the face-averaged outlet gas temperature of the test article and the gas temperature difference across the article, ΔT. The input gas temperature T_0 was 288.16 K, and the model converged on a face averaged outlet gas temperature T_{out} of 307±1 K, yielding a ΔT of 19±1 K.

The outlet gas temperature and ΔT are significant as they can both be measured experimentally by thermocouples positioned immediately upstream and downstream of the test article in the test stand setup. Because of this, the effectiveness of the ANSYS model can be directly validated by Phase II hardware testing.

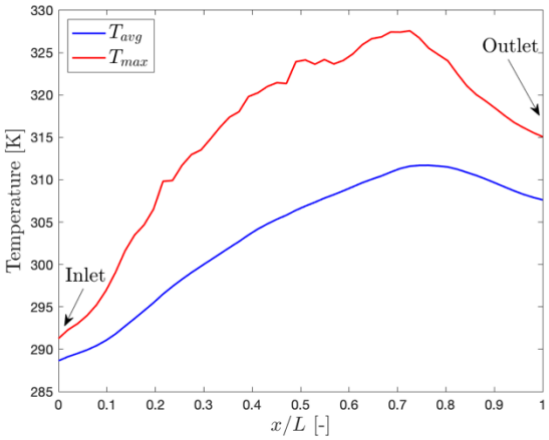

Fig. 5. Average and maximum gas temperatures as a function of distance from inlet x and total article length L.

All of the above results show that the Multiphysics ANSYS model developed was successful in producing physical results, and more importantly, an outlet gas temperature and ΔT that are measurable by standard thermocouples. This will allow Phase II hardware testing to fully verify the accuracy of the simulation and the effectiveness of modeling a multi-channeled reactor model.

However, the predicted T_{out} and ΔT create challenges for Phase III full-scale core testing. These temperatures are expected to decrease as the size of the test article and number of channels increase, and so the induction heater currently used may not be powerful enough to produce a measurable ΔT. Moreover, a much higher ΔT is needed to produce significant thrust. This issue will be corrected in subsequent testing by utilizing a different induction heater with an increased coil current and tighter coil loops to provide more power to the test article.

IV. CONCLUSION

The simulation of Hyperion-1 Phase II was successful and demonstrated that the current ANSYS modeling techniques effectively simulate the steady state induction heating of a multi-channel test article. These simulations also yielded an outlet gas temperature and ΔT across the test article that are significant and large enough to be experimentally validated. If Phase II hardware testing is successful in validating these results, the simulation process outlined in this paper will be used for simulation of the full-scale reactor core model of Phase III with 61 teardrop shaped channels.

IV.A. Continuation of Phase II

Preparation for Phase II hardware testing is currently underway. As discussed, hardware testing of Hyperion-1 Phase I affirmed the campaign's modeling technique and led to refinements in feed system design that will be implemented in Phase II.

Hardware testing will provide experimental results for gas outlet temperature and temperature difference which will be compared to the simulation results above. Additionally, a differential pressure transducer will be used to resolve the pressure drop across the test in order to prepare for Phase III testing of the full core reactor model. Lastly, a new induction heater will be obtained as discussed to provide the power increase needed to experimentally test the full core model.

ACKNOWLEDGMENTS

The ASPEN Laboratory would like to thank its advisors: Dr. Matthew Gilpin and Dr. Charles Radovich from the University of Southern California for their continuous support of the lab. Their guidance and expertise have been crucial to the success of the Hyperion-I campaign and in taking the campaign from concept to physical implementation. The dedication and work ethic of ASPEN's general lab members have also been essential to the progress of Hyperion-I, and the campaign would not be successful without their passion for the project. The ASPEN lab would like to thank the University of Southern California's Viterbi School of Engineering for its continuous financial support of the lab and for providing ASPEN with the facilities necessary to operate. The lab would also like to thank Northrop Grumman and Boeing for their sponsorships of the lab's endeavors.

REFERENCES

1. S. CENDRO et al., "Simulation and Experimental Validation of an Inductively Heated Solid-Core Nuclear Thermal Rocket Model," Nuclear and Emerging Technologies for Space, Knoxville, TN, 6-9 April (2020).
2. S.K. BOROWSKI, D.R. MCCURDY, and T.W. PACKARD, "Nuclear Thermal Propulsion (NTP): A Proven Growth Technology for Human NEO / Mars Exploration Missions," IEEE Aerospace Conference, Big Sky, MT, 3-10 March (2012).
3. W. J. EMRICH Jr., "Nuclear Thermal Rocket Element Environmental Simulator (NTREES)," NASA – Marshall Space Flight Center, M.S. ER24, Huntsville, Alabama 35812 (2008).
4. University of Southern California Center for Advanced Manufacturing: cam.usc.edu (current as of Jan. 28, 2021).

Nuclear and Emerging Technologies for Space
Sponsored by Oak Ridge National Laboratory, April 26th-30th, 2021.
Available online at https://nets2021.ornl.gov

DEVELOPMENT OF MULTI-PURPOSE DYNAMIC NUCLEAR THERMAL ROCKET SYSTEM MODELS*

J. D. Rader[1], T. P. Norby[1]

[1]*Oak Ridge National Laboratory, 1 Bethel Valley Rd, Oak Ridge, TN, 37831*

raderjd@ornl.gov

A Modelica-based dynamic system model of a nuclear thermal rocket engine has been created as part of a multi-agency effort to develop space nuclear propulsion technology. There is a need to provide the model to other team members in the fields of engine-vehicle integration and instrumentation and control in a form that is usable by computer codes suited for those purposes. To fulfill this need, the most recent version of the dynamic system model was augmented to support model export using the functional mock-up interface. This work describes the necessary changes to the model to update to the latest engine configuration and describes the model export process. The exported model has been shown to satisfactorily reproduce the baseline results and to run faster than real time.

I. INTRODUCTION

The US National Aeronautics and Space Administration (NASA) has been investigating space nuclear propulsion (SNP) technology for several decades using variable levels of funding. However, the last few years have seen a more focused effort and consistent funding for developing nuclear thermal propulsion (NTP) for ground testing or in-space demonstration. Given the confluence of space and nuclear technologies, there is a need for input and participation from several agencies or companies inside and outside the US Government. Researchers at Oak Ridge National Laboratory (ORNL) have been part of past SNP efforts and are participating in several aspects of the current program.

Due to the participation of several entities with various types of expertise, useful and accessible information and models must be disseminated to various project members. One such dynamic model of the nuclear thermal rocket (NTR) engine has been under development at ORNL since 2017. This Modelica-based model has many potential capabilities to support development of engine instrumentation and controls (I&C), engine-vehicle integration (EVI), human-machine interface (HMI), and other multiphysics modeling and simulation (M&S) needs. However, a demonstration run of the model outside of the Modelica integrated development environment (IDE) has not been conducted, so its utility has been limited.

Through recent efforts in model reorganization and improvements in the working fluid library, it is now possible to export the dynamic model to a functional mockup unit (FMU) using the functional mockup interface (FMI). When the model is exported to an FMU, it can act somewhat like a black-box in that it performs calculations according to the compiled model inside of the box that are driven by external forcing functions from the host environment. The host environment can be many things: Python, Matlab/Simulink, or SysML, among others. By using an FMU, the same model that was developed in the Modelica IDE can be used and tested in other environments tailored to specific analyses (e.g., I&C, EVI).

The work described here implemented changes to update the model to the most recent engine configuration and to support the export of the model for external users.

II. DYNAMIC MODEL

The dynamic model was been updated based on previous work[1,2] to better support parameterization and to reflect the most recent engine configuration. Also, the interface to the fluid property database was slightly updated to improve model export compatibility.

The basic layout of the model is shown in Figure 1. The engine is based on an expander power cycle with turbine bypass and hydrogen as the working fluid and propellant. The thermal spectrum reactor is fueled with high-assay low enriched uranium (HALEU). The hydrogen is stored in tanks and pumped into the engine, where the flow is divided into two paths to (1) the regenerative nozzle and control drums and (2) the moderator. The two paths merge before they reach the turbine(s) and turbine bypass. The bypass valve is modulated to control the flow through the turbine(s). The flows merge before entering the core, where the hydrogen is heated to 2,700 K, expanding through the nozzle to achieve 900 seconds of specific impulse.

The nuclear kinetics model uses the point kinetics assumption with reactivity feedback from several sources: moderator solid temperature, fuel solid temperature, hydrogen density in moderator channels, hydrogen density in fuel channels, and control drums. The feedback coefficients and control drum worth as a function of position are determined using separate neutronics calculations.

Only the moderator and fuel components make use of 1D discretized fluid volumes. Other fluid volumes are 0D. Pressure losses are accounted for using frictional losses in the discretized components, whereas flow resistors and

valves account for losses elsewhere. All pressure losses scale with the flow rate according to the type of pressure loss component specified.

Solid fuel and moderator materials are accounted for in the discretized components. A 1D discretized mass is included in the regenerative nozzle. These solid masses are important for a dynamic model because they add a delayed feedback mechanism which affects controllability.

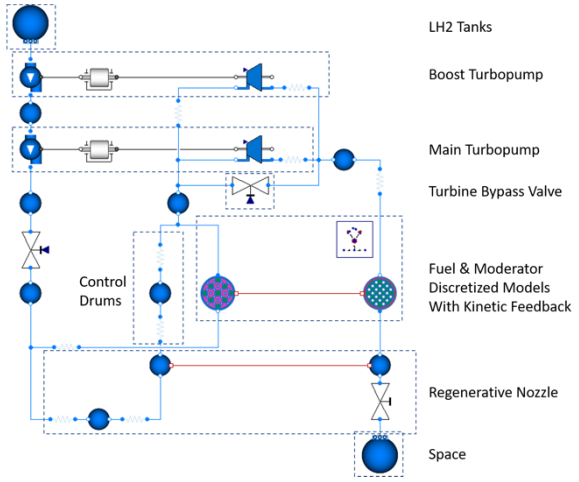

Fig. 1. Basic flow arrangement for NTR model. Blue lines indicate fluid connections, and red lines represent heat transfer connections.

Convective heat transfer occurs in the fuel and moderator channels. The power deposited into the solid regions of the fuel and moderator components is determined through separate neutronics calculations and is scaled by the fraction of total power. A small amount of power is deposited directly into the fluid regions of the fuel and moderator.

Heat transfer between the fuel and moderator solids through a thermal insulator is assumed to be 2% of full power. This heat source to the moderator is needed to drive the turbopump.

The model includes basic proportional-integral (PI) controls that use chamber temperature to control the control drum position and pressure to control the turbine bypass control valve position.

II.A. Codes

The majority of the dynamic NTR model was built using components from the ORNL-developed TRANSFORM library[3] with select components from the Modelica Standard Library (MSL). The model was developed in the Dymola v2021 IDE. The FMPy python library[4] was used to run the FMU. All simulations were run on a x86-64 Windows desktop machine. Software quality assurance for TRANSFORM is addressed through regression tests, version control, validation using exact solutions, and verification by modeling of experiments.

II.B. Model Updates

The NASA NTR engine design is constantly evolving to support current developments in other design disciplines. While design specific details are withheld for business proprietary and export control reasons, general updates and modeling strategy are described below.

II.B.1. Turbomachinery

The first update is the modeling of the turbomachinery. An additional turbopump was added to the model. The turbopump is a critical part of the system model and is composed of three components: a turbine, a shaft, and a pump.

The MSL includes basic turbine, shaft, and pump components, but TRANSFORM models are used for the turbine and pump to provide more detail. The shaft model is from the MSL.

The liquid hydrogen (LH2) stored in the tanks will likely be near the saturation point. As cryofluid management strategies for Mars and other years-long duration missions are still evolving, the engine must be able to accept LH2 at a variety of suboptimal conditions. Therefore, a lower speed boost pump has been included between the tank assembly and the main pump to reduce cavitation risk in the faster spinning main pump. The model is set up to accept LH2 pressure and temperature as a function of time. The continuous homologous pump curves are based on a NASA study of modeling the RL10 rocket engine.[6]

II.B.2 Fluid Property Database Updates

The MSL includes only two two-phase working fluids; however, it establishes a framework called `PartialTwoPhaseMedium` for creating custom working fluids. This framework has been exploited to interface with the CoolProp fluid property database[6] using an open-source Modelica library called ExternalMedia (EM). Even though the EM library is located in a public repository[7], it has not been significantly updated since 2015 and only includes 32-bit fluid property binaries using a compiler from 2012. This limitation prevents use of the dynamic NTR FMU in environments requiring 64-bit models. The latest EM commit is also limited to an outdated version of CoolProp v4.2.5.

While some public forks of the EM project have attempted to bring EM up to date with the latest version of CoolProp and are now using 64-bit fluid property binaries, the authors took on the task of formalizing this process using the latest compilers.[8] For this project, however, CoolProp v4.2.5 was still used, albeit with 64-bit libraries. Some features of the hydrogen properties were removed between CoolProp v4.2.5 and v6.x, so future work will

focus on updating CoolProp to include better hydrogen properties or to move away from the EM approach altogether.

II. MODIFICATIONS FOR FMU EXPORT

A few changes are required to optimize the model developed for use in the IDE so that it is most useful as an FMU; otherwise, the actual export process is quite simple.

II.A. Model Changes

To best accommodate using the model as an FMU, three features are required: external connectors, default values, and parameterization, as discussed below.

II.A.1. External Connectors

An FMU is most useful when it can be connected as part of a larger system in another code. External connectors are used to send information from the driver code to the FMU. Under the current FMI 2.0 specification, external connectors are restricted to primitive datatypes: Boolean, integer, real, and string. To exchange thermal-hydraulic information on the system boundaries, boundary conditions must be established that can receive time-dependent values as one of these four datatypes. In general, real connectors are used for this model for tank pressure and temperature, valve position, and control drum position. A Boolean connector is provided to deactivate the built-in PI controllers and to switch to external control. Integer and string connectors are not used in the current model version.

II.A.2. Default Values

When exported as an FMU, the model can be run standalone or as part of a larger system using external connectors. For debugging purposes, default values are useful so the model can be run standalone. Default values have been added to all external connectors for this work.

II.A.3 Parameterization

Model parameterization is the establishment of clearly defined static values that the simulation can use for model setup and initialization. Modelica distinguishes between time-dependent *inputs* and time-independent *parameters*.

Using parameters for an FMU allows a single model to be used for multiple iterations of a reactor core or engine design cycle. Example parameters include initial conditions, power shapes or distribution factors, heat transfer modification factors, and valve or flow resistor settings.

Acceptable parameters for an FMU are limited to those that do not affect the compilation, even if they are a model parameter in the IDE. Examples of this limitation include discretization of components. The number of nodes is fixed at the time of FMU compilation and cannot be changed. Distributed parameters like the power shape can be changed if the same number of points are used.

Even with these limitations, many parameters can be changed. Those considered the most likely to be changed or impactful to the behavior of the model are grouped together to make it easier for an FMU user to access. Other parameter obfuscation settings are available during FMU export which may be useful for an application in which a black-box approach is desired. For this work, exposing all parameters and variables is acceptable.

II.B. Fluid Property Library Changes

To support FMU export, a change to EM library compilation is required. The compilation scripts have been set up to simplify the change. As described in the ORNL fork of the EM compilation script comments, the user can simply change the library from a dynamic to a static linked library by making a single letter change to the compilation script. The dynamic library is used for simulation in Dymola, and the static library is used when exporting the model to FMU. The compiled dynamic library is included with the v4.2.5 tag, so the user must recompile the EM library as static linked before exporting an FMU.

II.C. Model Export

Once the changes described above have been made, the process to export the model using Dymola is simple. Through the graphical user interface (GUI), the user navigates to Simulation > Translate > FMU. The relevant model options used in this work were “Co-simulation using Dymola solvers,” version 2.0, and 64-bit binaries. The Dymola solver used is Sdirk34hw with a solution tolerance of 10^{-4}. Since a stiff solver is required to resolve the kinetics behavior, it is not clear if the current model can be immediately used in a real-time simulation environment. This aspect of dynamic NTR FMU use will be investigated further.

III. MODEL COMPARISONS

It is useful to compare the results of the FMU to the results from running in the IDE. An example transient is used for this comparison and is presented in Table I.

TABLE I. Chamber conditions for example transient

Time [s]	Pressure [%]	Temperature [%]
0	50	50
100	50	50
300	20	20
500	20	20
560	100	100
710	100	100
830	20	20
1,000	20	20

The transient establishes a steady-state condition at 20% chamber pressure and temperature by 500 seconds. Then, both values are ramped up to 100% over 60 seconds and held for 150 seconds. The engine is then brought back

down to the 20% condition over 120 seconds. The simulation concludes at 1,000 seconds. The use of 50% values at time equals zero helps to initialize since full-power design conditions are used as model defaults. The ramp-up starts at a lower power condition since this is what is expected to occur in a mission, although the details of the holding position before thrust-up has not been determined.

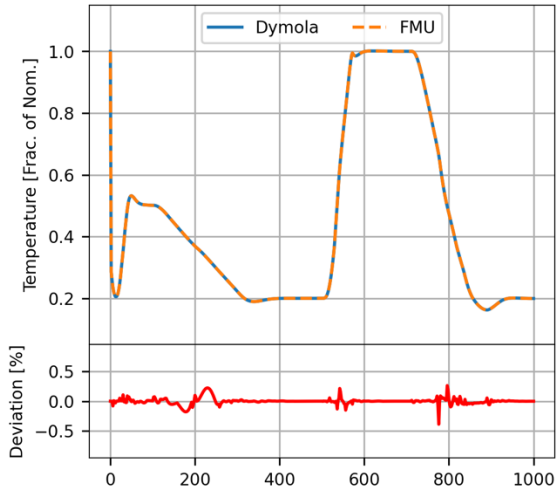

Fig. 2. Comparisons of temperature histories using FMU and Dymola.

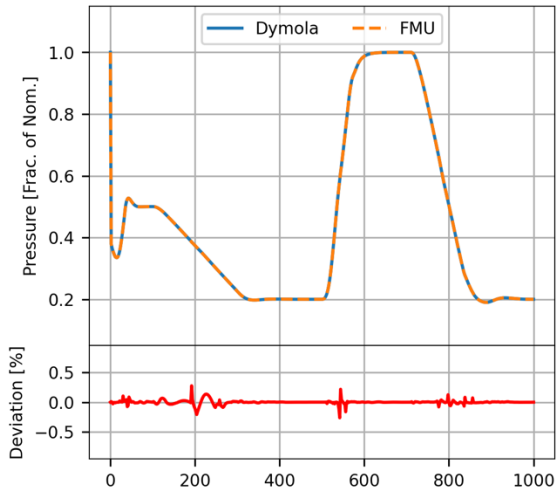

Fig. 3. Comparisons of pressure histories using FMU and Dymola.

Plots of the chamber pressure and temperature as functions of time for the Dymola-based simulation and the FMU simulation using FMPy are shown in Figs. 2 and 3. The trends overlap so closely that they are indistinguishable in the top graph. The percent difference is also shown as less than 0.5%. This provides confidence that the simulation performed in the IDE will be the same as the FMU in all meaningful characteristics. The simulation runs faster in the IDE at 182 vs 414 seconds. Although slower, the FMU still runs faster than real time. Improvement in FMU execution time is a subject of future work.

IV. CONCLUSIONS

A dynamic model of an NTR engine was updated to include the most recent system design features and to support model export with FMI for use outside the source code IDE. A comparison of the model results from the IDE and the FMU shows that there is very little difference in the results when the model is run outside the IDE. This feature should allow for improvements in the development of the engine I&C and EVI by increasing access to dynamic model results.

ACKNOWLEDGMENTS

This work was funded by NASA Marshall Space Flight Center.

REFERENCES

1. J. Rader et al., “Nuclear Thermal Propulsion Dynamic Modeling with Modelica,” NETS 2019, Richland, WA, USA. http://anstd.ans.org/NETS-2019-Papers.
2. J. Rader and M. Smith, “Dynamic Nuclear Thermal Rocket and Engine Modeling,” NETS 2020, Knoxville, TN, USA. https://nets2020.ornl.gov.
3. M. S. Greenwood, “TRANSFORM - Transient Simulation Framework of Reconfigurable Models.” Computer Software. https://github.com/ORNL-Modelica/TRANSFORM-Library. USDOE. 26 Sep. 2017. Web. DOI:10.11578/dc.20171025.2022.
4. CATIA Systems, “FMPy,” available online. https://github.com/CATIA-Systems/FMPy accessed on Feb. 10, 2021.
5. M. Binder, T. Tomsik, and J. Veres, “RL10A-3-3A Rocket Engine Modeling Project,” NASA Technical Memorandum 107318, January 1997. https://ntrs.nasa.gov/citations/19970010379
6. I. Bell, J. Wronski, S. Quoilin, and V. Lemort, *Industrial & Engineering Chemistry Research*. 2014, 53 (6), 2498–2508. DOI: 10.1021/ie4033999.
7. F. Casella and C. Richter, “ExternalMedia,” available online https://github.com/modelica-3rdparty/ExternalMedia accessed on Feb. 10, 2021.
8. ORNL-Modelica, “ExternalMedia” available online https://github.com/ORNL-Modelica/ExternalMedia accessed on Feb. 10, 2021.

Nuclear and Emerging Technologies for Space
Sponsored by Oak Ridge National Laboratory, April 26th-30th, 2021.
Available online at https://nets2021.ornl.gov

SAFETY DESIGN CONSIDERATIONS FOR NUCLEAR REACTOR POWERED SPACECRAFT

Robert W. Schleicher[1], Ron S. Faibish[2], and Gerald Lilienthal[1]

[1]*General Atomics Electromagnetic Systems, 16761 Via Del Campo Ct, San Diego, State, 92127*
[2]*General Atomics Electromagnetic Systems, 3000 K Street NW, Suite 250. Washington, District of Columbia, 20007*

Robert W. Schleicher Contact Information: 858-762-7553, bob.schleicher@ga.com

ABSTRACT

This paper examines how safety considerations may affect the design of nuclear reactor powered propulsion systems, be it either nuclear thermal propulsion (NTP) reactor or nuclear electric propulsion (NEP). From this assessment, it is clear that safety considerations derive from the full range of development and deployment stages beginning with ground testing and extending to space operation. Each stage can impose design requirements that will affect the overall propulsion system design. It is also recognized that different government organizations may have safety authority for the different deployment stages. For example, the Department of Energy (DOE) would have authority during ground testing at one of its national labs, whereas the Department of Transportation (DOT) has the authority to approve the launch of a vehicle containing a nuclear system. At present, there is not a cohesive set of safety design requirements for space reactors such as exists for terrestrial reactors. Due to the strategic importance and cost of these systems, articulating and consolidating a consistent set of guidelines and requirements is a necessary step for U.S. space nuclear propulsion development. The paper attempts to address each stage of propulsion reactor deployment and suggest design approaches that can practically be implemented to achieve an acceptable standard of safety.

I. SPACE SAFETY CONSIDERATIONS

As the U.S. enters into a new era of nuclear reactor powered propulsion development, it is necessary to identify and consolidate the safety requirements that must be addressed in the design process. This task is more complex than for terrestrial reactors because the deployment stages involve substantially differing environments and risks but also may have different regulating/authorizing organizations. The relevant deployment stages include:

- Ground testing
- Transportation to launch site
- Storage
- Launch / re-entry
- Space operation

The authority to approve the launch of a nuclear system rests with the President of the U.S. per NSPM-20, this launch authority has been delegated to the DOT [1]. The Department of Energy (DOE), National Aeronautical and Space Administration (NASA) and Department of Defense (DoD) may also have safety authority during certain stages, but as a practical matter, all involved organizations will collaborate with the DOE to establish safety requirements for the design, testing and operation of space nuclear propulsion reactor.

Some initial work toward this goal has been done. For example, the DOE has provided general guidance on space nuclear reactor safety design requirements in Ref. 2, and NASA has provided some guidance in Ref. 3. However, it is left to the designer of a nuclear propulsion system to translate this multi-agency guidance into practical systems and features that protect persons that could be exposed to some degree of risk from the nuclear propulsion system. This paper discusses a "designer's approach" to consolidating the space nuclear safety requirements from the ground testing, launch and space operation stages and translating them into practical systems and features.

I.A. Ground Testing Safety Design Requirements

It is difficult to conceive of deploying a NTP reactor or NEP reactor without some degree of ground testing of the full-scale, full-fidelity reactor. This would be especially true for manned space flights. During the ROVER/NERVA program, nine critical NTP experiments were carried out, some of which released radioactive fission products and fuel debris to the environment [4]. Even though these tests were carried out at a remote location (National Test Site in Nevada), such tests would never be allowed today. Ground testing will have to be carried out in a specially designed facility that can prevent release of radioactive debris and fission products to the environment in the event of fuel or any other failure.

Ground testing would most likely be done at a DOE laboratory such as the Idaho National Laboratory (INL) which has the necessary nuclear reactor test expertise or at a NASA laboratory such as the Stennis Center in Mississippi, which has the H_2 flow facilities and expertise. In either case, the reactor, in conjunction with the test facility, would have to meet safety requirements normally imposed upon terrestrial reactors. For the case of the INL site, these requirements are imposed and enforced by the DOE as required per 10 CFR 80 Subpart

B and 10 CFR 85 for facility safety. The reactor safety design criteria are set forth in DOE Order 5480.30, which identifies the Nuclear Regulatory Commission (NRC) Regulatory Guide 1.70 as a guide for the preparation of safety analysis reports. Because of these requirements, the combination of the reactor design and the test facility must meet many of the safety design requirements imposed upon terrestrial reactors.

The most important of these relates to containment of fission products. Although one can argue that fission product containment is not necessarily protect the crew of a spacecraft, containment is required to meet radiation exposure limits for the test facility staff and the public. The dose limitations of 10CFR20 and 10CFR100 and their implementation through regulatory guidelines would apply to the test facility. As a practical matter, this will necessitate that the reactor fuel elements incorporate one or more barriers to limit fission product release to the facility for both normal operation and anticipated transients. Any residual release from the reactor would have to be contained by the test facility.

Fission product retention is easier for an NTP reactor because of its short operating life (e.g. a few hours), even though the temperatures are much higher than for an NEP reactor. Fission product release is restricted by diffusion through the fuel itself and by a coating or cladding element that encapsulates the fuel. In many cases the cladding element also serves to prevent migration of the fuel itself. Thus, a safety requirement imposed by ground testing of an NTP reactor is that it incorporate an effective fuel cladding to prevent fission product release. The reactor system design should also incorporate the means to protect against cladding failure.

In the case of NEP reactors, the temperatures are lower, but the operating time is much longer (e.g. a few years). Thus the test period will be longer. This requires a more robust fission product containment design, which might be provided by a combination of fuel cladding and the reactor vessel. The test facility would constitute a third barrier comparable to a containment or confinement structure in a terrestrial reactor. Thus, a safety requirement imposed by ground testing is that the NEP reactor incorporate fuel encapsulation and a sealed vessel/primary system and that the reactor system be designed to protect the two fission product barriers against failure.

A second requirement affecting the propulsion reactor safety design is the need for safe shutdown reactivity insertion. As in the case of all U.S. terrestrial reactors, the test reactor must have two independent means of safely shutting down the reactor in response to an unanticipated event that would threaten the integrity of a fission product barrier. For most propulsion reactors, the main shutdown system would be rapid rotation of the control drums to the shutdown position. This likely would be accomplished by a spring-loaded mechanism with sufficient control drum redundancy to allow for a stuck drum. In fact, a practical design might allow for two stuck drums since a prudent operating requirement would which would allow for reactor startup with an initial stuck drum.

Ground testing of the propulsion reactor would also require an additional, independent shutdown system such as one or more control rods that could be injected into the core to render it subcritical i9n the event of failure of the control drums. This can be a challenge for a reactor with strict space and weight limits. Fortunately, there are several approaches that can be implemented to meet this requirement. For example, it may be possible to show that termination of H_2 flow in NTP reactors provides sufficient reactivity reduction to render the core subcritical, provided decay heat removal can still be safely accomplished. For NEP reactors, it will be necessary to have a separate reactivity insertion mechanism. For some reactor types, it may be possible to show that a strong negative temperature coefficient would safely reduce the power to near decay heat levels.

I.B Launch and Re-entry Safety Design Requirements

At the launch of a space propulsion reactor, it would not likely have operated and, therefore, would not contain fission products and nor generate decay heat. The principal safety requirements relate to preventing reactor criticality in the event of a launch failure causing reactor re-entry and preventing fuel dispersion such as in the case of the 1978 accidental re-entry of a Russian COSMOS 954 rocket carrying a TOPAZ II reactor fueled by high-enriched uranium (HEU). The spacecraft fell in northern Canada and HEU was dispersed over an area of 100,000 km^2 [5].

Criticality upon re-entry is postulated to occur by at least two scenarios. One is if the reactor should fall into a water body such that moderating water fills and surrounds the reactor. The reactor must remain subcritical in such an event. The drums must be locked in the shutdown position to prevent rotation upon impact. However, because most NTP reactor designs are under-moderated, this may not be sufficient to prevent criticality if submerged in water, so that a separate mechanism must be incorporated into the design to provide the needed negative reactivity. The challenge to implementing this requirement is that the additional mechanism must be eliminated when the reactor is safely in space to allow the reactor to start. This can be accomplished passively for some reactors with a hard neutron spectrum through rapidly depleting burnable poisons. For well-thermalized reactors, it would be necessary to incorporate a physical device into the core during launch and remotely remove it prior to startup in

space. Either method is a challenge that must be addressed in the design/development phase.

A second scenario for postulating reactor criticality is through compaction upon impact upon the earth surface. The design of the reactor in conjunction with the launch vehicle cargo faring must prevent compaction criticality. A closely related requirement is prevention of reactor breakup from heat and impact resulting in the spread of nuclear fuel material as in the case of the COSMOS 954 re-entry event.

One approach to meeting this requirement, is to incorporate a removable aeroshell for the launch operation. An aeroshell is a rigid heat-shielded shell that helps decelerate and protect a spacecraft vehicle from pressure, heat, and possible debris created by drag during atmospheric entry. The deceleration also helps reduce the impact shock. Its main components consist of a heat shield and a back shell. An example is shown in Fig. 1 [6]. Once the reactor is safety in orbit, the aeroshell would be removed and discarded.

Fig. 1. NASA aeroshell for Mars 2020 Space Exploration Program

Additionalsafety requirements apply to the case of an uncontrolled re-entry of a nuclear powered spacecraft that crashes into the public domain. NSPM-20 provides clear guidance regarding dose limits to a member of the public resulting from the crash. These limits are expressed in probabilistic terms in Table 1 and are very similar to requirements for terrestrial reactors [7]. For example, if a postulated accident is capable of exposing a member of the public to a dose of between 5 and 25 rem, then the spacecraft and reactor must be designed such that the calculatedprobability of such an event is no less than 1 in 10,000 for a single launch.

Table 1. Probabilistic Dose Limits for Accidental Crash of an Operating Space Reactor into the Public Domain

	Dose per Event, rem		
	0.025 – 5.0	**5.0 – 25**	**> 25**
Probability Limit	10^{-2}	10^{-4}	10^{-5}

I.C Space Operation Safety Design Requirements

The role of safety during manned space flight is not only to protect the spacecraft crew from radiation from the reactor but to move the crew quickly through the space mission and return them safely back to earth orbit. It is somewhat ironic that nuclear energy is, in fact, employed to reduce radiation exposure to the crew by reducing the mission time. The sources of this radiation are solar flares, galactic cosmic radiation and trapped ionized particles in the earth's magnetic field. The rate of exposure varies primarily with the solar cycle, but an average dose for an astronaut that spends six months in the International Space Station is 16 rem. The average dose for a 3-year Mars mission is 120 rem. For this reason, NASA has established an annual radiation dose limit for low earth orbit of 50 rem/year. This compares with 10 CFR 20 limits for terrestrial radiation workers of 5 rem per year and a total career dose limit of 25 rem. NASA's total career dose limit is based on the risk of an average of 3% loss of total lifespan, This results in the values given in Table 2 [7].

Table 2. NASA Career Radiation Dose Limits for Astronauts in Rem

Age	**25 yrs**	**35 yrs**	**45 yrs**	**55 yrs**
Female	100	175	250	300
Male	150	250	325	400

This leads to the question of what dose limit should be used for design of radiation shielding between the reactor and crew. The key difference between radiation from the reactor and from space is that the reactor designer has control over the dose from the reactor by design of the shielding. Thus, the principal of "As Low As Reasonably Achievable" (ALARA) applies. A reasonable limit would be the same value as applied to terrestrial radiation workers, i.e., 5 rem/year.

The other aspect of nuclear propulsion safety for space operation relates to prevention of transients that could disable the propulsion system to the point that it can no longer support the mission. This effectively is a conjunction of system reliability and safety. There is no practical ability to effect repairs other than control system corrections. The approach to this aspect of reactor safety is a combination of adequate system diagnostics and redundancy of critical subsystems and components.

Accurate information on system status and health requires a well-thought out approach to system diagnostics. Key parameters include core power distribution, H_2 flow distributions, component temperatures, vibration levels and mechanical strains in key structures. It would be unreasonable to expect the crew to continuously process all the information from the diagnostics, so the control system must be able to monitor key variables, process the information and take remedial

action or recommend remedial actions to the crew. This information must also be transmitted to earth, but it must be recognized that there could be a considerable time interval for transmission, perhaps up to an hour for a Mars mission. A significant effort must be expended in the design of the control and instrumentation system with incorporation of learning algorithms implemented during testing and parametric simulation of transient events.

All terrestrial reactors incorporate a safety system which shuts the reactor down if a condition arises that can cause a release of radioactivity. This may not be the highest priority for a space reactor. Rather, safety shutdown should be implemented primarily to terminate events that could cause irreparable damage to a propulsion engine such that it is rendered unable to accomplish a mission abort and return to earth.

The safety shutdown system is important area of redundancy for all reactors. For a space reactor, this applies to the control drums. An essential design approach would be to assure that reactor control and shutdown could be accomplished with at least one drum rendered inoperable, either in a full-out or full-in position. Ability to start the reactor with one stuck drum is just as important as the ability to shut it down. If the reactor is started with a stuck drum, then it may be necessary to require that it can be shut down with an additional stuck drum.

Ability to remove decay heat from a shutdown reactor is especially important for NTP systems where the reactor only operates for a short time during the mission but generates decay heat that lasts for a much longer period of time. When the reactor is shutdown, reactor heat is difficult the remove without flow of propellant. This would add an undesirable mass burden to the spacecraft and would require an energy source to flow propellant/coolant. The best practice approach is to construct the reactor design to be able to reject decay heat directly to space by radiation from the reactor vessel walls. This necessitates choosing materials with ability to withstand temperatures and have sufficient surface areas to support adequate radiative heat transport to space.

II. CONCLUSIONS

Although by no means complete, this discussion recognizes that propulsion system safety design considerations span the range of deployment stages from ground testing to space operation. It also recognizes that different government organizations may have safety authority for the different stages. At this pioneering time in nuclear propulsion development, it is left to the designer to create a single propulsion system design that meets meet the safety requirements for all deployment stages. At this time, well-thought out, consistent and comprehensive set of guidelines and/or regulations does not exist and would greatly assist the designer in this endeavor. In addition, to facilitate robust reactor safety design it would be helpful if the relevant government agencies establish formal working relationships to assure consistency in regulations. As an example, the Memorandum of Understanding for space nuclear cooperation between DOE and NASA [8] is a good start. It is suggested that this would be an important area for investment of space development funds.

REFERENCES

1. *National Security Presidential Memorandum 20, Launch of Spacecraft Containing Space Nuclear Systems*, April 20, 2019
2. *Nuclear Safety Criteria and Specifications for Space Nuclear Reactors*, U.S. DOE Office of Space Nuclear Projects, August, 1982.
3. *NASA General Safety Program Requirements, Chapter 6 Nuclear Safety for Launching of Radioactive Materials*, NPR 8715.3D, Effective August 1, 2017.
4. HASLETT, R.A., *Space Nuclear Propulsion Program Final Report,* Phillips Laboratory, May, 1995
5. GUMMER, W.K., F.R. CAMPBELL, G.B. KNIGHT, J.L. RICARD, *COSMOS 954, The Occurrence and Nature of Recovered Debris*, INFO-0006, Canadian Government Publishing Center, May 1980.
6. NASA Science website, https://mars.nasa.gov/resources/24752/mars-2020s-aeroshell/
7. NASA ebook, *Space Radiation*, https://www.nasa.gov/sites/default/files/atoms/files/space_radiation_ebook.pdf
8. Memorandum of Understanding between NASA and DOE, October 20, 2020.

Nuclear and Emerging Technologies for Space
Sponsored by Oak Ridge National Laboratory, April 26th-30th, 2021.
Available online at https://nets2021.ornl.gov

PROGRESS ON DECAY HEAT MODELING AND MITIGATION IN NTP SYSTEMS

Aaron Selby[1], Vishal Patel[1], Sarah Yue[1], Michael Eades[1]

[1]*USNC-Tech, 2356 W Commodore Way #120, Seattle, WA 98199*

Primary Author Contact Information: (865) 293-9367; a.selby@usnc-tech.com

Decay heat solutions are essential for maximizing the performance of NTP systems, reducing the amount of required cooldown hydrogen, and guaranteeing system safety. USNC-Tech's solution to NTP decay heat removal and utilization is high-temperature moderator elements with a moderator capable of operation at 1,000K. USNC-Tech is currently designing, building, and testing prototypic high-temperature tie tubes. These high-temperature moderator elements reduce the required cooldown hydrogen by over 50% and enable the co-power generation and RCS/OMS capabilities, enhancing the versatility of NTP for future space mission.

I. INTRODUCTION

Nuclear thermal propulsion systems (NTP) have historically used significant amounts of hydrogen to cool down the residual heat, known as decay heat, of an NTP system after operation. Decay heat solutions are essential for maximizing the performance of NTP systems and guaranteeing system safety. USNC-Tech has been performing an in-depth look into understanding and solving NTP decay heat by utilizing dual-mode power co-generation and a high-I_{sp} reactor-powered Reaction Control System (RCS)/Orbital Maneuvering System (OMS). USNC-Tech's solution to NTP decay heat removal and utilization is a high-temperature tie tube with a moderator capable of operation at 1,000K. USNC-Tech is currently designing, building, and testing prototypic high-temperature NTP moderators. These high-temperature moderators enable the co-power generation and RCS/OMS capabilities and enhance the versatility of NTP for a human Mars mission and other missions beyond low Earth orbit.[1]

Previous state of the art estimations state that up to 5% of the hydrogen used during a NTP burn is needed for cool down.[2] With advanced optimization and high-temperature tie tubes, USNC-Tech has shown that both the amount of cooldown hydrogen and the cooldown time can be reduced by more than a factor of two.

Increasing the temperature capabilities of an NTP system's hydride moderator is central to addressing decay heat. Hydride moderators are the lowest temperature component inside the NTP core and drive the temperature at which hydrogen removes decay heat from the core. During the decay heat removal phases of operation, providing hydrogen overpressure may not be possible or overly difficult so the temperature limit of hydride moderators is greatly reduced from full power operation. Furthermore, many co-power generation configurations for NTP systems make it impossible to provide hydrogen overpressure during power generation

Figure 1 shows the relationship between the maximum temperature capabilities of a tie tube and minimum hydrogen needed to cool the core.

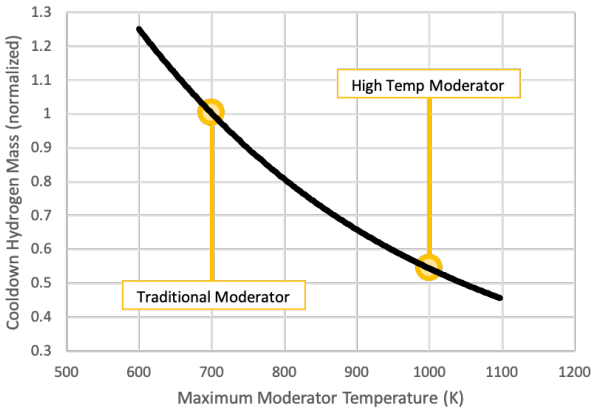

Fig. 1. Normalized Hydrogen Needed to Remove Decay Heat vs. Temperature Capability of Moderator

II. PROGRESS ON HIGH TEMPERATURE MODERATOR DEVELOPMENT

II.A. Moderator Development

II.A.1 ZrH Manufacturing

USNC-Tech is using two parallel approaches to manufacturing solid ZrH moderator elements. The direct hydride route uses a hydrogen furnace system to hydride solid Zr pellets. The other route involves hydriding a large amount of Zr feedstock, powderizing the resulting ZrH, and then compacting that into pellets. Those pellets are then canned to increase the temperature capability of the moderator. Both routes have advantages and disadvantages, and this project aims to understand which route will produce the best ZrH moderator elements to incorporate into tie tubes in NTP systems.

To perform the direct hydriding of Zr pellets, USNC-Tech has teamed up with PNNL to use their Sievert's Pressure System. The process of direct hydriding using PNNL's Sievert's Pressure System uses a hydrogen

absorption/desorption test to hydride the Zr. This involves using a volumetric method to determine the pressure difference between sample chamber and a calibrated volume, monitoring pressure, temperature, and time to observe the hydrogen absorption, desorption, and the rate. This process is very slow, taking over a week to hydride a 50mm long by 10mm diameter Zr rod to an H/Zr ratio of 1.8. The first scoping test produced a ZrH sample with 1.98 wt% H. This process results in a brittle, spongelike sample, as shown in Figure 2. The first sample broke in half, so research continues to determine the correct parameters for producing intact ZrH rods, such as changing the H loading, lowering the loading rate, and lowering the maximum pressure.

Fig. 2. ZrH as Manufactured Through Direct Hydride Method

The alternative approach to producing ZrH moderator elements is to produce ZrH powder and then compress the powder into pellets. A Zr sponge feedstock with low Hf content was selected and hydrided in a hydride furnace. The sponge was then milled and sieved to produce a fine ZrH powder. The powder was then compressed using a die and a cold uniaxial press to form solid ZrH pellets, as shown in Figure 3. The ZrH pellets were then analyzed. The density was ~70-80% and the H/Zr ratio was 1.65 – 1.79. Further research will be conducted to increase both the density and H/Zr ratio for the pressed ZrH powder route.

Fig. 3 Pressed Powder ZrH Pellets

It is also important to consider the type of Zr feedstock that is used for ZrH, because certain impurities are strong neutron absorbers. For the powder compaction route, USNC-Tech selected a high-purity Zr powder with <0.005% Hf. For the direct hydriding route, USNC-Tech selected a high-purity Zr with less than 2% Hf content and zircaloy-4, a nuclear-grade Zr alloy with 0.01% Hf. USNC-Tech will evaluate both pure Zr and zircaloy-4 for its use as ZrH moderator elements in high-temperature tie tubes.

II.A.1 Canning ZrH Moderator

To extend the life and increase the maximum operating temperature of the ZrH moderator in the NTP system, USNC-Tech is evaluating canning the ZrH in a hydrogen-resistant material. USNC-Tech is currently evaluating candidate materials and has down-selected to alumina and quartz. Both alumina and quartz have very low hydrogen permeability and have high melting points, making them excellent candidates for canning materials.

Exposing the ZrH moderators to high temperatures prior to the initiation of the hot hydrogen test runs the risk of degrading the hydrogen content within the ZrH. USNC-Tech is currently investigating methods for sealing the cans while keeping the ZrH temperature low.

II.B. Moderator Structural Component Selection

Historical tie tubes in high assay low-enriched uranium (HALEU) NTP systems were made of zircalloy, which has an optimistic maximum operating temperature of 700K and hydrogen embrittlement issues. To mitigate these issues and maximize the operation of the NTP system, USNC-Tech has investigated alternative tie tube materials, taking into account hydrogen compatibility, high-temperature performance, neutron transparency, density, availability, and manufacturability. After an extensive analysis, USNC-Tech down-selected to SiC-SiC composite and TZM, a molybdenum-based alloy. USNC-Tech is currently procuring these materials to be incorporated into the prototype high-temperature moderator element hot hydrogen experiments.

II.C. Hot Hydrogen Test Loop Development

USNC-Tech has teamed up with Pennsylvania State University (Penn State) to develop a hot hydrogen test loop experiment to test the prototype high-temperature moderator elements.

Penn State has developed the hot hydrogen test facility consisting of a hot hydrogen test loop used for testing the prototypical moderator elements and high temperature tie tubes in a pressurized, hot hydrogen environment.[3] Prototypical high-temperature moderator elements with canned ZrH will be tested up in pressurized, flowing, 1,000K hydrogen to simulate the NTP system operating conditions. Figure 4 shows a schematic of the test loop design. This loop can heat up hydrogen to >1,000K and

recirculate hydrogen at pressures up to 3,000 psi and with flow velocities up to 110 scfm. The loop pipe material is made of stainless steel 316 (SS316). SS316 has a melting onset temperature of 1648K, much higher than the 1,000K test temperature. The nickel-chrome -based heaters operate via radiant heat and will be wrapped in alumina fiber-based insulation in order to sustain high temperature heating during operation.

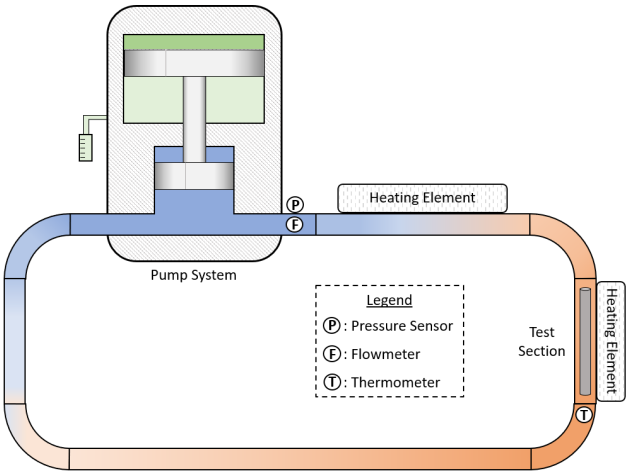

Fig. 4. Hot Hydrogen Test Loop Schematic

Inside the test section will be the high-temperature moderator element experiment test article, shown in Figure 5, which holds the prototypical moderator element with the canned moderator element and allows pressurized, hot hydrogen to flow through the moderator element.

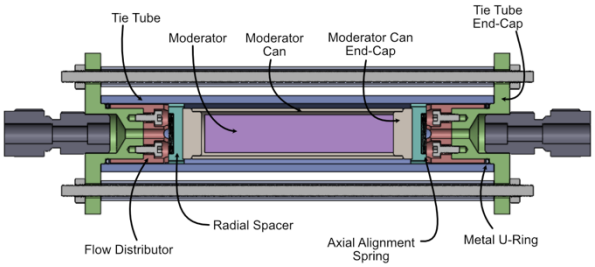

Fig. 5 High-temperature Moderator Element Experiment Test Article

III. PROGRESS ON HIGH FIDELITY MODELING

NTP systems require NTP-specific decay heat correlations for accurate predictions. USNC-Tech research has indicated that traditional decay heat correlations underpredict decay heat production. As a part of USNC-Tech's work in modeling and mitigating decay heat, USNC-Tech has developed methods of producing NTP-specific decay heat correlations.

For this work, a reference core was produced for modeling decay generation. This refence core uses the USNC-Tech "Cookie" fuel element with UN coated particles in a ZrC matrix to form a fully ceramic microencapsulated (FCM™)-derived fuel form. This fuel has internal circular channels for cooling. The fuel is placed in a structural/moderating Be metal matrix. Pins of $ZrH_{1.6}$ moderator are placed throughout the core to further increase moderator and reduce core sizes. Figure 6 shows this core.

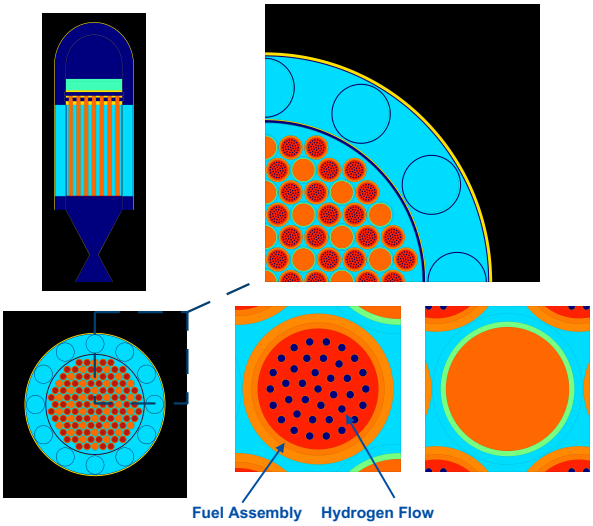

Fig. 6. Reference Core

III.B. Decay Heat Estimation

USNC-Tech has devised a method to calculate decay heat using MCNP to calculate reactor specific 1-group cross-sections and a 238-group flux to generate activation/decay libraries for use in ORIGEN. ORIGEN is then run in a mode to calculate heat produced during an NTP operational cycle.

ORIGEN is a package in Oakridge National Laboratories SCALE software code package that calculates fission production, decay chains, neutron sources, high-energy photon sources, alpha sources, and beta sources within a material.[4] This data is used to determine the decay heating given a neutron spectrum, power profile, external-to-fuel fission-induced heating, and fuel composition.

USNC-Tech also developed a separate methodology for calculating the expected decay heat using the Serpent code.[5] Specific details are found in (Denig and Eades, 2020).[6] First, an estimate of effective energy per fission is calculated by running a Serpent calculation with coupled burnup at a low power level. The total amount of heat absorbed in the reactor is calculated over time allowing for an estimate of the fission Q value taking into account neutron and photon leakage. This effective Q value curve is used with the power cycle schedule to calculate the expected number of fissions during operation. The number

of fissions predicted are used to calculate a Q-value to input to Serpent such that during a Serpent burnup calculation, the expected number of fissions will be recovered. A second Serpent burnup calculation is performed using the actual power cycle and many steps after the reactor is shutdown to calculate the heat generated from decay products after shutdown.

The main conclusions from the two studies using two different decay heat solvers are that they produced similar results and that the standard Todreas decay heat correlation underpredicts decay heat.[7] These conclusions are shown in Figure 7, in which various results are plotted that predicted decay heat after shutdown.

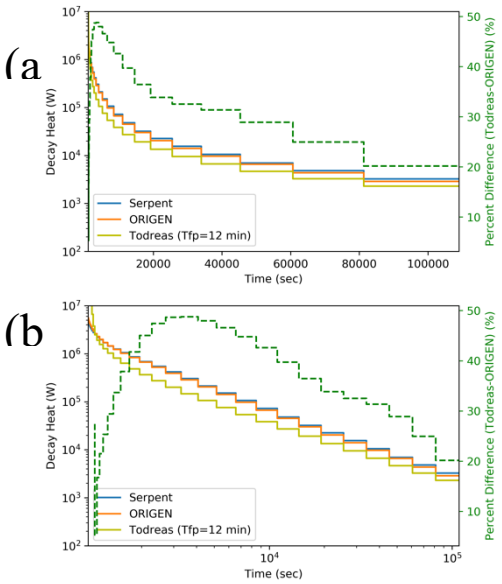

Fig. 7. Todreas Correlation Comparing Serpent and ORIGEN Decay Heat Calculations with Time Plotted on (a) a Linear X-Axis and (b) a Log X-Axis

Todreas underpredicts decay heat, because it assumes a larger energy release from fission than that assumed by the Monte-Carlo-informed methods performed by USNC-Tech. By assuming a larger energy release, less fissions are predicted to maintain desired core power. The prediction of less fissions results in reduced decay heat because, there are less fission products to produce decay heat.

The comparison between the two Monte-Carlo-informed methods is not in exact agreement; however, the trends are similar, and the total decay heat predicted agrees within 5%. USNC-Tech continues to investigate the reason for the differences.

There is not a clear best method for predicting decay heat between the two Monte-Carlo-informed methods. The Serpent method allows for use of a single code, while the ORIGEN method allows for speed. The current preference of USNC-Tech is the Serpent method, because it has better integration into our analysis framework. This is subject to change as the difference between the two Monte-Carlo informed methods is further investigated.

IV. CONCLUSIONS

USNC-Tech's solution to NTP decay heat removal and utilization is a high-temperature moderator with a moderator capable of operation at 1,000K. USNC-Tech is currently designing, building, and testing prototypic high-temperature moderator elements. These high-temperature moderator elements reduce the required cooldown hydrogen by more than a factor of two and enable the co-power generation and RCS/OMS capabilities, enhancing the versatility of NTP for future space missions.

ACKNOWLEDGMENTS

This work was funded under NASA's SBIR program under contract 80NSSC19C0202. The authors would like to thank Dr. Ewa Rennebro at Pacific Northwest National Lab for support in ZrH manufacturing and testing. The authors would also like to thank Dr. Leigh Winfrey and William Searight at Penn State for the development of the hot hydrogen test loop.

REFERENCES

1. M. G. Houts et. al., "Design Options for a Versatile Nuclear Thermal Propulsion (NTP) Stage," 2018 AIAA SPACE and Astronautics Forum and Exposition, Orlando, FL, (2018).
2. F. P. Durham, "Nuclear Engine Definition Study Preliminary Report, Volume 1 – Engine Description," *Los Alamos National Laboratory Informal Report,* LA-5044-MS Vol 1, Los Alamos, United States (1972).
3. W. Searight and L. Winfrey, "Design of a Hot Hydrogen Test Loop for Plasma-Material Interactions evaluation". *Fusion Science and Technology*, (2021).
4. B. T. Rearden and M. A. Jessee, "SCALE Code System," ORNL/TM-2005/39, version 6.2. 1.
5. J. Leppänen, et al. "The Serpent Monte Carlo code: Status, development and application in 2013," *Ann. Nucl. Energy* (2015).
6. A. Denig and M. Eades, "Monte Carlo–Informed Decay Heat Model for Cermet LEU-NTP Systems," *Nuclear Technology*, 206:8, 1171-1181, (2020).
7. N.E. Todreas, M.S. Kazimi, *Nuclear Systems I: Thermal Hydraulic Fundamentals*, Taylor and Francis, (1993).

Nuclear and Emerging Technologies for Space
Sponsored by Oak Ridge National Laboratory, April 26th-30th, 2021.
Available online at https://nets2021.ornl.gov

MIT REACTOR IRRADIATION CAPABILITIES FOR SPACE NUCLEAR TECHNOLOGY DEPLOYMENT

Koroush Shirvan[1], David Carpenter[2], Gordon Kohse[2] and Lance Snead[2]

[1]*Department of Nuclear Science and Engineering, Massachusetts Institute of Technology, Cambridge, MA, 02114*
[2] *Nuclear Reactor Lab, Massachusetts Institute of Technology, Cambridge, MA, 02114*

617-452-3017; kshirvan@mit.edu

MITR is a 6 MWth facility on Massachusetts Institute of Technology campus. With peak neutron fluxes of up to $6x10^{13}$ n/cm^2-s (thermal) and $1.2x10^{14}$ n/cm^2-s (fast), MITR provides a unique irradiation capability to support space nuclear technology deployment. Recent experience with handling fissionable materials (up to 100 grams of U235 equivalent) and hydrogen gas along with operating at high temperatures (up to 1600^{o}C) readily enables supporting of current nuclear space missions. Such unique irradiation capability with wide operating envelope provides an ideal platform for emerging fuel technology down selection. Particularly, with advent of advanced manufacturing and progress in material science, the design space for potential high performing materials for space application has considerably widened and requires support from a prototypic irradiation test bed. In the near future, over cubic meter of irradiation space will be available to perform testing on full size components such as fuel blocks, I&C kits, control drums for direct prototypic demonstration. This summary outlines the specific capabilities and recent progress with respect to supporting fission technologies for propulsion and surface power in space.

I. INTRODUCTION

Massachusetts Institute of Technology (MIT) has a long history in conducting materials and fuel irradiation experiments using its 6 MWth MIT Research Reactor (MITR). MITR has a wide range of irradiation facilities that offer neutron fluxes up to $6x10^{13}$ n/cm^2-s (thermal) and $1.2x10^{14}$ n/cm^2-s (fast). The MITR is a valuable test bed for research and development (R&D) related to current and next generation of nuclear technologies. The irradiation environment in the MITR core has very good access for installation and instrumentation and wide flexibility in operating protocols. The MITR reactor cycles are typically 60-65 days each. During a cycle the reactor operates continuously except for occasional scheduled outages for sample exchanges. There are several ports available for sample retrieval as desired while the reactor is operating.[1]

The renewed interest in deployment of micro-reactor and nuclear propulsion in the U.S., motivates overview of MITR relevant capability for such missions. The existing infrastructure and recent experience with irradiation and monitoring of fissile fuel at high temperature provides a critical foundation to accelerate nuclear technology development in space. Particularly, recent activity on achieving >1000^{o}C in-core, irradiation of advanced moderator materials and particle fuels, and in-core hydrogen (tritium) handling for molten salt irradiations,[2] forms a credible basis to support the current direction of nuclear thermal propulsion (NTP) technologies that are under development. The test samples are not only exposed to the intense radiation field but also can be adapted to the environment or objectives of interest. For instance, existing experience includes inducing stress on samples, to study irradiation-assisted stress corrosion cracking mechanisms. Irradiation response of high temperature irradiation-resistant reactor instrumentations such as thermocouples, optical fibers, self-powered detectors, ultrasonic sensors, etc., have also been recently explored. The equipment for macro-photography, optical digital microscopy, SEM/EDS, thermal diffusivity measurement, optical profilometry and digital image correlation are accessible for post irradiation examination (PIE). A variety of radiation detection equipment is also available, including liquid scintillation counting and HPGe detectors for beta and gamma spectroscopy.[1]

For nuclear fission applications, timely qualification of advanced fuels and in-core materials to enable meeting the mission's performance metrics is critical. A fuel and nuclear materials qualification campaign typically involves three steps: fabrication (2-3 years), irradiation testing (depending on application) and PIE to support code and model development that takes 2-3 years. A typical process involves 4 phases of the stated steps, starting with an initial fuel concept (Phase 1), down selection to promising variants (Phase 2), performing prototypical testing (Phase 3) and the final qualification phase (Phase 4). Luckily, in general, the NTP applications require relative low irradiation fluence, which can accelerate the irradiation time using high flux facilities such as MITR and shorten the PIE due to low radioactivity. Nevertheless, the fuel fabrication, characterization and modeling can still take ~20 years to reach qualification. With the growing need to meet shorter timeline and attain higher performances, the ability to rapidly test emerging materials at the prototypic scales (Phase 3) can significantly accelerate such time lines.

As such, we overview how MITR can support acceleration of R&D and serve as an irradiation test bed for space nuclear technology. The ability to perform irradiation on non-core components at full scale will also be discussed. We also present our recent progress in supporting nuclear space technologies with MITR. For generic nuclear technology applications and capability, readers are referred to the MITR user guide document.[1]

II. CAPABILITY FOR SPACE NUCLEAR

II.A. Rapid Turn Around Pneumatic Tube Facility

MTIR provides the ability to expose any material (including fissile material) in a "rabbit" pneumatic tube system under environment of choosing including hydrogen gas at low temperatures. The facility is not instrumented and cooled by air. The ports can accommodate up to 1.375'' diameter and 6.25'' irradiation space at the noted MITR peak fast and thermal fluence. The maximum sample mass can be 50 g and the time of irradiation can vary from few minutes to days.

Nuclear space technology, particularly for NTP, requires novel materials to continue to push the specific impulse (ISP) and thus propellant temperature beyond ~2600 K (based on NERVA-type engine designs with hydrogen as the propellant). At temperatures greater than 2600 K, refractory metals and ceramics that are difficult to morph in the optimal geometry are of high interest. In particular, the optimal geometry would involve incorporating ideal fission fuel material within a high temperature material matrix. With advent of advanced fabrication techniques, incorporation of such material to improve the NTP performance is more readily accessible.[3] However, advanced fabrication techniques can have profound impact on the material microstructure and its response to neutron and ionizing radiation. The pneumatic tube can provide a rapid and low cost test bed to perform such studies. Currently, testing of various spherical fuel particles that utilize novel fabrication methods are under way. The testing involves sealing few fuel particles in a capsule with desired fill gas. Then after irradiation, the capsule can be punctured and the off-gas can be analyzed for presence of Xe or Krypton fission products followed by macroscopic evaluation. The satisfactory results will then motivates testing in "3GV" facility discussed in section II.B.

The recent efforts to limit the fuel enrichment of a NTP core to less than ~20% U235 or High Assay Low Enriched Uranium (HALEU), motivates the exploration of thermal spectrum reactors that allow for lighter cores vs. fast spectrum reactors with HALEU. The conventional moderator of choice, Zirconium-hydride (ZrH_x) has limited temperature envelope. At high temperatures the outward diffusion of hydrogen can result in loss of local moderation and pressurization of its holding structure. As such, revisiting old high temperature moderators such as Yittrium-hydride[4] or novel high temperature moderators such as encapsulating ZrH_x[5] are of interest. Given the enormous number of possibilities in fabrication, stoichiometry and encapsulation material for only these two examples, initial rapid low cost testing with the pneumatic tube facility is desired to perform a logical down selection.

II.B. Prototypic Temperature and Environment in 3GV facility

The "3GV" vertical facility is located in MITR graphite reflector. The irradiation testing can be performed within a 2.5" ID and 18" in-core zone at $1.2x10^{13}$ n/cm^2-s thermal flux. The fast flux is markedly smaller (~10^{11} n/cm2-s) in this region of the MITR. However, the appreciable thermal flux can be used to boost the fast flux to ~$.5x10^{13}$ n/cm2-s with use of HALEU at under the 100 grams equivalent U235 allowable limit. The region is cooled with water cooling jackets that can be adjusted to meet a desired heat load. Samples and capsules can be inserted and retrieved while the MITR is operating at full power.

Since 3GV is outside of the core, it allows for more flexibility in the design space. The actual NTP operation time is also very small (~1 hour) with multiple startups that are limited to ~100 seconds based on the speed of rotation for control drums. As such, in addition to meeting the fluence target despite the lower power density in 3GV, we can also emulate the startup and shutdown of the NTP by a moving a cylindrical cadmium shield in the cooling jacked (~50 ^{o}C). This is feasible since 3GV is well outside of the core and Cd impact on core reactivity is minimal. We can also impose large temperature gradients governed by thermal fission to induce prototypic stresses in the sample by partially covering the experiments with a cadmium shield. We can also control temperature gradients by flowing gases of different conductivity and/or control the local fission rate with fluid boiling/condensation. These are all methods that are currently under investigation to support the NTP mission.

As mentioned, the fuel power density in 3GV will be substantially lower than an actual NTP application. We have recently performed MCNP calculations to understand the bounds of possible operating range. The results indicate that the fuel power densities of up to 400 W/cc can be accomplished. While this is low compared to NTP (~10,000 W/cc), it can meet the total energy deposition in 25x the NTPoperational time length (e.g. 25 hours). As for temperature, there are no theoretical upper limits for attainable temperature as long as the outer water jacket maintains its temperature under ~60^{o}C. The lower power density can reach prototypic temperatures by use of thermal insulators, such as gas gaps. Fig. 1 shows the preliminary design and thermal performance of such

facility with a cermet fuel sample specimen incased in a graphite block followed by layers of thermal shielding to reach maximum temperature of 2400 K with 400 K of temperature gradient across the cermet sample. The hydrogen flow path to the sample and detailed design of a similar facility for 3GV is current under investigation.

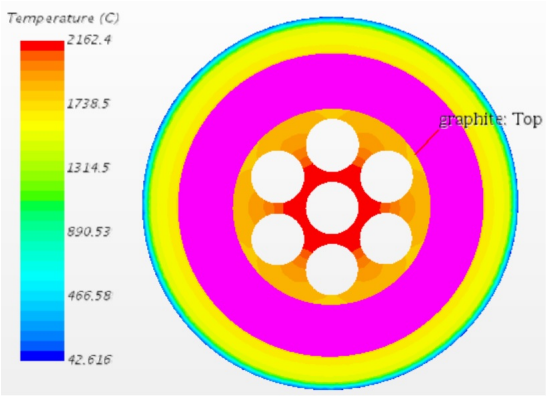

Fig. 1. The preliminary design and thermal calculation of a 3GV test section to meet NTP performance targets.

The combination of temperature, environment and reactivity/power control, makes 3GV an ideal test bed for new nuclear space fuel concepts. If deployed to its potential, the facility can reduce the mentioned ~20 years fuel qualification timeline by 6-12 years and allow for much wider evaluation of concepts to achieve a more optimum performance.

I.C. M3 Facility

The M^3 facility is currently being prepared to host a modular molten salt loop to support molten salt reactor (MSR) R&D and demonstration as supported by the recent DOE NEUP integrated research project led by MIT.[6] The loop is planned to be constructed in a modular fashion, such that it can be installed and removed flexibly to allow the space to be utilized for other experiments. The space as depicted in Fig. 2 in purple, is large enough to accommodate full scale NTP components such as control drums, I&C kits and fuel blocks. The space allows for specialized instrumentation to generate as much supporting data as desired.

Similar to 3GV, the thermal neutron beam can be used to generate the desired fast neutron level. Fig. 2 is based on a molten-salt-cooled, solid fuel in graphite block core that shares similarities to NERVA-type NTP designs. Since the M^3 facility is far away from the reactor, more substantial hydrogen flow is possible in addition to accommodating several fuel blocks or at least third of a typical NTP core. The fission reaction is driven by the fuel loading but the system is limited to a k_{eff} of less than 0.9.

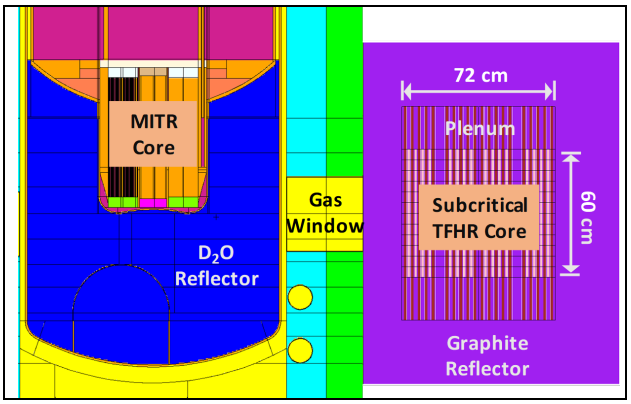

Fig. 2. Neutronic model of a subcritical Transportable Fluoride-salt-cooled HTR (TFHR) core element.[7]

II.D. In-Core Irradiation for High Fluence

The peak flux in-core (without sample fuel) is approximately $3.6x10^{13}$ n/cm^2-s thermal, and $1.2x10^{14}$ n/cm^2-s E>0.1 MeV. Thus, power density of 1,000 W/cc is achievable for fuel that can passively reject heat to the reactor coolant. While the power density is less than NTP targets, only handful of other facilities in the US can provide such flux levels and allow fissile fuel irradiation. Relative to the other ports in MITR, this region of the core is ideal to reach higher fluence, in particular to support surface power reactors.

The test with the highest temperature (1600ºC) at MITR took place in-core in the high temperature irradiation facility (HTIF) in 2006.[8] The schematic of this facility is shown in Fig. 3. The primary heating mechanism for the facility was the neutron and gamma absorption of molybdenum. The temperature was further enhanced by leveraging a gas gap where its composition can change. The primary motivation behind design of the facility was for TRISO fuel testing. which is of great relevance for current space nuclear technology.

Several tests were performed and the temperature was measured by thermal-couples. For instance, 1400 ºC was achieved both at 4 MWth with 100% Helium gas gap and at 3 MWth with 80% Helium-20% Neon gas gap. Currently, the MITR is licensed to 6 MWth and thus using 100% Neon gas, temperature of ~2400 ºC is achievable in this existing facility. The temperatures can be raised to 3000 ºC by including fissile fuel material in the capsule to boost the neutron and gamma flux and increase heating from the fission reaction. The gas gap also allows the online change of sample temperature without introducing radiation poisons that can be restrictive for an in-core testing location.

The long test section allows for loading multiple samples axially. Across the length of the test section, due to neutron leakage, substantial temperature gradient exists. For instance, measured temperature for one set of tests were 1350ºC in the middle, and 950 and 1050ºC 30

cm above and below the center, respectively. For such in-core facility, the test must last the length of the MITR fuel cycle (60-65 days) unless deemed mission critical.

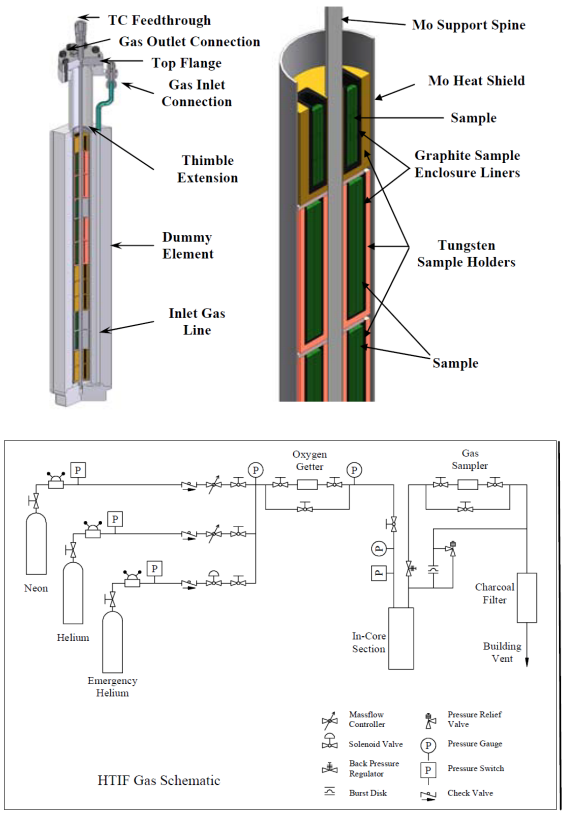

Fig. 3. The HTIF schematic including gas gap resistance.[8]

TABLE I. Summary of available capability with respect to nuclear fuel testing (exp.: experienced; Passive: requires double encapsulation and passive heat rejection; cost of relative neutron cost; Power densities are in W/cc)

Facility	Size	Temperature (K)	Power Density	Relative n Cost
Pneumatic	1.3''x6''	<500 K	800	1X
3GV	2.5''x18''	No Limit exp. 925 K	400	10-100X
In-Core	1.8''x24''	Passive exp. 1870 K	1,000	100X
M3	4'x4'x4'	No Limit exp. None	TBD	TBD

IV. CONCLUSIONS

The acceleration of high performing materials R&D is critical for advancement of space nuclear technology. MITR is currently performing irradiation service and designing facilities that can meet the target performance metrics for NTP and nuclear surface power applications. This includes the ability to meet very high temperatures, lifetime fluence and perform transient startup/shutdown testing for nuclear fissile fuel. Table I summarizes such capabilities. More complete information and up-to-date timeline of recent tests are listed in Ref. 9. As outlined, depending on objective, sample size, power density, fluence and cost target, there are multiple facilities that can be leveraged. MITR is part of the National Science User Facility (NSUF) and part of MIT as an educational non-profit institution. Limited seed fund irradiations are also available to the interested community.

REFERENCES

1. D. CARPENTER, G. KOHSE, L. HU, *MITR Users' Guide*, July 2012 <https://nrl.mit.edu/sites/default/files/documents/MITR_User_Guide.pdf>

2. K. DOLAN, G. ZHENG, K. SUN, D. CARPENTER, L. Hu., "Tritium generation, release, and retention from in-core fluoride salt irradiations," Progress in Nuclear Energy, *Progress in Nuclear Energy*, **131**, 103576 (2021). DOI: 10.1016/j.pnucene.2020.103576

3. A. M. RAFTERY, R. L. SEIBERT, D. R. BROWN, M. P. TRAMMELL, A. T. NELSON, K. A. Terrani, "Fabrication of UN-Mo CERMET Nuclear Fuel Using Advanced Manufacturing Techniques", *Nuclear Technology*, available online, (2020). DOI:10.1080/00295450.2020.1823187

4. L. N. YANNOPOULOS, R. K. EDWARDS, P. G. WAHLBECK, "The Thermodynamics of the Yttrium-Hydrogen System," *J. Phys. Chem.*, **69**, 2510 (1965) DOI: 10.1021/j100892a004

5. C. ANG, L. SNEAD, J. TRELEWICZ, "An Innovative Approach to Composite Moderators Containing Zirconium Hydrides," *ANS Transactions*, Washington D.C., Nov 17-21, Vol. 121, P. 683, ANS (2019)

6. https://neup.inl.gov/SitePages/FY20_IRP_Awards.aspx (Accessed 1/29/2021).

7. K. SUN, L. HU, C. FORSBERG, "Neutronics feasibility of an MIT Reactor–driven subcritical facility for the Fluoride-salt–cooled High-temperature Reactor," *Int J Energy Res.*, **41**, 2248 (2017) DOI:10.1002/er.3786

8. R.G. BALLINGER, P. HEJZLAR, M.S. KAZIMI, G.H. KOHSE, Y. OSTROVSKY, P.W. STAHLE, Z. XU, "A New Facility for Irradiation of Materials at Very High Temperatures," *Proceedings of ICAPP'06*, Reno, NV, June 4-8, paper 6431, p. 2163, (2006).

9. https://nrl.mit.edu/facilities/in-core/experiments (Accessed 1/29/2021)

Nuclear and Emerging Technologies for Space
Sponsored by Oak Ridge National Laboratory, April 26th-30th, 2021.
Available online at https://nets2021.ornl.gov

CORE LOADING PATTERN OPTIMIZATION OF A TIE-TUBE NUCLEAR THERMAL PROPULSION REACTOR USING A SIMULATED ANNEALING ALGORITHM FOR NODAL DIFFUSION SOLVERS

Corey Smith[1,2], Matthew Krecicki[1], Dan Kotlyar[1]

[1]*Georgia Institute of Technology, Atlanta, GA 30332*
[2]*Analytical Mechanics Associates, Inc., Huntsville, AL 35806*

Primary Author Contact Information: (678) 739-8494, corey.d.smith@ama-inc.com

ABSTRACT

Since the early 1950s, the key to deep space travel has hinged upon the use of high-temperature nuclear thermal or electric propulsion engines (NTP/NEP). Many design variants have been created by different government agencies, research laboratories, and technical universities, initiated by the Rover/NERVA (RN) program from the United States during the 1950s and 60s. Current and future NTP research designs require adequate moderation due to new restrictions on highly enriched uranium (HEU), posing several additional design challenges for potential mission operation. Both moderation and the use of high-assay low enriched uranium (19.75% w/o U-235) significantly increase core size and intraelemental power peaking which directly affects safety and performance metrics. To optimize key engine performance metrics, such as output specific impulse (Isp), thrust, and thrust to weight ratio, the core loading pattern should prioritize the minimization of the radial power peaking to increase the average element outlet coolant temperature. To perform this analysis, an iterative simulated annealing algorithm is used to couple material cross-section results from a Monte Carlo (MC) model with a computationally efficient nodal diffusion solver. This sequence can run thousands of different core configurations in the same amount of time required to run a single high-fidelity MC simulation.

I. CODES AND METHODS

I.A. Neutronics Software

Due to the complexity in geometry of a fuel element and moderator tie-tube NTP core design, code packages that can model hexagonal pin lattices had to be prioritized. For this optimization, SERPENT[2] will serve as the main MC neutron transport code, and DYN3D will be utilized for all nodal diffusion benchmarking.

SERPENT is an innovative and powerful tool for NTP core optimization due to the simplicity of the input decks and use of large depletion libraries for full-mission analysis. Produced at the VTT Technical Research Centre of Finland[2], it operates as a three-dimensional, continuous energy MC simulation system that utilizes conventional particle tracking in tandem with Woodcock delta-tracking methods. The software reads cross-sectional data from its ACE library which is based on various JEFF and ENDF library inputs. In addition, the code can produce multigroup cross-sections and assembly discontinuity factors (ADFs), which increases its applicability to nodal diffusion codes and this optimization study.

DYN3D is an industry-accepted nodal diffusion simulation system developed at the Helmholtz-Zentrum Dresden-Rossendorf Research Center. While it is traditionally used for light water reactor (LWR) square lattice designs, it can also be tailored to input hexagonal geometries as well. This solver can obtain neutronic and thermal hydraulic output data in computationally efficient amounts of time using MC-generated group-wise cross-sectional data. As a comparison, a sample test case in MC that takes several hours to run on multiple processors could run in seconds using a diffusion solver like DYN3D. However, this efficiency in terms of simulation time translates to increased output deviation when compared to high-fidelity, low statistical error MC results.

I.B. Cross-Section Generation

Nodal diffusion solvers operate by creating a system-specific geometry and inserting known cross-sectional data into a corresponding node. For example, an LWR fuel assembly can be represented by a single node with a homogenized cross-section profile. In an NTP reactor system, the fuel assemblies are represented by hexagonal fuel and moderator elements with a surrounding axial reflector annulus which must be appropriately modeled. For simplicity, the control drums and other structural materials are removed since they will not have sharp impacts on the trends in radial power peaking.

To provide a consistent comparison between all core configurations, two-dimensional (2D) cross-sections are generated in an infinite lattice geometry. As seen in Figure 1, cross-sections for the fuel are modeled by a single element with periodic boundary conditions, and by a supercell lattice for the moderator element. The fuel elements modeled include a uranium nitride kernel within a molybdenum-tungsten (MoW) ceramic metallic (CERMET) matrix for the top of the core and a tungsten CERMET matrix for the hotter end. The fuel cross-sections are modeled in two regions based on the split height of the core. The split height of a CERMET NTP

core refers to the ratio of length of the pure tungsten matrix section to the total length of the core[1]. In addition, infinite and leakage corrected cross-sections are generated to determine if the high leakage of NTP cores affects the simulated results.

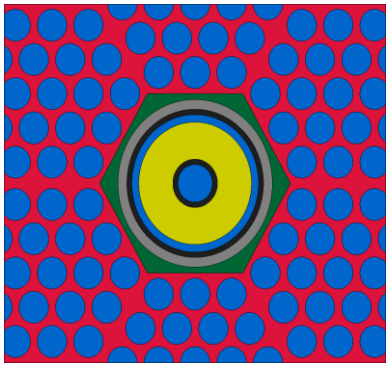

Fig. 1. Infinite supercell lattice with central moderator tie-tube surrounded by six identical fuel elements

I.C. Assembly Discontinuity Factors

A simple introduction into the relatively complex phenomenon of ADFs requires some knowledge of the flux distribution in the simulated core. Continuous energy codes like MCNP and SERPENT simulate flux profiles and surface flux values across material interfaces for the specific geometry. Basic reactor physics states that the heterogeneous flux must remain constant on both sides of a nodal mesh or at a material interface, but a discontinuity can arise when an averaged homogenous flux distribution is found[4]. In essence, ADFs measure the ratio between the heterogenous and the homogeneous flux for each energy group (Eq. 1), and a sample visual representation of the effect of homogenization at material interface is seen in the figure (Fig. 2). This ratio is assumed to be unity in nodal diffusion solvers; however, this unrealistic assumption has significant negative effects on the output power profiles, criticality eigenvalue, and thermal hydraulic outputs, if applicable.

$$ADF_{i,g} = \frac{\phi_{i,g}^{het}}{\phi_{i,g}^{hom}} \quad (1)$$

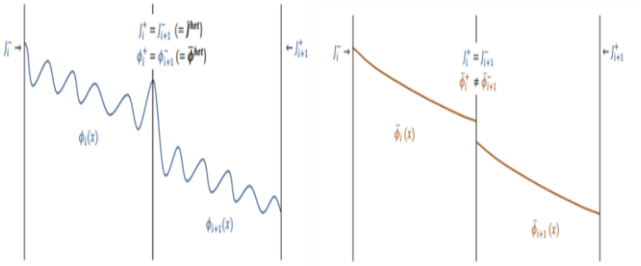

Fig. 2. Sample heterogeneous flux distribution at node interface with corresponding homogenized flux profile and discontinuity[3]

Earlier sensitivities to this project have been performed to test the impact of ADFs on the compatibility between DYN3D and SERPENT, and it is shown that it tends to decrease the accuracy of the results due to the extreme heterogeneity of the core. It is expected that higher fidelity results would be obtained if the nodal solver used radially dependent cross-sections instead of those defined from an infinite lattice model, but this level of detail would essentially nullify the computational efficiency. If cross-sections need to be generated for each radial design, then reactor designers should simply use the MC models for appropriate optimization. This study is focused on output trends, so the use of ADFs will not be necessary.

I.D. Simulated Annealing Algorithm

Minimization of the radial power peaking promotes elevated rocket performance with the same mass flow rate and exit gas temperature without higher concern for material integrity. Finding an optimum core configuration for any specific input parameter is difficult based on the variability of results to small changes in geometry, and small radial location changes for the fuel elements can have stark impacts on the radial power peaking. Subsequently, thousands of core configurations must be tested to find an optimum arrangement, thus the need for an optimization algorithm.

Simulated annealing (SA) is a probabilistic iterative scheme used to find the global maximum or minimum of a selected parent function. Most optimization techniques get trapped in local extrema instead of finding the global extrema, so SA is known for accepting worse cases on a probabilistic basis to escape these local points. Figure 3 shows an expected trend for a simulated annealing model with local extrema escape and location of a “true” global minimum.

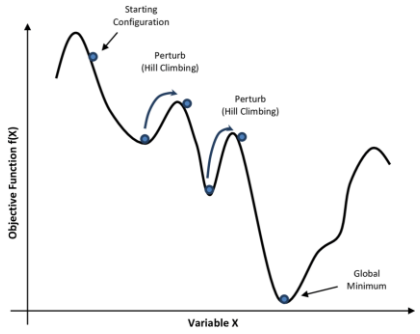

Fig. 3. Variation in the output objective function to demonstrate the effectiveness of a SA optimization model

The in-house SA code relies on the efficient simulation time of DYN3D and a unique convergence function fitted for power peaking. The framework of the iterative script involves:

1. Initial configuration defined by the user (Fig. 4)

2. Input generator script creates case specific DYN3D input deck
3. Simulates the radial power peaking in DYN3D
4. Switches a random fuel element to a random moderator element location (and vice-versa)
5. Simulates the new core in DYN3D

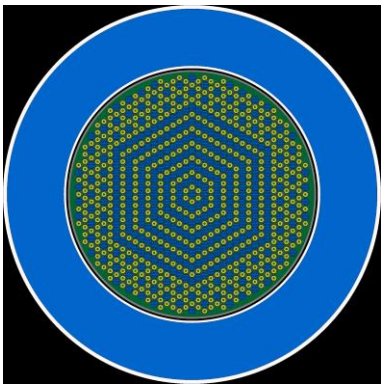

Fig. 4. Initial reference core configuration with fuel elements (dark blue), moderator tie-tubes (gold), and annular beryllium oxide reflector (blue)

An alternate form of this sequence replaces step 3 with a probabilistic methodology that varies a single random element to manipulate the moderator to fuel element (ME to FE) ratio. Boundary conditions are set for the upper limit for this case to inhibit impractical core designs.

If the radial power peaking of the new core is lower than the reference, the new geometry is accepted as the reference case for the next iteration. If the power peaking is higher, the code uses the SA probability, as seen in the equation below, to determine if the "worse" case can be accepted.

$$p_{sa} = exp(-\frac{k_a}{T_0} * (PP_1 - PP_0)) \quad (2)$$

In this equation, ka is the SA iteration number which increases by 1 for each accepted "worse" case, T_0 is the annealing temperature which is defined by the user, PP_0 is the reference radial power peaking, and PP_1 is the updated configuration's radial power peaking. This probability is compared with a randomly generated number between 0 and 1. If the random value is less than the annealing probability, then the less ideal case is accepted for the next iteration. For large iteration numbers, the exponential function gives smaller output probabilities, thus further reducing the likelihood of accepting the problematic cases.

II. RESULTS AND ANALYSIS

II.A. Two-Dimensional Sensitivities

Before a three-dimensional (3D) model can be used in the simulated annealing algorithm, a 2D model must show proper agreement between SERPENT and DYN3D power peaking results. The reference two-dimensional core (Fig. 4) is modeled in both neutronics solvers, and the output radial power peaking trends are displayed below.

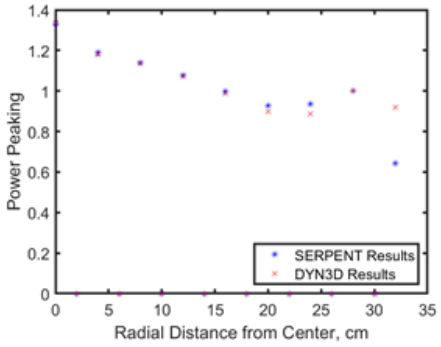

Fig. 5. 2D radial power peaking benchmark of DYN3D

Minor deviations are expected at the active core periphery since the annular reflector geometry cannot be mapped correctly using hexagonal nodes, but the deviation in the outer node is sizable. Since the higher-fidelity MC results display a minimum value at this location, it can be assumed the DYN3D model provides conservative results based on the heterogeneity at the core periphery and the lack of ADFs in the nodal diffusion system modeling.

With initial validation of the nodal diffusion model and the inputted cross-sections, an initial look at the SA algorithm tested the flexibility of the code with varying annealing temperatures. As mentioned in the previous section, larger annealing temperatures would yield a higher probability of accepting a "worse" radial core configuration. These sensitivities outputted an optimal annealing temperature of 2, and the results from 5000 iterations at this temperature are seen in the figure below.

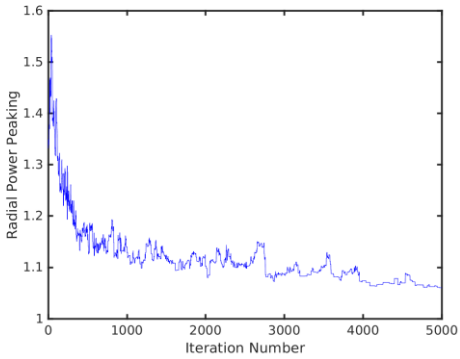

Fig. 6. Radial power peaking simulated annealing model with an annealing temperature of 2 for 5000 simulations

As expected, the max power peaking trends toward a global minimum with decreasing variation as the number of simulated cores increases. Since this model maintains a constant ME to FE ratio, it is shown that extreme flattening of the radial power profile is achievable by

simply rearranging the same volume of materials in the active core. To show the direct effect on the specific impulse, an NTP system code[4] simulated the average nozzle exit temperature based on the ME to FE ratio and the power peaking. The table below compares the Isp for the global minimum case (Fig. 7) with the initial reference case (Fig. 4)

TABLE I. Radial Power Peaking Effects on Isp

	Reference Core	Optimized Core
Max. Radial Power Peaking	1.3322	1.0605
Specific Impulse (Isp)	755.29	848.09

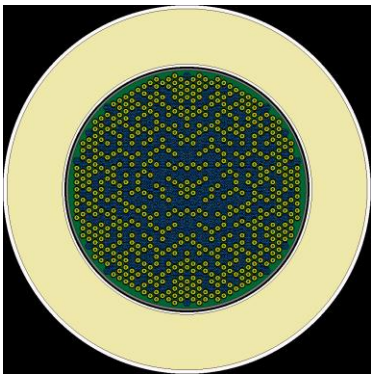

Fig. 7. SA-optimized core configuration with constant ME to FE ratio

II.B. Three-Dimensional Sensitivities

To perform axial and radial sensitivities on the NTP core, the capabilities of the DYN3D input generator were extended to include axial cross-sections. These cross-sections would vary with Doppler broadening with an extensive multigroup binning structure, but the use of two groups minimizes the effects of the axial temperature gradient. As discussed in Section I.B, the split height is also properly modeled by inputting varying fuel cross-sections into the axial nodes.

The framework of the SA algorithm remains the same, but sensitivities on the ME to FE ratio provide insight into varying core loading configurations previously unseen in the 2D model. For this sensitivity, 7500 different core configurations were simulated to provide trends between the two parameters. As seen in Figures 8 and 9, the max radial power peaking reaches higher magnitudes when compared with the 2D model due to added heterogeneity of the core. The SA results also show that the radial power peaking trends toward a global minimum as the ME to FE ratio increases. This trend is less ideal for NTP engines due to limited thrust and Isp extensibility. Additional coupling with the system's code can provide Isp trends for varying core configurations. Future analysis can use the same models with a lower maximum threshold for the ME to FE ratio to find a more ideal configuration.

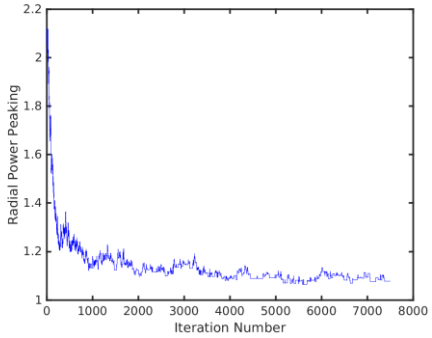

Fig. 8. 3D radial power peaking simulated annealing model with varying ME to FE ratio for 8000 simulations

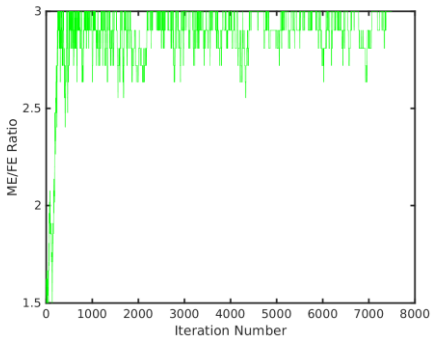

Fig. 9. ME to FE ratio simulated annealing trends for 8000 simulations

III. CONCLUSIONS

As seen in the results, strong optimization of key output rocket parameters can occur without changing the material volumes of a reference core. Flattening of the radial power peaking yields a higher average hydrogen temperature at the nozzle entrance which will boost specific impulse and thrust. A key takeaway from this study is the viability of nodal diffusion solvers like DYN3D to the optimization of an NTP core. In addition, simulated annealing algorithms were previously unproven in this research field, so this study proved that thousands of cores can be compared in a computationally efficient manner. Future studies can extend the SA framework to include radial enrichment zoning, control drums, and other core components to enhance its fidelity.

ACKNOWLEDGMENTS

I would like to thank Matthew Krecicki and Dr. Dan Kotlyar for providing the initial SERPENT models and technical guidance for this project. I would also like to acknowledge the 2020 NTP Senior Design team at the Georgia Institute of Technology for assisting with bulk post-processing scripts for the SERPENT models.

REFERENCES

1. R. J. ARMANI et al., “Nuclear Rocket Program Terminal Report,’ ANL-7236 Nuclear Reactors for Thermal Propulsion.” Argonne, IL: Argonne National Laboratory (1968).
2. J. LEPPANEN et al., "The Serpent Monte Carlo code: Status, development and applications in 2013." Ann. Nucl. Energy, 82 (2015) 142-150.
3. K. S. SMITH, “Assembly Homogenization Techniques for Light Water Reactor Analysis,” Progress in Nuclear Energy, Massachusetts Institute of Technology (1985).
4. D. KOTLYAR and M. KRECICKI, “Low Enriched Nuclear Thermal Propulsion Neutronic, Thermal Hydraulic, and System Design Space Analysis,” New York City, New York: Elsevier Inc (2019).

Nuclear and Emerging Technologies for Space
Sponsored by Oak Ridge National Laboratory, April 26th-30th, 2021.
Available online at https://nets2021.ornl.gov

DESIGN OF A LOW ENRICHMENT URANIUM NUCLEAR REACTOR TO POWER A FUTURE MARTIAN COLONY – THERMAL HYDRAULICS

Jacob Tellez, Conner Glatt, and Joffrey Dorville, and Jeffrey C. King

Nuclear Science and Engineering Program, Colorado School of Mines, Golden, Colorado

jtellez@mines.edu, cglatt@mines.edu, joffreydorville@mines.edu, kingjc@mines.edu

This work discusses the single channel analysis of hexagonal and cylindrical reactor configurations for use in a 2 MW_e Martian reactor targeting a 10-year operating lifetime with currently available materials and low enrichment uranium fuel. Each configuration uses a Mo-Re alloy cladding in combination with a closed CO_2 Brayton cycle. Fuels consist of uranium metal-hydrides employing either zirconium or yttrium as the metal for the hydride moderator. System efficiencies are estimated near 22% and 25% for the UZrH and UYH configurations, respectively. Average core mass fluxes are near 6700 kg/m^{2}s (46 kg/s) and 4000 kg/m^{2}s (20 kg/s) for the UZrH and UYH configurations, respectively. Peaking factors for the central fuel elements require flow rates to be increased by as much as a factor of two when compared with the average fuel element. The flow rates in the central channels result in significant pressure drops in the zirconium hydride moderated cores, primarily due to the temperature limit set to limit potential hydrogen migration out of the hot regions in the moderator.

I. INTRODUCTION

Establishment of extraterrestrial bases has captured the focus of scientists, engineers, and others for many decades. The eventual development of these bases into small colonies creates a greater demand for power. Fission power systems offer the capability for reliable, extended operation with a wide range of potential missions for kilowatt and megawatt class power systems. This work discusses the thermal hydraulic analysis of a megawatt class (2 MW_e), gas-cooled Martian reactor using currently available materials and fueled with Low Enrichment Uranium (LEU, uranium containing less than 20% uranium-235).

Analysis of fluid flow and cooling mechanisms in the reactor core channels is a critical component of nuclear reactor design. For gas-cooled reactors, these problems fall in the realm of single-phase, nonlinear heat transfer problems. An analytical model based on the Homogeneous Equilibrium Model[2] explores the single-phase heat transfer in the coolant channels and fuel elements of the MINERAL reactor. Companion papers analyzing the neutronics and heat rejection can be found in these proceedings[1,2].

II. REACTOR COOLING SYSTEM

The reactor cooling system employs a supercritical CO_2 Brayton cycle in the primary heat removal loop, with a combination of convective and radiative panels located above the core and power conversion system to manage heat rejection. The primary flow loop in the core brings cold coolant down around the outside of the core and then sends it up through the channels and to the power conversion system. Figure 1 shows this flow path. Within the core, the coolant flows through the inner portion of annular channels which penetrate the solid fuel matrix. The channel geometry differs slightly between the thermal hydraulic and neutronic analyses. Specifically, the neutronics model considers the coolant channel in a hexagonal lattice[1]; however, the thermal hydraulic modeling employs a cylindrical annulus with an equivalent radius that preserves the cross-sectional fuel area. Figure 3 presents this channel and its equivalent cell. After leaving the core, the coolant flows into the power conversion system, through the heat rejection system, and then back to the core. The heat rejection system manages excess heat with several convective and radiative panels[2]. Figures 1 and 2 show these systems and a companion paper describes their operation in detail[2].

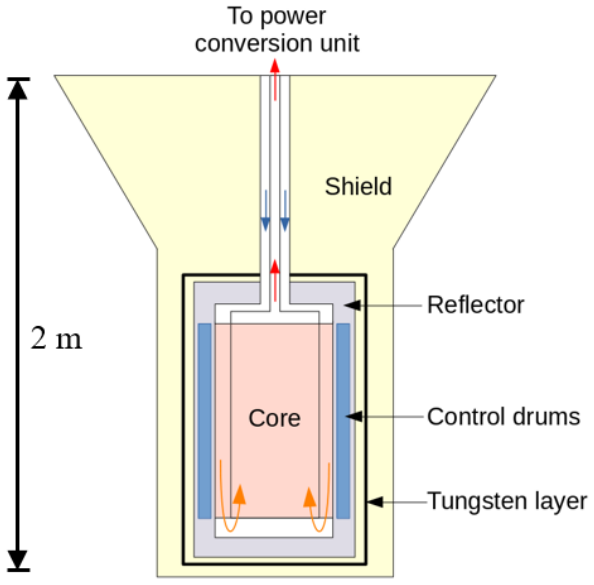

Fig. 1. Coolant flow path through the core (not to scale).

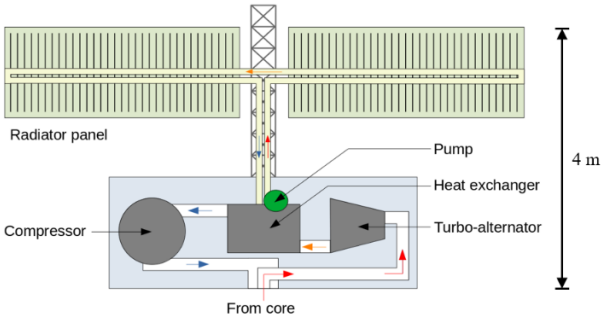

Fig. 2. Overview of the heat rejection system that sits on above core (not to scale).

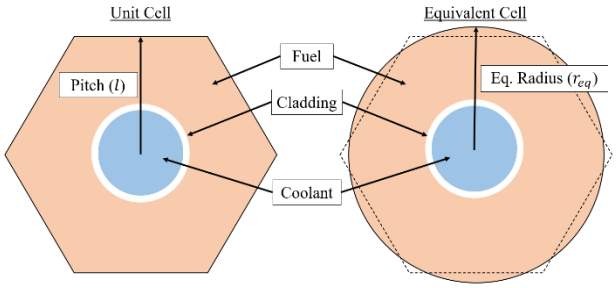

Fig. 3. Coolant channel unit cell (left) and the equivalent cell (right) used for the single channel analysis (not to scale).

III. HEAT TRANSFER MODEL

The single-phase model heat transfer model, derived from the Homogeneous Equilibrium Model[3], relies on coupled differential equations describing the development of pressure and enthalpy throughout the channel. Throughout the development of the model, liquid-gas mixture properties remain for general development of the equations despite the absence of liquid in the single-phase system. The CoolProp library[4] provides the equations of state for carbon dioxide in the MINERAL reactor.

III.A Mass Balance

The model begins with the mass balance where the system is assumed to operate at steady state. This, in combination with assuming the net mass transfer between the channels is zero, gives a definition for the mass flux in the channel, G,

$$G = \rho v = \text{constant in } \hat{z}. \tag{1}$$

III.B Momentum Balance

The general form of the momentum balance is also modified to apply to the problem. In these systems, the only applied body force is gravity in $\hat{z}$. Using the expression for the single-phase flow viscous stress tensor, exploiting the dependence of the specific volume on pressure, and then rearranging to find the pressure change in $\hat{z}$, the momentum balance gives an incomplete expression for the pressure drop (the quality is unknown):

$$-\frac{dP}{dz} = \frac{-\frac{\xi_w}{A_{flow}}\frac{f_i G^2 \underline{v}_m}{2} + G^2 \underline{v}_{fg}\frac{\partial \chi}{\partial z} + \frac{g}{\underline{v}_m}}{1 + G^2\left(\chi\frac{\partial \underline{v}_g}{\partial P} + (1-\chi)\frac{\partial \underline{v}_f}{\partial P}\right)}. \tag{2}$$

The derivative of the quality remains in the expression, despite being the system being single-phase, so that the momentum and energy balances can be related in the next portion of the solution. Additionally, Eq. (2) allows for evaluation of the specific volume and its derivative from state tables.

III.C Energy Balance

Assuming that body force and frictional heating effects are insignificant, and that there is no heat generation in the coolant, the steady state form of the energy balance is:

$$\frac{d(\rho_m h_m v)}{dz} = G\frac{dh_m}{dz} = \frac{q''(z)\xi_H}{A_{flow}}. \tag{3}$$

Exploiting the dependence of the mixture enthalpy on pressure, as seen with specific volume in the momentum balance, allows the equilibrium flow quality to be found. With some manipulation, an expression for the pressure drop can also be derived:

$$-\frac{dP}{dz} = \frac{\alpha f_i G^2 \underline{v}_g + \frac{G\underline{v}_{fg}\xi_H}{A_{flow} G \underline{h}_{fg}} q''(z) + \frac{g}{\underline{v}_g}}{1 + G^2\left(\frac{d\underline{v}_g}{dP} - \frac{\underline{v}_{fg}}{\underline{h}_{fg}}\frac{d\underline{h}_g}{dP}\right)}. \tag{4}$$

With the pressure drop fully defined, identifying suitable correlations for the heat transfer between the coolant and channel wall is the last remaining task.

IV. HEAT TRANSFER CORRELATIONS

The flow conditions in the coolant channels involve both fully developed and turbulent flow throughout the entire channel. These conditions permit use of the Dittus-Boelter correlation for convective heat transfer[3]. This correlation relies on thermophysical properties of the coolant, which are extracted from the state equations in CoolProp[4].

The friction factor is the second flow parameter requiring a correlation. This parameter takes on different expressions for laminar and turbulent flow; though, the flow is predominantly turbulent, so both the Dittus-Boelter and turbulent friction factor correlations suffice for this system. For turbulent flow, the friction factor takes on the form outlined by McKeon et al.[5] where f is a solution of

$$\frac{1}{f^{1/2}} = 1.930 \cdot \log\left(Re \cdot f^{\frac{1}{2}}\right) - 0.537. \qquad (5)$$

V. TEMPERATURE DISTRIBUTION IN THE FUEL

In the case of low thermal conductivity or large heat flux, the fuel materials can undergo large temperature gradients which may significantly affect the thermophysical properties of the fuel. These effects, when significant, cause nonlinearities in the governing equations and the problem cannot be accurately solved with constant material properties. Consequently, evaluation of the problem with a nonlinear heat transfer model allows for a more accurate determination of the fuel temperatures.

In the nonlinear model, only the thermal conductivity is taken to be temperature dependent, while the heat generation is given to be independent of the temperature by assuming that the reactor operates in a steady state. Additionally, axial and azimuthal heat transfer are neglected. Applying the nonlinear model demonstrated that the centerline fuel temperature increased by less than 4 K compared to the linear model for all cores. The differences between linear and nonlinear solutions were smaller elsewhere in the fuel. Consequently, all further analyses employs the linear model.

In the linear model, the heat diffusion equation is broken into regions for the fuel matrix and cladding. Continuity of temperature and heat flow are applied as boundary conditions between the interfaces. The temperature gradient is set to zero at the outer fuel boundary and the convective heat transfer condition is used at the cladding-coolant interface with the bulk coolant temperature completing the equations as a known value from the heat flow out of the wall at the previous position in the coolant channel. These conditions provide the following solutions for the temperature profiles in the fuel:

$$T_{fuel}(r,z) = \frac{-q'''(z)r^2}{4k_{fuel}} + c_0 \ln(r) + c_1, \qquad (6)$$

$$T_{clad}(r,z) = c_2 \ln(r) + c_3. \qquad (7)$$

The linear system produces a closed-form, analytical solution assuming that the bulk fluid temperature is known. These solutions arise from the assumptions that there is no heat generation in the moderator or fluid and that the power generation profile of the fuel maintains a sinusoidal profile that approximates the axial power generation profile of the core. It should also be noted that, with no data available for the thermal conductivity of the UYH fuel, the correlation for UZrH fuel was used but evaluated at a higher average temperature. This rough estimation represents the lowest conductivity scenario being since YH is more conductive than ZrH in this temperature range[6]. In addition, alternative fuels considered for a heterogeneous fuel-moderator matrix in this design have higher thermal conductivities than the UZrH in this design[7]. For the linear model, the thermal conductivities were taken as the mean value from the nonlinear solution.

VI. RESULTS

Four different core configurations, consisting of UZrH and UYH fuels in two different geometries, were run. Geometric details of each can be found in Table I. Detailed descriptions of each core can be found in a companion paper in these proceedings[1] Each core configuration was optimized to meet the neutronic requirements; then, an iterative procedure coupling the heat rejection system and primary coolant loop (core, turbine, heat rejection, and compressor) converged the core inlet temperature and mass flow rate based on a maximum allowable material temperature. In all cases, the fuel-moderator matrix set the lowest temperature limit in attempting to prevent hydrogen diffusion. A summary of relevant parameters for each configuration can be found in Table I. Figures 4 and 5 show results for the UYH fuel matrix with a cylindrical core perimeter.

The channel temperature distributions demonstrate that the high heat flux caused the fuel-moderator temperature to peak just before the end of the channel. When attempting to maximize the system efficiency, the maximum allowable temperature for ZrH and YH constrain the mass flow rate and inlet temperatures for each configuration. Absolute temperature limits are set by the migration of hydrogen out of ZrH_x and YH_x near 900 K and 1173 K, respectively[6,8]; however, to avoid premature migration of the moderating hydrogen, the maximum design temperature of the moderator may not to exceed 66% of these values, providing design limits of 594 K (UZrH) and 774 K (UYH).

TABLE I. Geometric and thermophysical parameters for the four reactor configurations.

	UZrH	UYH
Pitch [cm]	3.52	3.6
Channel Radius [cm]	0.83* / 0.81**	0.70* / 0.66**
Clad. Thickness [cm]	0.2	0.2
Core Height [cm]	90	90
Number of Rings	7	7
Fuel Thermal Conductivity[9] [W/mK]	18.57	19.35
Cladding Thermal Conductivity[10] [W/mK]	37.0	37.0

* Cylindrical Core

** Hexagonal Core

The radial peaking factor is estimated from a Bessel function approximation of the radial flux profile, giving a peaking factor of 1.64 and forcing a large mass percentage of coolant through the central channel to maintain the fuel and moderator temperatures near the center below the specified temperature limits. In theory, the distribution of coolant to inner and outer pins could be controlled by orifices at the entrances to the core in the coolant flow path; however, the coolant channel diameter could be altered to flatten the neutronic peaking profile and increase the surface area between the coolant and cladding. The mass flux required to compensate for the peaking factor in the cylindrical UYH core was 8096 kg/m^{2}s, or 2.017 times larger than the average channel mass flux. Similar results were obtained for the three other cores.

The moderator temperature limits severely increased the mass flow rates required in the peak channels. Pursuit of the original 594 K moderator temperature limit was not practical. This limit required a channel mass flow rate exceeding 1.02 kg/s, which dropped the pressure below the limits outlined by CoolProp. Permitting a temperature increase in the central fuel cells of up to 650 K reduced the flow rate drops 0.76 kg/s. Further extending the moderator limit to 700 K decreased the required flow rate to 0.45 kg/s. However, increasing the moderator temperature limits will increase the chance of significant hydrogen transport and loss over the lifetime of the reactor. A better understanding of long-term hydrogen diffusion in hydride moderators will be necessary to increase the allowable operating temperature in moderated space nuclear reactors.

The separation of the fuel temperature from the trend of the coolant temperature could be mitigated by increasing the flow rate; however, this might put strain on the efficiency by requiring significant power to pump the coolant. As of now, there is no gap to allow thermal expansion of the cladding and fuel. Inclusion of a gap will increase the peak fuel temperature and will impose further design challenges for the moderator by creating a large separation of cladding and fuel-moderator temperatures. The fuel temperature distribution can be found in Figure 5. An understanding of the pressure drop through the core is not as critical for a gas reactor as it is with a light water reactor, though it serves as a relevant point for verifying code functionality. The pressure drop across the average coolant channel in the current reactor is about 0.142 MPa. A detailed summary of other relevant core results can be found in Table II.

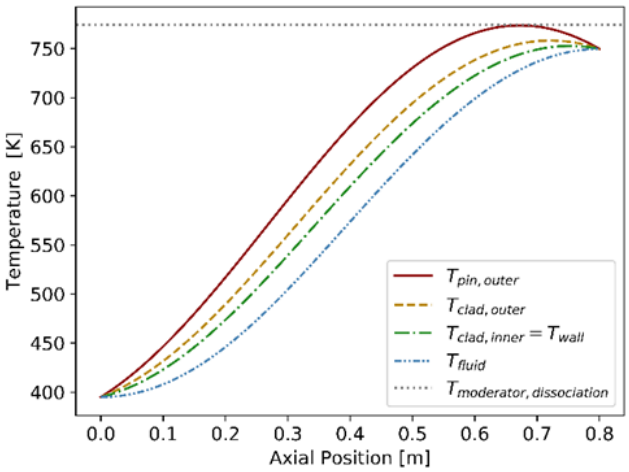

Fig. 4. Temperature distribution for the fuel matrix, cladding, and coolant in an average fuel element in the cylindrical UYH core configuration.

VI.A. Coolant Loss Analysis

One consideration for the selection of the coolant for this reactor system is the atmospheric environment on Mars. With a carbon dioxide composition of about 95.7% (Ref. 11), the Martian atmosphere shows potential for acting as a coolant source in the event of an accident. While the raw atmosphere would require minor purification, the atmosphere could serve as an emergency coolant if

TABLE II. Core parameters for each core type.

	UZrH				UYH			
	Cylindrical		Hexagonal		Cylindrical		Hexagonal	
Mass Flow Rate (Core)	46.22	kg/s	46.77	kg/s	19.62	kg/s	19.87	kg/s
Mass Flux (Core)	6726	kg/m^{2}s	7146	kg/m^{2}s	4014	kg/m^{2}s	4572	kg/m^{2}s
Mass Flux Peaking Factor	*2.074		*2.129		2.017		2.097	
Coolant Pressure (Inlet)	7.09	MPa	7.09	MPa	7.09	MPa	7.09	MPa
Coolant Pressure (Outlet)	6.89	MPa	6.86	MPa	6.95	MPa	6.81	MPa
Coolant Temperature (Inlet)	359	K	359	K	359	K	359	K
Coolant Temperature (Outlet)	571	K	570	K	750	K	746	K
Fuel Temperature Max.	594	K	594	K	774	K	774	K
Cladding Temperature Max.	579	K	577	K	758	K	755	K
Efficiency	21.6	%	21.6	%	25.2	%	25.2	%

* Requires increasing the moderator temperature limit to 650 K.

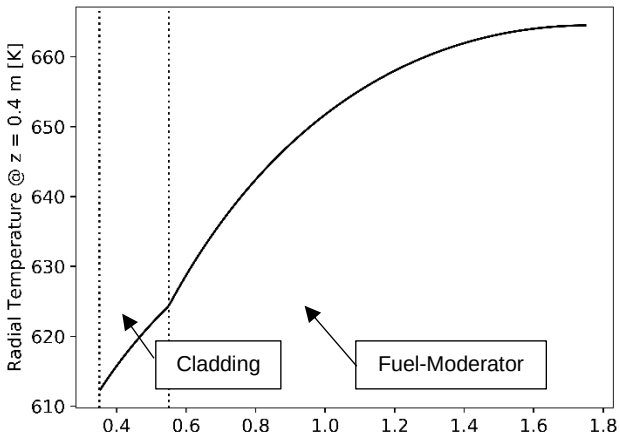

Fig. 5. Temperature profile of the average equivalent fuel cell at the middle of the core in the cylindrical UYH configuration.

necessary. Alternatively, the option to re-pressurize the primary loop to full or partial pressure could be an option in the event of a small primary loop leak. The lowest channel inlet pressure evaluated is 2.03 MPa. At this pressure, most of the thermal hydraulic results were nearly identical to that of the full pressure system, except for the mass flow rate, which increased from 19.62 to 21.42 kg/s, and the pressure drop, which increased from 0.141 to 0.549 MPa. At an inlet pressure of 3.55 MPa, the mass flow rate increased to 20.967 kg/s and the pressure drop increased to 2.98 atm.

VI.B. Alternate Configurations

Results for the three other configurations are shown in Table II. Table II does not include temperature profiles due to their similarity to the cylindrical UYH core. The primary difference between the UZrH and UYH configurations is the temperature limits required by the zirconium hydride moderator, which severely lowers the allowable maximum fuel temperature. The development of these configurations does not account for a thermal expansion gap between the fuel-moderator and cladding, though this will be considered in future. Additionally, other coolants, such as a He-Xe mixture, may also be evaluated.

VII. SUMMARY AND CONCLUSIONS

The thermal hydraulics of four megawatt-class reactors, designed for a 10-year operation lifetime with LEU fuel, are analyzed via single channel analyses. The reactors employ cylindrical and hexagonal geometries as well as both zirconium and yttrium hydride moderators integrated in a uranium fuel matrix. Each core also makes use of a Mo-Re cladding and a closed CO_2 Brayton cycle.

Uranium yttrium hydride fuels demonstrate better potential performance compared to zirconium hydride containing fuels based on their ability to operate at higher temperatures without hydrogen migration away from the hot regions in the fuel. This elevated operation temperature permits a higher efficiency and thus longer operation lifetime and reduced system mass. The UYH fuel reactor configurations possess mass flow rates near 19 kg/s, proportional to other comparable gas cooled reactors; however, the lower temperature limits of UZrH fuel increase the required flow rate to nearly twice that of the UYH fueled reactors. In addition, both fuel types have central fuel channels that require mass flow rates nearly twice that of the average channels. This issue might be mitigated by increasing the inner coolant channel diameters. This may decrease the power generation near the core center and decrease the neutronic peaking factor.

The use of a supercritical CO_2 Brayton cycle allows for the potential using the Martian atmosphere as a coolant in emergency scenarios. Further evaluation of the impact of a thermal expansion gap between the cladding and fuel matrix is needed. If the gap increases the fuel matrix temperature too much, the development of a heterogeneous fuel-moderator system may be required. Additionally, the potential use other coolants such as He-Xe mixtures should be evaluated.

NOMENCLATURE

G – Mass flux of the coolant
ρ – Coolant mass density
v – Coolant mean velocity
$\hat{z}$ – Vertical direction aligned with the pin length
$\hat{r}$ – Radial direction normal to $\hat{z}$
ξ_w – Wetted perimeter of the channel
ξ_H – Heated perimeter of the channel
A_{flow} – Flow area of the channel
f – Friction factor
$\underline{v_m}$ – Specific volume of the mixed phase coolant
$\underline{v_f}$ – Specific volume of the condensed-phase coolant
$\underline{v_g}$ – Specific volume of the gas-phase coolant
$\underline{v_{fg}} = \underline{v_g} - \underline{v_f}$
χ – Flow quality
g – Gravitational constant of Mars
P – Coolant pressure
h_m – Enthalpy of the mixed phase coolant
h_f – Enthalpy of the condensed phase coolant
h_g – Enthalpy of the gas-phase coolant
$h_{fg} = h_g - h_f$
q'' - Surface heat flux through the cladding-coolant interface
q''' - Volumetric heat generation rate in fuel
Re – Reynold's number
k_i – Thermal conductivity of material i

REFERENCES

1. J. DORVILLE et al., “Design of a Low Enrichment Uranium Nuclear Reactor to Power Future a Martian Colony - Neutronic Aspects”, *Nuclear and Emerging Technologies for Space (NETS-2021)*, April 26-30, paper 35996, Oak Ridge National Laboratory (2021).
2. C. GLATT et al., “Design of a Low Enrichment Uranium Nuclear Reactor to Power A Future Martian Colony – Heat Rejection”, *Nuclear and Emerging Technologies for Space* (NETS-2021), April 26-30, paper 35998, Oak Ridge National Laboratory (2021).
3. E. TODREAS and M. S. KAZIMI, *Nuclear System I: Thermal Hydraulic Fundamentals*, Ed. 2, Taylor and Francis (1993).
4. I. H. BELL et al., “Pure and Pseudo-pure Fluid Thermophysical Property Evaluation and the Open-Source Thermophysical Property Library CoolProp,” *Industrial & Engineering Chemistry Research*, **53**, 6 (2014). DOI:10.1021/ie4033999
5. B. J. McKEON et al., “Friction Factors for Smooth Pipe Flow,” *Journal of Fluid Mechanics*, **511**, 41-44 (2004). DOI: 10.1017/S0022112004009796
6. J. ZYMBALUK et al., “A Survey of High-Temperature Moderators for Space Nuclear Reactor Applications”, *Nuclear and Emerging Technologies for Space (NETS-2021)*, April 26-30, paper 35995, Oak Ridge National Laboratory (2021).
7. L. GRANDE et al., “Thermal Aspects of Uranium Carbide and Uranium Dicarbide Fuels in Supercritical Water-Cooled Nuclear Reactors,” *Journal of Engineering for Gas Turbines and Power*, **133**, 2 (2011). DOI: 10.1115/1.4001299.
8. J. L. ANDERSON et al., “Reactivity control of fast-spectrum reactors by reversible hydriding of yttrium zone,” *National Aeronautics and Space Administration*, NASA TN D-4615 (1968).
9. D. STAHL, “Fuels for Research and Test Reactors,” Technical Report ANL-83-5, Argonne National Laboratory, (1982).
10. L. B. LUNTLBERG, “A Critical Evaluation of Molybdenum and Its Alloys for Use in Space Reactor Core Heat Pipes,” *Los Alamos Scientific Laboratory*, LA-8685-MS (1981).
11. H. B. FRANZ et al., “Initial SAM calibration gas experiments on Mars: Quadrupole mass spectrometer results and implications,” Planet. Space Sci., **138**, pp. 44–54. DOI:10.1016/j.pss.2017.01.014.

Nuclear and Emerging Technologies for Space
Sponsored by Oak Ridge National Laboratory, April 26th-30th, 2021.
Available online at https://nets2021.ornl.gov

DESIGN OF NERVA-DERIVED HALEU REACTOR ("EMU") FOR NUCLEAR THERMAL PROPULSION

Teyen Widdicombe[1], Avery Grieve[2], Steve Herring[3] and Brad Kirkwood[4]

[1]*University of Idaho, twiddicombe@uidaho.edu*
[2]*University of Michigan, agrieve@umich.edu*
[3]*Center for Space Nuclear Research, Universities Space Research Association, jherring@usra.edu*
[4]*Idaho National Laboratory, brad.kirkwood@inl.gov*

During the CSNR 2020 summer program a Nuclear Thermal Propulsion reactor based on NERVA (Nuclear Engines for Rocket Vehicle Applications) designs was investigated. Use of HALEU (High Assay Low Enriched Uranium) fuel in a zirconium carbide matrix mitigates the NERVA issue of fuel vaporization. A larger number of flow tubes than used in NERVA designs are composed of refractory metal alloys to improve heat transfer. The reactor was characterised in both Serpent and MCNP in the interest of dividing labour and playing to each code's strengths.

I. INTRODUCTION

Project Rover was set up in 1955 by the U.S. Air Force, and transferred to the newly created National Aeronautics and Space Administration in 1958, with the aim of constructing a nuclear thermal rocket engine for spacecraft propulsion[1]. The project designed and built more than half a dozen reactors, even destruction-testing one in the KIWI-TNT test. Research has since continued, with work at present being in support of NASA's intention to return to the moon and travel on to Mars.

II. DESIGN APPROACH

Our reactor was designed for a thermal power of 500MW, and maximum thrust of 25klbf (111kN). Each fuel element (3/4" (19mm) across the hexagonal flats) was to contain equally spaced flow tubes each 1mm in diameter, numbering 127 in all. The original NERVA reactors employed 19 flow tubes per element between imperial equivalents of 2.4 and 2.8 mm in diameter respectively, leading to a higher heat flux across the tube walls. The vast majority of reactor dimensions were taken from the NERVA type engines, with the exception being the reactor radius, which was reduced assuming a constant power density to around 70% of its original value. Each element was clad in 30 μm of refractory metal or carbide, whilst the flow tubes were 50μm in wall thickness (vapour deposition territory). In the inner part of the core, tungsten enriched in W-184 was used for the flow tubes to improve neutron transparency and resist the high temperatures. The flow tubes in the cooler outer core were composed of a creep-resistant nanostructured 0.7% lanthana-molybdenum[2]. Zirconium carbide is anticipated to be used in the tungsten alloys for high temperature hydrogen creep resistance via grain growth inhibition, but was not included in the model due to minimal neutronic effect compared with the ZrC fuel matrix. Beryllium axial and radial reflectors 4.5" (11.4cm) in thickness were used, with the former mounted atop the core. The 12 control drums were 5cm in diameter with 1cm thick 120 degree boron aluminide shims. The whole assembly was radially surrounded with a 1cm thick aluminium shell. Slightly different directions were investigated using these materials and basic geometry with MCNP and Serpent.

II.A. Serpent

Following the above specification, a model reactor was built in Serpent[3] as shown in figure 1. Simulations were run using 100 cycles of 30,000 histories per cycle, with 25 cycles being discarded.

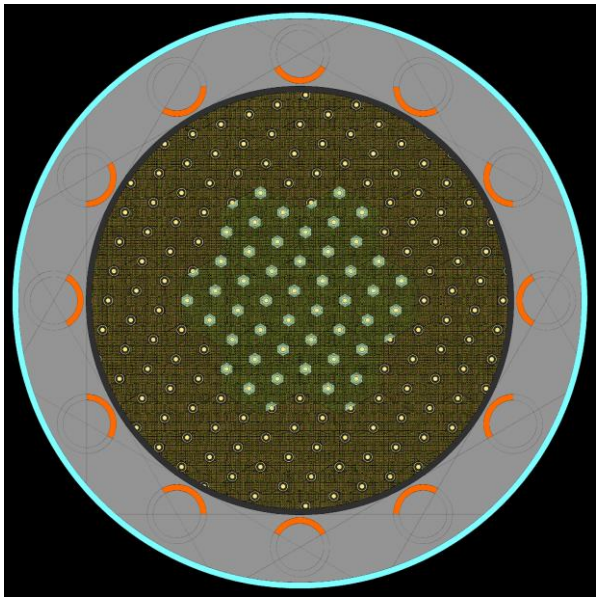

Fig. 1. Radial cross-section of Serpent reactor geometry

II.A.1. Characterisation

For the Serpent model, elements with 19 coolant tubes and a 70:30 ratio of uranium carbide to zirconium carbide in the inner core and UC to graphite in the outer core was found to be critical. A variety of parameters were investigated for the model. The first was the variation of keff as a function of drum angle, for which the control drums were rotated by 20 degrees at a time. The point of criticality was deliberately set at 120 degrees by varying materials to arrive at the described configuration.

Secondly, creating layers within the core as shown in Figure 2 and setting up energy deposition detectors allowed quantitative power profiles to be generated.

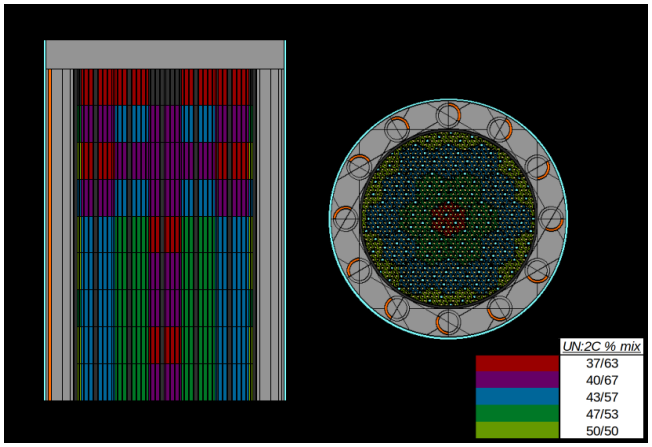

Fig. 2. Serpent core zones with key

Various axial and radial concentration profiles were investigated as shown in figure 3 in an attempt to damp out harmonics found to exist with constant fuel concentration and arrive at an axial power profile, which was found to be approximately:

$$\frac{P}{P_{max}} = \sqrt{\left[cos\left(\frac{0.95z}{z_{max}} - \frac{1}{2}\right)\right] e^{\sqrt{2}\frac{z}{z_{max}}}}$$

where ***P*** is power and ***z*** is height within the core.

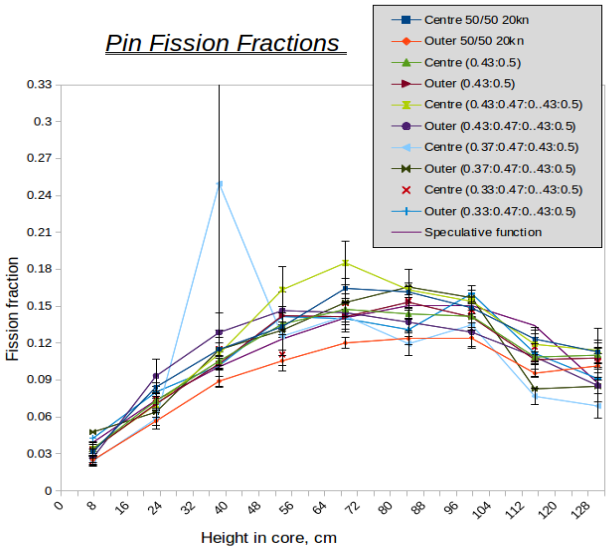

Fig. 3. Axial power profiles- the large uncertainty and visible "spike" are due to an unknown processing error

A qualitative flux / fission plot generated natively by the code is shown in figure 4, with the former in blue and the latter in orange, with increasing values denoted by increasing pixel brightness.

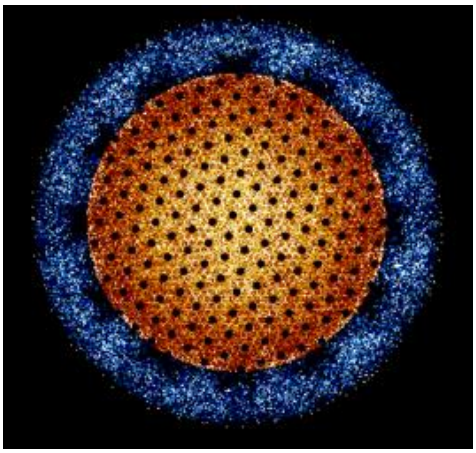

Fig. 4. Serpent flux / fission plot

Thirdly the decay heat generated by the reactor was investigated, with a total burn time of 5 hours in 30 minute steps and also a Mars mission profile, assumed to be 30, 20, 20 and 30 minute burns with 90, 120 and 90 day wait times in between. In the former case, initial decay power was seen to increase very slightly with burn time in a nonlinear fashion, whilst for the latter, heat was found to fit the correlation:

$$\frac{P}{P_d} = \frac{\sum(\tau)}{55.5\tau}\left(t^{-1/4} - (t+\tau)^{-1/4}\right)$$

where ***t*** is time since the burn and is ***τ*** burn time, in days.

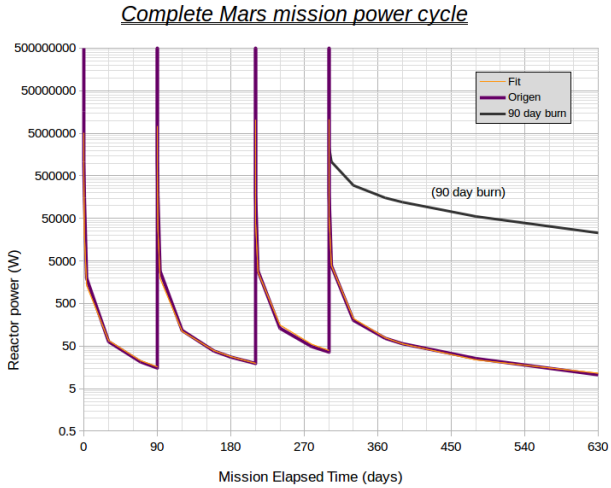

Fig. 5. Power for complete Mars round trip from LEO

The method for decay heat simulations was to pass the burned fuel material files from Serpent through ORIGEN[4]. Though theoretical decay heat correlations do exist for NTRs (Nuclear Thermal Rockets)[5], their results are much higher (closer to the 90 day curve plotted in figure 5). The original NERVA reports and the aforementioned published correlations suggest that the

initial decay power for their tests was extremely high (on the order of 1/5 of P0[6]) - however many of the curves in question are explicitly the product of simulations, and measurements are difficult to interpret, indicating that further research into this area is required.

II.A.2. MCNP check

Geometries diverged between the Serpent and MCNP models over the course of the project as labour was divided, but for the purpose of validation the former was modified to match the latter at the halfway stage. The biggest change was the geometry of the central moderator element and increasing the number of flow tubes from 19 to 127 to match the MCNP geometry, as shown in figure 6. Enriched W-4Re was used for 50μm thick flow tube walls and element clad, whilst the cooling structures were changed to zircaloy, and the majority of the moderator to zirconium hydride. Finally, the radial reflector was thickened by 1cm. 3x106 histories produced keff values (1.01504+/- 0.00032; 0.94829 +/- 0.00034) which matched MCNP's (1.01587 +/- 0.00071; 0.94820 +/- 0.00072) to the third decimal place (0.83‰).

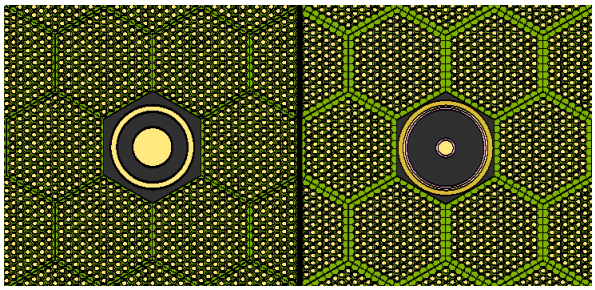

Fig. 6. Original (left) and MCNP-replica core elements

II.B. Monte Carlo N-Particle

II.B.1. Realistic Core Edge

The main issue with the geometry as developed in Serpent and the early matching MCNP model was having the outer edges of the core cut off at the graphite moderator interface. To fix this, the full fuel bundle as shown in figure 7 was initially taken as the primary building block of the reactor. The fuel bundle geometry was based off the Kiwi-type fuel from Project Rover that run the length of the active core. Six fueled elements, containing 127 1mm diameter coolant channels, surround a central support element containing moderator and coolant channels. The coolant passages and fueled element perimeter were clad with tungsten enriched in 184-W or molybdenum-lanthana alloy depending on reactor heat region. The full bundle is shown in figure 7.

Of particular note is the central element of this bundle, which has been adapted from the geometry of the center element in Gates et al[7]. A central hydrogen flow channel is clad with a thin layer of Zircaloy-4. The middle region (tan) is a zirconium hydride moderator. Gates et al. asserts that hydrogen flowing in the support element should nominally be 600 K, and with the material limit for zirconium hydride being about 1000 K, there is a safety factor built in. Outside of the ZrH_2, there is another hydrogen flow channel clad on the outer edge with Zircaloy-4 again. The outermost ring is then zirconium carbide, and the remainder of the hexagon is graphite.

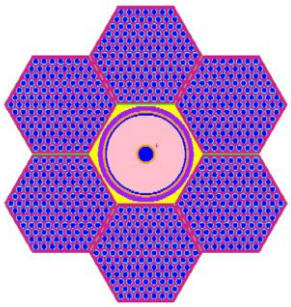

Fig. 7. A full single fuel bundle

Utilizing just the full bundle as the building block of the core left a good deal of empty space near the core edges that could be filled with more fuel and moderator elements as seen in the left hand image of figure 8. Therefore the "full-bundle" core was used as a template to rebuild using a hexagonal lattice. After copying the design with the lattice, extra elements were added around the edge to utilize space more effectively and increase fuel density. The right hand image in figure 8 shows the same area of the reactor after improvements to close packing with a pure lattice. This work was important because packing as much fuel as possible is necessary to maintain the positive reactivity needed for a Mars mission.

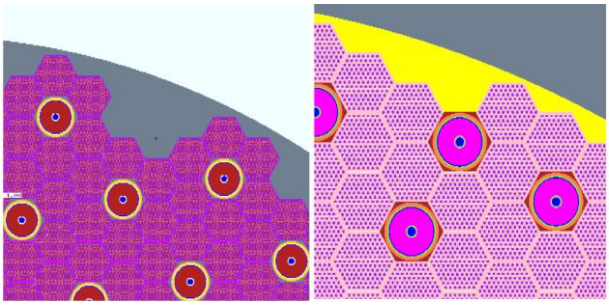

Fig. 8. Core edge geometry with full bundle (left) and single element (right) arrays

II.B.2. Reactor Heat Regions

Both Serpent and MCNP model used two fuel heat regions, with a more realistic interface in the latter. The expected maximum operating temperature is approximately 2500 to 3000 K in the high power area near the center of the core. This heat decreases as the power profile decreases, so the edges of the core will be somewhat cooler. The MCNP model was designed with two distinct heating regions: the center at 2500 K and the outer core at 1200 K. This can be easily seen in figure 9.

Using these two heat regions provided a more realistic look at the multiplication factors of the reactor in operation compared with a homogeneous temperature reactor. Further, two separate regions allowed the use of different clad materials as described in §II. In both regions, the coolant channel and element clad layers are 50 µm thick. The central support element temperatures match the bulk temperatures of their regions.

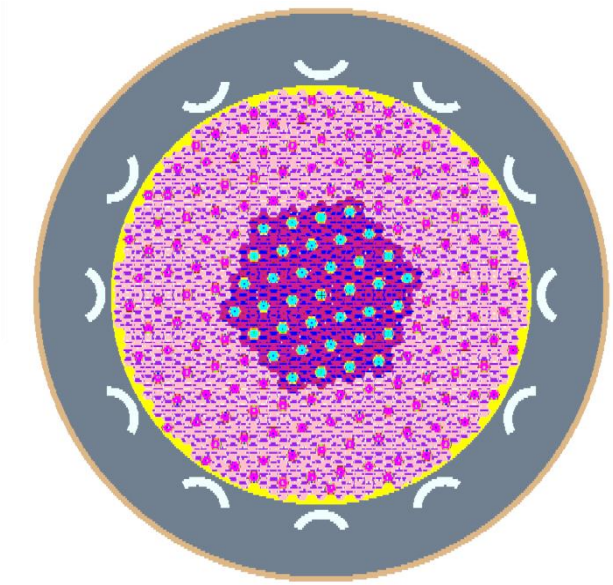

Fig. 9. Full MCNP core with distinct heat regions.

II.B.3. Control Drum Worth and K Eigenvalue Behavior

For the final MCNP geometry, a series of simulations were performed to determine the multiplication factor for various control drum positions- this had been done in Serpent but found to be inaccurate. In figure 10, the x axis corresponds to the angle from drums fully in (0 degrees) to the drum centerline, with 180 degrees corresponding to drums fully out. The smooth sinusoidal shape of the line matches the expected behavior given by the solid angle of neutron poison seen by the reactor as the drum rotates. In MCNP, kcode simulations were run with 20000 histories per cycle with 30 cycles discarded and 500 cycles tallied.

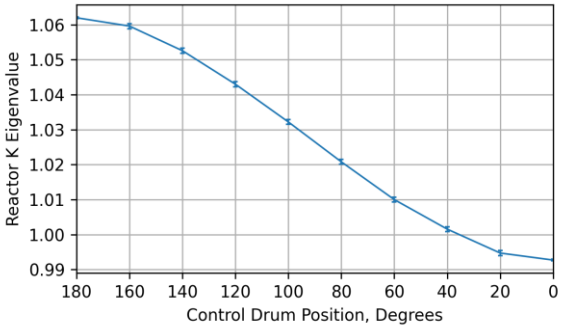

Fig. 10. Plot of the value for k as drums rotate inwards

III. CONCLUSIONS

MCNP and Serpent make good complimentary codes for neutronics investigations beyond just division of labour, as there are some tasks (for example flux/fission plots) which are possible only in Serpent, and others (for example rotational symmetry) which are so only in MCNP. Realistic geometry produced in MCNP can be "ported" to other neutronics codes for further exploration of transient effects. Future work involves refining the geometry by allowing temperature region gradients, more realistic coolant channel temperatures, and geometry for the rest of the supporting structure (including fuel vessel and rocket nozzle), as well as defining criticality lifetime and coefficients of reactivity. The reactor design itself, with improvements to those of NERVA as described, was found to be eminently feasible with both codes, but the use of larger numbers of flow tubes imposed a neutronic penalty sufficient to require MLIS (Molecular Laser Isotope Separation) enrichment in order for criticality to be achieved at operating temperature.

REFERENCES

1. J. FINSETH, *Rover nuclear rocket engine program: Overview of rover engine tests. final report*, Sverdrup Technology (1991).
2. O. R. MIRELES, *NTP 101 Short Course*, NASA Marshall Spaceflight Center (2015).
3. J. LEPPÄNEN, M. PUSA, T. VIITANEN, V. VALTAVIRTA, and T. KALTIAISENAHO, "The Serpent Monte Carlo Code: Status, Development and Applications in 2013," *Joint International Conference on Supercomputing in Nuclear Applications and Monte Carlo*, p. 06021, EDP Sciences (2014).
4. B. T. REARDEN, M. E. DUNN, D. WIARDA, C. CELIK, K. B. BEKAR, M. L. WILLIAMS, D. E. PEPLOW, C. M. PERFETTI, I. C. GAULD, W. A. WIESELQUIST, et al., "Overview of scale 6.2", *Proceedings of ANS NCSD 2013*, Wilmington, North Carolina, September 29-October, Vol. 3, American Nuclear Society (2013).
5. A. DENIG and M. EADES, "Monte Carlo–Informed Decay Heat Model for CERMET LEU_NTP Systems," *Nuclear Technology*, pp. 1–11 (2020).
6. W. HOWARTH and F. RETALLICK, *Decay Heat Cooling Analysis of a Nuclear Rocket Engine*, Westinghouse Electric Corp., Pittsburgh; Naval Postgraduate School, Monterey (1962).
7. J. Gates, A. Denig, R. Ahmed, V. Mehta, and D. Kotlyar, *Low-enriched cermet-based fuel options for a nuclear thermal propulsion engine*, Georgia Institute of Technology (2018).

Nuclear and Emerging Technologies for Space
Sponsored by Oak Ridge National Laboratory, April 26th-30th, 2021.
Available online at https://nets2021.ornl.gov

ALTERNATIVES FOR ELECTRICAL POWER PRODUCTION FROM A NUCLEAR THERMAL PROPULSION ENGINE

Emily Wood[1] and Dr. L. Dale Thomas[2]

[1] Department of Mechanical and Aerospace Engineering, The University of Alabama in Huntsville, 301 Sparkman Drive, Huntsville, AL, 35899
[2]Department of Industrial and Systems Engineering and Engineering Management, The University of Alabama in Huntsville, 301 Sparkman Drive, Huntsville, AL, 35899

256-824-8100 egw0015@uah.edu

This paper discusses the concept of a Minimally Intrusive Power generation System (MIPS) for use with a Nuclear Thermal Propulsion (NTP) engine for a crewed Mars Transfer Vehicle (MTV). In order to keep the fuel elements in the nuclear reactor above their ductile-to-brittle transition temperature (DBTT), the reactor will not be turned off after each burn, but instead will idle in a low power mode. The goal of the MIPS is to remove enough of the idle heat so that the reactor core will not be damaged, and convert this thermal energy into an adequate amount of electricity to power the vehicle, without compromising the reactor design. Three alternatives will be considered; thermoelectric generators, a closed-loop Brayton cycle, and a Stirling cycle. This paper describes the candidate systems and the design requirements of the MIPS, then goes on to outline how the systems were modeled and what attributes will be considered when deciding which system is best for this intended use.

I. INTRODUCTION

In 2015, the Nuclear Thermal Propulsion Project was established as part of NASA's Space Technology Mission Directorate with the intention to "determine the feasibility and affordability of a low-enriched uranium-based Nuclear Thermal Propulsion (NTP) engine with solid cost and schedule confidence" [1]. NTP offers very high energy density and specific impulse roughly double that of the highest performing traditional chemical propulsion systems. NTP may offer the only viable option for human exploration missions to Mars and beyond, where solar arrays can no longer provide sufficient energy and chemical propulsion would require prohibitively high mass of propellant and/or long mission durations.

Although the NTP project was not established until 2015, NASA's interest in NTP dates back to the 1960s with the Nuclear Engine for Rocket Vehicle Applications (NERVA). Testing on NERVA engines was conducted through the 1960s and early 1970s until the program was terminated due to shifting focuses and budget cuts. During the NERVA tests, thrust levels up to 75,000 pounds were observed along with specific impulse of nearly 900 seconds [2]. In the context of a human exploration mission to Mars, NTP also provides the ability to abort the mission and return to Earth at any time within three months of Earth departure and also includes the ability to return immediately upon arrival at Mars, or anywhere in the mission profile, whereas other propulsion architectures do not allow for this [3].

In most exploration mission scenarios, multiple burns of the propulsion system are needed at different points in the trajectory, primarily to exit or enter orbits of planets or moons. After the nuclear reactor is used to provide thrust for the first burn, it cannot be completely shut down or else the fuel elements will cool past their ductile-to-brittle transition temperature (DBTT) [1]. Past this temperature, the fuel elements will experience embrittlement issues[1]. This issue is unique to the tungsten cermet fuel elements, as carbide-based cores do not experience this [4]. This is due to the difference in the coefficient of thermal expansion [5].

Following a burn, instead of shutting the reactor completely down, the power output will be reduced to idle in which the reactor will continue to generate sufficient heat to keep the fuel elements above the DBTT of 373 K. When in its idle mode, the reactor is estimated to generate 10 MWt [6]. While the fuel elements located nearest the exterior of the reactor can effectively radiate this heat, the fuel elements located more interior must have heat actively removed by a non-propulsive hydrogen coolant loop in order to prevent damage to the reactor. Bimodal Nuclear Thermal Propulsion attempts to convert all of this idle mode heat into electricity for the vehicle. The ESCORT bimodal design gained much attention in 2005 for its proposed capability to provide 50 kWe of power and its potential for substantial mass savings, but it was ultimately cancelled because it required intrusive changes to the reactor design [1]. This paper proposes the concept of a Minimally-Intrusive Power generation System (MIPS) which can remove some of the heat generated by the reactor in idle mode and convert it to usable power to the vehicle without any changes to the reactor core and minimal changes to the engine.

If feasible, a MIPS will be able to convert the idle heat into usable electricity to power the vehicle and the hydrogen cooling system. The specific application mission for this MIPS study is for a crewed Mars

Transport Vehicle (MTV) for a round-trip mission to Mars.

II. DESIGN REQUIREMENTS

For this study, it is assumed that the MTV requires between 25 kWe, twice that of the Orion Spacecraft [7] and 100 kWe, approximately that of the International Space Station [8]. In order to achieve enough electricity to power the vehicle, the nuclear reactor idle heat must be converted through a power conversion cycle. There are several alternative technologies for this power conversion. Candidate technologies include:

- Thermoelectric generators (TEGs)
- Closed-loop Brayton cycle, and
- Stirling cycle

The first candidate for power conversion is thermoelectric generators. Thermoelectric generators convert heat energy directly into electrical energy without any moving parts such as turbines. Thermoelectric generators work by exploiting a temperature gradient between two sides of a generator to produce a voltage potential. Thermoelectric generators with a radioisotope as a heat source were used on Voyager 1, Voyager 2, Cassini, and New Horizons spacecraft [9]. Therefore, thermoelectric generators have already been proven to be reliable in a deep-space environment.

Candidates two and three consist of two dynamic power conversion systems: a closed-loop Brayton cycle and a Stirling cycle. The cooling system for the Near Infrared Camera and Multi-Object Spectrometer (NICMOS) on the Hubble Space Telescope used a closed-loop Brayton cycle to power the cryocoolers from 2002 to 2008. This technology was chosen because of its long-life operation and minimal vibration effects [10].

Glenn Research Center successfully demonstrated the power capabilities of a Stirling converter with their Technology Demonstration Converters (TDCs) which generated about 100 watts of electrical power each, while weighing just over 18 kg [11],[12]. TDC #13 holds the record for longest-running heat engine as of 2018 and it still shows no sign of wear [12]. Initially, this study included a Rankine cycle as an alternative, but it was eliminated because Rankine conversion cycles have never been used in a space environment. Therefore, the trade space for this study was confined to systems which have previously been used in space applications, or thoroughly researched for space applications.

Mass is always a consideration in spacecraft and space transportation vehicle design. In order to make a MIPS worthwhile, the mass of the system needs to be minimized. Specifically, it needs to be less massive than the solar arrays that the spacecraft would be forced to carry otherwise. The MIPS only needs to generate enough power for the vehicle, any more power would be wasted. Therefore, instead of being efficiency driven, like for most terrestrial systems, this study will be mass driven. In other words, as long as the candidate systems are capable of generating the target power level, initially, the mass of each system will be the primary consideration when deciding the best system for a round-trip mission to Mars. Future studies will include reliability and cost analysis.

Once the nuclear reactor is turned off, it will continue to generate decay heat due to the continued reactive decay of the fission products. Post-operational heat is a function of the power level at which the reactor operated before shutdown and the length of time in which it operated at this power level. As stated before, this heat must be removed in order to prevent damage to the reactor [1]. The baseline approach for decay heat removal is the blowdown procedure which requires up to 4,000 kg of additional hydrogen to be pulsed through each core after each burn [1] until the reactor reaches idle conditions. The heat generated in the idle state differs from the decay heat of the cooldown transients. The decay heat occurs due to the continued radioactive decay of fission product in the core after the control drums have been rotated to make the fission process subcritical. The reactor in cooldown mode will continue to generate thermal power at a decaying rate until it reaches idle conditions [13]. In idle mode, the reactor power is maintained to generate enough heat to stay above the DBTT of 373 Kelvin [14] until the power is increased for a subsequent burn. The MIPS will not only remove this idle heat without the use of additional propellant, but it will also generate power to the vehicle while the engine is at an idle state. For a nominal four-burn mission profile, there will be three idle periods in which the rector is not needed for propulsion. The first idle period will last 159 days between burns 1 and 2, the second will last 622 days between burns 2 and 3, and the final will last 159 days between burns 3 and 4 [1].This totals to 940 days in which the reactor will be operating at idle conditions. The mission profile is shown below in Figure 1.

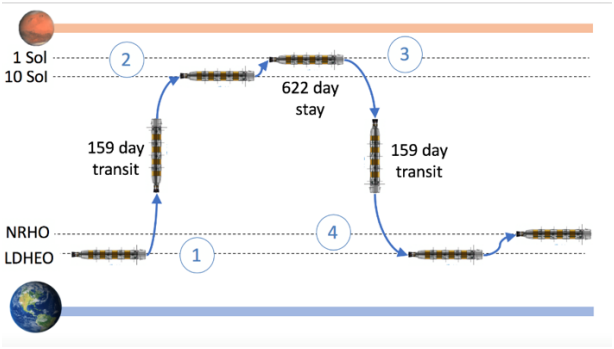

Fig. 1. Mars NTP Mission Bat Chart [1]

III. MODELING AND ANALYSIS

The mathematical modeling for this study was performed using MATLAB. As stated previously, the MTV is assumed to require between 25 kWe and 100 kWe. For the sake of simplicity, the input heat from the reactor at idle will be treated as a constant 10 MWt.

The first power conversion system to be modeled was the TEGs and then the subsequent dynamic power conversion cycles. The power output for the thermoelectric generators depends greatly on the material properties. The material for this study was selected as Silicon-germanium (SiGe), which was the material used for the radioisotope thermoelectric generators (RTGs) on the Voyager 1, Voyager 2, Cassini, and New Horizons [9]. The use of this material also allows for the Thompson effect to be neglected, which simplifies the equation for power output [15]. The mathematical model is shown below in Eq. 1.

$$P = \eta \dot{Q}_{in} \qquad \text{(Eq. 1)}$$

The power output of the closed-loop Brayton cycle, shown in Figure 2, is limited to the maximum temperature in which the turbine blades can withstand and by the working fluid properties. Nitrogen was chosen as the working fluid because in the study included in Reference 15, it was proven to produce the highest efficiencies for a Brayton cycle for space applications [16],[17]. The mathematical model for the Brayton cycle is shown below in Eqs. 2 and 3 where h is the specific enthalpy at each state and $\dot{m}$ is the mass flow rate of the working fluid.

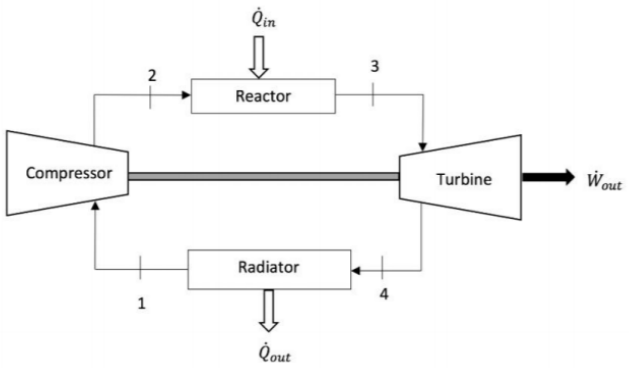

Fig. 2 Closed-loop Brayton Cycle [18]

$$\dot{W}_{cycle} = \dot{m}[(h_3 - h_4) - (h_2 - h_1)] \qquad \text{(Eq. 2)}$$

$$P = G\dot{W}_{cycle} \qquad \text{(Eq. 3)}$$

As for the Stirling cycle, a beta configuration was chosen for this study with helium as the working fluid because of its high gas constant [19]. The equations for the Stirling cycle are shown below along with a Pressure vs Volume diagram in Figure 4 and a Temperature vs Entropy diagram in Figure 5.

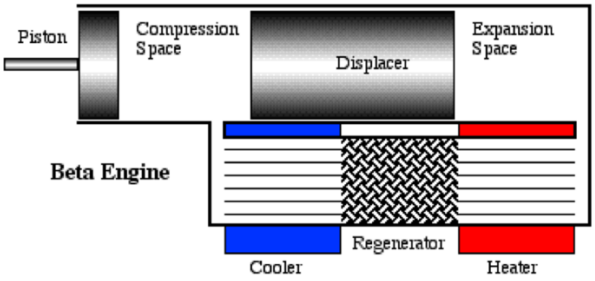

Fig. 3. Stirling Cycle Beta Configuration [19]

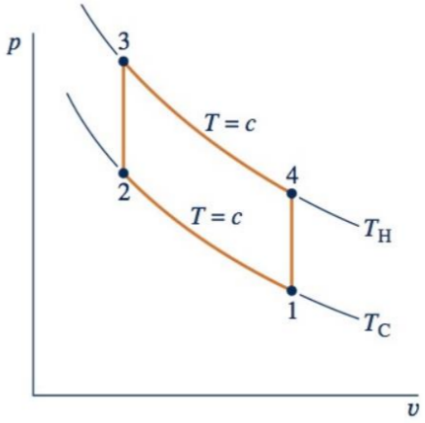

Fig. 4. Stirling Cycle Pressure vs Volume [18]

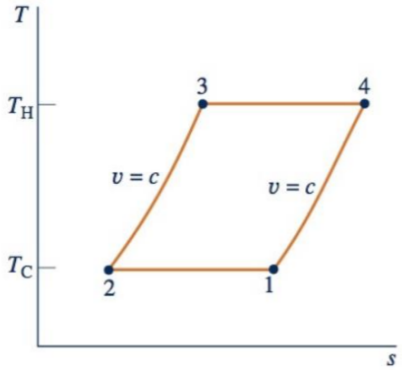

Fig. 5. Stirling Cycle Temperature vs Entropy [18]

The equations for calculating the power output by the Stirling cycle are shown below in Eqs 4 through 8. First, the ideal compression ratio is calculated using Eq. 4.

$$CR = \frac{T_H}{T_C} \qquad \text{(Eq. 4)}$$

Here, T_H is the hot temperature of the working fluid and T_C is the cold temperature of the working fluid. The mass of the working fluid in the system is found by Eq. 5.

$$m = \frac{Q_{in}}{c_v(T_H - T_C) + c_v T_C \ln(CR)} \quad \text{(Eq. 5)}$$

Here, c_v is the specific heat capacity of the working fluid and Q_{in} is the heat input coming from the reactor. The next step is to calculate the efficiency, η, of the Stirling engine using Eq. 6.

$$\eta = \frac{mc_v T_C \ln(CR)}{mc_v(T_H - T_C) + mc_v T_C \ln(CR)} \quad \text{(Eq. 6)}$$

The work out, $\dot{W}_{out}$, is calculated using Eq. 7, below.

$$\dot{W}_{out} = \eta Q_{in} \quad \text{(Eq. 7)}$$

Finally, the generator efficiency is taken into account in Eq. 8.

$$P = G\dot{W}_{out} \quad \text{(Eq. 8)}$$

For all of these models, the results of most interest are power output and mass of the power conversion system. The thermoelectric generator model for this study was based on the General-Purpose Heat Source Radioisotope Thermoelectric Generator (GHPS-RTG). Except the module for this study has no plutonium capsule or heat shield, since we are only interested in the thermoelectric generator parts. Instead of a plutonium radioisotope, like in the GPHS-RTG, the MIPS will use the heat from the nuclear reactor at idle as its heat source. Since the whole GPHS-RTG weighs 123.238 pounds, and the mass of the plutonium capsule and the heat shield is 56.747 pounds, the mass of the TEG equipment alone can be taken to be 66.491 pounds. Therefore, the mass of the TEG modules for this study were decidedly 66.491 pounds each. Next, calculations were performed to determine how many TEG modules were needed to reach the given power level, and for however many modules were required, what that equated to in mass.

For the dynamic power conversion cycles, Creo Parametric was used to model the components of the power conversion cycles to estimate the mass of these proposed systems. The 25 kWe Brayton engine was modeled using the dimensions and material specifications found in the *NASA Document for the Solar Dynamic Power System for Space Station Freedom* [20]. The Creo model of the 25 kWe engine turboalternator components was then scaled up by scaling factors that came from calculations and iterations to get the mass of the engine's turboalternator components to match that of the scaling curve given by historical data for each of the remaining power increments. The scaling curve for the Brayton engine turboalternator components is shown below in Figure 6. Figure 6 shows that the mass of the turboalternator components scale logarithmically. This is because of the fact that the specific power of the turboalternator components scale with logarithmic decay [21].

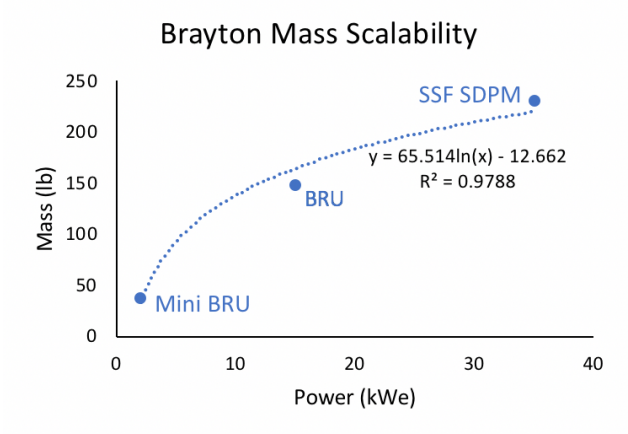

Fig. 6. Brayton Mass Scalability [21]

The mass of the Stirling engine was determined by first modeling the engine dimensions and material specifications shown in NASA's *SPDE/SPRE Final Summary Report* [20], a conference paper on NASA Lewis Stirling SPRE testing [22], and a contractor report for the SPDE [23]. The 25 kWe engine was then scaled up by scaling factors to get the mass of the engine to reach the mass given by the scaling curve shown in Figure 7.

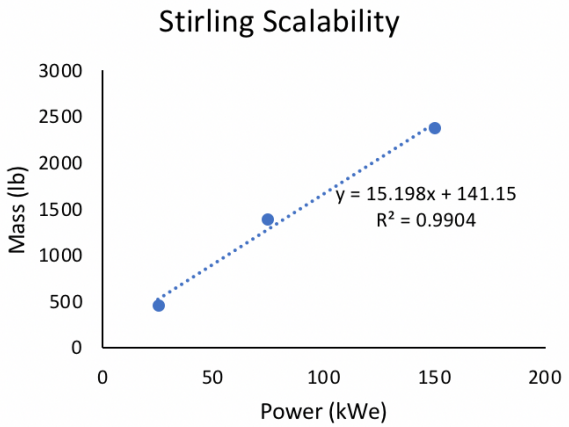

Fig. 7. Stirling Mass Scalability [24]

The necessary surface area of the solar arrays was found using Eqs (9) through (14) where R_{mars} is the average distance from the sun to Mars in km x 10^6, I_d is the inherent losses of the solar array, θ is the sun incident angle, and L_d is the life degradation of the solar arrays.

$$P_0 = 301 \times H_1 \quad \text{(Eq. 9)}$$

$$H_1 = \left(\frac{149.6}{R_{mars}}\right)^2 \quad \text{(Eq. 10)}$$

$$P_{BOL} = P_0 I_d cos\theta \quad \text{(Eq. 11)}$$

$$L_d = \left(1 - {}^{degradation}/_{year}\right)^{life\ in\ years} \quad \text{(Eq. 12)}$$

$$A = \frac{P}{P_{BOL}} \quad \text{(Eq. 13)}$$

IV. RESULTS

Assuming the TEGS for this study will have the same efficiency as that of the GPHS-RTG used on the Cassini and New Horizons missions, at 6.3%, the power outputs can be achieved with 195 TEG modules for the 25 kWe power level, 389 modules for the 50 kWe power level, 583 modules for the 75 kWe power level, and 774 modules for the 100 kWe power level

For the Brayton cycle, the turbine inlet temperature, T_1, is limited by the moderator's melting temperature. Assuming the moderators are made of LiH [25], the turbine inlet temperature should be about 500 K. Furthermore, a common Brayton cycle pressure ratio of 13 was assumed, since the normal range is between 11 and 20 [18]. The radiator sink temperature, T_3, was assumed to be 278 K [26]. The specific enthalpies at each state were determined using CoolProp and then the power generated by the system was calculated using Eq. 2 and 3.

Many assumptions had to be made to calculate the power output of the Stirling cycle. The temperatures of the working fluid and the size of the Stirling engine mirrored those from a study performed in 2016 at Glenn Research Center [27]. The hot temperature of the working fluid, T_H, was assumed to be 500 K, as it was with the Brayton cycle, and the cold temperature of the working fluid, T_C, was assumed to be 323 K [27]. Additionally, the length the piston travels was taken as 6 mm. This length was the same as the length the piston traveled in the study mentioned above. The generator efficiency was considered to be 30%, the same as it was for the Brayton cycle calculations. The heat coming from the reactor was assumed to be 10 MWt.

For the solar arrays, it was assumed that the solar arrays would be flex-fold out with a mass area density of 1.9 kg/m^2 and that the solar arrays would be multi-junction with a power output coefficient of 301 W/m^2. The value for R_{mars} was taken to be 228.0 km x 10^6. Furthermore, it was assumed that the solar arrays would have a degradation of about 0.5% per year and that the sun's incident angle would be at worst-case-scenario 45° [28].

The mass of the radiators used to radiate out any heat not taken in by the MIPS was calculated using heat transfer equations with the following assumptions: the material of the radiator is a carbon-carbon composite and the temperature of the radiator is 323 K. For this study, these radiators were referred to as "Idle Mode Radiators," or IMRs.

The following plot shows the mass of the MIPS alternatives plus the mass of the IMRs compared to the mass of the solar arrays plus the IMRs.

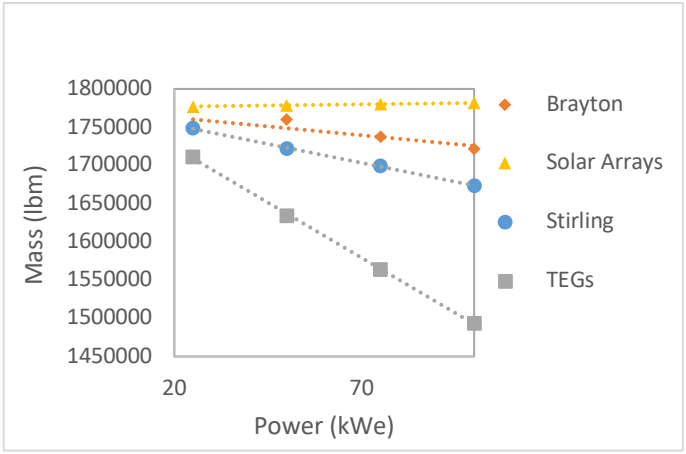

Fig. 6. Mass of Power Generation Systems with IMRs

It can be seen that all three MIPS alternatives result in a lower mass than the solar arrays. The TEG MIPS configuration is the least massive, followed by the Stirling engine, and then the Brayton engine.

V. CONCLUSIONS

NTP is a viable option for missions to Mars and beyond, but in its idle state, excess heat is an immediate issue for the reactor. The bimodal nuclear thermal propulsion concept has previously been favored for its ability to take all of this idle heat and convert it to usable power for the vehicle, but it would require substantial changes to the reactor design [1]. Conceptually, a MIPS could tap into the thermal energy from the non-propulsive hydrogen coolant loop and convert this thermal energy into an adequate amount of electricity to power the vehicle, without compromising the reactor design. Since all three of the MIPS alternatives result in mass savings compared to solar arrays and their associated IMRs, further consideration of the MIPS as the primary power source for the MTV is merited.

VI. FUTURE WORK

It is likely that the idle temperature of the reactor will change, therefore sensitivity analysis will be conducted on the effects of this parameter and of other

selected parameters. Furthermore, reliability of the systems and cost analysis will be considered in addition to the systems power output capabilities and masses in order to better influence a well-rounded suggestion of which system would be best for use in the MTV.

ACKNOWLEDGMENTS

Thank you to Samantha Rawlins for her contributions to this research and to Dr. Jason Cassibry for his guidance and encouragement. This work was supported by the National Aeronautics and Space Administration.

REFERENCES

[1] Rawlins, S. B., and Thomas, D. L. D. "A PROPOSED SOLUTION TO ADDRESS NUCLEAR THERMAL PROPULSION FUEL EMBRITTLEMENT AND CRYOGENIC HYDROGEN REQUIREMENTS." p. 5.

[2] Finseth, J. L. Overview of Rover Engine Tests Final Report. https://ntrs.nasa.gov/archive/nasa/casi.ntrs.nasa.gov/19920005899.pdf. Accessed May 18, 2020.

[3] Hall, L. Nuclear Thermal Propulsion: Game Changing Technology. *NASA*. http://www.nasa.gov/directorates/spacetech/game_changing_development/Nuclear_Thermal_Propulsion_Deep_Space_Exploration. Accessed May 19, 2020.

[4] Burns, D., and Johnson, S. "Nuclear Thermal Propulsion Reactor Materials." *Nuclear Materials*, 2020. https://doi.org/10.5772/intechopen.91016.

[5] Hickman, R. R., Broadway, J. W., and Mireles, O. R. "Fabrication and Testing of CERMET Fuel Materials for Nuclear Thermal Propulsion." p. 23.

[6] Jennings, T., "Space Technology Mission Directorate Game Changing Development Program Nuclear Thermal Propulsion Project: STM2.0 Reactivity Closed Loop Control," Aerojet Rocketdyne, September 2019

[7] "Orion: America's Next Generation Spacecraft," NP-2010-10-025-JSC

[8] Garcia, M. International Space Station Solar Arrays. *NASA*. http://www.nasa.gov/mission_pages/station/structure/elements/solar_arrays.html. Accessed Jul. 27, 2020.

[9] Cheng, F. "Calculation Methods for Thermoelectric Generator Performance." *Thermoelectrics for Power Generation - A Look at Trends in the Technology*, 2016. https://doi.org/10.5772/65596.

[10] SUCCESS STORIES. Creare.

[11] Wolverton, M. Stirling in Deep Space. *Scientific American*. https://www.scientificamerican.com/article/stirling-in-deep-space/. Accessed Aug. 13, 2020.

[12] It Keeps Going and Going: Stirling Engine Test Sets Long-Duration Record at NASA Glenn - SpaceFlight Insider. https://www.spaceflightinsider.com/space-centers/glenn-research-center/it-keeps-going-and-going-stirling-engine-test-sets-long-duration-record-at-nasa-glenn/. Accessed Jan. 26, 2021.

[13] Buden, D. *Nuclear Thermal Propulsion Systems*. Polaris Books, Lakewood, CO, 2011.

[14] Wronski, A., and Foukdeux, A. "The Ductile-Brittle Transition in Polycrystalline Tungsten." *Journal of the Less Common Metals*, Vol. 8, No. 3, 1965, pp. 149–158. https://doi.org/10.1016/0022-5088(65)90042-1.

[15] Powering the Voyager Spacecraft with Radiation: The RTG (Radioisotope Thermoelectric Generator) - News. https://www.allaboutcircuits.com/news/voyager-mission-anniversary-rtg-radioisotope-thermoelectric-generator/. Accessed Jan. 27, 2021.

[16] Tarlecki, J., Lior, N., and Zhang, N. "Analysis of Thermal Cycles and Working Fluids for Power Generation in Space." *Energy Conversion and Management*, Vol. 48, No. 11, 2007, pp. 2864–2878. https://doi.org/10.1016/j.enconman.2007.06.039.

[17] Nitrogen or Air Versus Helium for Nuclear Closed Cycle Gas Turbines. *Atomic Insights*. https://atomicinsights.com/nitrogen-or-air-versus-helium-for-nuclear-closed-cycle-gas-turbines/. Accessed Jul. 28, 2020.

[18] Moran, M. J., Shapiro H. N., Boettner, D. D., and Bailey, M. B., *Fundamentals of Engineering Thermodynamics,* 8th Edition, 2014

[19] Asnaghi, A., Ladjevardi, S. M., Saleh Izadkhast, P., and Kashani, A. H. Thermodynamics Performance Analysis of Solar Stirling Engines. *ISRN Renewable Energy*. Volume 2012, e321923. https://www.hindawi.com/journals/isrn/2012/321923/. Accessed Jul. 27, 2020.

[20] Staff of Solar Dynamic Power System Branch, "Solar Dynamic Power System Development for Space Station Freedom," NASA Reference Publication 1310, July 1993

[21] Mason, L. S., Shaltens, R. K., Dolce, J. L., and Cataldo, R. L. Status of Brayton Cycle Power Conversion Development at NASA GRC. In *SPACE TECHNOLOGY AND APPLICATIONS INTERNATIONAL FORUM- STAIF 2002*, No. 608, Albuquerque, New Mexico (USA), 2002, pp. 865–871.

[22] Wong, W. A., Cairelli, J. E., Swec, D. M., Doeberling, T. J., Lakatos, T. F., and Madi, F. J. NASA Lewis Stirling SPRE Testing and Analysis with Reduced Number of Cooler Tubes. Presented at the 27th Intersociety Energy Conversion Engineering Conference (1992), 1992.
[23] Dochat, G. “SPDEjSPRE Final Summary Report.” p. 98.
[24] Mechanical Technology Incorporated, "Space Power Free-Piston Stirling Engine Scaling Study," NASA CR-182218
[25] Nam, S. H., Venneri, P., Kim, Y., Lee, J. I., Chang, S. H., and Jeong, Y. H. “Innovative Concept for an Ultra-Small Nuclear Thermal Rocket Utilizing a New Moderated Reactor.” *Nuclear Engineering and Technology*, Vol. 47, No. 6, 2015, pp. 678–699. https://doi.org/10.1016/j.net.2015.06.003.
[26] Pietsch, A., and Brandes, D. J. Advanced Solar Brayton Space Power Systems. Presented at the Proceedings of the 24th Intersociety Energy Conversion Engineering Conference, 1989.
[27] Briggs, M. H. Improving Power Density of Free-Piston Stirling Engines. Presented at the 14th International Energy Conversion Engineering Conference, Salt Lake City, UT, 2016.
[28] Higdon, K., "MAE 468/568 Elements of Spacecraft Design: Spacecraft Power," 2020

Nuclear and Emerging Technologies for Space
Sponsored by Oak Ridge National Laboratory, April 26th-30th, 2021.
Available online at https://nets2021.ornl.gov

A SURVEY OF HIGH-TEMPERATURE MODERATORS FOR SPACE NUCLEAR REACTOR APPLICATIONS

Jaden G. Zymbaluk, Jesus A. Mendoza, Melissa L. Breathwaite, Jeffrey C. King

Colorado School of Mines, 1500 Illinois St, Golden, CO 80401

jzymbaluk@mines.edu, jmendoza1@mines.edu, mbreathwaite@mines.edu, kingjc@mines.edu

This paper surveys the existing literature on high-temperature solid moderators and provides derived nuclear and physical property data for beryllium, beryllium oxide, graphite, lithium hydride, yttrium hydride, and zirconium hydride. While zirconium hydride has been used as a moderator in previous space nuclear reactors, the higher disassociation temperature of yttrium hydride, combined with its higher thermal conductivity, make yttrium hydride a strong candidate for use in future Low Enrichment Uranium (LEU)-fueled space nuclear reactors.

I. INTRODUCTION

Space Directive 6, issued by the White House on December 16, 2020, encouraged the development of nuclear fission power sources to support future space exploration efforts.[1] The directive specifically referenced the development of a 40 kW_e fission power source to enable long-term habitation of the Moon and a future mission to Mars. The directive also specified that future space nuclear reactors will be fueled with Low Enrichment Uranium (LEU, uranium containing less than 20% uranium-235), unless the specific mission could not be accomplished without the use of Highly Enriched Uranium (HEU, uranium containing more than 20% uranium-235). Previous work demonstrated that kilowatt-class space nuclear reactors fueled with LEU are conceptually possible; however, several significant engineering challenges remain.[2] Specifically, in order to achieve a reactor size and mass comparable to that of an HEU-fueled kilowatt-class reactor, it will likely be necessary to incorporate a moderator into the reactor core.[2] The inclusion of a moderator decreases the average neutron energy in the core, which increases the effective fission cross-section of the uranium-235 in the core. This, in turn, can compensate for the lower uranium-235 atom density inherent to LEU-based reactor fuels.

Moderator technologies for terrestrial reactors are well-understood, with water as the most common moderator in terrestrial power reactors. However, the need for higher conversion efficiencies, and, thus higher-operating temperatures, makes water infeasible as a moderator in a space nuclear reactor. Several high-temperature solid moderators have received significant historical attention[3]; and, several newer candidates have become available in the past several years.[4,5,6,7] This paper provides an introductory survey of the properties of several high-temperature solid moderators with a focus on space nuclear power and propulsion applications.

II. POTENTIAL MODERATORS

Historically, the list of potential high-temperature solid moderators included beryllium, beryllium oxide, graphite, lithium hydride, and zirconium hydride. More recently, yttrium hydride has become economically available.[8] Additionally, recent sponsored research has considered the development of encapsulated moderator materials, where hydride-based moderators are encapsulated in an aluminum oxide or magnesium oxide matrix.[4] This section considers the properties of historic and newly available high-temperature solid moderators to identify those most relevant to space nuclear power and propulsion applications.

II.A. Historic Moderators

Historically, high-temperature moderator research focused on beryllium, beryllium oxide, graphite and metal hydrides such as lithium and zirconium hydride.[3] These historic moderators were chosen, in essence, for their ability to effectively thermalize neutrons without parasitically absorbing a large fraction of the resulting thermal neutrons.[9] Minimizing the number of collisions required to thermalize a fast neutron was an important additional requirement. Thus, historic moderators were selected for their high neutron scattering cross section, low neutron absorption cross section, and an abundance of atoms with a low atomic number.

However, none of these moderators are perfect candidates for use in the high-temperature environment of a space nuclear reactor. Lithium and zirconium hydride experience hydrogen disassociation at elevated temperatures (993 K and 900 K, respectively), which will significantly decrease the moderating ability of these materials and leads to concerns regarding hydrogen diffusion and transport in hydride-moderated space nuclear reactors.[10] Both beryllium and beryllium oxide moderators would require the handling of beryllium during fabrication and assembly. Exposure to beryllium can be toxic to humans, making the production and handling of these moderators challenging.[11] Finally, graphite may undergo

significant dimensional changes under neutron irradiation, which may contribute to a shortened lifetime in reactor environments.[12] Recently, these drawbacks have led to a search for newer, potentially more effective, moderator materials that pose fewer concerns when considered for use in a space nuclear reactor.

II.B. Recent Developments

Recent research on new high temperature moderator materials has yielded several promising candidates. Suggestions for newer high-temperature moderators include two-phase composite moderators[4], micro-encapsulated moderators[5], radiogenic lead[13], and beryllium carbides.[6] Two-phase composite moderators[4] and micro-encapsulated moderators[5] function similarly. Both rely on a primary moderator material, generally a historic moderator such as zirconium hydride or beryllium, while employing a second material, usually a ceramic, to extend the operating temperature of the primary moderating phase. The main difference between these two advanced moderator concepts lies in the amount of secondary phase. In the two-phase composite moderators, the secondary ceramic phase comprises most of the composite moderator's mass[4], while a micro-encapsulated moderator relies on a secondary ceramic phase that is only a few atomic layers thick.[5] In both cases, the secondary phase serves to stabilize the primary moderator. For example, the ceramic layer used in the micro-encapsulated moderators is intended to serve as a diffusion barrier when applied to metal hydrides, allowing the micro-encapsulated moderator to be used at temperatures above the traditional dissociation temperatures of the metal hydrides.

Other options include radiogenic lead[13], alternate beryllium compounds such as beryllium carbide[6], and ternary zirconium-yttrium hydrides.[7] Radiogenic lead is promising as the dominant constituent, lead-208, exhibits a respectable scattering cross section and diminutive absorption cross section. A recent study evaluated four potential moderators (beryllium carbide, beryllium oxide, silicon carbide, and magnesium oxide) for use in a fluoride salt-cooled high temperature reactor by comparing them to graphite.[6] This study found that both beryllium carbide and beryllium oxide can operate at temperatures above 1300 K while maintaining a k_{eff} >1 for longer time periods than graphite at a burn-up of 160.6 MWd/kgU.[6] Based on this study, beryllium carbide may be an effective moderator material with a melting temperature of approximately 2400 K.[6] Another recent study evaluated a technique for producing bulk, crack free zirconium-yttrium hydrides, with an additional benefit of showing that the addition of yttrium to the zirconium hydride system can inhibit the delta to epsilon phase transition, preventing a prime mechanism of crack production.[7]

Yttrium hydride historically posed several issues that prevented it from becoming a widely used moderating material. Primarily, pure yttrium was historically too expensive to be implemented economically[14] and it was difficult to fabricate bulk yttrium hydride without considerable cracking.[15] Recently, however, the price of pure yttrium has decreased considerably[8]; and, technological improvements have led to the advent of a programmable hydriding system that produces bulk, crack free yttrium hydride.[16] These two developments make yttrium hydride a viable moderator material, especially considering that it exhibits a considerably greater thermal stability than other metal hydrides.[16]

II.C. Moderators Included In This Survey

This survey considers the five historic moderators discussed in Section II.A, as well as yttrium hydride. These materials are commercially available and could be readily incorporated into a near-term space nuclear reactor. In contrast, while other new moderating materials have been proposed, there is currently not enough information on their respective physical and nuclear properties to consider them in the near-term. Table I presents the limiting temperatures and densities of the moderators considered in this survey.

III. NUCLEAR PROPERTIES

The nuclear properties of any material selected for use in a nuclear reactor core need to be thoroughly considered. Since moderators serve to decrease the energy of neutrons produced by fission in the core, the slowing down decrement and the moderating ratio are the main nuclear properties of interest for this analysis of high-temperature moderators.

This survey defines the neutron energy ranges as follows: thermal neutrons range from 0 – 0.0253 eV; epithermal neutrons range from 0.0253 eV – 100 keV; and, fast neutrons range from 100 keV – 4 MeV. The Monte Carlo N-Particle, Version 6.2 neutron transport code (MCNP6.2)[26] provided energy-averaged cross sections in the defined ranges based on the ENDF/B-VIII.0 neutron cross section libraries[27], as well as cross-sections averaged

TABLE I. Physical Properties of Selected Materials

	Limiting Temperature (K)	Density (g cm^{-3})
Beryllium	1558[17] §	1.86[22]
Beryllium Oxide	2843[18] §	2.8[18]
Graphite	4073-5073[19] §	1.6[19]
Lithium Hydride	993[20]↓	0.8[23]
Yttrium Hydride	1173[21]↓	4.2[24]
Zirconium Hydride	900[21]↓	5.7[25]

§ Indicates Melting
↓Indicates Hydrogen Desorption

over the watt fission spectrum. The cross-section calculations used a mono-directional beam of neutrons with energies uniformly sampled from the defined energy ranges. The neutrons pass through two F1 tallies with the elastic scattering and absorption cross section multiplier cards for the individual elements in the moderators.

III.A. Slowing Down Decrement

Neutron moderation occurs as a result of energy loss from a neutron scattering event with a nucleus. Effective moderators for thermal systems must be able to efficiently remove large amounts of energy from fission neutrons and slow the neutrons down to an ideal energy range without the neutrons being removed by resonance absorption by uranium-238. The logarithmic energy decrement (ξ) can be used to determine the moderation effectiveness of a particular nucleus with an atomic weight given by A:

$$\xi = 1 + \frac{(A-1)^2}{2\,A} * ln\left(\frac{A-1}{A+1}\right). \quad (1)$$

The logarithmic energy decrement is only applicable to individual nuclei. When considering heterogeneous materials, the average logarithmic energy decrement must be considered. The average logarithmic energy decrement weights the logarithmic energy decrement of each isotope in the mixture by the macroscopic scattering cross section (Σ_s) of that isotope to determine a weighted average value for the energy decrement of the material as a whole:

$$\bar{\xi} = \frac{Sum(\xi_i * \Sigma_{si})}{Sum(\Sigma_{si})}. \quad (2)$$

Table II displays the calculated average logarithmic energy decrement of the potential moderators in the thermal, epithermal, fast, and Watt fission energy ranges, as well as a historical value based on tabulated cross sections.[28, 29] In this table, the highest energy decrement comes from the materials containing hydrogen. This is the expected outcome given that the energy transfer between a neutron and a proton can be nearly 100%. As the atomic weight of the materials increases, the average energy loss from a collision between a neutron and the nuclei decreases. This is most evident with the beryllium and carbon-based moderators, where the higher atomic mass results in a decreased energy loss per collision. The average energy decrement of the single component moderators does not change significantly with incident neutron energy, as the cross section portion of the calculation cancels out.

III.B. Moderating Ratio

The slowing down decrement of materials is geared towards the scattering of neutrons in a material. In order to fully consider a material's effectiveness as a moderator, neutron absorption must also be considered. The moderating ratio provides a way to compare the scattering potential and the energy decrement of each scattering event to the absorption potential of the material to more accurately measure a material's effectiveness as a moderator.

The moderating ratio can be computed by incorporating the total macroscopic scattering cross section (Σ_s) and the total macroscopic absorption of the material (Σ_a) of the material in the following manner:

$$MR = \frac{\bar{\xi} * \Sigma_s}{\Sigma_a}. \quad (3)$$

Table III lists the calculated moderating ratios for each of the moderators considered in this paper. A higher moderating ratio is considered better, since it indicates that the moderating potential is greater than the possibility of absorption. The values provided in the table are consistent with expectations given that a decrease in neutron energy generally indicates an increase in cross section.

Beryllium has a neutron absorption threshold reaction in the fast region (> 1.758 MeV) where it absorbs a neutron and emits two neutrons.[27] This reaction constitutes 72.6% of beryllium's fast neutron absorptions which indicates that the drop in the fast and Watt fission spectrum moderating ratios is not detrimental to the neutron life cycle properties of the beryllium-based moderators.

Table II. Average logarithmic energy decrement of the moderators selected in this survey.

	Thermal	Epithermal	Fast	Watt Fission	Historical
Beryllium	0.21	0.21	0.21	0.21	0.21
Beryllium Oxide	0.18	0.17	0.16	0.16	0.14
Graphite*	0.16	0.16	0.16	0.16	0.16
Lithium-7 Hydride	0.98	0.96	0.76	0.78	0.99
Yttrium Hydride‡	0.93	0.81	0.64	0.63	0.96
Zirconium Hydride‡	0.94	0.77	0.62	0.62	0.99

* Assuming crystalline graphite

‡ Zirconium hydride and yttrium hydride assume a 1:2 atom ratio (ZrH_2 and YH_2)

TABLE III. Moderating ratios of the moderators selected in the survey.

	Thermal	Epithermal	Fast	Watt Fission	Historical
Beryllium	8.21×10^{1}	1.11×10^{5}	2.93×10^{0}	3.72×10^{0}	1.38×10^{2}
Beryllium Oxide	1.07×10^{2}	4.19×10^{4}	4.62×10^{0}	3.83×10^{0}	4.24×10^{2}
Graphite*	1.21×10^{2}	5.43×10^{4}	8.39×10^{3}	3.83×10^{2}	2.59×10^{2}
Lithium-7 Hydride	6.80×10^{1}	4.83×10^{4}	9.12×10^{4}	8.65×10^{4}	1.16×10^{0}
Yttrium Hydride‡	2.63×10^{1}	1.30×10^{3}	1.45×10^{3}	1.44×10^{3}	8.44×10^{1}
Zirconium Hydride‡	5.99×10^{1}	9.98×10^{2}	7.94×10^{2}	8.10×10^{2}	2.44×10^{2}

* Assuming crystalline graphite

‡ Zirconium hydride and yttrium hydride assume a 1:2 atom ratio (ZrH_2 and YH_2)

Table III indicates that the least absorbent moderators are graphite and the beryllium-based moderators with some consideration for lithium hydride, given that fission neutrons are generally fast neutrons. Given hydrogen's potential for moderation, the moderating ratio is not a definitive method for analyzing moderators; but, it does give insight for how a moderating material can be used. As a result of neutron absorption, an ideal amount of a hydride moderator would be less than the ideal amount of a non-hydrogen-based moderator; and, given the average logarithmic energy decrement, the hydride moderators would generally provide a higher effective multiplication factor using similar amounts of material.

IV. PHYSICAL PROPERTIES

Figures 1-3 present recommended values for the thermal conductivity, the specific heat, and the thermal expansion coefficient as a function of the temperature of the selected moderator materials. A full catalogue of the phase changes these materials experience, and their triggers, will be included in a future journal publication. To determine these recommended values, it was necessary to gather a database of reported property values. Following this, each reported data set was fitted with a fourth order polynomial, which was then used to generate an equal number of points for all of the data sets, within the scope of the data. These equally spaced data sets were then fitted with a fourth order polynomial as single data set, with this regression serving as the recommended value for that particular property and material. A full set of citations for each historic data set will be included with the upcoming journal publication.

It is worth noting that many of the selected moderator materials are generally isotropic with regards to their thermophysical properties, with several notable exceptions. The thermophysical properties of graphite are usually anisotropic. In this survey, the graphite properties are given for the planes parallel to the extrusion axis. In this specific case, the properties in the planes perpendicular to the extrusion axis are quite small in comparison to the parallel planes. One significant example of anisotropy takes place in the thermal expansion of zirconium hydride.[29] The epsilon phase, face-centered tetragonal in structure, of zirconium displays significant thermal expansion anisotropy; however, the delta phase of zirconium hydride displays isotropic thermal expansion.[29] In this survey, the delta phase, oftentimes the face-centered cubic phase by convention, of the materials is considered, as the hydrogen content is closest to the stoichiometric composition for lithium and yttrium hydride . Furthermore, the delta phase of zirconium hydride is. By far, the most isotropic phase exhibited.[30]

Figure 1 indicates that lithium hydride has a significantly higher specific heat (4118 J/kg-K at 300 K) than the other moderators in this survey, while yttrium hydride and zirconium hydride have the lowest (384 J/kg-K and 339 J/kg-K at 300 K, respectively). A higher specific heat may contribute to increasing the thermal mass of the reactor, which can become important in considering the reactor's transient behavior.

Figure 2 shows that beryllium, beryllium oxide, and graphite have significantly higher thermal conductivities (189 W/m-K, 265 W/m-K and 191 W/m-K at 300 K, respectively) than the other moderators, while the thermal conductivity of lithium hydride and zirconium hydride are significantly lower (11 W/m-K and 17 W/m-K at 300 K, respectively). Thermal conductivity directly impacts the peak fuel and moderator temperatures in a reactor, and yttrium hydride's increased thermal conductivity compared to zirconium hydride (76 W/m-K compared to 17 W/m-K at 300 K, respectively) may be another advantage to its use in space nuclear reactors.

The thermal expansion of materials must be accounted for in the design of any reactor system, and the thermal expansion of moderating materials can have a strong impact on a reactor's thermal feedback coefficients. The significantly high thermal expansion coefficient of lithium hydride (37×10^{-6} /K at 300 K) may increase the magnitude of the moderator thermal feedback coefficient of a reactor containing significant amounts of lithium hydride. The linear thermal expansion coefficients of beryllium,

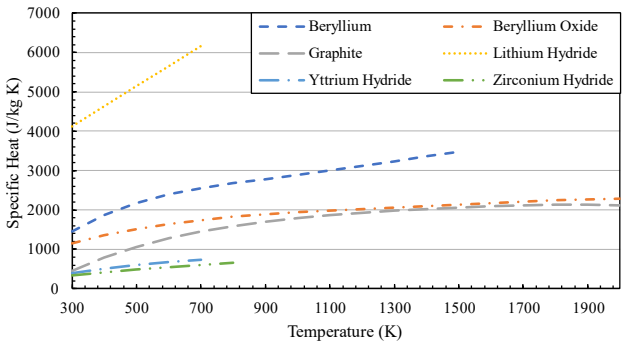

Fig. 1. Specific heat as a function of temperature of the moderators selected in this survey.

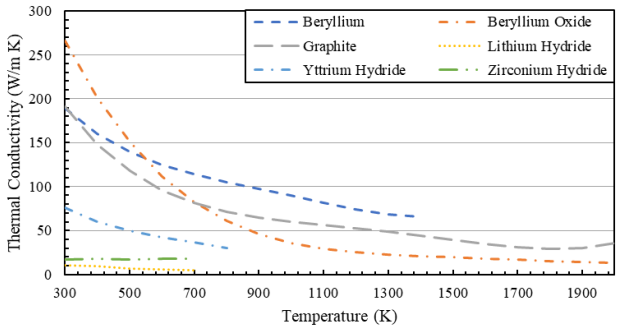

Fig. 2. Thermal conductivity as a function of temperature of the moderators selected in this survey.

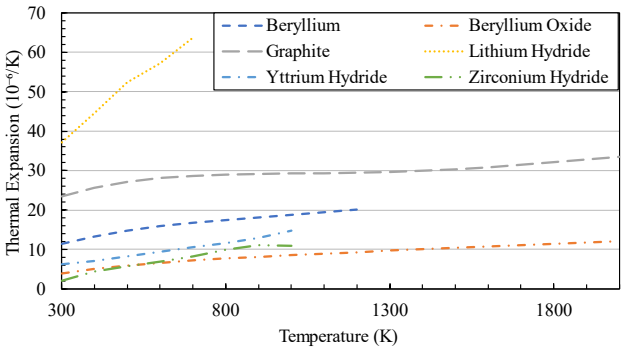

Fig. 3. Linear thermal expansion coefficient as a function of temperature of the moderators selected in this survey.

beryllium oxide, yttrium hydride, and zirconium hydride at 300 K are between 5-31% (11, 4.0, 6.2, and 2.0 x 10^{-6} /K, respectively) of lithium hydride, with graphite having a linear thermal expansion coefficient that is 63% (24 x 10^{-6} /K at 300 K) that of lithium hydride.

V. SUMMARY AND CONCLUSIONS

The renewed interest in space nuclear power as well as the push towards Low Enrichment Uranium (LEU, uranium containing less than 20% uranium-235)-fueled space reactor systems, suggests a future need for advanced high-temperature moderators to reduce to the system and mass of future space nuclear reactors. This paper surveys the existing literature on high-temperature solid moderators and provides derived nuclear and physical property data for beryllium, beryllium oxide, graphite, lithium hydride, yttrium hydride, and zirconium hydride. While zirconium hydride has several properties that make it very attractive as a moderator, hydrogen disassociation will begin to occur at 900 K, which will constrain the operating temperature of space nuclear reactors moderated by this material. While the moderating ratio of yttrium hydride is lower than that of zirconium hydride, its higher disassociation temperature (1173 K), combined with its higher thermal conductivity, make yttrium hydride a strong candidate for consideration as a moderator in future LEU-fueled space nuclear reactors.

REFERENCES

1. Department of Energy, Presidential Policy Directive 6 (Space Policy), "National Strategy for Space Nuclear Power and Propulsion," Office of the Secretary, *Department of Energy*, 85 FR 83923, (2020).
2. L.d.H. MENCARINI and J. C. KING, "Fuel geometry options for a moderated low-enriched uranium kilowatt-class space nuclear reactor," *Nuclear Engineering and Design*, **340**, 122-132 (2018). DOI:10.1016/j.nucengdes.2018.09.017.
3. W. MUELLER, "Metal Hydrides," Chapter 2: Hydrides in Nuclear Reactor Applications, Academic Press, Cambridge, MA (1968).
4. L. SNEAD, N. BROWN, J. TRELEWICZ, et al., "Fabrication of Two-Phase Composite Moderators as Potential Lifetime Reactor Components," *Transactions of the American Nuclear Society*, **121**, 1445-1447, (2019). DOI:10.1312/T31286.
5. C. ANG, L. SNEAD, and J. TRELEWICZ, "An Innovative Approach to Composite Moderators Containing Zirconium Hydrides," *Transactions of the American Nuclear Society*, **121**, 683-685 (2019). DOI:10.13182/t31283.
6. V. KRISHNA, C. HIONG, and S. XIAO, "Assembly design of a fluoride salt-cooled high temperature commercial-scale reactor: Neutronics evaluation and parametric analysis." *Annals of Nuclear Energy*, **141**, (2020). DOI:10.1016/j.anucene.2019.107288.
7. J. PENG, M. WU, F. DU, et al., " Thermodynamic Modelling of Y–H and Y–Zr–H System Aided by First-Principles and its Application in Bulk Hydride Moderator Fabrication," *Journal of Nuclear Materials*, **531**, 152035 (2020). DOI:10.1016/j.jnucmat.2020.152035.

8. U.S. Geological Survey, Mineral Commodity Summaries 2020, *United States Geological Survey*, 186-187, Reston, VA (2020).

9. P. NICHOLS, E. WOODRUFF, and R. NIGHTINGALE,, "Nuclear Graphite," Chapter 4, Academic Press, Cambridge, MA (1962).

10. R. VAN HOUTEN and W. G. BAXTER, "Titanium, Zirconium, and Yttrium Hydrides as Space Shielding Materials," *Journal of Spacecraft and Rockets*, **2**, no. 3, 469-472 (1965). DOI:10.2514/3.28212.

11. C. STRUPP, "Beryllium Metal II. A Review of the Available Toxicity Data," *Ann. Occup. Hyg.*, **55**, no. 1, 43-56 (2010). DOI:10.1093/annhyg/meq073.

12. C. H. WU, J. P. BONAL, and B. KRYGER, "The effect of high-dose neutron irradiation on the properties of graphite and silicon carbide," *Journal of Nuclear Materials*, **208**, 1-7 (1994). DOI:10.1016/0022-3115(94)90191-0.

13. A. SHMELEV, G. KULIKOV, V. APSE, et al., "Radiogenic lead with dominant content of ^{208}Pb: New coolant and neutron moderator for innovative nuclear facilities," *Science and Technology of Nuclear Installations*, (2011). DOI:10.1155/2011/252903.

14. R. VAN HOUTEN, "Selected engineering and fabrication aspects of nuclear metal hydrides (Li, Ti, Zr, and Y0," *Nuclear Engineering and Design*, **31**, no. 3, 434-448 (1974), DOI:10.1016/0029-5493(75)90178-8.

15. J. VETRANO, "Hydrides as neutron moderator and reflector materials," *Nuclear Engineering and Design*, **14**, no. 3, 390-412 (1971). DOI:10.1016/0029-5493(70)90159-7.

16. X. HU, D. SCHAPPEL, C. SILVA, et al., "Fabrication of yttrium hydride for high-temperature moderator application," *Journal of Nuclear Materials*, **539**, 152335 (2020). DOI:10.1016/j.jnucmat.2020.152335.

17. J. DICKINSON, "Method of Making Beryllium," United States Patent Application, 504,770, Dundee, IL (1921).

18. G. SAMSONOV, "The Oxide Handbook," Plenum Press, New York, NY (1973).

19. A. SAVVATIMSKIY, "Measurements of the melting point of graphite and the properties of liquid carbon (a review for 1963-2003)," *Carbon*, **43**, 1115-1142, (2005). DOI:x

20. W. GROCHALA and P. EDWARDS, "Thermal decomposition of the non-interstitial hydrides for the storage and production of hydrogen," *Chemical Reviews*, **104**, 1283-1315 (2004). DOI:10.1021/cr030691s.

21. J. L. ANDERSON, W. MAYO, and E. LANTZ, "Reactivity Control of Fast-Spectrum Reactors by Reversible Hydriding of Yttrium Zones," NASA TN-D-4615, Lewis Research Center, Cleveland, OH (1968).

22. N. PINTO, R. FLOYD, and J. LOWE, "Beryllium Science and Technology: Volume 2," Chapter 2, Springer US, New York, NY (1979).

23. R. SMITH and J. MISER, "Compilation of the properties of lithium hydride," NASA Technical Memorandum X-483, Cleveland, OH (1963).

24. M. ITO, J. MATSUNAGA, D. SETOYAMA, et al. "Thermal properties of yttrium hydride," *Journal of Nuclear Materials*, **344**, 295-297 (2005). DOI:10.1016/j.nucmat.2005.04.058.

25. S. YAMANAKA, K. YAMADA, K. KUROSAKI, et al., "Characteristics of zirconium hydride and deuteride," *Journal of Alloys and Compounds*, **330-332**, 99-104 (2002). DOI:10.1016/S0925-8388(01)01448-7.

26. C. J. WERNER, J. S. BULL, C. J. SOLOMON, et al., "MCNP Version 6.2 Release Notes," *Los Alamos National Laboratory* Technical Report LA-UR-18-20808, Los Alamos, NM, (2018). DOI:10.2172/1419730.

27. D. A. BROWN, M. B. CHADWICK, R. CAPOTE, et al., "ENDF/B-VIII.0: The 8th Major Release of the Nuclear Reaction Data Library with CIELO-project Cross Sections, New Standards and Thermal Scattering Data", *Nuclear Data Sheets*, **148**, 1-142, (2018). DOI: 10.1016/j.nds.2018.02.001.

28. J. R. LAMARSH and A. J. BARATTA, "Introduction to Nuclear Engineering - Third Edition," Prentice-Hall, Inc., Upper Saddle River, NJ (2001).

29. V. F. SEARS, "Neutron Scattering Lengths and Cross Sections," *Neutron News*, **3**, no. 3, 29-37, (2006).

30. M. CINBIZ, X. HU, and K. TERRANI, "Thermal expansion behavior of δ-zirconium hydrides: Comparison of δ hydride powder and platelets," *Journal of Nuclear Materials*, **509**, 566-576, (2018). DOI:10.1016/j.nucmat.2018.07.026.